Precursor Synthesis and Chemical Vapour Deposition of Group 13 Oxides

This thesis is submitted in partial fulfilment of the requirements for the Degree of Doctor of Philosophy (Chemistry)

Siama Basharat

University College London

Christopher Ingold Laboratories,

20 Gordon Street,

WC1H 0AJ

2007

ProQuest LLC
789 East Eisenhower Parkway
P.O. Box 1346
Ann Arbor, MI 48106-1346

I, Siama Basharat, confirm that the work presented in this thesis is my own. Where information has been derived from other sources, I confirm that this has been indicated in the thesis.

Abstract

This thesis is primarily concerned with the precursor synthesis and chemical vapour deposition of group 13 oxides. The gas sensing properties of some of the films prepared have also been investigated. **Chapter 1** gives an introduction to techniques used for deposition, in particular chemical vapour deposition (CVD). **Chapter 2** describes the synthesis of gallium and indium alkoxides incorporating donor functionalised ligands. The donor-functionalised alkoxides $[R_2M(OR')]_2$ (M = Ga, R = Et; M = In, R = Me; R' = $CH_2CH_2NMe_2$, $CH(CH_2NMe_2)_2$, CH_2CH_2OMe, $CH(CH_3)CH_2NMe_2$, $C(CH_3)_2CH_2OMe$) were synthesised by the 1 : 1 reaction of R_3M with R'OH in toluene at room temperature.

Gallium and indium bis-alkoxides $[RM(OR')_2]$ (M = Ga, R = Et; M = In, R = Me; R' = $CH_2CH_2NMe_2$, $CH(CH_2NMe_2)_2$, CH_2CH_2OMe, $CH(CH_3)CH_2NMe_2$, $C(CH_3)_2CH_2OMe$) have also been synthesised by the 1 : 6 reaction of R_3M with R'OH in toluene under reflux conditions. Homoleptic gallium trisalkoxides $[Ga(OR)_3]_2$ have been prepared by the 1 : 6 reaction of $[Ga(NMe_2)_3]_2$ with R'OH. Decomposition of all the compounds have been studied by thermal gravimetric analysis in **Chapter 3**. The formation of thin-films of gallium oxide *via* single-source low pressure chemical vapour deposition (LPCVD) methodology was investigated including detailed film growth studies and characterisation. The compounds described above were used as precursors and deposition was achieved at 550 °C. Chapter 3 also investigates the formation of thin-films of gallium and indium oxide using aerosol assisted chemical vapour deposition (AACVD). This involved the *in situ* reaction of $[Ga(NMe_2)_3]_2$ or R_3M with a donor functionalised alcohol (R'OH). Gas sensing experiments on selected Ga_2O_3 films deposited by AACVD are described in **Chapter 4**.

Acknowledgements

First, I would like to thank my supervisor, Dr. C. J. Carmalt, for well everything. I thank her for invaluable guidance, support and enthusiasm. In particular I am grateful to the immense patience she has shown me over the years and for keeping my focused. I would also like to thank Professor I. P. Parkin, my secondary supervisor for supervising me whilst Dr C. J Carmalt was on maternity leave.

In particular, I am grateful to Dr. Chris. Blackman, for helping me with practical work concerning many aspects of this work. I thank Dr. Derek Tocher and Dr. Sarah Barnett for carrying out all the X-ray crystallography. I thank Dr. Abil Aliev for all his help elucidating my spectra. I thank Dr. Steve Firth for useful discussions about thermal analysis. I thank Lisa Harris and John Hill for Mass spec and Jill Maxwell for elemental analysis. I am extremely grateful to Kevin Reeves for WDX, EDXA and SEM. I would also like to thank Rob Palgrave, who recorded the X-ray photoelectron spectra and Dr. Russell Binions for carrying out the gas sensing experiments.

Many thanks go to my friends for their support and encouragement over the years. I would like to thank Jalpa Patel, Dr. Christina Baskaran, Dr. Dina Solanki, Dr. Ashti Rampaul, Sobia Ashraf, Naima Narband and Caroline Knapp. I am grateful to Nicolas Boscher for all his help with the CVD aspects. I would all like to thank all the other people who have worked in Lab 308 for creating an enjoyable place to work and socialise. I would also like to thank a very close friend, Sakhila for her support and encouragement.

Most importantly I would like to thank my family. I am eternally grateful to my parents, my sisters; Abru and Samara and brothers; Shubber and Bubbar for putting up with me over the years. I thank them for their love, encouragement and support, without whose support I would not have completed this thesis.

Contents

List of Figures

Chapter 1 Introduction

Chapter 2 Synthesis of Group 13 Alkoxides

Chapter 3 Chemical Vapour Deposition of Group 13 Oxides

Chapter 4 Gas Sensing Properties of Gallium Oxide

List of Tables

Chapter 1 Introduction

Chapter 2 Synthesis of Group 13 Alkoxides

Chapter 3 Chemical Vapour Deposition of Group 13 Oxides

Chapter 4 Gas Sensing Properties of Gallium Oxide

List of Schemes

Chapter 2 Synthesis of Group 13 Alkoxides

List of Abbreviations

Å	Angstrom
AACVD	Aerosol assisted chemical vapour deposition
APCVD	Atmospheric pressure chemical vapour deposition
Ar	Aryl
Calc.	Calculated
CI	Chemical Ionisation
cm	Centimeter
CVD	Chemical vapour deposition
Cy	Cyclohexyl
d	Doublet
δ	Chemical shift / ppm
DSC	Differential scanning calorimetry
Et	Ethyl
EDXA	Energy dispersive X-ray analysis
eV	electron volts
g	Gram
h	Hour
J	Coupling constant
^{i}Bu	iso-butyl
^{i}Pr	iso-propyl
^{n}Bu	Normal-butyl
^{t}Bu	Tertiary-butyl
IR	Infra-red
LPCVD	Low pressure chemical vapour deposition
m	Medium (in IR spectra)
m	Multiplet (in NMR spectra)
Me	Methyl
mmol	Millimole
MOCVD	Metalorganic Chemical Vapour Deposition
MS	Mass spectrometry

Py	Pyrdine
^{n}Pr	Normal-propyl
NMR	Nuclear magnetic resonance
PECVD	Plasma enhanced chemical vapour deposition
Ph	Phenyl
ppm	Parts per million
PVD	Physical vapour deposition
q	Quartet (in NMR spectra)
quin	Quintet (in NMR spectra)
R	Organic substituent
SEM	Scanning electron microscopy
s	Singlet (in NMR spectra)
s	Strong (in IR spectra)
Sept	Septet (NMR)
$SiMe_3$	Trimethyl silyl
t	Triplet
THF	Tetrahydrofuran
TGA	Thermal gravimetric analysis
tmp	Trimethylpyridine
UV	Ultraviolet
vis	Visible
vs	Very strong
vw	Very weak
W	Weak
WDX	Wavelength dispersive analysis
XRD	X-ray diffraction
XPS	X-ray photoelectron spectroscopy

Chapter 1

Introduction

Chapter 1 Introduction

The aim of this work was to synthesis and characterise a range of gallium and indium alkoxide complexes using donor-functionalised ligands. Group 13 alkoxides have been used extensively in organic reactions, however this work involves their use as precursors to group 13 oxides. Gallium oxide (Ga_2O_3) is considered to be one of the most ideal materials for application as thin-film gas sensors at high temperatures and finds many uses in optoelectronic devices. Gallium oxide (Ga_2O_3) is an electrical insulator at room temperature and semiconducting above 400 °C. Indium oxide containing materials are of interest due to their application in transparent conducting electrodes. Chemical vapour deposition (CVD) is the most practical method for preparing thin-films for large-scale applications. The versatility of metal alkoxides as single-source precursors to metal oxides *via* CVD processes is widely recognised; they are easy to prepare and purify and are intrinsically non-corrosive. The advantages of using single-molecular precursors over existing methods include potential low temperature synthesis and removal of the use of toxic/volatile reagents.

This introductory chapter describes the structure and applications of gallium and indium oxides, which have been produced in thin film form in this work. The synthesis and characterisation of a range of gallium and indium alkoxides are discussed in Chapter 2. Chapter 3 investigates the suitability of these alkoxide complexes as precursors to chemical vapour deposition. This is assessed by thermogravimteric analysis (TGA) and differential scanning calorimetry (DSC) of the complexes in order to deduce the decomposition process. In addition, deposition of thin films of gallium and indium oxide by aerosol assisted chemical vapour deposition (AACVD) and low-pressure chemical vapour deposition (LPCVD) is described. Chapter 4 describes the gas sensing properties of the gallium oxide films produced by AACVD. The final chapter discusses the findings of this work.

1.1 Deposition of Thin Films

There are several routes, which can be used to deposit thin films of materials. Solution phase techniques include dip coating, spraying and sol gel methodology.

Vapour phase routes are now increasingly being employed to prepare high quality thin films of technologically important materials. A thin film is a solid layer of a material on a surface, usually a few atoms to a few microns in thickness, which has different properties to those of the substrate. Films maybe be amorphous, epitaxial or polycrystalline.

1.1.1 Physical vapour deposition

Physical vapour deposition (PVD) is a process, which involves laying down a thin solid film, by forming gaseous species from a solid target by processes such as evaporation, sputtering, sublimation and molecular beam epitaxy.

Evaporation is one of the easiest ways to grow a film by vaporising a pure material and allowing the vapour phase molecules to deposit on a cooler surface. The choice of the evaporation source is governed by the material to be evaporated, as well as other considerations such as deposition rate.[1] Examples of the source include vacuum deposition, electron bombardment and flash evaporation.[2] Alternatively, sputtering is a physical process that uses high-energy ions to bombard the surface of the precursor material. This causes the atoms from the surface to be ejected in an ionised form. These ionised atoms are accelerated towards the surface of the substrate by an applied electric field, where the substrate forms part of one of the electrodes.[2,3]

Molecular Beam Epitaxy (MBE) is a used for forming crystalline films, which are lattice matched to the substrate (10^{-10} Torr).[4] This results in the production of high purity films as pure elemental sources are used and the ultra high vacuum leads to low concentration of gases such as oxygen. The use of ultra high vacuum makes the technique very expensive but at the same time it is precise, and single monolayer films may be produced.

1.1.2 Chemical Vapour Deposition

Chemical vapour deposition (CVD) is a process, which involves depositing a thin film from gas phase reactions.[2,5] In general, in a CVD reaction, one or more volatile inorganic, metal-organic or organometallic precursors are transported in the gas phase, often by a carrier gas or under vacuum, into a reaction chamber. Within the chamber, gas phase reactions may occur between the precursor molecules, forming intermediate species (Figure 1.1). These species may be transported to the substrate and adsorption of

the product to the surface can occur. Surface reactions take place on the heated substrate during which the precursors decompose to form the material of the final film. During the decomposition of the precursors volatile byproducts are also formed, which desorb from the substrate and are transported out of the chamber by either vacuum or the carrier gas. The atoms of the film are weakly bound to the substrate mainly through van der Waals type interactions and are hence free to diffuse. The atoms diffuse across the surface of the film until nucleation occurs by several atoms bonding together, which leads to growth of the desired solid thin film.

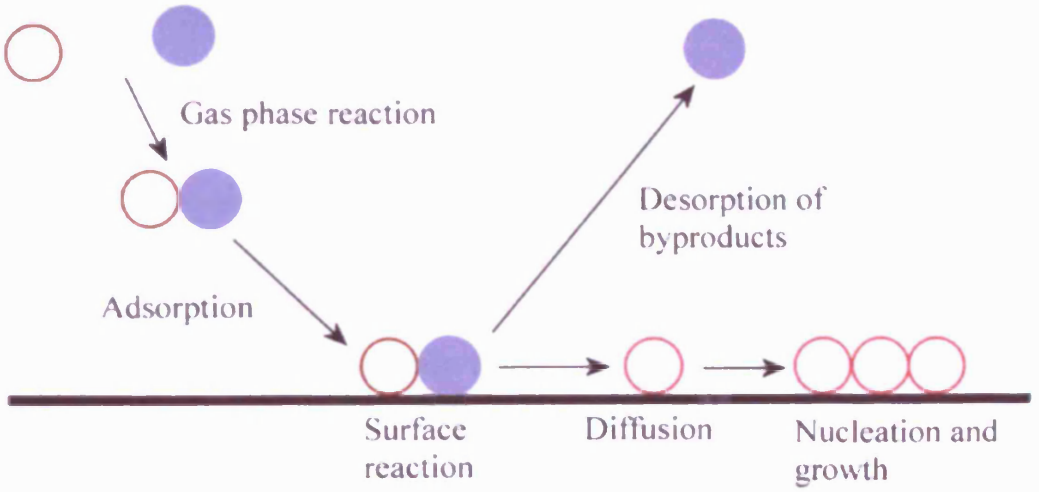

Figure 1.1: Overview of the CVD process

There are a number of advantages of CVD over traditional methods, such as PVD. These include:

- CVD produces highly dense and pure materials.
- Uniform films with good adhesion and reproducibility are formed.
- Crystal structure, surface morphology and orientation of products can be controlled by varying CVD parameters.
- Reasonable deposition costs.
- A wide range of precursors can be utilised.
- Relatively low deposition temperatures.
- Deposition rates can be adjusted.

- CVD is a non line-of-sight process with good throwing power. Therefore it can be used to uniformly coat complex shaped components and deposit films with good conformal coverage.[6]

1.1.2.1 Dual-Source Chemical Vapour Deposition

In CVD reactions to form films with simple compositions, for example GaN, two precursors are often used (e.g. Me_3Ga and NH_3 for GaN, Eq. 1.1). This type of reaction is termed a dual-source reaction and each precursor contains one of the elements of the final film.

$$Me_3Ga + NH_3 \xrightarrow{> 900\,^{\circ}C} GaN + 3\,CH_4 \qquad \textbf{(1.1)}$$

Dual source CVD reactions can have the following problems:

1. A large excess of one of the precursors must be present (e.g. NH_3 for GaN).
2. It is often difficult to control the exact stoichiometry of the final film and films are often inhomogeneous.
3. High temperatures are often used.
4. Precursors used are sometimes very reactive (e.g. Me_3Ga is pyrophoric) and toxic; this leads to problems with handling on a large scale.

These problems may be overcome by the use of single-source precursors.

1.1.2.2 Single-Source Chemical Vapour Deposition

A single-source precursor is a simple molecule, which contains all of the appropriate atoms required for the film. Single-source precursors contain preformed bonds between the elements of the film and sometimes the elements are present in the same stoichiometric ratio as the final film.[7] This facilitates greater control over the stoichiometry and can lead to homogenous films.

Single-source precursors potentially display a range of advantages over dual-source routes, including:

1. Lower temperature growth is possible.
2. Air and moisture stability of the precursors is possible.
3. Less toxic and less reactive compounds than conventional precursors.

Important requirements of a single-source precursor are that they should be volatile and stable in the vapour phase and possess easily removable terminal ligands. An example of a single source precursor for GaN is shown in Eq. 1.2.[3] On heating, the compound $[Cl_2GaNH(SiMe_3)]_2$ readily loses Me_3SiCl and HCl resulting in the formation of GaN.

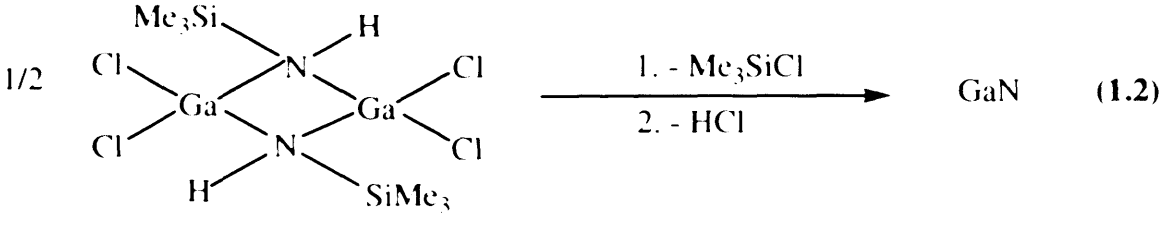

(1.2)

1.1.2.3 Low Pressure Chemical Vapour Deposition

Low pressure chemical vapour deposition (LPCVD) is the most common form of CVD. In this process a vacuum is used to aid the transport of precursors to the substrate. Typically LPCVD processes operate between 1×10^{-3}-1×10^{-7} atm. No carrier gases are required in LPCVD, although sometimes these are added. Normally in LPCVD a single-source precursor is used. LPCVD is widely used in the electronics industry for making metal interconnects on Si-chips. LPCVD gives good conformality, but relatively slow growth rates, typically 100-200 nmh^{-1}. Problems arise from the incomplete decomposition of the precursor leading to contamination, such as carbon incorporation, in the resulting film. Further experimental details about LPCVD are discussed in Chapter 3.

1.1.2.4 Aerosol- Assisted Chemical Vapour Deposition

Aerosol-assisted (AA)CVD uses an aerosol vaporisation technique.[8] The precursor is dissolved in a suitable solvent and an aerosol mist is generated using a

piezoelectric transducer. Ultrasonic waves pass through the precursor solution producing a wave pattern on the surface of the liquid. When the height of the wave is sufficient, the wave crests become unstable and form droplets that are ejected from the surface thus generating an aerosol mist.[9] The generated mist is then transported to the reaction chamber using an inert carrier gas at atmosphere pressure. In the reaction chamber, which is usually heated in excess of 200 °C, the solvent is evaporated and the precursors undergo a chemical reaction to deposit the thin film required. Further detail will be discussed later in Chapter 3.

1.2 Group 13 Oxides

1.2.1 Structure

1.2.1.1 Gallium oxide

Gallium(III) Oxide, Ga_2O_3, is the most stable form of gallium oxide and exists in several crystalline forms depending upon the conditions of preparation. Five forms have been reported,[10] as listed in Table 1.1.

Table 1.1: Crystal structures of gallium oxide

Form	Crystal structure
α -Ga_2O_3	Trigonal *R3c*
β-Ga_2O_3	Monoclininc, *C2/m*
γ-Ga_2O_3	Cubic, *Fd3m*
δ-Ga_2O_3	Cubic, *Ia3*
ε-Ga_2O_3	Orthorhombic

Gallium sesquioxide has been reported to crystallise with five structures, the stable forms being trigonal α-Ga_2O_3 and monoclinic β-Ga_2O_3.[11] The oxygen ions in the structure of α-Ga_2O_3 are in an approximately hexagonal close packed array with all the Ga^{3+} ions octahedrally coordinated to O^{2-} ions. Also, in the α-phase, octahedra share edges and faces which brings the metal ions very close to each other. The α-phase is known to be metastable.

The β-Ga_2O_3 structure (Figure 1.2) is quite different from that of α-Ga_2O_3. The oxygen ions in β-Ga_2O_3 are arranged in a "distorted cubic" close packed array.[12] The unit cell consists of two crystallographically non-equivalent gallium and three non-equivalent oxygen ions. Each Ga^{3+} ion is surrounded by a distorted tetrahedron of oxygen ions. β-Ga_2O_3 is the thermodynamically stable room temperature phase,[13] because of its low density. The average bond distances of the two known stable gallium oxide structures are highlighted in Table 1.2.

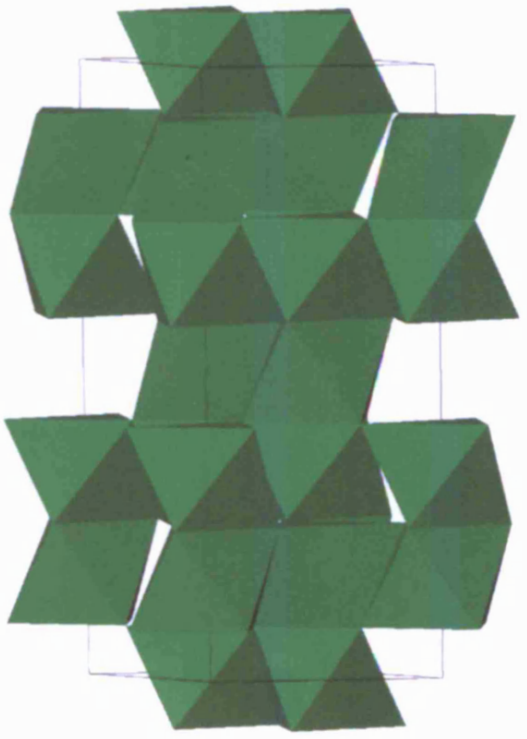

Figure 1.2: Perspective view of the arrangement of the oxygen octahedra and tetrahedra in β-Ga_2O_3.

Table 1.2: Average bond distances of the two gallium oxide structure.

	Ga–O	**O–O**
α-Ga_2O_3 [11]	2.00	2.80
β-Ga_2O_3 [13]	2.00	2.84

1.2.1.2 Indium oxide

The crystal structure of indium sesquioxide is known to have the cubic *C* modification (Zachariasen, 1927).[14] The unit cell consists of two crystallographically non-equivalent indium atoms and only one type of oxygen atom. The indium atoms are six coordinate, whilst the oxygen is four coordinate.[14] Each In is surrounded by six equidistant oxygen atoms, which lie nearly at the corners of a cube with two-body diagonally opposite corners unoccupied. Also, another In atom is surrounded by six oxygen atoms which lie nearly at the corners of a cube, leaving two face-diagonally opposite corners unoccupied. In this polyhedra, there are three different sets of In–O distance (*av.* 2.18 Å). The polyhedra arrangement is shown in Figure 1.3.

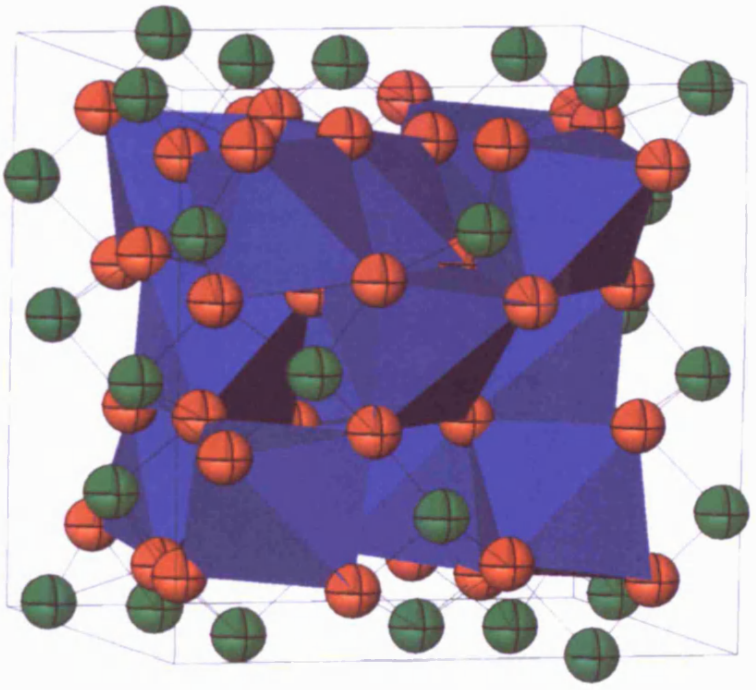

Figure 1.3: The polyhedra arrangement of In and O atoms in In_2O_3 (Red sphere = In, Green sphere = O).

1.2.2 Applications

1.2.2.1 Gallium Oxide

Gallium oxide (Ga_2O_3) is considered to be one of the most ideal materials for application as thin-film gas sensors at high temperatures and finds uses in

optoelectronic devices.[15,16] Gallium oxide (Ga_2O_3) is an electrical insulator at room temperature and semiconducting above 500 °C.[17] It is thermally stable and adopts a monoclinic structure. At temperatures above 900 °C[18] the electric conductivity changes depending on the concentration of oxygen. Hence the oxygen concentration can be monitored. Oxygen gas sensors have practical use in monitoring and controlling oxygen concentrations in exhaust gases of automobiles, as well as waste gases and chemical processes.[19] Below 900 °C, gallium oxide thin film operates as a surface-control-type sensor to reducing gases, *e.g.* EtOH and CO.[20,21] Thus it is possible to switch the function of the sensor with temperature. Gallium oxide films also have potential practical uses outside of sensors. β-Ga_2O_3 and amorphous Ga_2O_3 has received attention as a new phosphor host material for thin film electroluminescent (TFEL) devices.[22-24] This property arises upon optical excitation through the band gap, β-Ga_2O_3 can exhibit up to three different emissions, UV, blue and green depending on the dopant and preparation of the sample.[24] Other applications include use as catalysts because of their high ion-exchange selectivity and capacity.[25-27] Tin doped β-Ga_2O_3 films is a unique oxide films which are transparent to deep UV light and at the same time electrically conductive.[28] They are used for applications such as UV transparent electrodes for UV light emitting diodes.[29] Gallium oxide also has uses as a nanomaterial,[30-32] for example, gallium oxide nanowires have been produced by electric arc discharge of GaN powders mixed with small amounts of Ni and Co on oxygen ambient.[30]

1.2.2.2 Indium Oxide

Indium oxide thin films (doped and undoped) are attractive materials for use as transparent conductors, in applications such as display panels and solar cell windows.[32] Undoped indium oxide finds use in industrial and technological applications such as toxic / dangerous gas detection in chemical plants due to both its transparency and conductivity. Indium oxide has a direct band gap of 3.75 eV[34,35] for single crystals. Indium oxide can be doped with other metals to enhance its electronic properties. Tin doped indium oxide (ITO) can be prepared with an optical band gap of more than 3.4 eV.[36] ITO thin films are widely used in optoelectronic devices such as transparent electrodes for light emitting diodes (LEDs)[37-41] and flat panel displays (FPDs)[41,42], and photovoltaic cells[43-46] due to their high transparency in the visible light region, low electric resistivity, chemical stability and excellent adhesion to substrate.[47]

1.3 References

1. J. L.Vossen and W. Kern, *Thin Film Processes II*, Academic press, 1991.
2. M. Ohring, *The Materials Science of Thin Films*, Academic Press, London, 1992.
3. M. L. Hitchman, K. F. Jensen Eds, *Chemical Vapour Deposition Principles and Applications*, Academic Press, London, 1993.
4. G. B. Stringfellow, *Rep. Prog. Phys*, 1982, 45, 469.
5. W. S. Rees Jr. Ed, *CVD of Nonmetals*, VCH Publishers, New York, 1996.
6. K. L. Choy, *Progress in Materials Science*, 2003, 48, 57.
7. T. S. Lewkebandara and C. H. Winter, *Adv. Mater*, 1994, 6, 237.
8. C. J. Carmalt, J. D. Mileham, A. J. P. White, D. J. Williams and J. W. Steed, *Inorg. Chem*, 2001, 40, 6035.
9. T. T. Kodas and M. J. Hampden-Smith, *Aerosol processing of materials*, 1999, Wiley-VCD. New York.
10. A. J. Downs, *Chemistry of Aluminium, Gallium, Indium and Thallium*, Chapman and Hall, Springer, 1 Edition, 1993.
11. M. Mareizo and J. P. Remeika, *J. Chem. Phys*, 1966, 46 (5), 1862.
12. S. Geller, *J. Chem. Phys*, 1960, 33 (3), 676.
13. L. M. Foster and H. C. Stump, *J. Am. Chem. Soc*, 1951, 73, 1590.
14. M. Marezio, *Acta Cryst*, 1996, 20, 723.
15. M. Fleischer, L. Hollbauer, H. Mexiner, *Sensors and Aquators B*, 1994, 18-19, 119.
16. M. Ogita, K. Higo, Y. Hatanaka, *Applied Surface Science*, 2001, 175, 721. M. Ogita, S. Yausa, K. Kobayashi, Y. Yamada, Y. Natanishi, Y. Hatanaka, *Applied Surface Science*, 2003, 212, 397.
17. M. Fleischer, H. Mexiner, *Sensors and Actuators B*, 1995, 26-27, 81.
18. T. Schwebel, M. Flesischer, H. Mexiner, C. - D. Kohl, *Sensors and Actuators B*, 1998, 49, 46.
19. Y. Li, A. Trinchi, W. Wlodarski, K. Galatsis, K. Kalantar-Zadeh, *Sensors and Actuators B*, 2003, 93, 431.
20. M. Fleischer, S. Kornely, T. Weh, J. Frank, H. Meixner, *Sensors and Actuators B*, 2000, 69, 205.

21. M. Ogita, N. Saika, Y. Nakanishi, Y. Hatanaka, *Applied Surface Science*, 1999, 142, 188.

22. T. Miyata, T. Nakatkani, T. Minami, *Thin Solid Films*, 2000, 373, 145.

23. J. Hao, M. Cocivera, *J. Phys . D. Appl. Phys*, 2002, 35, 433.

24. L. Binet, D. Gourier, *J. Phys. Chem. Solids*, 1998, 59, 1241.

25. A. L. Petre, J. A. Peredigon-Melon, M. Hirano, H. Hosono, *Thin Solid Films*, 2002, 411, 134.

26. A. L. Petre, A. Auroux, P. Gelin, M. Caldararu, N. I. Ionescu, *Thermochin. Acta*, 2001, 379, 177.

27. C. O. Arean, A. L. Bellan, M. P. Menruit, M. R. Delagdo, G. T. Palomino, *Microporous Mesoporous Mater*, 200, 40, 35.

28. M. Orita, H. Hiramatsu, H. Ohta, M. Hirano, H. Hosono, *Thin Solid Films*, 2002, 411, 135.

29. H. Ohta, K. Kawamura, M. Orita, M. Hirano, N. Sarukura, H. Hosono, *Appl. Phys. Lett*, 77, 475, 2000.

30. G. S. Park, W. B. Choi, J. M. Kim, Y. C. Choi, Y. H. Lee, C. B. Lim, *J. Cryst. Growth*, 2000, 220, 494.

31. Z. R. Dai, W. Pan, Z. L. Wang, *J. Phys .Chem B*, 2002, 106, 902.

32. S. Sharma, M. K. Sunkara, *J. Am. Chem. Soc*, 2002, 124, 12288.

33. J. N. Avaritsiotis and R. P. Howson, *Thin Solid Films*, 1980, 80, 63.

34. R. L .Weiher and R. P. Ley, *J. Appl. Phys*, 1966, 37, 299.

35. H. K. Muller, *Phys. Status Solid*, 1969, 27, 723.

36. C. Xirouchaki, G. Kiriakidis, T. F. Pedersen and H. Fritzsche, *J. Appl. Phys*, 79, 1996, 9349.

37. C. W. Tang and S. A. Van Slyke, *Appl. Phys. Lett*, 51, 1987, 913.

38. J. H. Burroughes, D. D. C. Bradley, A. R. Brown, R. N. Marks, K. Mackay, R. H. Friend, P. L. Burns and A. B. Holmes, *Nature*, 347, 1990, 539.

39. J. R. Sheats, H. Antoniadis, M. Hueschen, W. Leonard, J. Miller, R. Moon, D. Roitman and A. Stocking, *Science*, 273, 1996, 884.

40. J. M. Leger, S. A. Carter, B. Ruhstaller, H.- G. Nothofer, U. Scherf, H. Tillman and H.- H. Horhold, *Phys. Rev. B*, 68, 2003, 054209.

41. S. - F. Hsu, C. - C. Lee, S. - W. Hwang and C. H, *Chem. Apply. Phys. Lett*, 86, 2005, 1.

42. B. H. Lee, I. G. Kim, S. W. Cho and S. H. Lee, *Thin Solid Films*, 1997, 302, 25.

43. R. B. H. Tahar, T. Ban, T. Ohaya and Y. Takahashi, *J. Appl. Phys*, 1998, 83, 2631.

44. A. J. Breeze, Z. Schlesinger, S. A. Carter and P. J. Brock, *Phys. Rev. B*, 2001, 64, 125205.

45. F. Zhang, M. Johansson, M. R. Anderson, J. C.Hummelen and O. Inganas, *Adv. Mater*, 2002, 14, 662.

46. E. Kymakis and G. A. J. Amaratunga, *Appl. Phys. Lett*, 80, 2002, 112.

47. Z. Z. You and J. Dong, *Journal of Colloid Sceince*, 2006, 300, 697.

Chapter 2

Synthesis of Group 13 Alkoxides

Chapter 2 Synthesis of Group 13 Alkoxides

2.1 Introduction

This chapter describes the synthesis and characterisation of a range of gallium and indium alkoxides. These compounds were prepared for application as single and dual source precursors for the CVD of gallium and indium oxide thin films. Section 2.1 gives an overview on known gallium and indium alkoxide complexes in the literature. The synthesis and characterisation of the group 13 alkoxides prepared in this project are discussed in section 2.2, with experimental details given in section 2.3.

2.1.1 Mono(alkoxides)

A number of different methods have been used to synthesise mono(alkoxides) of gallium(III) and indium(III). The most common method is the reaction of trivalent gallium or indium organometallics R_3M with alcohols at elevated temperatures, Eq. 2.1.

$$R_3M + R'OH \longrightarrow 1/2\,[R_2MOR']_2 + RH \qquad (2.1)$$

Another efficient and widely used route for the synthesis of gallium and indium mono (alkoxides) is salt elimination. This involves the reaction of organometallic halide complexes $[R_2MX]$ (R = alkyl or aryl, M = Ga or In, X = halide) with early main group reagents (e.g. LiOR'), Eq. 2.2.

$$R_2MX + LiOR' \longrightarrow 1/n\,[R_2MOR']_n + LiX \qquad (2.2)$$

An alternative route to group 13 mono(alkoxide) complexes involves amine-alcohol exchange, Eq. 2.3.

$$[R_2M(NR'_2)]_n + R'OH \longrightarrow 1/n\,[R_2MOR']_n + HNR'_2 \qquad (2.3)$$

Group 13 mono(alkoxides), of the type $[R_2MOR']_n$ (R = akyl or aryl; M = Ga or In; R' = alkyl, aryl), have been structurally characterised for both gallium(III) and indium(III), as discussed in this section. The structure of these compounds is governed by

electronic and steric properties of both the alkoxide and alkyl/aryl ligands. Gallium and indium alkoxides are generally air/moisture sensitive compounds and highly soluble in a range of organic solvents. However, the structure of these compounds can vary, due to electronic and steric properties of both the alkoxide and alkyl/aryl ligands. Two main structural types have been identified for gallium and indium alkoxides either, dimers with alkoxy bridges or monomers.

The dimeric structure is derived from two sp^2 hybridised M atoms, which are then bridged by two alkoxide ligands forming a M_2O_2 ring, according to Figure 2.1. Thus, the first alkoxide ligand forms an M–O bond and lies within the equatorial plane of M. The second bridging alkoxide ligand forms a dative covalent M–O bond *via* electron pair donation from O into a vacant p-orbital on M and lies axial to the M centre. The situation is reversed for the second M and each alkoxide ligand is sp^3 hybridised at O.[1]

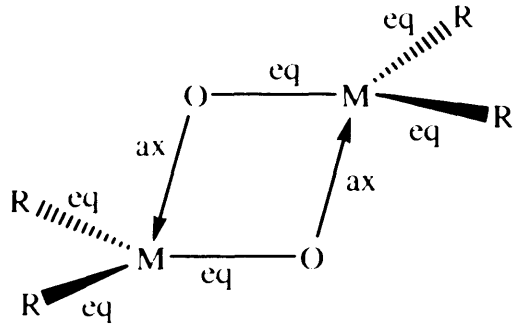

Figure 2.1: Representation of the formation of the M_2O_2 ring in the formation in mono(alkoxides).

2.1.1.1 Gallium

Dimethylgallium methoxide $[Me_2Ga(OMe)]_3$ was reported over 50 years ago.[3] This compound was prepared from the reaction of Me_3Ga and methanol, according to Eq. 2.4. A series of related complexes, $[Me_2Ga(OR')]_n$ (R' = CH_3, CD_3, C_2H_5), were subsequently reported and the IR and Raman spectra indicated that the methyl derivatives are trimeric with puckered six-membered M_3O_3 ring systems.[4] Other compounds also described include $[Me(Cl)GaOMe]_n$, $[Cl_2Ga(OMe)]_n$ and

$[Et_2Ga(OMe)]_n$. Similarly, the reaction of R_3Ga with one equivalent of ^tBuOH yielded the complex $[R_2Ga(O^tBu)]_2$ (R = CH_3, ^tBu).[5,6]

The related complexes $[Me_2Ga(OR)]_n$ were also prepared by the reaction of Me_3Ga with ROH to yield $[Me_2Ga(OR)]_n$ (R = ^tBu, ^nBu, Me, $PhCH_2$) and Et_3Ga with EtOH to give $[Et_2Ga(OEt)]_n$.[7-9] However, some of these compounds had been previously reported.[5,6] The reaction of Me_3Ga with CyOH has been reported recently, to yield the dimeric complex $[Me_2Ga(OCy)]_2$, Eq. 2.4, *via* evolution of methane.[10] The X-ray structure showed the compound to be dimeric, consisting of a planar Ga_2O_2 ring (Ga–O = 1.953(4) and 1.954(4) Å). However, the similar reaction of Me_3Ga with excess $PhCH_2OH$ resulted in the isolation of the sesquialkoxide $[Ga(MeGa(OCH_2Ph)_3)_3]$.[10] Other compounds of the type $[R_2GaOR]_2$ have also been reported and described in an extensive review recently published.[1]

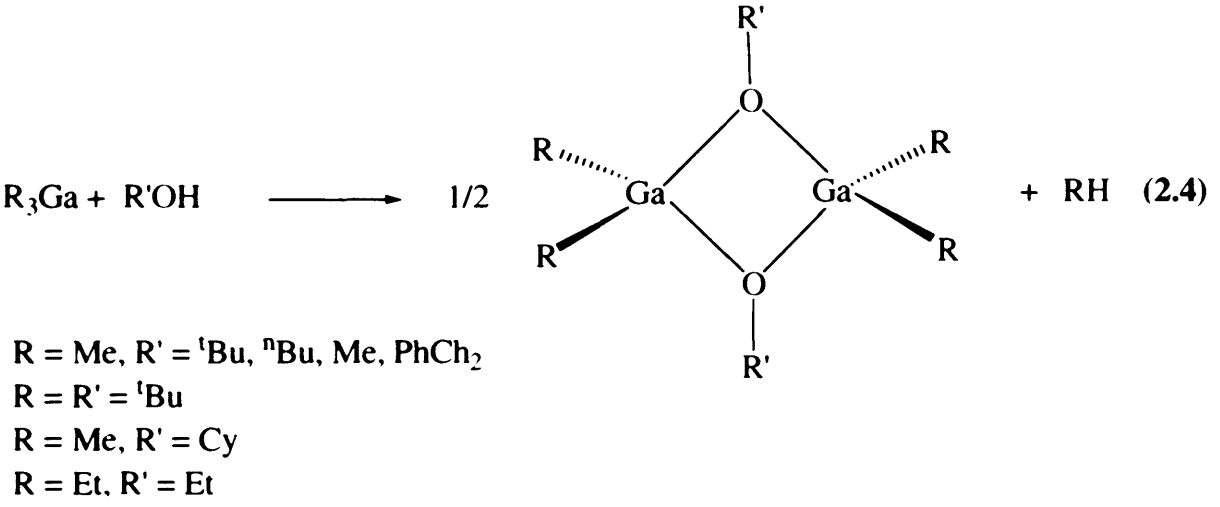

The first range of examples of gallium monoalkoxides incorporating donor functionalised alkoxides were reported in 1953.[11] However, the first complex to be crystallographically characterised was reported almost 20 years later by Rettig *et al.*[12] The reaction of Me_3Ga with one equivalent of $HOCH_2CH_2NMe_2$ afforded colourless crystals of $[Me_2Ga(OCH_2CH_2NMe_2)]_2$, as shown in Eq. 2.5.

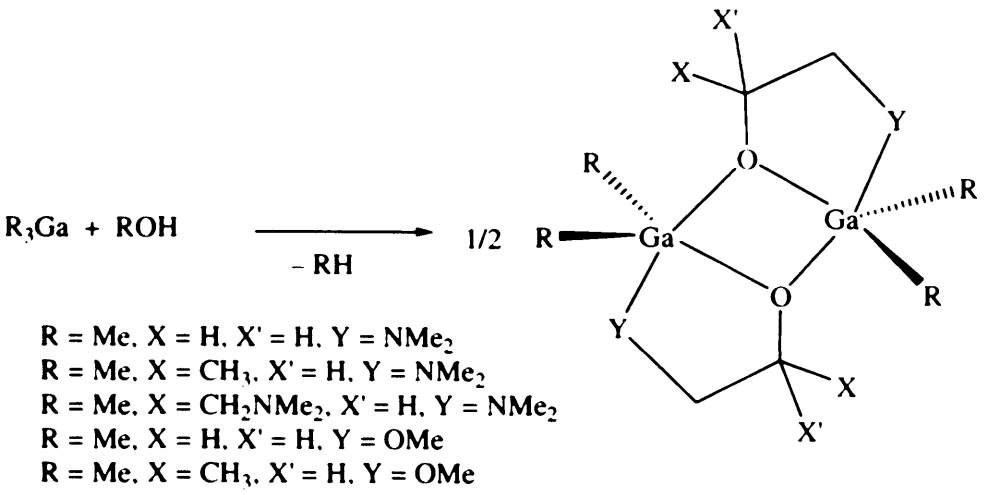

(2.5)

Treatment of $[GaH_3(NMe_3)]$ with $HOCH_2CH_2NMe_2$ yielded $[H_2Ga(OCH_2CH_2NMe_2)]_2$, according to Eq. 2.6.

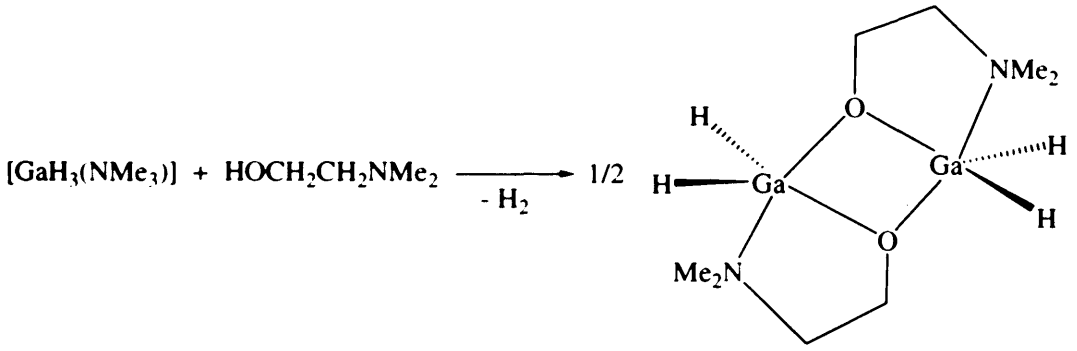

(2.6)

The crystal structures of $[Me_2Ga(OCH_2CH_2NMe_2)]_2$ and $[H_2Ga(OCH_2CH_2NMe_2)]_2$ were investigated by X-ray diffraction and showed dimers with the formation of four-membered Ga_2O_2 rings resulting in centrosymmetric molecules with three fused rings.[1] The gallium centres in both compounds adopt distorted trigonal bipyramidal coordination geometries with the nitrogen atoms occupying axial positions and the oxygen atoms occupying an equatorial site on one gallium and an axial position on the second gallium atom.[4,12] The two remaining equatorial positions are occupied by methyl groups in $[Me_2Ga(OCH_2CH_2NMe_2)]_2$ and hydrogen atoms in $[H_2Ga(OCH_2CH_2NMe_2)]_2$. The Ga_2O_2 rings in both compounds are planar with Ga–O (equatorial and axial) bond distances of 1.913(3) and 2.078(3) Å in $[Me_2Ga(OCH_2CH_2NMe_2)]_2$ and 1.911(3) and 2.053(3) Å in $[H_2Ga(OCH_2CH_2NMe_2)]_2$. X-ray crystallography revealed the structure of $[Me_2Ga(OCH(CH_3)CH_2NMe_2)]_2$ to

consist of a central four-membered ring Ga_2O_2 ring with Ga–O (equatorial and axial) bond distances of 1.919(2) and 2.097(2) Å similar to $[Me_2Ga(OCH_2CH_2NMe_2)]_2$.

The 1 : 1 reaction of Me_3Ga and 2,3-epoxy-1-propanol resulted in the formation of the dimeric species $[Me_2Ga(OCH_2CHCH_2O)]_2$, as shown in Eq. 2.7.[13] The ^1H NMR of the product indicated that the structure is similar to the aforementioned dialkyl gallium alkoxides derived from donor functionalised alcohols, for example, $[Me_2Ga(OCH_2CH_2NMe_2)]_2$.[12-16] Each gallium atom was found to be coordinated in a distorted trigonal bipyramidal manner by two methyl groups in axial, two alkoxide groups in axial and equatorial and the N atom of the aminoalkoxide group in equatorial position.[14]

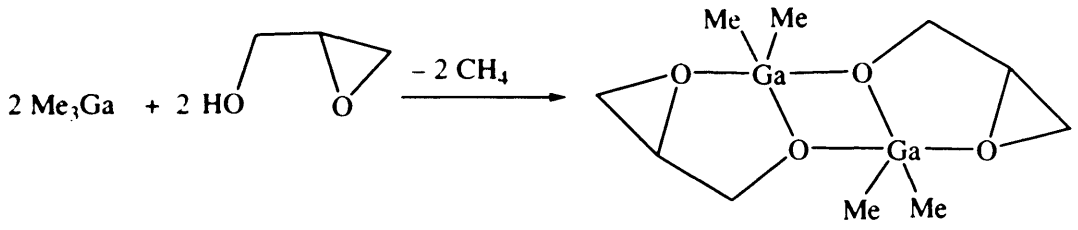

(2.7)

The tetranuclear adduct $[Me_2Ga(OCH_2CHCH_2O)GaMe_3]_2$, was formed from the reaction of two equivalents of Me_3Ga with 2,3-epoxy-1-propanol, as depicted in Scheme 2.1.

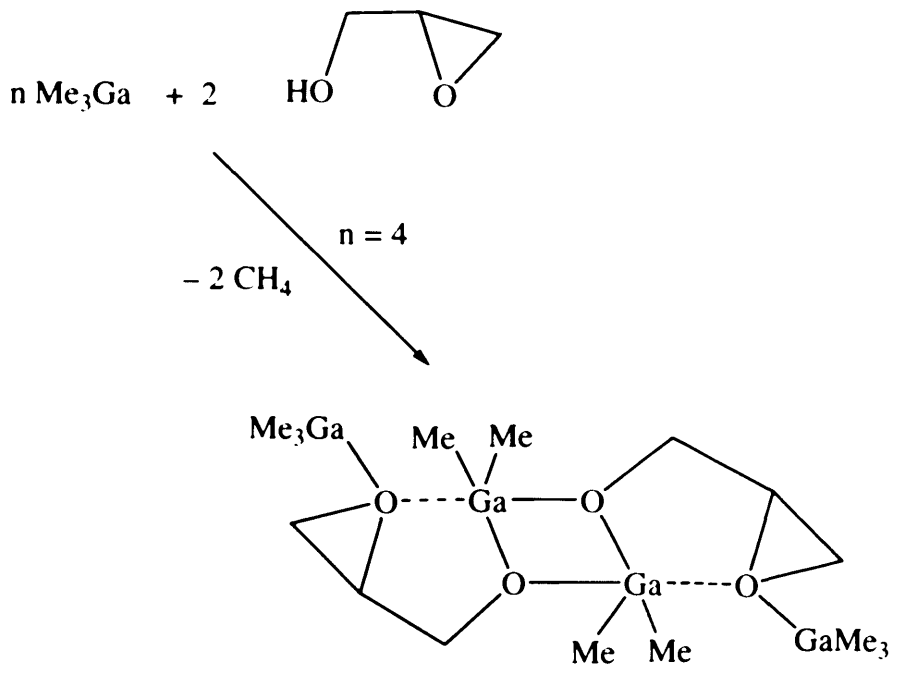

Scheme 2.1: Reaction of Me_3Ga and 2,3-epoxy-1-propanol

X-ray crystallography of $[Me_2Ga(OCH_2CH(CH_2O)GaMe_3]_2$ showed that the structure is dimeric, with the epoxide oxygen atoms double coordinate to different Lewis acid centres. The central Ga_2O_2 ring is planar with the epoxide oxygen atoms being in the same plane. The central gallium atoms adopt a distorted trigonal bipyramidal geometry with Ga–O bridging bond distances of 1.951(3) and 1.991(3) Å.[1]

The reaction of Me_3Ga with the related alcohols, 2-methoxybenzyl alcohol and *o*-methyoxyphenyl-1-ethanol afforded the dimeric complexes $[Me_2Ga(OCHRC_6H_4\text{-}2\text{-}OMe)]_2$ (R = H, Me) (Figure 2.2).[16,17] The dimeric nature of $[Me_2Ga(OCHRC_6H_4\text{-}2\text{-}OMe)]_2$ (R = Me) was confirmed by X-ray diffraction and revealed a planar Ga_2O_2 core. The Ga–O distances of 1.951(2) and 1.957(2) Å, are similar to those observed in other dimeric complexes, for example $[Me_2Ga(OCH_2CHCH_2O)GaMe_3]_2$.[18] Interestingly, the gallium atoms adopt tetrahedral coordination geometry, thus, the oxygen atoms of the methoxy substituents do not coordinate to the gallium centre. However, no structural data is available for $[Me_2Ga(OCHRC_6H_4\text{-}2\text{-}OMe)]_2$ (R = H).[16]

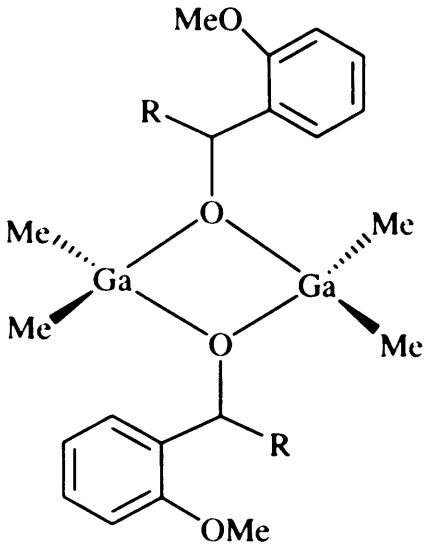

R = H, Me

Figure 2.2: Structure for $[Me_2Ga(OCHRC_6H_4\text{-}2\text{-}OMe)]_2$ (R = H, Me)

More recently treatment of Me_3Ga with fluorinated aminoalcohols resulted in the formation of the monomeric complexes $[Me_2Ga(OC(CF_3)_2CH_2NRR')]$ (R = H, R' = Me, R = H, R' = ^tBu, R = R' = Me) (Figure 2.3).[19] The structure of $[Me_2Ga(OC(CF_3)_2CH_2NRR')]$ (R = R' = Me) was determined by X-ray crystallography, which revealed that the gallium centre is four-coordinate and adopts a distorted tetrahedral environment with bond angles in the range 107.6–125.0°. The Ga–N bond distance of 2.082(2) Å is significantly shorter than the Ga–N bond length observed in related dimeric gallium complexes incorporating non-fluorinated aminoalkoxide ligands, such as $[Me_2Ga(OCH(CH_3)CH_2NMe_2)]_2$ (Ga–N 2.525(2) Å).[14] Thus, it appears that the coordinative unsaturation of the gallium atom is satisfied by the dative interaction with the nitrogen atom.[1] The presence of electron-withdrawing CF_3 groups on the aminoalkoxide, as well as steric repulsion, reduces the bridging capability of the oxygen atom and thus preventing dimer formation. The Ga–O bond distance of 1.890(2) Å is comparable to that observed in the monomeric compound $[Me_2Ga(OCPh(CH_2Ph)CH(CH_3)CH_2NMe_2)]$.[17]

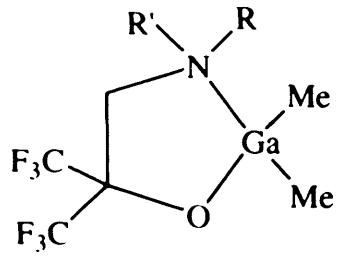

R = H, R' = Me
R = H, R' = ^{t}Bu
R = R' = Me

Figure 2.3: Structure for $[Me_2Ga(OC(CF_3)_2CH_2NRR')]$ (R = H, R' = Me, R = H, R' = ^{t}Bu, R = R' = Me)

The related compounds $[Me_2Ga(BINOL\text{-}R)]$ (R = Me, CH_2Ph, ^{t}Bu), Figure 2.4, were synthesised from the reaction of binapthol monoethers (*R*)-BINOL-Me, (*R*)-BINOLBz and (*R*)-BINOL-^{t}Bu with 1 equivalent of Me_3Ga.[20] Unfortunately, no structural data are available for these compounds, however they are thought to be monomeric based on mass spectral evidence.

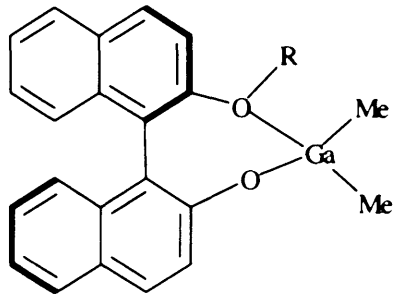

R = Me, Bz, ^{t}Bu

Figure 2.4: Structure of $[Me_2Ga(BINOL\text{-}R)]$ (R = Me, CH_2Ph, ^{t}Bu)

2.1.1.2 Indium

Early routes to dialkylindium mono(alkoxides) involved the reaction of Me_3In with ROH.[21,22] The compounds $[R_2In(OR')]_n$ (R = Me, R' = Me, CD_3, ^tBu, $SiMe_3$; R= Et, R' = Me, Et) were isolated and characterised.[21,23-27] The compounds $[^tBu_2In(OR)]_2$ (R= Et, Me) were also reported and prepared using different synthetic procedures.[80,81] Salt elimination was used for the preparation of the compound $[^tBu_2In(OR)]_2$ (R = Et) *via* the reaction of $[^tBu_2InCl]_2$ with two equivalents of Li(tmp) in diethyl ether, as shown in Scheme 2.2. It was assumed that lithium ethoxide was produced from the reaction of Li(tmp) with diethyl ether.[1]

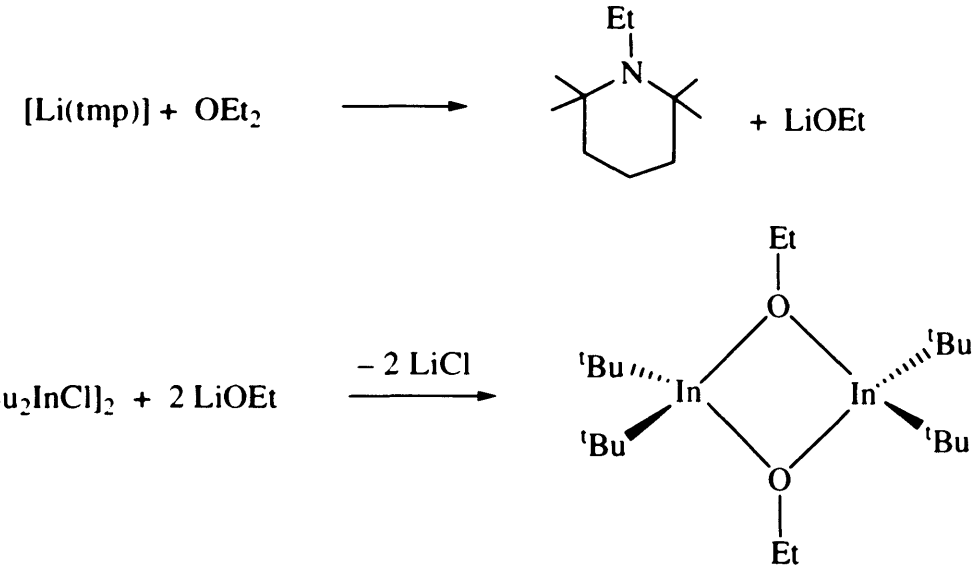

Scheme 2.2: Synthesis of compound $[^tBu_2In(OR)]_2$ (R = Et)

Dialkylindium alkoxides incorporating donor functionalised ligands have also been reported.[30,31] Reaction of R_3In with $HOCH_2CH_2NMe_2$ yielded the complex $[R_2In(OCH_2CH_2NMe_2)]_2$, (R = Me, Et). No structural data is available for $[R_2In(OCH_2CH_2NMe_2)]_2$, although these complexes are expected to be dimeric, according to Figure 2.5.

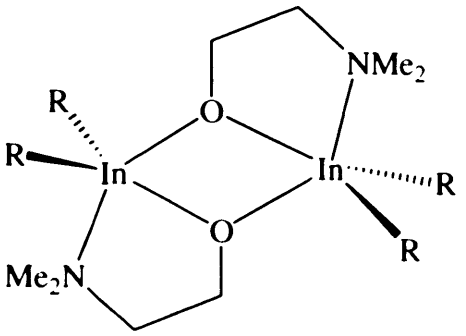

R = Me, Et

Figure 2.5: Proposed structure of $[R_2In(OCH_2CH_2NMe_2)]_2$, (R = Me, Et).

Similarly, reaction of R_3In with 8-hydroxyquinoline afforded the compounds $[R_2In(Oquin)]_2$, Figure 2.6 (R = Me, Et). Molecular weight determinations suggested that these compounds are also dimeric.

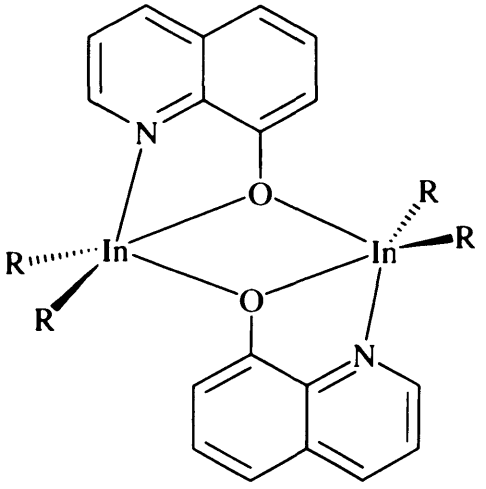

Figure 2.6: Proposed structure for $[R_2In(Oquin)]_2$ (R = Me, Et)

A series of dimethylindium aminoalkoxide complexes have been reported recently.[31] Reaction of Me_3In with $HOC(CF_3)_2CH_2NHR$ resulted in the formation of the dimeric complexes $[Me_2In(OC(CF_3)_2CH_2NHR)]_2$ (R = $(CH_2)_2OMe$, Me and ^tBu). In addition, the compound $[Me_2In(OC(CF_3)_2CH_2NMe_2)]_2$ was isolated from the reaction between Me_3In and $HOC(CF_3)_2CH_2NMe_2$. The existence of a dimeric In_2O_2 core structure in the solid state was confirmed with the amino group located *trans* to the

alkoxide ligands for these compounds. X-ray crystallography of $[Me_2In(OC(CF_3)_2CH_2NHR)]_2$ (R = $(CH_2)_2OMe$) revealed a centrosymmetric, four-membered nearly planar In_2O_2 ring.[32] The structure is similar to the related gallium complexes such that the bridging alkoxide groups are located in both equatorial and axial positions while the nitrogen atom of the aminoalkoxide group is in the other axial position.[19] The In–O equatorial bond length of 2.2034(8) Å is significantly shorter than the In–O axial distance of 2.3959(8) Å.

2.1.2 Bis(alkoxides)

Only a limited number of examples of monoalkyl gallium and indium bis(alkoxide) compounds have been reported in the literature. These are rare species, in contrast to the well-known diorganoalkoxometallanes of gallium and indium.[1] However, reaction of a gallane or indane with two equivalents or an excess of alcohol does not yield the expected gallium and indium bis(alkoxide) compounds, $[RM(OR')]_n$, in most cases. Instead reaction of Me_3M with an excess of alcohol often results in the formation of sesquialkoxides.[12]

The synthesis and characterisation of the few examples of gallium and indium bis(alkoxide) complexes reported in the literature are described in Sections 2.1.2.1 and 2.1.2.2.

2.1.2.1 Gallium

The only structurally characterised example of a gallium bis(alkoxide) incorporating a simple monodentate alkoxide group is $[HGa(O^tBu)_2]_2$.[34] This complex was synthesised by the 1 : 2 reaction of $[GaH_3(OEt_2)]$ and ^tBuOH in diethyl ether at 0 °C, followed by fractional sublimation or distillation under vacuum, as shown in Eq. 2.8.

$$[GaH_3(OEt_2)] + 2\,{}^tBuOH \xrightarrow[-\,Et_2O]{-\,2\,H_2} 1/2 \quad \text{(2.8)}$$

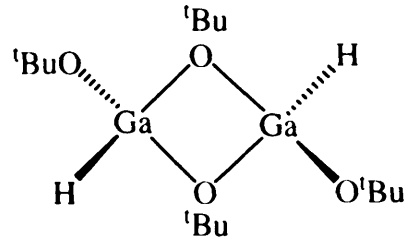

The structure of $[HGa(O^tBu)_2]$ was determined and was found to be dimeric with each gallium centre being four-coordinate and approximately tetrahedral (terminal

Ga–O 1.783(4) Å; *av.* bridging Ga–O 1.906(4) Å). The bridging oxygen atoms were found to be in a trigonal planar environment.

The alkane elimination reaction between Me_3Ga and one equivalent of the chelating ligand BINOL (2,2'-dihydroxy-1,1,-binaphthyl) led to the formation of a dimeric gallium bis(alkoxide), as shown in Scheme 2.3.[35]

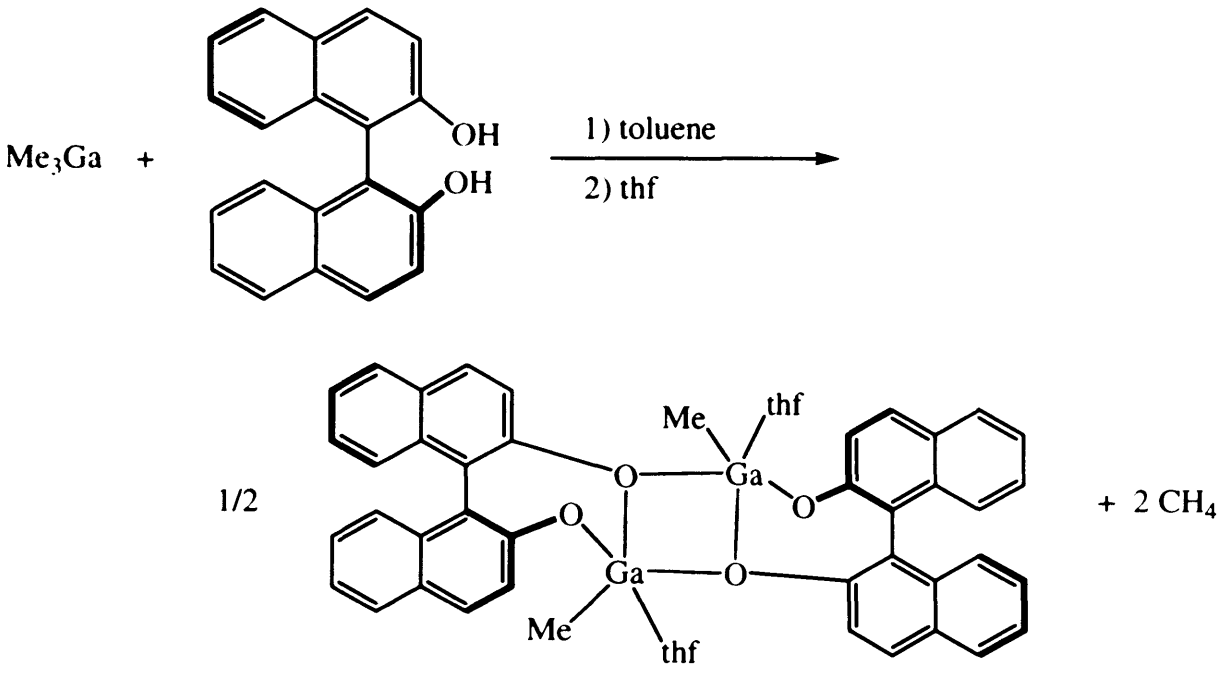

Scheme 2.3: Reaction of Me_3Ga and 2,2'-dihydroxy-1,1,-binaphthyl

The initial poorly soluble white solid was suggested to comprise of a coordination polymer of the type $[MeGa((S)\text{-BINOLate})]_n$.[1] The polymer was recrystallised from thf inorder to break the polymer chains to give the dimer $[(THF)MeGa((S)\text{-BINOLate})]_2$. The structure was found to be dimeric by X-ray crystallography each gallium centre adopting a distorted trigonal bipyramidal geometry with the thf and O atom of one BINOLate ligand in the axial positions and the Cl atom. two bridging O atoms from the BINOLate ligands in equatorial positions (bridging Ga–O 2.072(4) Å; terminal Ga–O (BINOLate) 1.834(6) Å).[1]

Recently, a monomeric gallium bis(alkoxide) incorporating donor functionalised ligand was prepared by the reaction of Et_3Ga with an excess of $HOCH_2CH_2NMe_2$ under reflux conditions.[4] Sublimation of the reaction mixture resulted in the isolation of a 1 : 1

mixture of $[Et_2Ga(OCH_2CH_2NMe_2)]_2$ and the gallium bis(alkoxide) $[EtGa(OCH_2CH_2NMe_2)_2]$, as shown in Eq. 2.9.

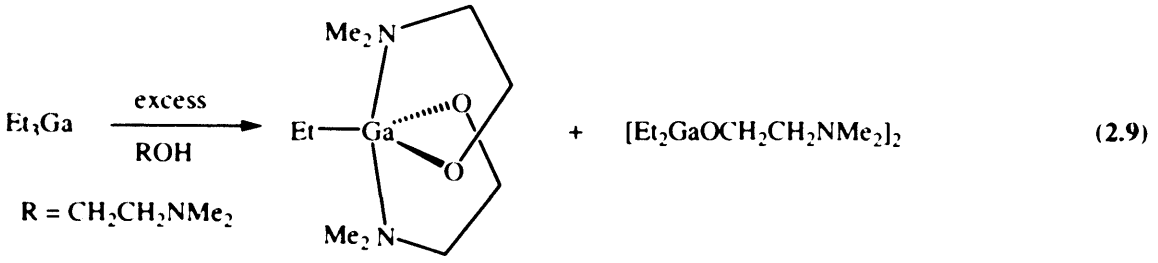

(2.9)

X-ray crystallography of $[EtGa(OCH_2CH_2NMe_2)_2]$ confirmed that the compound was monomeric and showed that the gallium centre adopts a trigonal bipyramidal geometry, with the oxygen atoms of each alkoxide and an ethyl ligand occupying the three equatorial positions and the N atoms of the NMe_2 group in the axial positions.[36] The Ga–O bond distances are (1.8522(13) and 1.8534(13) Å) and comparable to the terminal Ga–O(alkoxide) bond length in [(THF)MeGa((*S*)-BINOLate)]$_2$.

Other known examples of gallium bis(alkoxides) are the disubstituted compounds, of the type $[ClGa(OR)_2]$, prepared by the reaction of $GaCl_3$ with two equivalent of NaOR (Scheme 2.4), (R = $C(CF_3)_2CH_2NMe_2$, $C(CF_3)_2CH_2C(CH_3)NMe$).[19] The structures of these compounds are similar to that previously reported for compound $[EtGa(OCH_2CH_2NMe_2)_2]$,[36] and a trigonal bipyramidal geometry is adopted at the monomeric Ga centre. The chloride and alkoxy groups occupy the equatorial positions and the nitrogen donors are located in the axial sites. The Ga–O and Ga–N bond distances are similar to those observed in compound $[EtGa(OCH_2CH_2NMe_2)_2]$, although the Ga–N distances in $[ClGa(OC(CF_3)_2CH_2C(CH_3)NMe_2)_2]$ (2.087(2) and 2.092(2) Å) are shorter due to the formation of a stronger donor–acceptor bond for the imino N atom.

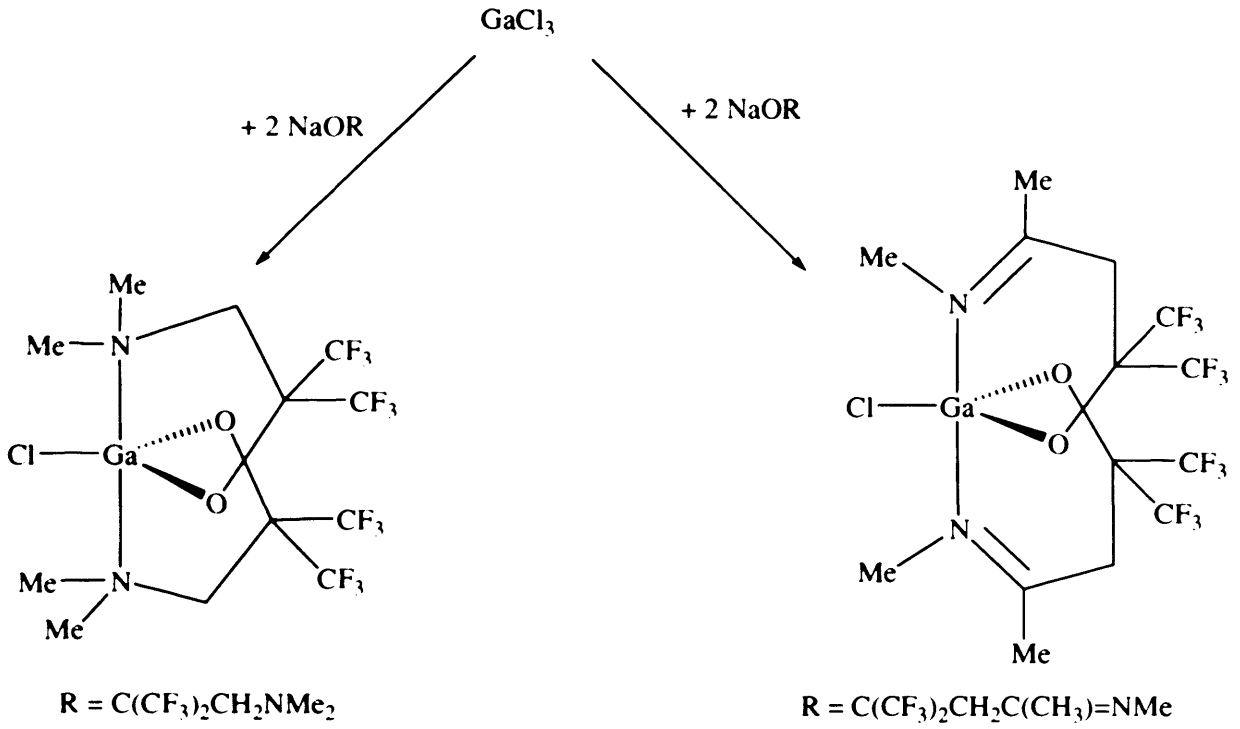

Scheme 2.4: Reaction of $GaCl_3$ and NaOR (R= $C(CF_3)_2CH_2NMe_2$, $C(CF_3)_2CH_2C(CH_3)$ NMe).

2.1.2.2 Indium

One of the only structurally characterised example of an indium bis(alkoxide) incorporating a monodentate alkoxide is $[MeIn(O^tBu)_2]_2$.[32] This compound was synthesised from amine/alcohol exchange reactions, as shown in Scheme 2.5. Initially, the amido complex $[Me(Cl)InN(SiMe_3)_2]_2$ was reacted with two equivalents of ^{t}BuOH to give the indium mono(alkoxide) $[Me(Cl)InO^tBu]_2$. Reaction of $LiN(SiMe_3)_2$ with $[Me(Cl)InO^tBu]_2$ followed by ligand exchange with ^{t}BuOH resulted in the formation of $[MeIn(O^tBu)_2]_2$

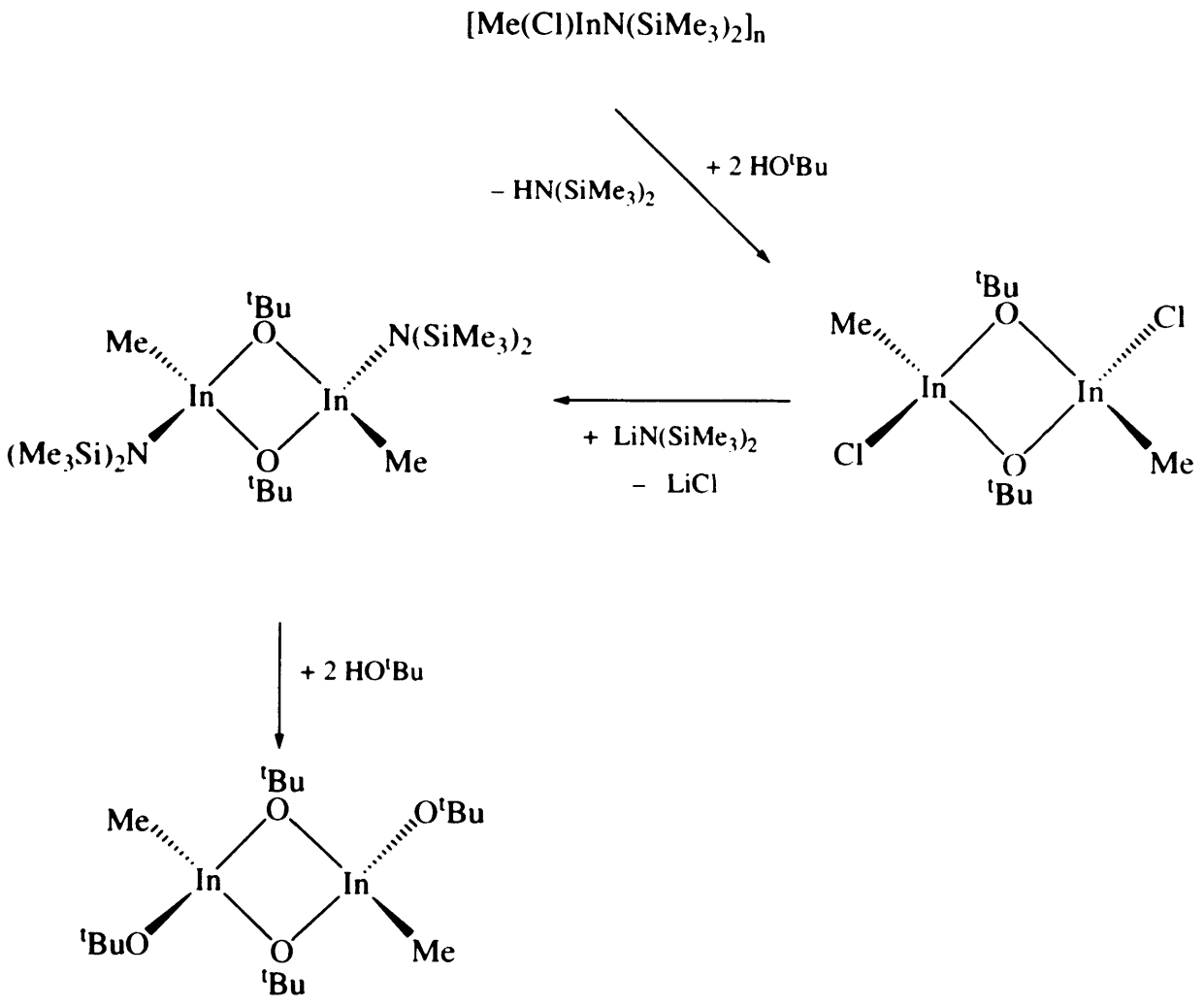

Scheme 2.5: Synthetic route for the formation of $[MeIn(O^tBu)_2]_2$.

The solid-state structure of $[MeIn(O^tBu)_2]_2$ comprises of a dimeric molecule with bridging alkoxide groups (In–O–In 103.6(2)°. O–In–O 76.4(2)°).[1] The indium centre adopts a distorted tetrahedral coordination geometry with the In–O bond lengths to the terminal oxygen atoms being 0.12 Å shorter than the bond lengths in the In_2O_2 ring (bridging In–O 2.128(8) Å; terminal In–O 2.006(4) Å).

An indium bis(alkoxide) incorporating a donor functionalised ligand has also been reported.[37] This was achieved by the reaction of $InCl_3$ with two equivalents of $Me_2NCH_2CH_2OLi$ giving the compound $[ClIn(OCH_2CH_2NMe_2)_2]$. No structural information was reported.

2.1.3 Tris(alkoxides)

A number of synthetic routes have been employed for the formation of homoleptic gallium and indium alkoxides $[M(OR)_3]_n$. The general procedures include reaction of the metal trihalide with NaOR, alkoxide/alcohol exchange, amine/alcohol exchange and transesterification reactions, as shown in Eqs. (2.10)–(2.13).[1]

$$MCl_3 + 3\,NaOR \longrightarrow [M(OR)_3] + 3\,NaCl \quad \textbf{(2.10)}$$

$$[M(OR)_3] + 3\,R'OH \longrightarrow [M(OR')_3] + 3\,ROH \quad \textbf{(2.11)}$$

$$[M(OR)_3] + 3\,MeCO_2R' \longrightarrow [M(OR')_3] + 3\,MeCO_2R \quad \textbf{(2.12)}$$

$$[M(NR_2)_3] + 3\,R'OH \longrightarrow [M(OR')_3] + 3\,R_2NH \quad \textbf{(2.13)}$$

2.1.3.1 Gallium (III)

One of the earliest reported attempts of the synthesis of homoleptic gallium alkoxide compounds $[Ga(OR)_3]_n$ (R = alkyl) were by Mehrotra and Mehrotra[38] and Funk and Paul.[39] The report detailed the reaction of $GaCl_3$ with 3 equivalents of NaOR, (R = Et, ^{i}Pr) which resulted in the formation of gallium tris(ethoxide) and gallium tris(isopropoxide), respectively, as summarised in Eq. 2.14.

$$GaCl_3 + 3\,NaOR \longrightarrow [Ga(OR)_3] + 3\,NaCl \quad \textbf{(2.14)}$$
$$R = Et, {}^iPr$$

Routes towards the synthesis of homoleptic gallium alkoxides have been widely studied and prepared *via* an alkoxide/alcohol exchange reaction. Gallium tris(isopropoxide) has been prepared from the reaction of $[Ga(OEt)_3]$ and three equivalents of ^{i}PrOH, according to Eq 2.15.[40] In the same year, Funk and co-workers reported the synthesis of $[Ga(OMe)_3]$ and $[Ga(OEt)_3]$ *via* exchange of the appropriate alcohol with $[Ga(OPh)_3]$.[41] A series of gallium alkoxides were also reported by Mehrotra and co-workers from the alcohol exchange reactions of $[Ga(O^iPr)_3]$ with ROH (Eq. 2.15).[42]

$$[Ga(OR)_3] + 3\,R'OH \longrightarrow [Ga(OR')_3] + 3\,ROH \qquad \textbf{(2.15)}$$

R = ^{i}Pr, R' = Me, Et, ^{n}Pr, ^{n}Bu, ^{t}Bu
R = Et, R' = ^{i}Pr
R = Ph, R' = Me, Et

This series of compounds provided the first information regarding possible structures of the gallium tris(alkoxide) complexes.[1] The gallium ethoxide, propoxide and butoxide derivatives were proposed to be tetramers based on ebullioscopic molecular weight determinations. In contrast, the isopropoxide and t-butoxide complexes were determined to be dimeric with the proposed structure $[Ga(\mu\text{-}OR)(OR)_2]_2$. The dimer formulation for $[Ga(O^tBu)_3]_2$ was established using ^{1}H NMR spectroscopy.[43] Oliver and Worrall also demonstrated that $[Ga(O^iPr)_3]$ existed in solution as an equilibrium mixture of tetramer and dimer, as shown Eq. 2.16.[44,45] Furthermore, phase studies showed that gallium isopropoxide reacts with pyridine to form the 1 : 1 adduct $[Ga(O^iPr)_3(py)]$, as characterised by ^{1}H NMR and molecular weight studies.[46]

$$\underset{\text{tetramer}}{[Ga[(\mu\text{-}O^iPr)_2Ga(O^iPr)_2]_3]} \rightleftharpoons \underset{\text{dimer}}{2\,[Ga(\mu\text{-}O^iPr)(O^iPr)_2]_2} \qquad \textbf{(2.16)}$$

Recently, the reaction of $[Ga(NMe_2)_3]_2$ with ^{i}BuOH and ^{i}PrOH resulted in the formation of the tetramers $Ga[(\mu\text{-}OR)_2Ga(OR)_2]_3$, where R = ^{i}Bu and ^{i}Pr, respectively via amide/alcohol exchange.[47] The homoleptic gallium alkoxides were the only products formed, as shown by the ^{1}H NMR spectra. X-ray crystallography confirmed that the structure $Ga[(\mu\text{-}O^iPr)_2Ga(O^iPr)_2]_3$ was tetrameric. This compound was found to consist of a six-coordinate central Ga atom surrounded by three four coordinate Ga atoms (Scheme 2.6). The structure was found to be similar to the related tetramers $Al[(\mu\text{-}O^iPr)_2Al(O^iPr)_2]_3$[48] and $In[(\mu\text{-}OCHEt_2)_2In(OCHEt_2)_2]_3$.[49]

The reaction of $[Ga(NMe_2)_3]_2$ with 6 equivalents of ^{t}BuOH or $EtMe_2COH$ gave mixtures of $[Ga(\mu\text{-}OR)(OR)_2]_2$ (R = ^{t}Bu and CMe_2Et) and the amine adduct $[Ga(OR)_3(HNMe_2)]$ (R = ^{t}Bu and CMe_2Et) in 1 : 2 to 1 : 4 ratios, as shown in Scheme 2.6. However, similar reactions involving $^iPrMe_2COH$ and Et_2MeCOH formed $[Ga(OR)_3(HNMe_2)]$ (R = $CMe_2{}^iPr$ and $CMeEt_2$) and no dimer formation was detected by ^{1}H NMR spectroscopy. The X-ray structure of $[Ga(\mu\text{-}OCMe_2Et)(OCMe_2Et)_2]_2$

confirmed the complex to be dimeric. This compound consists of an edge shared tetrahedron structure[1] common to dimeric group 13 alkoxide complexes.

Homoleptic gallium alkoxide dimers, of the type $[Ga(\mu\text{-}OR)(OR)_2]_2$ (R = ^{t}Bu, CMe_2Et, $CMe_2{}^iPr$, $CMeEt_2$), have also been isolated by heating the mixtures formed from the reaction of $[Ga(NMe_2)_3]_2$ and ROH or $[Ga(OR)_3(HNMe_2)]$ under dynamic vacuum (R = ^{t}Bu or CMe_2Et) or refluxing toluene solutions (R = CMe_2, ^{i}Pr or $CMeEt_2$). It was found that moderate heating of the solid (50 °C for 2–3 h) was required for sterically smaller R groups (^{t}Bu or CMe_2Et) whereas prolonged heating (toluene reflux for >2 days) was necessary when R was larger ($CMe_2{}^iPr$ or $CMeEt_2$). Hence, sterically demanding R groups favour retention of the amine ligand. An X-ray crystallographic study showed that $[Ga(O^tBu)_3(HNMe_2)]$ consists of a four-coordinate Ga centre with a distorted tetrahedral geometry.

Gallium alkoxides incorporating fluoroalkoxide groups, of the type $[Ga(OR)_3(HNMe_2)]$ (R = $CH(CF_3)_2$, $CMe_2(CF_3)$, $CMe(CF_3)_2$) have also been prepared from the reaction of $[Ga(NMe_2)_3]_2$ and six equivalents of ROH (Scheme 2.6).[50]

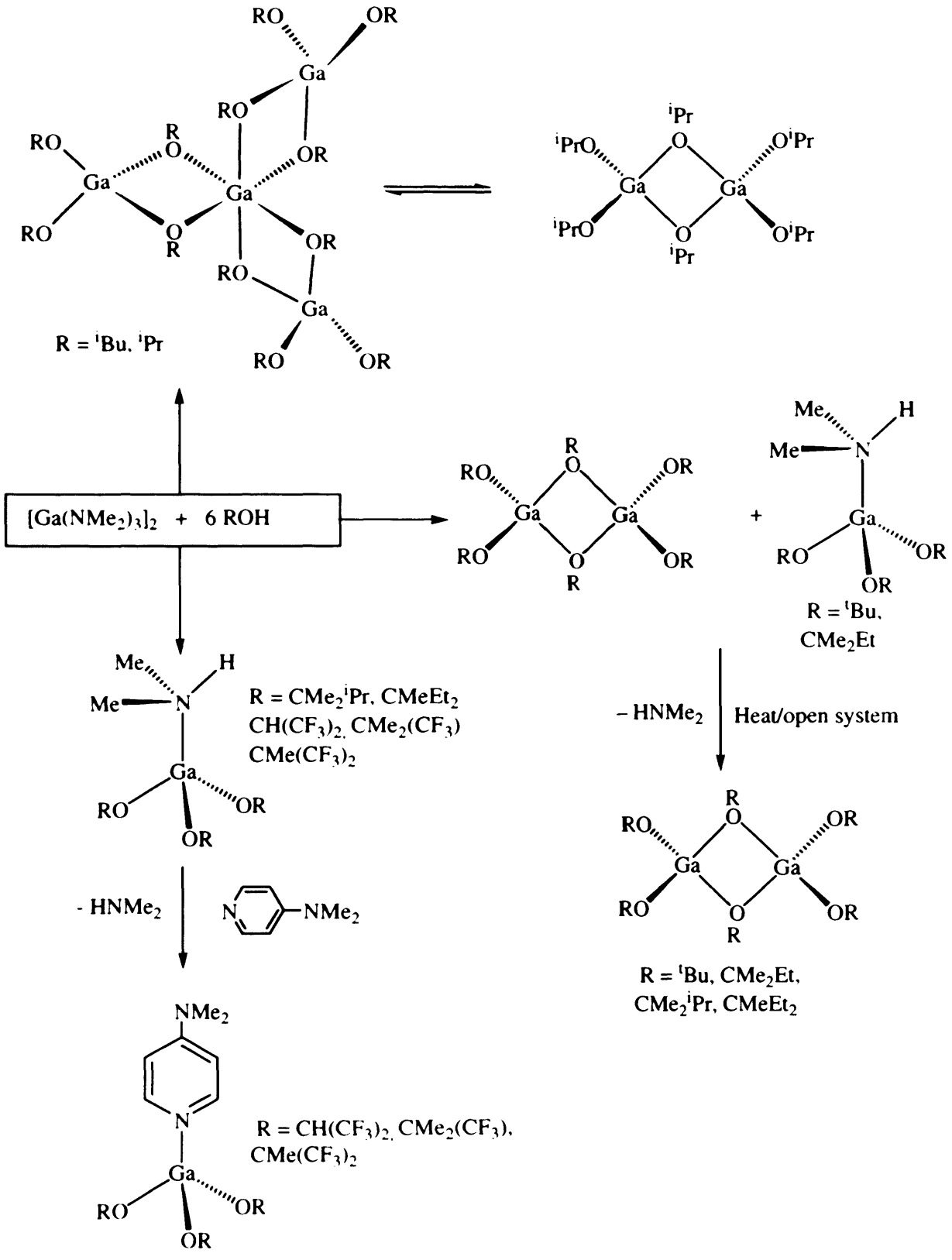

Scheme 2.6: Reaction of $[Ga(NMe_2)_3]_2$ and ROH.

The reaction of $[Ga(OR)_3(HNMe_2)]$ with 4-dimethylaminopyridine resulted in the formation of $[Ga(OR)_3(4\text{-}Me_2Npy)]$ (R = $CH(CF_3)_2$, $CMe_2(CF_3)$ and $CMe(CF_3)_2$), as shown in Scheme 2.6. X-ray analysis showed that the compounds $[Ga(OR)_3(4\text{-}Me_2Npy)]$ ((R = $CH(CF_3)_2$ or $CMe_2(CF_3)$) adopt a distorted tetrahedral geometry at the central Ga atom.

Other gallium alkoxides of type $[Ga(\mu\text{-}OR)(OR)_2]_2$ (R = $CH_2CH_2NMe_2$,CH_2CH_2OMe) were isolated from the reaction of either $[Ga(N(SiMe_3)_2)_3]$ or $[Ga(NEt_2)_3]_2$ with ROH. As expected, the sterically encumbered gallium amide, $[Ga(N(SiMe_3)_2)_3]$, was found to be less reactive than $[Ga(NEt_2)_3]_2$, thus the reaction required refluxing in toluene for 6 h, Eq. 2.17.[36] No structural information is available for these compounds, which were characterised by ^1H NMR.

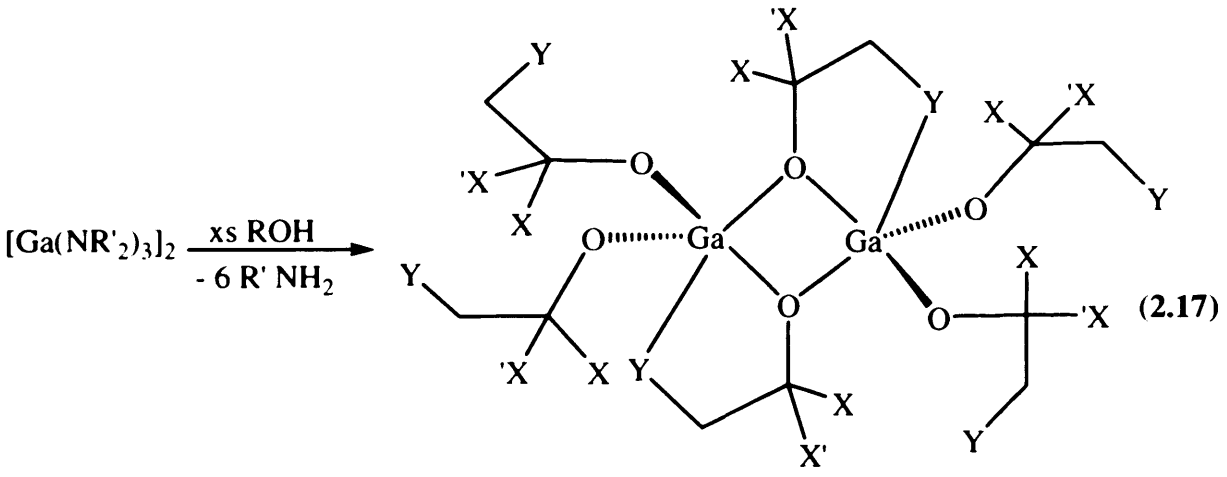

(2.17)

R' = Et or $SiMe_3$, X = H, X' = H, Y = NMe_2
R' = Et, or $SiMe_3$, X = H, X' = H, Y = OMe

2.2 Results and Discussion

2.2.1 Methods used

Three different routes were attempted towards the synthesis of gallium and indium alkoxides incorporating donor functionalised ligands. The use of gallium amides (route 1) for the synthesis of the corresponding alkoxide was prompted by the earlier successes of this route, as shown in Scheme 2.6. This method was investigated in an attempt to isolate gallium tris(alkoxides) incorporating donor functionalised ligands. The aim was to develop volatile precursors, which are less sensitive to air and moisture due to the stabilisation of the metal centre. In addition, compounds of the type $[Ga(OR)_3]_2$, possess a 1 : 3 ratio of Ga : O and should therefore serve as precursors to Ga_2O_3 (ratio 1 : 1.5 Ga : O).

$$[Ga(NMe_2)_3]_2 + x\,ROH \longrightarrow [Ga(OR)_3]_2 + x\,Me_2NH \quad \textbf{Route 1}$$

Route 2 involved the reaction of R_3M (R = Et, M = Ga; R = Me, M = In) with alcohols in a 1 : 1 ratio. The methodology in route 2 should result in the formation of dialkyl gallium or indium mono(alkoxides). These complexes should serve as precursors to gallium or indium oxide thin films and α- or β-hydrogen elimination should minimise carbon contamination in the resulting films. Donor functionalised ligands were chosen again to increase the volatility of the complexes for LPCVD and solubility for AACVD.

$$R_3M + R'OH \longrightarrow [R_2MOR]_2 + RH \quad \textbf{Route 2}$$

The related reaction shown in route 3 was attempted in order to isolate gallium or indium bis(alkoxides). It was hoped that due to the presence of excess alcohol and the high temperatures employed that the novel bis(alkoxides) would be isolated. Previous attempts to prepare gallium bis(alkoxides) using simple monofunctional alcohols have failed and generally result in the formation of gallium mono(alkoxides) or sesquialkoxides (section 2.1). Therefore, once again donor functionalised alcohols were chosen in an attempt to stabilise and isolate bis(alkoxides). Gallium and indium bis(alkoxides) as well as being novel compounds are expected to be superior precursors

to the respective metal oxide. The M : O ratio in the bis(alkoxides) are 1 : 2 rather than 1 : 1 in the mono(alkoxides). A ratio of 1 : 1.5 is required for the resulting M_2O_3 material and therefore the mono(alkoxides) could lead to oxygen deficient films. Furthermore, the bis(alkoxides) incorporating donor functionalised ligands are expected to be monomeric and hence more volatile.

$$R_3M + xs\ R'OH \longrightarrow [RM(OR)_2] + RH \qquad \textbf{Route 3}$$

2.2.2 Reaction of $GaCl_3$ and $LiNMe_2$

Treatment of $GaCl_3$ with 3 equivalents of $LiNMe_2$ resulted in a colourless solution, which upon solvent removal afforded a white crystalline solid (**1**) in a 62% yield. The ^1H and ^{13}C NMR spectra were consistent with the formation of the dimeric complex $[Ga(NMe_2)_3]_2$ **1**. The ^1H NMR spectum of **1** showed resonances at δ 2.69 (integrated to 12 bridging NMe_2 protons) and δ 2.68 (integrated to 24 terminal NMe_2 protons). ^{13}C NMR spectrum of **1** showed resonances at δ 42.9 (terminal NMe_2 carbon) and δ 43.2 (bridging NMe_2 carbon). The proposed composition is in accord with the elemental analysis data (%C, %H and %N).

2.2.3 Synthesis of gallium tris(alkoxides)

2.2.4 Reaction of $[Ga(NMe_2)_3]_2$ and $HOCH_2CH_2NMe_2$

Treatment of $[Ga(NMe_2)_3]_2$ with an excess of $HOCH_2CH_2NMe_2$ in toluene under reflux conditions resulted in a colourless solution which, upon solvent removal afforded a pale viscous oil (62% yield). Spectroscopic data for the oil suggested that the major product formed is $[Ga(OCH_2CH_2NMe_2)_3]_2$ (**2**) with a small amount of $[Ga(OCH_2CH_2NMe_2)_2Cl]$ (**3**), formed as a side product, as shown in Eq. 2.18.

$$[Ga(NMe_2)_3]_2 + 6\,HOCH_2CH_2NMe_2 \xrightarrow[-\,6\,Me_2NH]{} \underset{\textbf{(2)}}{[Ga(OCH_2CH_2NMe_2)_3]_2} + \underset{\textbf{(3)}}{[Ga(OCH_2CH_2NMe_2)_2Cl]} \quad \textbf{(2.18)}$$

The formation of **3** must result from the incomplete substitution of all chloride ligands in the preparation of compound **1**. Incomplete substitution would lead to a mixed chloro/amido complex $[Ga(NMe_2)_2Cl]$, which on reaction with $HOCH_2CH_2NMe_2$ would yield **3**, as shown in Eq. 2.19.

$$[Ga(NMe_2)_2Cl] + 2\,HOCH_2CH_2NMe_2 \xrightarrow[-2\,Me_2NH]{} [Ga(OCH_2CH_2NMe_2)_2Cl] \quad \textbf{(2.19)}$$

The mass spectrum of the product was obtained as a solution in toluene. A molecular ion peak at *m/z* = 281 was observed for $[Ga(OCH_2CH_2NMe_2)_2Cl]$ and additional fragmentation peaks (e.g. 194 [M]–$OCH_2CH_2NMe_2$). A molecular ion was not observed for the dimer $[Ga(OCH_2CH_2NMe_2)_3]_2$, although previous studies have shown that this compound is dimeric.[36] However peaks were observed at *m/z* = 474 and 405, which could arise from fragmentation of the dimeric structure. A peak at *m/z* = 334 for the monomer $[Ga(OCH_2CH_2NMe_2)_3]$ was observed along with fragmentation peaks (245, 194 and 158). The ^1H NMR spectrum of the mixture showed only one set of resonances attributable to the three proton environments of the alkoxide ligand. Thus, the ^1H NMR spectrum revealed resonances at δ 2.00 (CH_2, integrated to 6 protons), δ 2.27 (NMe_2, integrated to 12 protons) and δ 3.93 (CH_2, integrated to 6 protons) attributable to the three proton environments of the alkoxide ligand. These results suggest that only one of the compounds is present or that the resonances for both **2** and **3** occur at the same ppm. It is likely that compound **3** is a minor product and so not detected by ^1H NMR spectroscopy. FT-IR absorptions were observed at 623 and 561 cm^{-1} attributable to characteristic Ga_2O_2 ring modes, as would be expected for dimeric $[Ga(OCH_2CH_2NMe_2)_3]_2$. On standing at room temperature for 24h, a small yield of colourless crystals were obtained from the oil. An X-ray crystallographic study (section 2.2.5) was carried out on the colourless crystals and showed that the crystals were monomeric $[Ga(OCH_2CH_2NMe_2)_2Cl]$ **3**. As discussed above, the analytical and spectroscopic data for **1** showed a good agreement for the formation of $[Ga(NMe_2)_3]_2$

rather than [Ga(NMe$_2$)$_2$Cl]. Therefore, compound **3** is thought to be a minor product (hence the NMR spectrum of the mixture showing only one set of resonances for the alkoxide ligands) with the major product being the gallium tris(alkoxide), [Ga(OCH$_2$CH$_2$NMe$_2$)$_3$]$_2$ (**2**). Unfortunately X-ray quality crystals of **2** could not be obtained.

2.2.5 X-ray data of [Ga(OCH$_2$CH$_2$NMe$_2$)$_2$Cl] (3)

The crystal structure of compound **3** was determined by X-ray crystallography and the results are shown in Figure 2.7; selected bond lengths and angles are given in Table 2.1. Compound **3** crystallised into the Orthorhombic, *Pna*2$_1$ space group. As shown in Figure 2.7, the gallium atom adopts a distorted trigonal bipyramidal geometry, with the oxygen atoms of each alkoxide ligand and a chlorine atom occupying the equatorial positions. The N atoms of the NMe$_2$ group reside in the axial positions. However, the mutually *trans* N-functionalities of the alkoxide ligand provide stability at gallium *via* the donation of electron density into the same vacant Ga p-orbital (Figure 2.7). The Ga–N distances (*av.* 2.131 Å) are significantly shorter than the sum of the van der Waals radii and so indicative of a strong dative bonding interaction. Similar trigonal bipryamidal geometry at the gallium centre has been noted in the related intramoleculary stabilised gallium monoalkoxide complexes of the type [ClGa(OR)$_2$] (R = C(CF$_3$)$_2$CH$_2$NMe$_2$ and C(CF$_3$)$_2$CH$_2$C(CH$_3$)=NMe).[19] The Ga–O and Ga–N bond distances in these compounds are similar to those observed in **3**. Although compound **3** was obtained as a side product it is of interest due to the lack of gallium bis(alkoxides) in the literature. The direct reaction between ClGa(NMe$_2$) and two equivalents of HOCH$_2$CH$_2$NMe$_2$ was attempted and ^{1}H NMR studies showed that compound **3** could be prepared by this route.

Table 2.1: Selected bond lengths (Å) and angles (°) for $[Ga(OCH_2CH_2NMe_2)_2Cl]$ **(3)**

Ga1–O1	1.841(2)	Ga1–N1	2.161(3)
Ga1–O2	1.842(3)	Ga1–N2	2.118(3)
Ga1–Cl1	2.2433(8)		
O1–Ga1–O2	135.08(13)	O2–Ga1–N2	84.89(12)
O1–Ga1–N2	91.27(11)	O1–Ga1–Cl1	114.18(9)
O1–Ga1–N1	83.45(11)	O2–Ga1–N1	89.37(12)
O2–Ga1–Cl1	110.70(10)	N2–Ga1–N1	165.55(11)

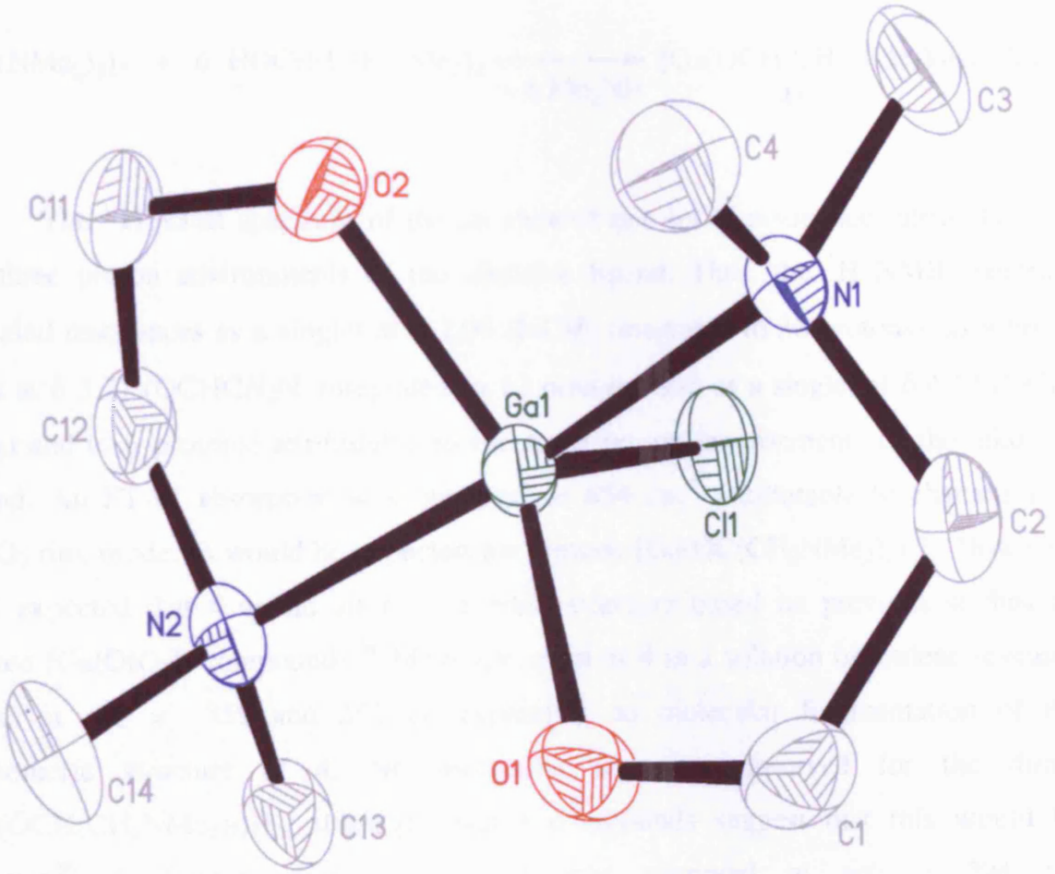

Figure 2.7: X-ray structure of $[Ga(OCH_2CH_2NMe_2)_2Cl]$ **(3)**

2.2.6 Reaction of $[Ga(NMe_2)_3]_2$ and $HOCH(CH_2NMe_2)_2$

The reaction of $[Ga(NMe_2)_3]_2$ with an excess of $HOCH(CH_2NMe_2)_2$ in toluene under reflux conditions resulted in a pale yellow solution, which upon solvent removal afforded a yellow viscous oil. Spectroscopic data indicated that the product $[Ga(OCH(CH_2NMe_2)_2)_3]$ (**4**) had formed, as shown in Eq. 2.20.

$$[Ga(NMe_2)_3]_2 + 6\ HOCH(CH_2NMe_2)_2 \xrightarrow[-\ 6\ Me_2NH]{} \underset{(4)}{[Ga(OCH(CH_2NMe_2)_2)_3]_2} \quad (2.20)$$

The ^{1}H NMR spectrum of the oil showed one set of resonances attributable to the three proton environments of the alkoxide ligand. Thus, the ^{1}H NMR spectrum revealed resonances as a singlet at δ 2.09 (NCH_3, integrated to 36 protons), as a broad peak at δ 3.77 ($OCHCH_2N$, integrated to 12 protons) and as a singlet at δ 4.12 (OCH, integrated to 6 protons) attributable to the three proton environments of the alkoxide ligand. An FT-IR absorption was observed at 654 cm^{-1} attributable to characteristic Ga_2O_2 ring mode, as would be expected for dimeric $[Ga(OC(CH_2NMe_2)_2)_3]_2$. However, it is expected that **4** would adopt a dimeric structure based on previous studies on related $[Ga(OR)_3]_2$ compounds.[36] Mass spectrum of **4** in a solution of toulene revealed peaks at *m/z* = 359 and 251 corresponding to molecular fragmentation of the monomeric structure of **4**. No molecular ion was observed for the dimer $[Ga(OCH(CH_2NMe_2)_2)_3]_2$, although related compounds suggest that this would be dimeric.[36] A further strong ion peak was observed at *m/z* = 394 for $[Ga(OCH(CH_2NMe_2)_2Cl]$ suggesting, that as with compounds **2** and **3**, a gallium bis(alkoxide) was formed as a side product due to incomplete substitution.

2.2.7 Reaction of $[Ga(NMe_2)_3]_2$ and $HOCH(CH_3)CH_2NMe_2$

Reaction of $[Ga(NMe_2)_3]_2$ with six equivalents of $HOCH(CH_3)CH_2NMe_2$ in toluene under reflux conditions resulted in a pale brown solution which, upon solvent removal afforded a pale yellow viscous oil (55% yield). Spectroscopic data for the oil suggested that the major product formed is $[Ga(OCH(CH_3)CH_2NMe_2)_3]_2$ (**5**) with a small amount of $[Ga(OCH(CH_3)CH_2NMe_2)_2Cl]_2$ (**6**), formed as a side product, as shown in Eq. 2.21.

$$[Ga(NMe_2)_3]_2 + 6\ HOCH(CH_3)CH_2NMe_2 \xrightarrow[-6\ Me_2NH]{} \underset{\textbf{(5)}}{[Ga(OCH(CH_3)CH_2NMe_2)_3]_2} + \underset{\textbf{(6)}}{[Ga(OCH(CH_3)CH_2NMe_2)_2Cl]} \quad \textbf{(2.21)}$$

Again, the formation of **6**, as with **3** must be due to the incomplete substitution of all chloride ligands in the preparation of **1**. Incomplete substitution would lead to a mixed chloro/amido complex $[Ga(NMe_2)_2Cl]$, which on reaction with $HOCH(CH_3)CH_2NMe_2$ would yield **6**, as shown in Eq. 2.22.

$$[Ga(NMe_2)_2Cl] + 2\ HOCH(CH_3)CH_2NMe_2 \xrightarrow[-\ 2\ Me_2NH]{} \underset{\textbf{(6)}}{[Ga(OCH(CH_3)CH_2NMe_2)_2Cl]} \quad \textbf{(2.22)}$$

The ^1H NMR spectrum of the mixture showed only one set of resonances attributable to the four proton environments of the alkoxide ligand, as previously observed for **2**. The ^1H NMR spectrum showed a doublet at δ 1.09 (18 protons, $OCH(CH_3)$), a broad peak at δ 2.21–2.11 (12 protons, $OCHCH_2N$), another broad peak at δ 2.31 (36 protons, NCH_3), and a multiplet at δ 3.86 (6 protons, $OCH(CH_3)CH_2$). These results suggest that one of the compounds is present as a major product or the peaks for the two compounds overlap. The Infra-red spectrum showed absorptions at 539, 496 and 579 cm^{-1} attributable to Ga_2O_2 ring modes of **5**. In the mass spectrum obtained from a solution of the product in toluene, a small ion peak at m/z = 309 is observed corresponding to the monomeric structure of **6**. No molecular ion was observed for the dimer **5**, although previous studies on related compounds suggest that it would be dimeric.[36] However, intense peaks (m/z = 273 and 102) corresponding to molecular fragmentation of the monomeric structure of **5** are observed.

On standing at room temperature for 24h, a small yield of colourless crystals were obtained from the oil. An X-ray crystallographic study (section 2.2.8) was carried out on the colourless crystals and showed that $[Ga(OCH(CH_3)CH_2NMe_2)_2Cl]$ **(6)** had formed.

2.2.8 X-ray data of $[Ga(OCH(CH_3)CH_2NMe_2)_2Cl]$ (6)

The X-ray structure of compound **6** was determined by X-ray crystallography, the results are shown in Figure 2.8; selected bond lengths and angles are given in Table

2.2. Compound **6** crystallised into the triclinic space group, $P\bar{1}$. As shown in Figure 2.8, the gallium atom adopts a distorted trigonal bipyramidal geometry as observed for **3**. The oxygen atoms of each alkoxide and a chlorine atom occupying the three equatorial positions and the N atoms of the NMe_2 group the axial positions. The mutually *trans* N-functionalities of the alkoxide ligand provide stability at gallium *via* the donation of electron density into the same vacant Ga p-orbital. The Ga–N distances (*av.* 2.161 Å) are significantly shorter than the sum of the van der Waals radii and so indicative of a strong dative bonding interaction.

Similar trigonal bipryamidal geometry at the gallium centre has been noted in the closely related intramoleculary stabilised gallium monoalkoxide complexes of the type $[ClGa(OR)_2]$ (R = $C(CF_3)_2CH_2NMe_2$ and $C(CF_3)_2CH_2C(CH_3)=NMe$).[19] The Ga–O and Ga–N bond distances in these compounds are similar to those observed in **3**. The Ga–O bond distances in **6** (Ga(1)–O(1) 1.8381(16) Å; Ga(1)–O(2) 1.8386(16) Å) are also comparable to the Ga–O bond distances in $[(THF)MeGa(BINOL)]_2$ (Ga(1)–O(1) 1.8522(13) Å; Ga(1)–O(2) 1.8534(13) Å).

Table 2.2: Selected bond lengths (Å) and angles (°) for $[Ga(OCH(CH_3)CH_2NMe_2)_2Cl]$ **(6)**

Ga1–O1	1.8381(16)	Ga1–O2	1.8386(16)
Ga1–N1	2.1529(19)	Ga1–N2	2.1683(19)
Ga1–Cl1	2.2123(6)		
O1–Ga1–O2	118.80(8)	O1–Ga1–N1	84.31(7)
O2–Ga1–N1	90.32(7)	O1–Ga1–N2	89.78(7)
O2–Ga1–N2	84.25(7)	N1–Ga1–N2	168.86(8)
O1–Ga1–Cl1	121.63(6)	O2–Ga1–Cl1	119.57(6)
N1–Ga1–Cl1	95.41(5)	N2–Ga1–Cl1	95.73(5)

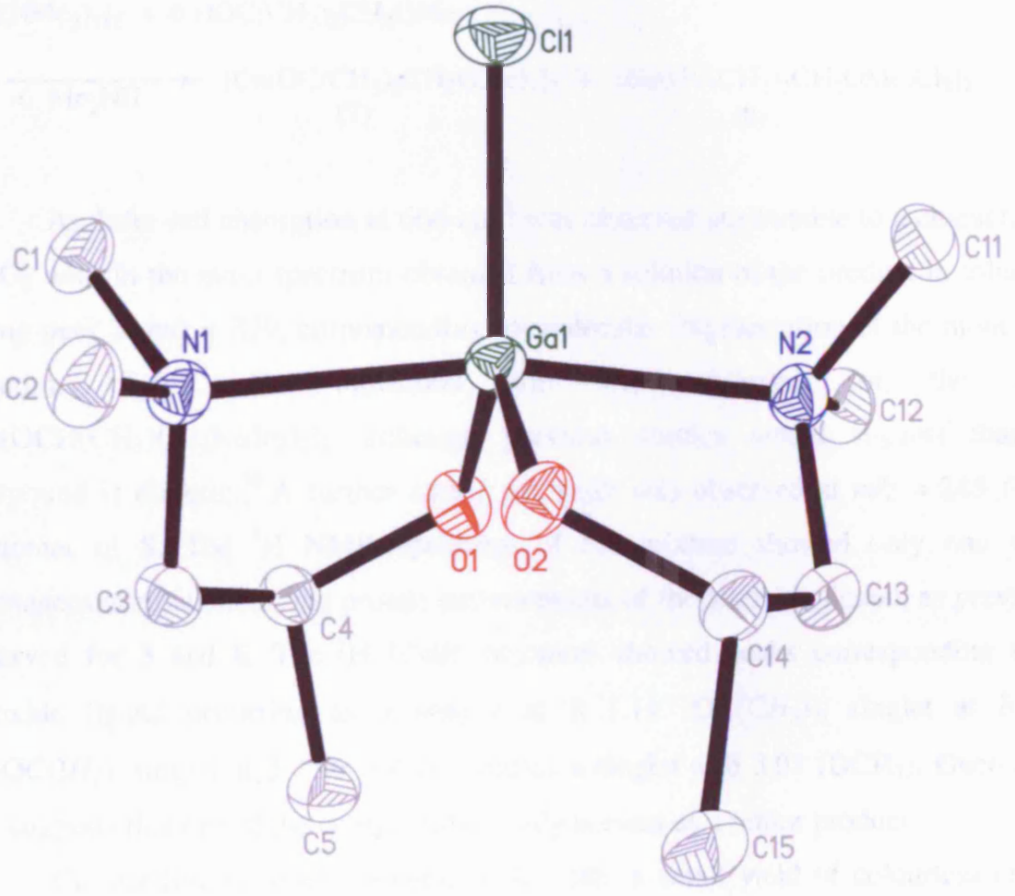

Figure 2.8: X-ray structure of $[Ga(OCH(CH_3)CH_2NMe_2)_2Cl]$ **(6)**

2.2.9 Reaction of $[Ga(NMe_2)_3]_2$ and $HOC(CH_3)_2CH_2OMe$

The analogous reaction of $[Ga(NMe_2)_3]_2$ with an excess of $HOC(CH_3)_2CH_2OMe$ in toluene under reflux conditions resulted in a brown solution, which upon solvent removal afforded a pale brown viscous oil (61% yield). Spectroscopic data for the oil suggested that the major product formed is $[Ga(OC(CH_3)_2CH_2OMe)_3]_2$ **(7)** and a small amount of $[Ga(OC(CH_3)_2CH_2OMe)Cl_2]$ **(8)**, formed as a side product, as shown, in Eq. 2.23.

$$[Ga(NMe_2)_3]_2 + 6\,HOC(CH_3)_2CH_2OMe \xrightarrow[-6\ Me_2NH]{} \underset{\textbf{(7)}}{[Ga(OC(CH_3)_2CH_2OMe)_3]_2} + \underset{\textbf{(8)}}{[Ga(OC(CH_3)_2CH_2OMe)Cl_2]_2} \qquad \textbf{(2.23)}$$

An Infra-red absorption at 666 cm^{-1} was observed attributable to a characteristic Ga_2O_2 unit. In the mass spectrum obtained from a solution of the product in toluene, a strong peak at m/z = 379, corresponding to molecular fragmentation of the monomeric structure of **7**. No molecular ion was observed for the dimer $[Ga(OCH(CH_3)CH_2NMe_2)_3]_2$, although previous studies would suggest that this compound is dimeric.[36] A further strong ion peak was observed at m/z = 245 for the monomer of **8**. The ^1H NMR spectrum of the mixture showed only one set of resonances attributable to the proton environments of the alkoxide ligand, as previously observed for **3** and **6**. The ^1H NMR spectrum showed peaks corresponding to the alkoxide ligand occurring as a singlet at δ 1.11 ($OC(CH_3)$), singlet at δ 2.89 ($GaOCCH_2$), singlet at δ 2.96 (OCH_3) and as a singlet at δ 3.01 (OCH_3). Once again, this suggests that one of the compounds is only present as a minor product.

On standing at room temperature for 24h, a small yield of colourless crystals were obtained from the oil. An X-ray crystallographic study (section 2.2.10) was carried out on the colourless crystals and showed that the crystals were $[Ga(OC(CH_3)_2CH_2OMe)Cl_2]$ **(8)**. Elemental analysis confirmed the crystals to be $[Ga(OC(CH_3)_2CH_2OMe)Cl_2]$. As observed for compounds **3** and **6**, the formation of **8** must be due to incomplete substitution of all chloride ligands in the preparation of **1**.

2.2.10 X-ray data of [Ga(OC(CH$_3$)$_2$CH$_2$OMe)Cl$_2$] (8)

The X-ray structure of compound **8** was determined by X-ray crystallography, the results are shown in Figure 2.9; selected bond lengths and angles are given in Table 2.3. Compound **8** crystallised into the monoclinic space group $P2_1/n$. As shown in Figure 2.9, the compound exhibits a dimeric molecular arrangement. The centrosymmetric, four-membered Ga_2O_2 ring is planar, and each gallium atom is coordinated in a distorted trigonal bipyramidal geometry with two chlorine groups in equatorial positions. The bridging alkoxide subsituents are located in both axial and equatorial positions, while the methoxy group is in the other axial position. The equatorial Ga1–O1 (1.9753(17) Å) bond length is significantly shorter than the axial one Ga–O2 (2.1613 (19) Å). The average O2'–Ga–O1 bond angle to the opposite, axial alkoxide group is 154.27 (8)°. This large deviation from 180° is due to the constraints of the internal O2'–Ga–O2 angle 76.30(9) ° in the Ga_2O_2 ring and the geometry of the ligand.

Similar distorted trigonal bipryamidal geometry at the gallium centre has been noted in the closely related intramoleculary stabilised gallium monoalkoxide complexes of the type [Me$_2$GaOR]$_2$ (R = $OCH_2CH_2NMe_2$, OCH_2CH_2OMe, $OCH(CH_3)CH_2NMe_2$ and $OCH(CH_3)CH_2OMe$).[51, 52, 53] These structures are also dimeric in the solid state and consist of planar or nearly planar Ga_2O_2 rings. The gallium centres are also coordinated in distorted trigonal bipyramidal geometry with comparable bond lengths and angles.

Table 2.3: Selected bond lengths (Å) and angles (°) for $[Ga(OC(CH_3)_2CH_2OMe)Cl_2]$ **(8)**

Ga1–O2#1	1.9753(17)	Ga1–Cl2	2.1595(8)
Ga1–O1	2.1613(19)	Ga1–Cl1	2.1715(8)
Ga1–O2	1.886 (2)		
O2–Ga1–O2#1	76.30(9)	O2–Ga1–Cl2	120.54(7)
O2#1–Ga1–Cl2	102.35(6)	O2–Ga1–O1	77.98(7)
O2#1–Ga1–O1	154.27(8)	Cl2–Ga1–O1	91.29(6)
O2–Ga1–Cl1	122.49(7)	O2#1–Ga1–Cl1	100.69(6)
Cl2–Ga1–Cl1	116.19(3)	O1–Ga1–Cl1	92.44(5)

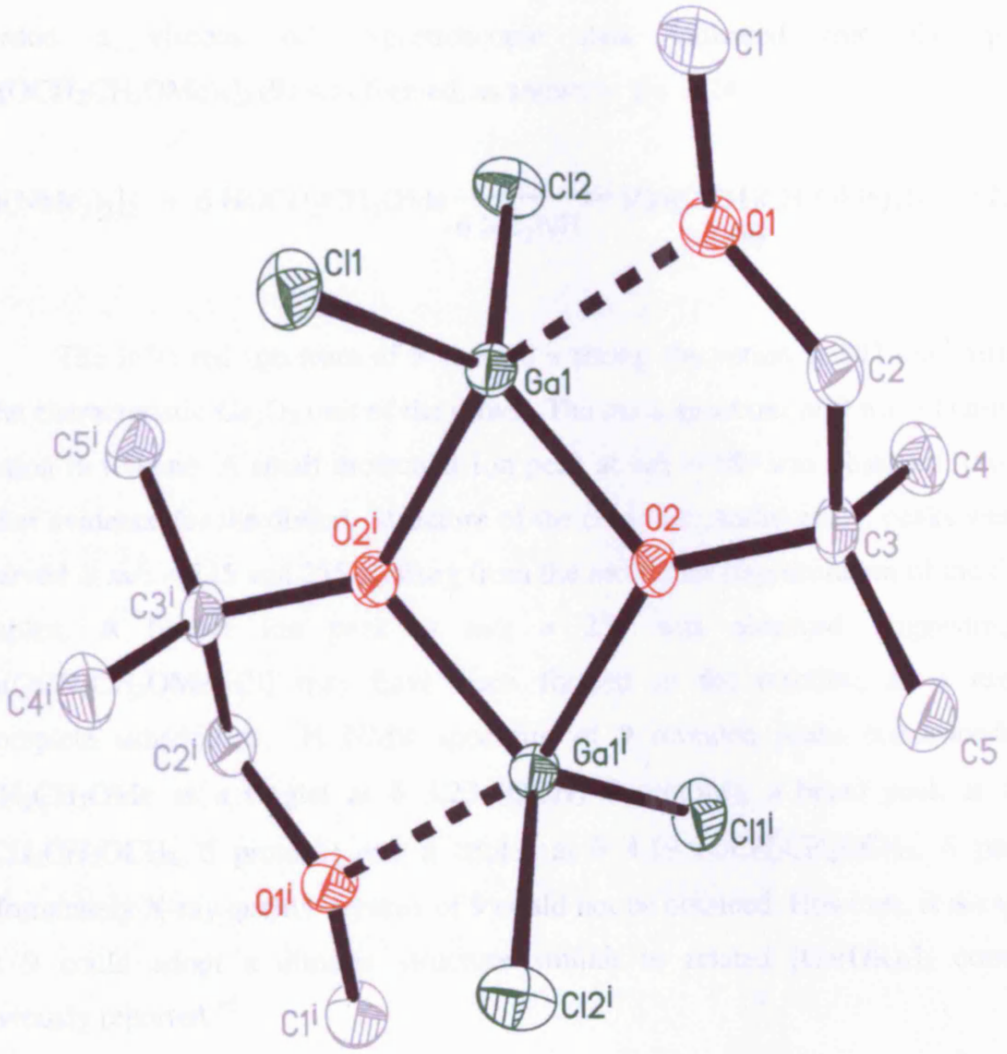

Figure 2.9: X-ray structure of $[Ga(OC(CH_3)_2CH_2OMe)Cl_2]_2$ **(8)**

2.2.11 Reaction of $[Ga(NMe_2)_3]_2$ and $HOCH_2CH_2OMe$ (9)

Treatment of $[Ga(NMe_2)_3]_2$ with an excess of $HOCHCH_2CH_2OMe$ in toluene under reflux conditions resulted in a clear solution which, upon solvent removal afforded a viscous oil. Spectroscopic data indicated that the product $[Ga(OCH_2CH_2OMe)_3]_2$ (**9**) was formed, as shown in Eq. 2.24.

$$[Ga(NMe_2)_3]_2 + 6\,HOCH_2CH_2OMe \xrightarrow[-6\,Me_2NH]{} \underset{(9)}{[Ga(OCH_2CH_2OMe)_3]_2} \quad (2.24)$$

The Infra-red spectrum of **9** showed a strong absorption at 697 cm^{-1} attributed to the characteristic Ga_2O_2 unit of the dimer. The mass spectrum of **9** was obtained as a solution in toluene. A small molecular ion peak at *m/z* = 589 was observed, providing further evidence for the dimeric structure of the complex. Additionally, peaks were also observed at *m/z* = 515 and 255 arisisng from the molecular fragmentation of the dimeric complex. A further ion peak at *m/z* = 255 was observed, suggesting that $[Ga(OCH_2CH_2OMe)_3Cl]$ may have been formed in the reaction, as a result of incomplete substitution. ^1H NMR spectrum of **9** revealed peaks corresponding to OCH_2CH_2OMe as a singlet at δ 3.23 (OCH_3, 9 protons), a broad peak at δ 3.43 ($OCH_2CH_2OCH_3$, 6 protons) and a triplet at δ 4.19 ($OCH_2CH_2OCH_3$, 6 protons). Unfortunately X-ray quality crystals of **9** could not be obtained. However, it is expected that **9** could adopt a dimeric structure similar to related $[Ga(OR)_3]_2$ complexes previously reported.[36]

2.2.12 Synthesis of gallium mono(alkoxides)

The reaction of triethyl gallium Et_3Ga, with donor functionalised alcohols has been investigated to synthesise a range of mono(alkoxides) of gallium(III). These are particularly useful as precursors for chemical vapour deposition, as they are less air/moisture sensitive, have increased solubility and volatility. Furthermore, ethyl ligands may facilitate a favourable decomposition pathway to gallium oxide in the form of β-elimination.[54]

2.2.13 Reaction of Et_3Ga and $HOCH_2CH_2NMe_2$

Treatment of Et_3Ga with one equivalent of $HOCH_2CH_2NMe_2$ in toluene at -78 °C gave rise to a strongly exothermic reaction with violent evolution of ethane gas. After work up, the resulting colourless oil was left to stand at room temperature for several days. X-ray quality colourless crystals of **(10)** in a 91% yield were obtained. Analytical and spectroscopic data for **10** indicated that dimeric $[Et_2Ga(OCH_2CH_2NMe_2)]_2$ had formed, as shown in Eq. 2.25.

$$Et_3Ga + HOCH_2CH_2NMe_2 \longrightarrow 1/2\ [Et_2Ga(OCH_2CH_2NMe_2)]_2 + C_2H_5 \quad \textbf{(2.25)}$$
$$\textbf{(10)}$$

The Ga_2O_2 moiety of dimeric gallium mono(alkoxides) typically display strong absorptions in the low-frequency infrared spectral range. Infra-red absorptions were observed at 552, 504, 430 cm^{-1} for **10**, attributable to characteristic Ga–C stretch and Ga_2O_2 ring modes, respectively. The ^1H NMR spectrum of **10** showed resonances at δ 0.44 (quartet) and δ 1.29 (triplet) for the CH_2 and CH_3 groups, respectively, of the ethyl ligand. Peaks corresponding to the alkoxide ligand occur as a singlet at δ 1.98 (NCH_3), triplet at δ 2.01 (OCH_2CH_2N) and a triplet at δ 3.49 (OCH_2CH_2N). The peaks for the alkoxide and ethyl ligands, each integrate to 10 protons, thus suggesting the formation of a dialkyl gallium mono(alkoxide). The mass spectrum of **10** was obtained as a solution in toluene. A small molecular ion peak at m/z = 433 was observed, providing further evidence for the dimeric structure of the complex. Strong ion peaks were also observed at m/z = 403 and 344 arising from molecular fragmentation of the dimeric structure. Additionally, a small peak for the monomer of **10** was observed, suggesting a monomer-dimer equilibrium in solution, although this is not observed in the NMR. This fragment may also arise from the symmetric cleavage of the Ga_2O_2 ring. The structure of compound **10** was confirmed by X-ray crystallography, the details of which are described in section 2.2.14.

2.2.14 X-ray structure of $[Et_2Ga(OCH_2CH_2NMe_2)]_2$ (10)

The X-ray structure of compound **10** was determined by X-ray crystallography and the results are shown in Figure 2.10; selected bond lengths and angles are given in Table 2.4. Compound **10** crystallised into the monoclinic space group $P2_1/n$. As shown

in Figure 2.10, the compound adopts a dimeric molecular arrangement. The centrosymmetric, four-membered Ga_2O_2 ring, that is common to this type of complex,[1] is nearly planar. Each gallium atom adopts a distorted trigonal bipyramidal geometry with two ethyl groups in equatorial positions. The bridging alkoxide groups are located in both axial and equatorial positions, while the nitrogen atom of the aminoalkoxide group is in the axial position with the average N–Ga–O bond angle to the opposite, axial alkoxide group being 149.37(4)°. This large deviation from 180° is due to the constraints of the internal O–Ga–O angles (73.48(4)° and 73.70(4)°) in the Ga_2O_2 ring and the geometry of the ligand. The sum of the bond angles in the equatorial plane of **10** is 359.7°, which is a measure of the planarity of the equatorial groups. The equatorial Ga–O bond lengths (*av.* 1.9283 Å) are significantly shorter than the axial Ga–O bond distances (*av.* 2.07895 Å) indicative of two active bonding Ga–O bond types. The Ga–N distances (*av.* 2.43775 Å), can be attributed to N→ Ga dative bonding and are slightly longer than the N→Ga in the related compound $[Me_2Ga(OCH_2CH_2NMe_2)]_2$.[12] This bond length is also longer than the sum of the covalent radii of N(sp^3) and Ga (2.19 Å) and so indicative of a strong dative bonding interaction. The Ga–N bond distance in **10** is also longer than these observed in compounds **2** (*av.* 2.0875 Å) and **6** (*av.* 2.161 Å). This can be explained in terms of the steric effect of the ethyl group and electronic effect of the Cl in **10**, thus making the Ga–N distance longer in **10** and shorter in **2** and **6**.

Similar distorted trigonal bipryamidal geometries at gallium have been observed in the closely related intramoleculary stabilised gallium mono(alkoxide) complexes, of the type $[Me_2GaOR]_2$ (R = $CH_2CH_2NMe_2$, CH_2CH_2OMe, $CH(CH_3)CH_2NMe_2$ and $CH(CH_3)CH_2OMe$).[51,52,53] These structures are also dimeric in the solid state and consist of planar or nearly planar Ga_2O_2 rings. The gallium centres are also coordinated in distorted trigonal bipyramidal geometry with comparable bond lengths and angles.

Table 2.4: Selected bond lengths (Å) and angles (°) for $[Et_2Ga(OCH_2CH_2NMe_2)]_2$ **(10)**

Ga1–O1	1.9229(10)	Ga1–C7	1.9786(14)
Ga1–C5	1.9843(14)	Ga1–O2	2.0669(9)
Ga1–N1	2.5068(12)	Ga2–O1	2.0910(9)
Ga2–O2	1.9337(9)	Ga2–C15	1.9848(14)
Ga2–C13	1.9586(14)	Ga2–N2	2.3727(11)
O1–Ga1–C7	116.47(5)	O1–Ga1–C5	117.84(5)
C7–Ga1–C5	125.35(6)	O1–Ga1–O2	74.48(4)
C7–Ga1–O2	98.58(5)	C5–Ga1–O2	100.90(5)
O1–Ga1–N1	75.24(4)	C7–Ga1–N1	96.84(5)
C5–Ga1–N1	91.12(5)	O2–Ga1–N1	149.63(4)
O2–Ga2–C15	116.82(5)	O2–Ga2–C13	119.24(5)
C15–Ga2–C13	123.86(6)	O2–Ga2–O1	73.70(4)
C15–Ga2–O1	100.89(5)	C13–Ga2–O1	97.00(5)
O2–Ga2–N2	75.45(4)	C15–Ga2–N2	94.42(5)
C13–Ga2–N2	96.43(5)	O1–Ga2–N2	149.11(4)

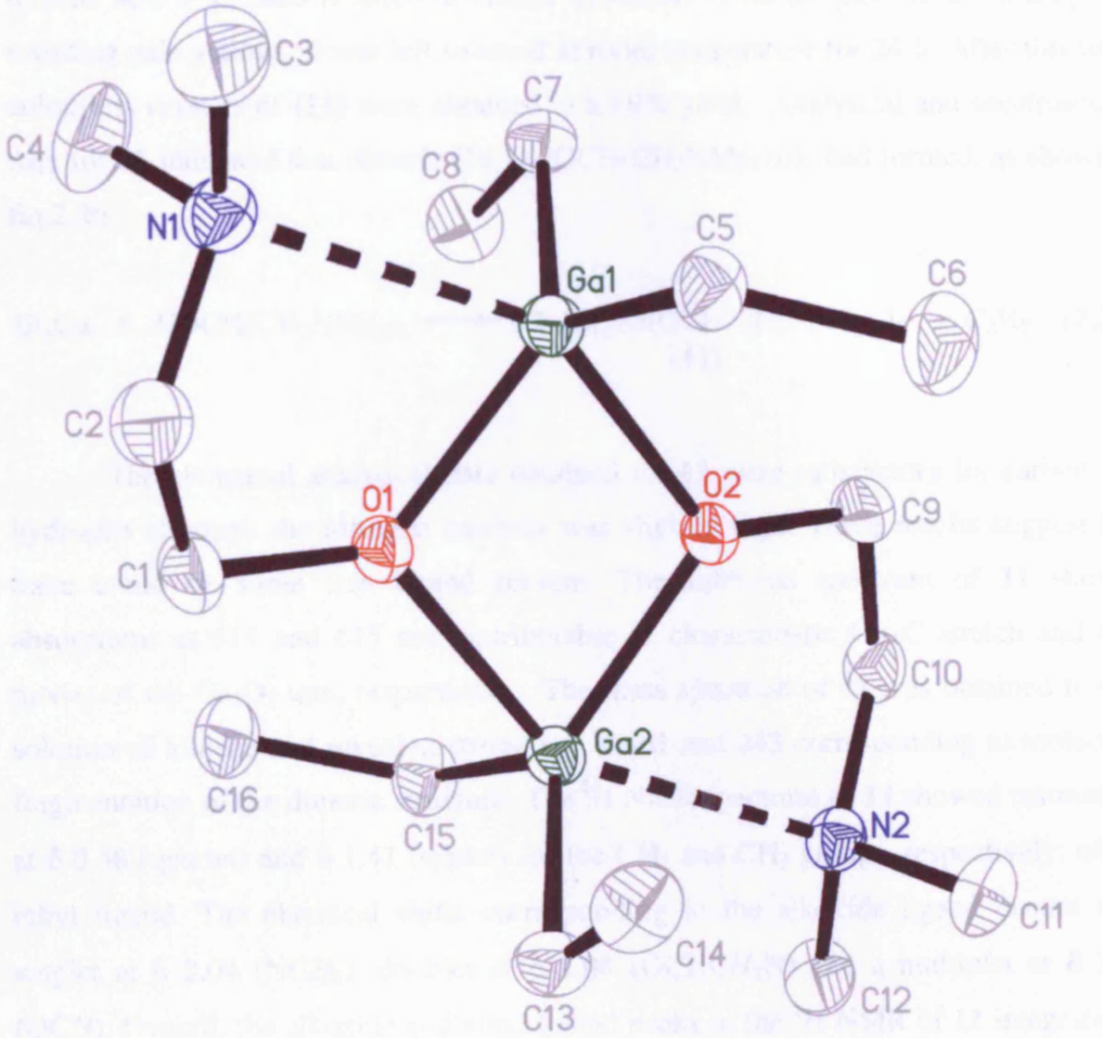

Figure 2.10: X-ray structure of $[Et_2Ga(OCH_2CH_2NMe_2)]_2$ **(10)**

2.2.15 Reaction of Et_3Ga and $HOCH(CH_2NMe_2)_2$

The analogous reaction of Et_3Ga with one equivalent of $HOCH(CH_2NMe_2)_2$ in toluene at -78 °C also resulted in violent evolution of ethane gas. After work up, the resulting pale yellow oil was left to stand at room temperature for 24 h. After this time, colourless crystals of **(11)** were obtained in a 89% yield. Analytical and spectroscopic data for **11** indicated that dimeric $[Et_2Ga(OCH(CH_2NMe_2)_2)]_2$ had formed, as shown in Eq.2.26.

$$Et_3Ga + HOCH(CH_2NMe_2)_2 \longrightarrow 1/2\ [Et_2Ga(OCH(CH_2NMe_2)_2]_2 + C_2H_5 \quad \textbf{(2.26)}$$
$$\textbf{(11)}$$

The elemental analytical data obtained for **11** were satisfactory for carbon and hydrogen although the nitrogen analysis was slightly high. These results suggest that there could be some free ligand present. The Infra-red spectrum of **11** showed absorptions at 611 and 615 cm^{-1} attributable to characteristic Ga–C stretch and ring modes of the Ga_2O_2 unit, respectively. The mass spectrum of **11** was obtained from a solution of toluene and revealed strong *m/z* = 401 and 243 corresponding to molecular fragmentation of the dimeric structure. The ^1H NMR spectrum of **11** showed resonances at δ 0.58 (quartet) and δ 1.41 (triplet) for the CH_2 and CH_3 groups, respectively, of the ethyl ligand. The chemical shifts corresponding to the alkoxide ligand occurs as a singlet at δ 2.04 (NCH_3), doublet at δ 2.08 ($OCHCH_2N$) and a multiplet at δ 3.81 (OC*H*). Overall, the alkoxide and ethyl ligand peaks in the ^1H NMR of **11** integrates to 17 and 10 protons, respectively, thus confirming the formation of a dialkyl gallium monoalkoxide. The structure of **11** was determined by X-ray crystallography, the details which are described in section 2.2.16.

2.2.16 X-ray structure of $[Et_2Ga(OCH(CH_2NMe_2)_2)]_2$ (11)

The X-ray structure of compound **11** was determined by X-ray crystallography, the results are shown in Figure 2.11; selected bond lengths and angles are given in Table 2.5. Compound **11** crystallised into the triclinic space group, $P\bar{1}$. As shown in Figure 2.11, compound **11** also exhibits a dimeric molecular arrangement similar to **10**. The centrosymmetric, four-membered Ga_2O_2 ring is planar, and each gallium atom adopts distorted trigonal bipyramidal geometry with two ethyl groups in equatorial

positions. The Ga–N bond distance of 2.5038(13) Å indicates a weak dative bond, which is longer than observed in **10**. This could be due to unfavourable steric interactions, which arise between the alkyl groups of the aminoalkoxide ligand and ethyl groups attached to the gallium. The alkoxide groups are located in both axial and equatorial positions, while one of the nitrogen atoms of the aminoalkoxide group is in the axial position with the *av.* N–Ga–O bond angle to the opposite, axial alkoxide group being 151.7°. The equatorial Ga(1)–O(1) bond length of 1.9152(11) Å is significantly shorter than that to the axial alkoxide oxygen atom with Ga(2)–O(1') distance of 2.0965(11) Å. All other bond lengths and angles observed in **11** are similar to those found in **10**.

Table 2.5: Selected bond lengths (Å) and angles (°) for $[Et_2Ga(OCH(CH_2NMe_2)_2)]_2$ **(11)**

Ga1–O1	1.9152(11)	Ga1–C8	1.9738(19)
Ga1–C10	1.9764(19)	Ga1–O1#1	2.0965(11)
Ga1–N2	2.5038(13)	Ga1–N2'	2.5690(17)
O1–Ga1–C8	118.30(7)	O1–Ga1–C10	114.50(7)
C8–Ga1–C10	126.92(9)	O1–Ga1–O1#1	74.83(5)
C8–Ga1– O1#1	100.37(7)	C10–Ga1– O1#1	97.89(7)

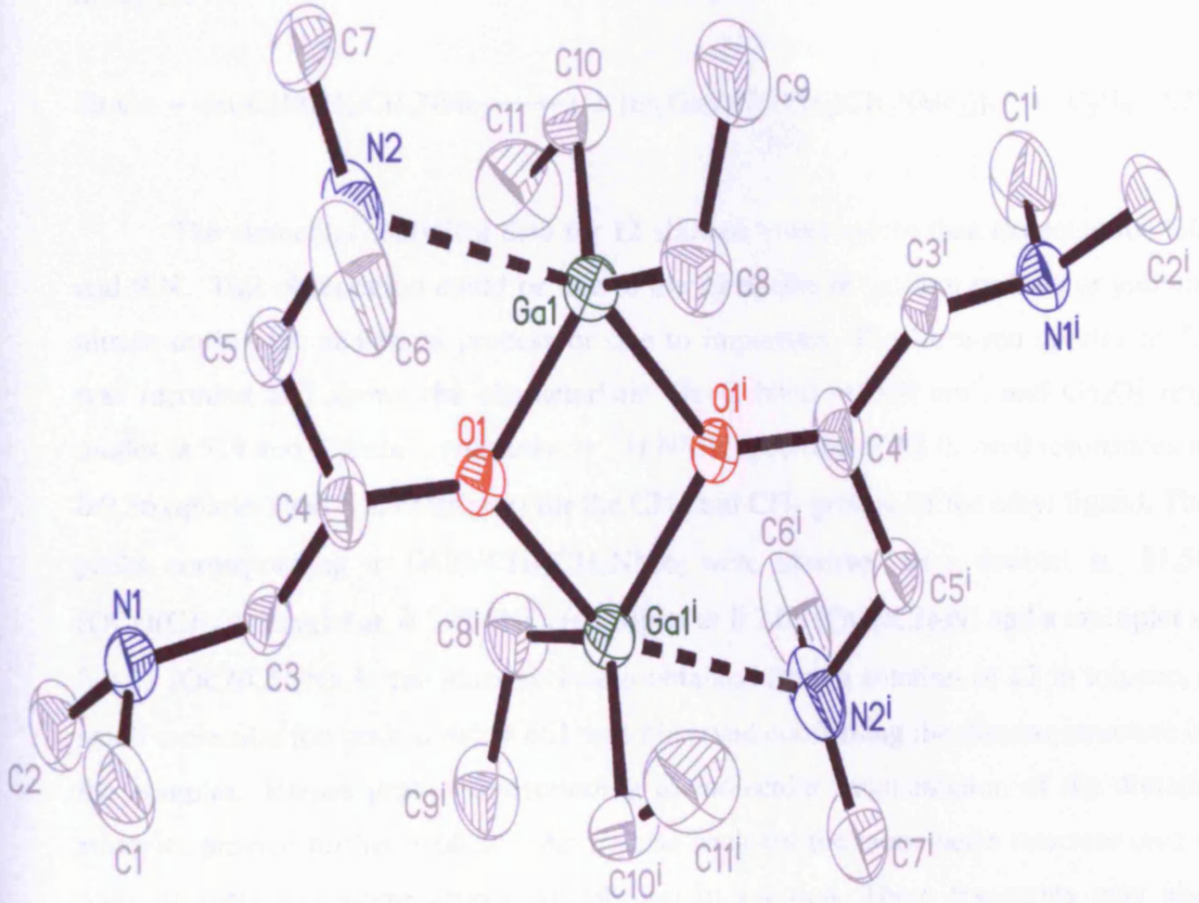

Figure 2.11: X-ray structure of $[Et_2Ga(OCH(CH_2NMe_2)_2)]_2$ **(11)**

2.2.17 Reaction of Et_3Ga and $HOCH(CH_3)CH_2NMe_2$

Reaction of Et_3Ga with one equivalent of $HOCH(CH_3)CH_2NMe_2$ in toluene at -78 °C resulted in a strongly exothermic reaction with evolution of ethane. After work up, the resulting pale yellow oil was left to stand at room temperature for 24 h. Colourless crystals of **12** were isolated in a 92% yield. Analytical and spectroscopic data for **12** indicated that dimeric $[Et_2Ga(OCH(CH_3)CH_2NMe_2)]_2$ had formed, as shown in Eq. 2.27.

$$Et_3Ga + HOCH(CH_3)CH_2NMe_2 \longrightarrow 1/2\ [Et_2Ga(OCH(CH_3)CH_2NMe_2)]_2 + C_2H_5 \quad (2.27)$$
$$(12)$$

The elemental analytical data for **12** showed lower values than expected for %C and %N. This observation could be due to the formation of gallium carbide or gallium nitride during the analytical process or due to impurities. The Infra-red spectra of **12** was recorded and shows the characteristic Ga–C bond at 619 cm^{-1} and Ga_2O_2 ring modes at 519 and 422 cm^{-1}, respectively. ^1H NMR spectrum of **12** showed resonances at δ 0.56 (quartet) and δ 1.39 (triplet) for the CH_2 and CH_3 groups, of the ethyl ligand. The peaks corresponding to $OCH(CH_3)CH_2NMe_2$ were observed as a doublet at δ1.56 ($OCH(CH_3)$), singlet at δ 1.90 (NCH_3), triplet at δ 2.08 ($OCHCH_2N$) and a multiplet at δ 3.81 ($OCHCH_2N$). In the mass spectrum obtained from a solution of **12** in toluene, a small molecular ion peak at *m/z* = 461 was observed confirming the dimeric structure of the complex. Intense peaks corresponding to molecular fragmentation of the dimeric structure provide further evidence. An intense peak for the monomeric structure (*m/z* = 358) suggests a monomer-dimer equilibrium in solution. These fragments may also arise from the symmetric cleavage of the Ga_2O_2 ring. The structure of **12** was confirmed by X-ray crystallography, the details which are described in section 2.2.18.

2.2.18 X-ray structure of $[Et_2Ga(OCH(CH_3)CH_2NMe_2)_2]_2$ (12)

X-ray structure of compound **12** was determined by X-ray crystallography, the results are shown in Figure 2.12; selected bond lengths and angles are given in Table 2.6. Compound **12** crystallised into the triclinic space group, $P\bar{1}$. As shown in Figure 2.12, this compound also exhibits a dimeric molecular arrangement as observed in **10** and **11**. The crystal structure of **12** consists of two independent molecules in the unit

cell. The centrosymmetric, four-membered Ga_2O_2 ring is planar in both molecules, and each gallium atom adopts a distorted trigonal bipyramidal geometry with two ethyl groups in equatorial positions. The Ga–N bond distances of 2.5524(28) Å and 2.6005(30) Å indicates, weak dative bonds, which are longer than observed in **10** but similar to **11**. This could be due to unfavourable steric interactions, which arise between the alkyl groups of the aminoalkoxide ligand and ethyl groups attached to the gallium. The alkoxide groups are located in both axial and equatorial positions, while the nitrogen atom of the amino alkoxide group is in the axial position with the *av.* N–Ga–O bond angle to the opposite, axial alkoxide group being 149°. The equatorial Ga(1)–O(1) bond lengths of 1.919(2) Å and 1.920(2) Å are significantly shorter than those to the axial alkoxide oxygen atom Ga(2)–O(2) distance of 2.074(2) Å and Ga(1)–O(1') distance of 2.088(2) Å.

Table 2.6: Selected bond lengths (Å) and angles (°) for $[Et_2Ga(OCH(CH_3)CH_2NMe_2)]_2$ **(12)**

Ga1–O1	1.919(2)	Ga1–C8	1.978(3)
Ga1–C6	1.982(3)	Ga1–O1#1	2.088(2)
Ga2–O2	1.920(2)	Ga2–C16	1.974(3)
Ga2–C18	1.982(3)	Ga2–O2#2	2.074(2)
Ga1–N1	2.5524(28)	Ga2–N2	2.6005(30)
O1–Ga1–C8	116.77(12)	O1–Ga1–C6	115.78(12)
C8–Ga1–C6	127.04(14)	O1–Ga1–O1#1	75.07(10)
C8–Ga1–O1#1	98.38(12)	C6–Ga1–O1#1	100.72(12)
O2–Ga2–C16	114.93(13)	O2–Ga2–C18	115.46(12)
C16–Ga2–C18	128.90(15)	O2–Ga2–O2#2	75.63(10)
C16–Ga2– O2#2	99.51(13)	C18–Ga2– O2#2	100.39(12)

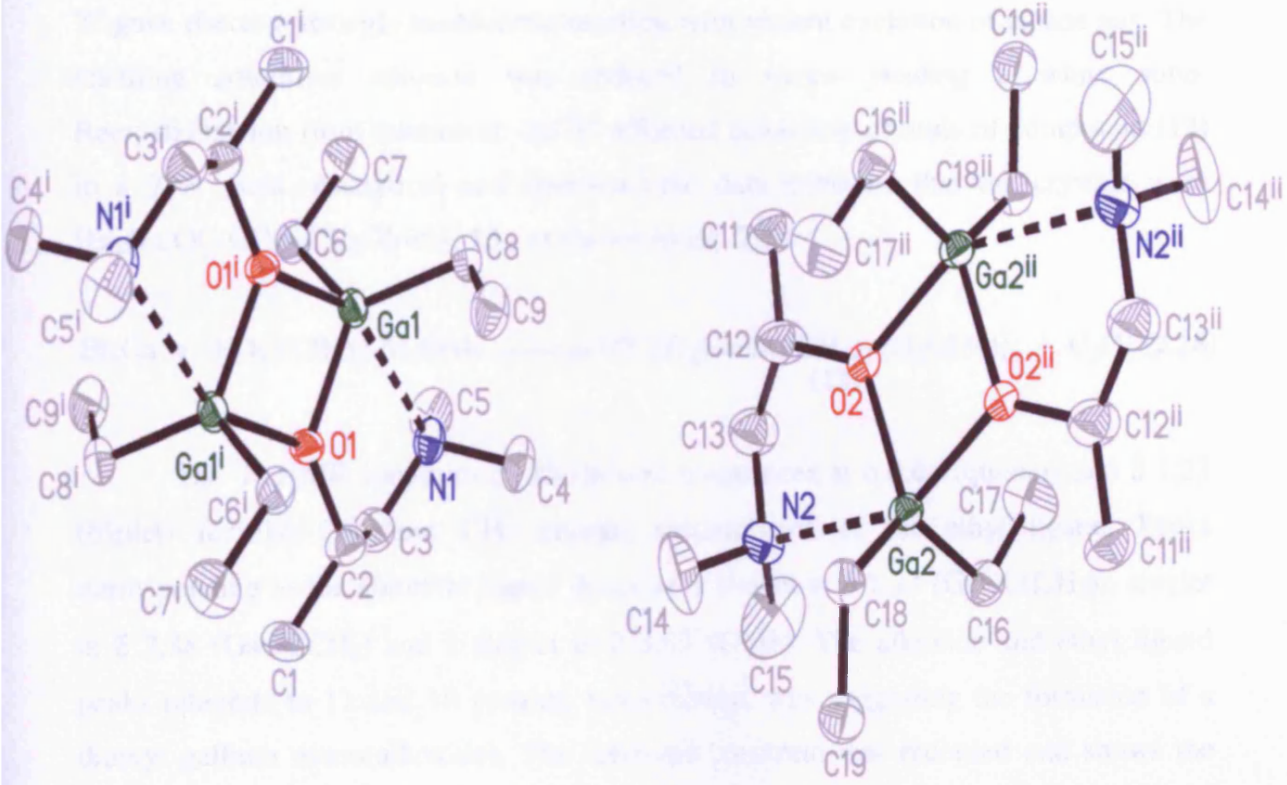

Figure 2.12: X-ray structure of $[Et_2Ga(OCH(CH_3)CH_2NMe_2)]_2$ **(12)**

2.2.19 Reaction of Et_3Ga and $HOC(CH_3)_2CH_2OMe$

Treatment of Et_3Ga and one equivalent of $HOC(CH_3)_2CH_2OMe$ in toluene at -78 °C gave rise to a strongly exothermic reaction with violent evolution of ethane gas. The resulting colourless solution was reduced in *vacuo* yielding a white solid. Recrystallisation from toluene at -20 °C afforded colourless crystals of compound **(13)** in a 97% yield. Analytical and spectroscopic data indicated that the crystals were $[Et_2Ga(OC(CH_3)_2CH_2OMe)]_2$ **13** , as shown in Eq. 2.28.

$$Et_3Ga + HOC(CH_3)_2CH_2OMe \longrightarrow 1/2\ [Et_2Ga(OC(CH_3)_2CH_2OMe)]_2 + C_2H_5 \quad \textbf{(2.28)}$$
$$\textbf{(13)}$$

The ^1H NMR spectrum of **13** showed resonances at δ 0.64 (quartet) and δ 1.23 (triplet) for the CH_2 and CH_3 groups, respectively, of the ethyl ligand. Peaks corresponding to the alkoxide ligand occur as a singlet at δ 1.23 ($GaOC(CH_3)$), singlet at δ 2.88 ($GaOCCH_2$) and a singlet at δ 3.03 (OMe). The alkoxide and ethyl ligand peaks integrate to 11 and 10 protons, respectively, thus suggesting the formation of a dialkyl gallium mono(alkoxide). The infra-red spectrum was recorded and shows the expected peaks at 658, 633 and 556 cm^{-1}, which are attributable to a characteristic Ga–C stretch and ring modes of the Ga_2O_2 unit, respectively. The mass spectrum was obtained from a solution of **13** in toluene. Although no peak was observed for the molecular ion, an intense peak for the monomeric structure (*m/z* = 359) was observed, again suggesting a monomer-dimer equilibrium in solution resulting from molecular fragmentation of the dimeric structure. Strong ion peaks are observed at *m/z* = 358, 231 and 201 arising from molecular fragmentation of the dimeric structure. The structure of **13** was confirmed by X-ray crystallography, the details which are described in section 2.2.20.

2.2.20 X-ray of $[Et_2Ga(OC(CH_3)_2CH_2OMe)]_2$ (13)

X-ray structure of compound **13** was determined by X-ray crystallography, the results are shown in Figure 2.13; selected bond lengths and angles are given in Table 2.7. Compound **13** crystallised into the triclinic space group, $P\bar{1}$. As shown in Figure 2.13, this compound also exhibits a dimeric molecular arrangement as observed in **10**, **11** and **12.** The centrosymmetric, four-membered ring Ga_2O_2 is also planar, and each gallium atom adopts a distorted trigonal bipyramidal geometry with two ethyl groups in

equatorial positions. The bridging alkoxide groups are located in both axial and equatorial positions, while the oxygen atom of the methoxy group is in the axial position with the O–Ga–O bond angle to the opposite, axial alkoxide group being 148.3°. The equatorial Ga(1)–O(1') bond length of 1.9229(9) Å is slightly shorter than that to the axial alkoxide oxygen atom with Ga(2)–O(1) distance of 2.0141 (9) Å. As expected the largest Ga–O bond length is the Ga–OMe interaction (2.6266(10) Å. The bond lengths observed in this compound are similar to those observed in the methyl derivative, $[Me_2Ga(O(CH_3)_2CH_2OMe)]_2$.[16] The equatorial Ga(1)–O(1) bond length in $[Me_2Ga(O(CH_3)_2CH_2OMe)]_2$ is 1.914(4) Å with the axial Ga(2)–O(2) distance being 1.999 (4) Å.

Table 2.7: Selected bond lengths (Å) and angles (°) for $[Et_2Ga(OC(CH_3)_2CH_2OMe)]_2$ **(13)**

Ga1–O1#1	1.9299(9)	Ga1–C8	1.9737(13)
Ga1–C6	1.9748(13)	Ga1–O1	2.0141(9)
		Ga1–O2	2.6266(10)
O1#1–Ga1–C8	116.04(5)	O1#1–Ga1–C6	113.58(5)
C8–Ga1–C6	125.06(6)	O1#1–Ga1–O1	77.27(4)
C8–Ga1–O1	106.73(5)	C6–Ga1–O1	105.70(5

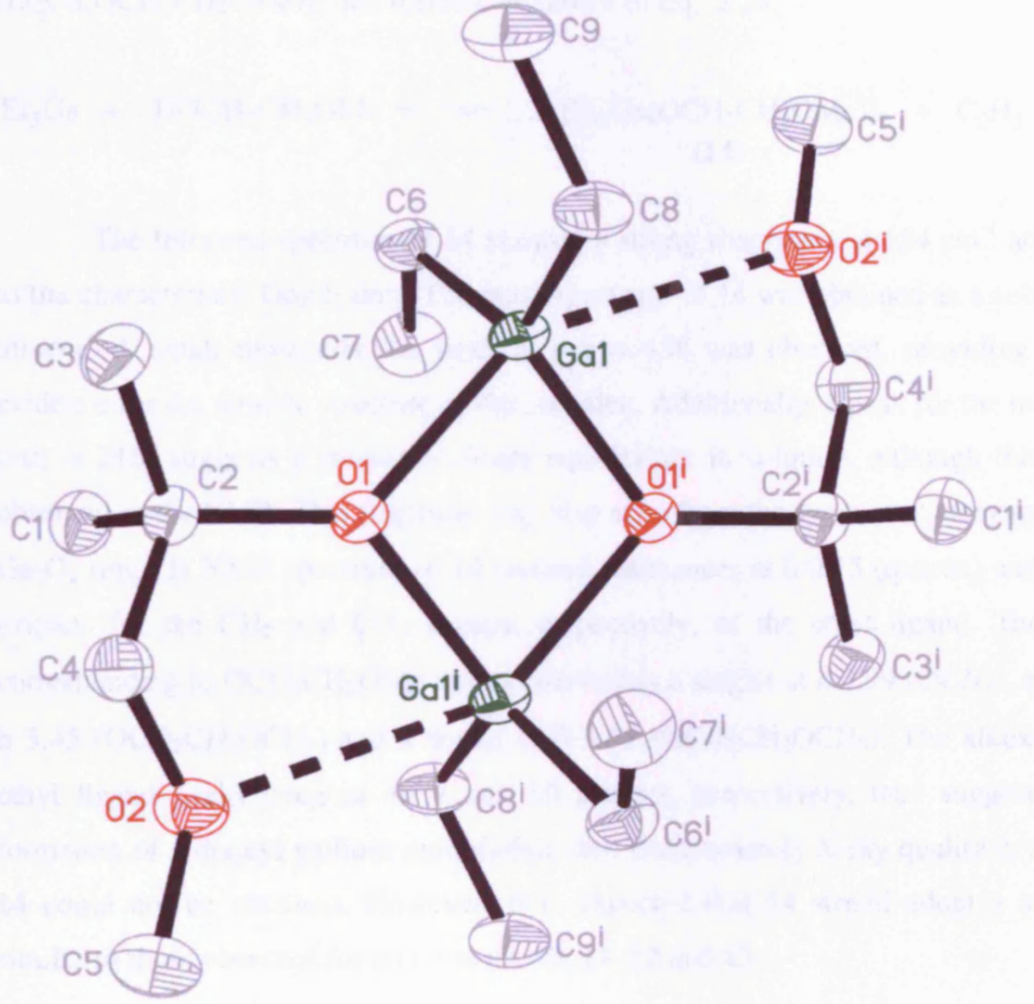

Figure 2.13: X-ray structure of $[Et_2Ga(OC(CH_3)_2CH_2OMe)]_2$ **(13)**

2.2.21 Reaction of Et_3Ga and $HOCH_2CH_2OMe$

The reaction of Et_3Ga with one equivalent of $HOCH_2CH_2OMe$ in toluene at -78 °C resulted in a strongly exothermic reaction with evolution of ethane. After work up, the resulting pale yellow oil was left to stand at room temperature for 24 h. Compound **(14)** was isolated in a 71% yield. Spectroscopic data for **14** indicated that dimeric $[Et_2Ga(OCH_2CH_2OMe)]_2$ had formed, as shown in Eq. 2.29.

$$Et_3Ga + HOCH_2CH_2OMe \longrightarrow 1/2\ [Et_2Ga(OCH_2CH_2OMe)]_2 + C_2H_5 \quad \textbf{(2.29)}$$
$$\textbf{(14)}$$

The Infra-red spectrum of **14** showed a strong absorption at 654 cm^{-1} attributed to the characteristic Ga_2O_2 unit. The mass spectrum of **14** was obtained as a solution in toluene. A small molecular ion peak at *m/z* = 438 was observed, providing further evidence for the dimeric structure of the complex. Additionally, a peak for the monomer (*m/z* = 218) suggests a monomer-dimer equilibrium in solution, although this is not observed in the NMR. This fragment may also arise from the symmetric cleavage of the Ga_2O_2 ring. ^1H NMR spectrum of **14** showed resonances at δ 0.75 (quartet) and δ 1.58 (triplet) for the CH_2 and CH_3 groups, respectively, of the ethyl ligand. The peaks corresponding to OCH_2CH_2OMe were observed as a singlet at δ 2.99 (OCH_3), triplet at δ 3.45 ($OCH_2CH_2OCH_3$) and a triplet at δ 3.83 ($OCH_2CH_2OCH_3$). The alkoxide and ethyl ligand peaks integrate to 7 and 10 protons, respectively, thus suggesting the formation of a dialkyl gallium mono(alkoxide). Unfortunately X-ray quality crystals of **14** could not be obtained. However, it is expected that **14** would adopt a structure similar to those observed for compounds **10**, **11**, **12** and **13**.

2.2.22 Reaction of Et_3Ga and isoproponol

Compounds **10-14** all contain donor functionalised aligands. To provide a comparison, a gallium mono(alkoxide) with a simple monofunctional alkoxide has been prepared.

Treatment of Et_3Ga with one equivalent of isoproponal in toluene at -78 °C gave rise to a strongly exothermic reaction with violent evolution of ethane gas. After work up, a white microcrystalline solid in a 90% yield was obtained. Analytical and

spectroscopic data for **(15)** indicated that dimeric $[Et_2Ga(OCH(CH_3)_2)]_2$ had formed, as shown in Eq. 2.30.

$$Et_3Ga + HOCH(CH_3)_2 \longrightarrow \underset{\textbf{(15)}}{1/2\,[Et_2Ga(OCH(CH_3)_2)]_2} + C_2H_5 \quad \textbf{(2.30)}$$

In the mass spectrum obtained from a solution of **15** in toluene, a small molecular ion peak at *m/z* = 374 was observed providing evidence for the dimeric structure of the complex. A further peak at *m/z* = 317 corresponding to molecular fragmentation of the dimeric structure was also observed. An intense peak for the monomeric structure (*m/z* = 186) suggests a monomer-dimer equilibrium in solution. These fragments may also arise from the symmetric cleavage of the Ga_2O_2 ring. The ^1H NMR spectrum of **15** showed resonances at δ 0.62 (quartet) and δ 1.32 (triplet) for the CH_2 and CH_3 groups, respectively, of the ethyl ligand. The peaks corresponding to $OCH(CH_3)_2$ were observed as a doublet at δ 0.99 ($OCH(CH_3)_2$) and as a septet at δ 3.91 (*OCH*). The alkoxide and ethyl ligand peaks integrate to 7 and 10 protons, respectively, thus suggesting the formation of a dialkyl gallium mono(alkoxide). The Infra-red spectra of **15** was recorded and shows the characteristic Ga–C bond at 553 cm^{-1} and Ga_2O_2 ring modes at 653 and 603 cm^{-1}.

2.2.23 Synthesis of monoalkyl gallium bis(alkoxides)

Only limited examples of monoalkyl gallium and indium bis(alkoxides) have been reported, as discussed in section 2.1.2 . In an attempt to fill this gap in group 13 chemistry, the reaction of triethylgallium and trimethylindium with an excess of donor functionalised alcohols, under reflux conditions was investigated. As described above the 1 : 1 reaction of Et_3Ga and ROH resulted in high yields of $[Et_2GaOR]_2$. The presence of excess alcohol in the reaction mixture at elevated temperatures was investigated in an attempt to overcome the stability of the gallium mono(alkoxides) and isolate bis(alkoxides).

2.2.24 Reaction of Et_3Ga and 6 equivalents of $HOCH_2CH_2NMe_2$

The reaction of Et_3Ga with excess $HOCH_2CH_2NMe_2$ under reflux conditions did not lead to the anticipated monoalkyl gallium bis(alkoxide), but instead the

corresponding dialkyl gallium mono(alkoxide) complex **10**, as characterised by ^{1}H NMR, ^{13}C NMR, IR and Elemental Analysis. This is in contrast to a previous report where the reaction of Et_3Ga and $HOCH_2CH_2NMe_2$ afforded a 1 : 1 mixture of **10** and $[EtGa(OCH_2CH_2NMe_2)_2]$[4] (section 2.1.2.1). The reaction between Et_3Ga and excess $HOCH_2CH_2NMe_2$ under different conditions was repeated a number of times. However, in every reaction only compound **10** was isolated after work up. This could be a result of differences in concentrations of the reaction mixture or due to a different batch of Et_3Ga/ROH employed.

2.2.25 Reaction of Et_3Ga and 6 equivalents of $HOCH(CH_2NMe_2)_2$

The analogous reaction of Et_3Ga with excess $HOCH(CH_2NMe_2)_2$ in toluene under reflux conditions for 24 h afforded a 1 : 8 mixture of the diethylgallium alkoxide $[Et_2Ga(OCH(CH_2NMe_2)_2)]_2$ **(11)** and the ethylgallium bis(alkoxide) $[EtGa(OCH(CH_2NMe_2)_2)_2]$ **(16)**. Spectroscopic data confirmed the formation of a 1 : 8 mixture of compounds **16** and **11**.

$$Et_3Ga + 6\,HOCH(CH_2NMe_2)_2 \xrightarrow{\Delta} 1\,[Et_2Ga(OCH(CH_2NMe_2)_2)]_2 + 8\,[EtGa(OCH_2(CH_2NMe_2)_2)_2] \qquad (2.32)$$

(11) **(16)**

The ^{1}H NMR spectrum of the product from the reflux of Et_3Ga and $HOCH(CH_2NMe_2)_2$ identified a mixture of the dimeric diethylgallium mono(alkoxide) complex **11** and the monoethylgallium bis(alkoxide) $[EtGa(OCH(CH_2NMe_2)_2)_2]$ **16**. These two complexes can be distinguished by the difference in peak positions of the $GaCH_2CH_3$ and $GaCH_2CH_3$ resonances. In complex **11**, the $GaCH_2CH_3$ peak is found at δ 0.57 (integrated to 8 protons) and in complex **16** at δ 0.55 (integrated to 16 protons). The $GaCH_2CH_3$ peak in complex **11** is observed at δ 1.41 (integrated to 12 protons) and in complex **16** at δ 1.44 (integrated to 24 protons). Analysis of the observed proton integrations correlate to the calculated values for a 1 : 8 product mixture of **11** and **16**. It is interesting to note that the proton resonances of the alkoxide ligand appear to vary little within both complexes and so cannot be distinguished. The ^{13}C NMR of the product shows the presence of both complex **11** and complex **16**. Two environments for each of the carbon groups of the ethyl and alkoxide group are observed in the ^{13}C NMR.

The mass spectrum of the product also confirmed the presence of both complexes. Strong molecular ion peaks at *m/z* = 273 and *m/z* = 243 identified for the monomer of the mono(alkoxide) complex **11** and the bis(alkoxide) complex **16**, respectively, were observed. Unfortunately, even after repeated crystallisations using a range of solvents, X-ray quality crystals of **16** could not be isolated. Furthermore, attempts to isolate crystals of **16** *via* sublimation also failed.

2.2.26 Reaction of Et_3Ga and 6 equivalents of $HOCH(CH_3)CH_2NMe_2$

Treatment of Et_3Ga with excess $HOCH(CH_3)CH_2NMe_2$ in toluene under reflux conditions for 24 h afforded a 1 : 8 mixture of the diethylgallium mono(alkoxide) $[Et_2Ga(OCH(CH_3)CH_2NMe_2)]_2$ **12** and the ethylgallium bis(alkoxide) $[EtGa(OCH(CH_3)CH_2NMe_2)_2]$ **(17)** as shown in Eq. 2.33. Spectroscopic data confirmed the formation of a 1 : 8 mixture of compounds **12** and **17**.

$$Et_3Ga + 6\,HOCH(CH_3)CH_2NMe_2 \xrightarrow{\Delta} 1\,[Et_2Ga(OCH(CH_3)CH_2NMe_2)]_2\ (\mathbf{12}) + 8\,[EtGa(OCH(CH_3)CH_2NMe_2)_2]\ (\mathbf{17}) \qquad (2.33)$$

The ^1H NMR spectrum of the product identified a mixture of the dimeric diethyl gallium mono(alkoxide) **12** and monoethyl gallium bis(alkoxide) **17**. In complex **12**, the $GaCH_2$ peak is found at δ 0.50 (integrated to 8 protons) and in complex **17** at δ 0.65 (integrated to 16 protons). The $GaCH_3$ peak in complex **12** is observed at δ 1.38 (integrated to 12 protons) and in complex **17** at δ 1.40 (integrated to 24 protons). ^{13}C NMR of the product (Figure 2.14) shows two environments for each of the carbon atoms of the ethyl and alkoxide groups further confirming the presence of two species, complex **12** and complex **17**. However, some free alcohol is also present in the ^{13}C NMR spectrum.

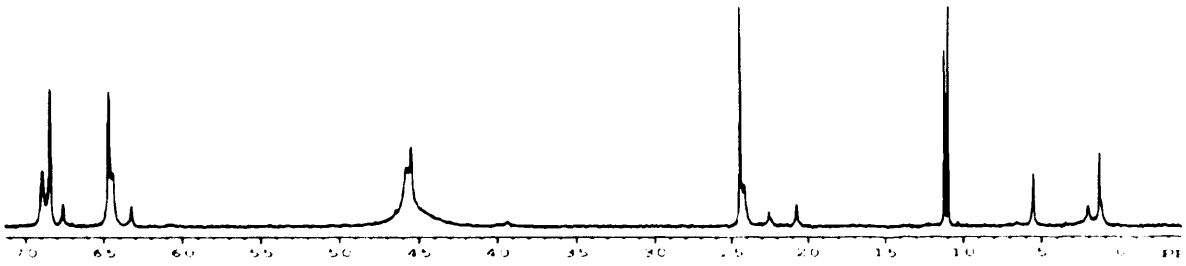

Figure 2.14: ^{13}C NMR spectrum for the reaction of Et_3Ga and six equivalents of $HOCH(CH_3)CH_2NMe_2$.

Mass spectrum (Figure 2.15) of the product also confirmed the presence of both complexes. A molecular ion peak at *m/z* = 230 is observed from the monomeric structure of **12**. In addition, strong molecular ion peaks *m/z* = 431 and 373 corresponding to molecular fragmentation of the dimeric structure of complex **12** were found. A strong molecular ion peak at *m/z* = 303 for the monomeric structure of complex **17** was also observed. Unfortunately, even after repeated crystallisations using a range of solvents, X-ray quality crystals of **17** could not be isolated. Furthermore, attempts to isolate crystals of **17** *via* sublimation also failed.

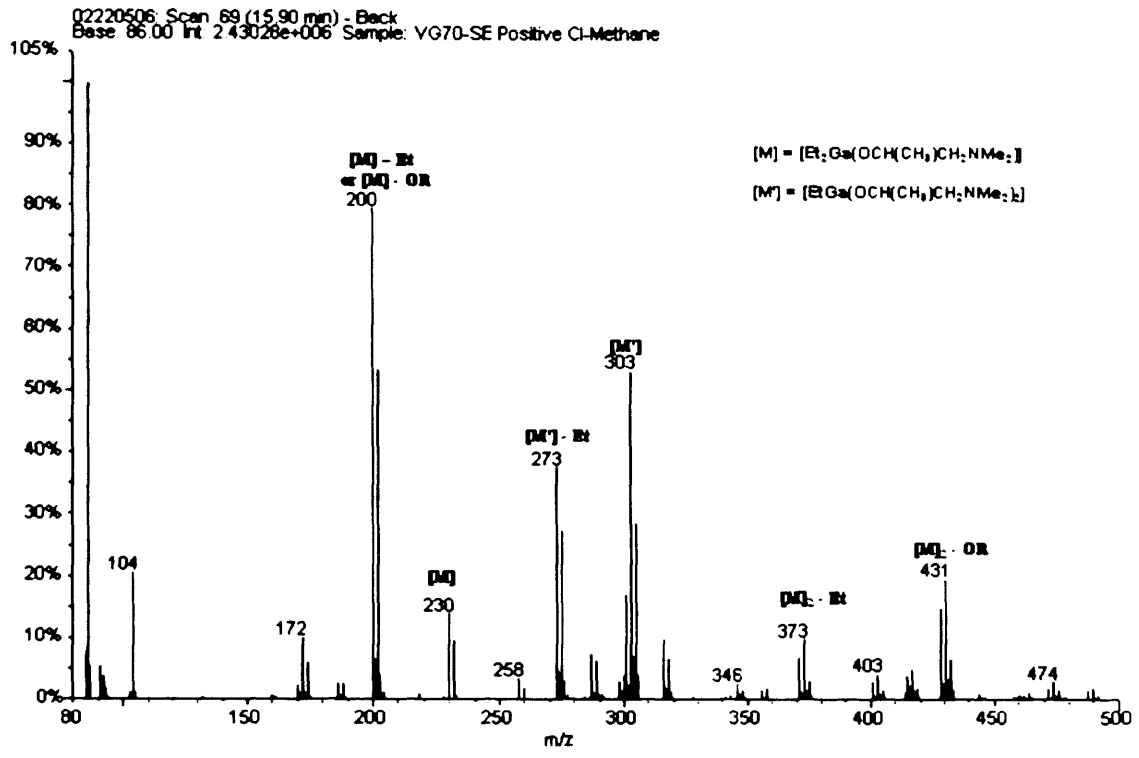

Figure 2.15: Mass spectrum for the reaction of Et_3Ga and six equivalents of $HOCH(CH_3)CH_2NMe_2$.

The mixture of **12** and **17** was obtained as an oil after work of the reaction mixture. Numerous attempts to obtain crystals of **17** failed with only X-ray quality crystals of **12** being isolated. However, it is assumed that **17** would adopt a structure similar to $[EtGa(OCH_2CH_2NMe_2)_2]$, **3** and **6**.

2.2.27 Reaction of Et_3Ga and 6 equivalents of $HOC(CH_3)_2CH_2OMe$

Reaction of Et_3Ga with excess $HOC(CH_3)_2CH_2OMe$ in toluene under reflux conditions for 24 h afforded a 1 : 3 mixture of the diethylgallium mono(alkoxide) $[Et_2Ga(OC(CH_3)_2CH_2OMe)]_2$ **13** and the ethylgallium bis(alkoxide) $[EtGa(OC(CH_3)_2CH_2OMe)_2]$ **(18)**. Spectroscopic data confirmed the formation of a 1 : 3 mixture of compounds **13** and **18**.

$$Et_3Ga + 6\,HOC(CH_3)_2CH_2OMe \xrightarrow{\Delta} [Et_2Ga(OC(CH_3)_2CH_2OMe)]_2 + 3\,[EtGa(OC(CH_3)_2CH_2OMe)_2] \quad (2.34)$$

(13) **(18)**

The ^1H NMR spectrum of the product identified a mixture of the dimeric diethyl gallium mono(alkoxide) **13** and monoethylgallium bis(alkoxide) **18**. These two complexes can be distinguished by the difference in peak positions of the $GaCH_2CH_3$ and $GaCH_2CH_3$ resonances. In complex **13**, the $GaCH_2CH_3$ peak is found at δ 0.64 (integrated to 8 protons) and in complex **18** at δ 0.60 (integrated to 6 protons). The $GaCH_2CH_3$ peak in complex **13** is found at δ 1.38 (12H) and in complex **18** at δ 1.27 (9H). Analysis of the observed proton integrations for the ethyl group correlate to the calculated values for a 1 : 3 product mixture of **13** and **18**. The proton resonances of the alkoxide ligand vary little within both complexes and so cannot be distinguished. The ^{13}C NMR confirms that both the dimeric diethylgallium monoalkoxide complex **13** and complex **18** are present, as two environments are observed for both the ethyl and alkoxide groups. The mass spectrum of the product also confirmed the presence of both complexes. Strong molecular ion peaks are observed at *m/z* = 433, 359 and 230 arising from the molecular fragmentation of the dimeric structure **13**. A strong molecular ion peak *m/z* = 301 is identified for the monomeric complex **18**. The mixture of **13** and **18** was isolated as a white crystalline compound after work up of the reaction mixture. In a similar manner to compounds **16**, and **17**, recrystallisation of the mixture only yielded single crystals of **13** and it was not possible to separate the two compounds.

2.2.28 Reaction of Et_3Ga and 6 equivalents of $HOCH_2CH_2OMe$

Treatment of Et_3Ga with excess of $HOCH_2CH_2OMe$ in toluene under reflux conditions for 24h afforded a 1 : 1 mixture of the diethylgallium mono(alkoxide) $[Et_2Ga(OCH_2CH_2OMe)]_2$ **14** and the gallium bis(alkoxide) $[EtGa(OCH_2CH_2OMe)_2]$ **(19)**. Spectroscopic data confirmed the formation of a 1 : 1 mixture of compounds **14** and **19**.

$$Et_3Ga + 6\,HOCH_2CH_2OMe \xrightarrow{\Delta} [Et_2Ga(OCH_2CH_2OMe)]_2 + [EtGa(OCH_2CH_2OMe)_2] \quad (2.35)$$

(14) **(19)**

The ^1H NMR spectrum of the product identified a mixture of the dimeric diethylgallium mono(alkoxide) complex **14** and monoethylgallium bis(alkoxide) complex **19**. In complex **14**, the $GaCH_2CH_3$ peak is found at δ 0.68 (integrated to 8 protons) and in complex **19** at δ 0.71 (integrated to 2 protons). The $GaCH_2CH_3$ peak in complex **14** is observed at δ 1.24 (integrated to 12 protons) and in complex **19** at δ 1.32 (integrated to 3 protons). Analysis of the observed proton integrations correlate to the calculated values for a 1 : 1 product mixture of **19** and **14**. Furthermore, the ^{13}C NMR shows two environments for each of the carbon atoms of the ethyl and alkoxide groups, further confirming the presence of two complexes, complex **14** and complex **19**. The mass spectrum of the product revealed a strong ion peak at *m/z* = 173, arising from the molecular fragmentation of the dimeric structure **14**. A strong molecular ion peak at *m/z* = 404 corresponding to the dimeric structure of **14** was also observed. Additionally, strong ion peaks at *m/z* = 377, 331 and 202 are observed arising from the molecular fragmentation of the monoethylgallium bis(alkoxide) **19**. It was not possible to separate compound **19** from **14** *via* crystallisation. These compounds were obtained as a crystalline white solid and using a range of solvents for recrystallisation only yielded crystals of **14**.

2.2.29 Summary

In general, a number of methods were attempted to separate the diethylgallium mono(alkoxide) from the ethylgallium bis(alkoxide). Sublimation was attempted, particularly where oils were obtained as the crude product. Thus, the oils were warmed gently under vacuum. This was the method was successful in yielding X-ray quality crystals of $[EtGa(OCH_2CH_2NMe_2)_2]$.[36] However, all attempts with these mixtures were unsuccessful. Fractional crystallisation methods also failed to separate the compounds and isolate the ethylgallium bis(alkoxide). Due to all the mixtures being oils elemental analysis could not be obtained. It is likely that these complexes could only be isolated from a more direct synthesis. For example, the side products $[ClGa(NMe_2)_2]$ on reaction with ROH yielded $[ClGa(OR)_2]$ (section 2.2.2).

2.2.30 Synthesis of dialkyl indium mono(alkoxides)

As described earlier the 1 : 1 reaction of Et_3Ga and ROH resulted in high yields of $[Et_2GaOR]_2$. In a similar manner, the reaction of Me_3In and ROH was also investigated to yield donor functionalised indium mono(alkoxides) of the type, $[Me_2InOR]_2$, for precursors for use in chemical vapour deposition.

2.2.31 Reaction of Me_3In and one equivalent of $HOCH_2CH_2NMe_2$

Treatment of Me_3In with one equivalent of $HOCH_2CH_2NMe_2$ in toluene at -78 °C gave rise to a strongly exothermic reaction with violent evolution of methane gas. After work up, the resulting colourless oil was left to stand at room temperature for several days. X-ray quality colourless crystals of compound **(20)** were obtained in a 58% yield. Analytical and spectroscopic data for **20** indicated that dimeric $[Me_2In(OCH_2CH_2NMe_2)]_2$ had formed, as shown in Eq. 2.36.

$$Me_3In + HOCH_2CH_2NMe_2 \longrightarrow \underset{\textbf{(20)}}{1/2\ [Me_2In(OCH_2CH_2NMe_2)]_2} + CH_4 \qquad \textbf{(2.36)}$$

The ^1H NMR spectrum of **20** showed a resonance at δ 0.04 (singlet) corresponding to the methyl ligand. Peaks corresponding to the alkoxide ligand occur as a broad singlet at δ 2.99 (NCH_3), broad singlet at δ 3.89 (OCH_2CH_2N) and as a singlet at δ 4.13 (OCH_2CH_2N). The peaks for alkoxide and methyl ligands, each integrate to 10 and 6 protons, thus confirming the formation of a dialkylindium mono(alkoxide). The infra-red spectrum was recorded and shows the expected peaks at 658, 633 and 556 cm^{-1}, which are attributable to a characteristic In–C stretch and ring modes of the In_2O_2 unit, respectively. The mass spectrum was obtained from a solution of **20** in toluene, and an intense molecular ion peak at m/z = 642 was observed confirming the dimeric structure of the complex. In addition, at m/z = 556, an intense peak, corresponding to molecular fragmentation of the dimeric structure was observed. A molecular ion peak for the monomeric structure (m/z = 320) was also observed suggesting monomer-dimer equilibrium in solution; these fragments may also arise from the symmetric cleavage of the In_2O_2 ring. Interestingly a large peak corresponding to the ligand fragment ($OCH_2CH_2NMe_2$) is present and could provide some evidence of a potential

decomposition pathway to indium oxide. The structure of **20** was confirmed by X-ray crystallography, the details of which are described in section 2.2.32.

2.2.32 X-ray structure of $[Me_2In(OCH_2CH_2NMe_2)]_2$ (20)

The crystal structure of compound **20** was determined by X-ray crystallography, the results are shown in Figure 2.14; selected bond lengths and angles are given in Table 2.8. Compound **20** crystallised into the orthorhombic, *Pccn* space group. As shown in Figure 2.14, the compound adopts a dimeric molecular arrangement. The centrosymmetric, four-membered In_2O_2 ring, that is common to this type of complex,[32] is planar. Each indium atom in **20** adopts a distorted trigonal bipyramidal geometry with two methyl groups in equatorial positions. The bridging alkoxide groups are located in both axial and equatorial positions, while the nitrogen atom of the aminoalkoxide group is in the axial position with the N–In–O bond angle to the opposite, axial alkoxide group being 144.08(5)°. This large deviation from 180° is due to the constraints of the internal O–In–O angle (71.75(6) °) in the In_2O_2 ring and the geometry of the ligand. The sum of the bond angles in the equatorial plane of **20** is 359.93°, which is a measure of the planarity of the equatorial groups. The equatorial In–O bond length (2.1432(14) Å) is significantly shorter than the axial In–O bond distance (2.2358(14) Å) indicative of two active bonding In–O bond types. This In–O bond length is longer than the Ga–O bond lengths in analogous gallium compound **10**. This can be attributed to the larger covalent radius of indium (1.50 Å). Similar distorted trigonal bipryamidal geometry has been observed in the closely related intramoleculary stabilised indium mono(alkoxide) complexes of the type $[InMe_2(OC(CF_3)_2CH_2NHR)]_2$, R = CH_2CH_2OMe.[54] This structure is also dimeric in the solid state and consists of a planar In_2O_2 ring. The indium centre is also coordinated in a distorted trigonal bipyramidal geometry with comparable bond lengths and angles. The In–N distance (2.5161(16) Å) in **20**, can be attributed to N→ In dative bonding and is slightly longer than the N→Ga bond length in **10** (*av.* 2.43775 Å) .[12] The longer bond distance in the indium derivative is due to the larger covalent radius of indium with respect to gallium and the greater Lewis acidity of indium. The bond angles for C–Ga–C (125.35°) and O–Ga–N (149.63°) in **10** are smaller than corresponding angles in **20**, C–In–C 133.99(9)° and O–In–N 144.08(5)°. Thus, the elongation of the In–O bonds and constraints of the ligand cause a considerable deformation of the coordinate sphere of indium. The significant widening of the C–M–

C angles in the indium derivative has been observed previously in some related dimeric five coordinated diorganometallic compounds of group 13.[55] It is thought that the electron-pair repulsion of the M–C bonds could affect the C–M–C angles. In addition, this angle is also sensitive to the substituents on the bridging moiety.

Table 2.8: Selected bond lengths (Å) and angles (°) for $[Me_2In(OCH_2CH_2NMe)]_2$ **(20)**

In1–O1	2.1432(14)	In1–C5	2.1555(18)
In1–C6	2.1563(18)	In1–O1#1	2.2358(14)
In1–N1	2.5161(16)		
O1–In1–C5	116.33(7)	O1–In1–C6	109.61(7)
C5–In1–C6	133.99(9)	O1–In1–O1#1	71.75(6)
C5–In1–O1#1	96.98(8)	C6–In1–O1#1	99.35(8)
O1–In1–N1	72.66(5)	C5–In1–N1	94.35(8)
C6–In1–N1	96.90(8)	O1#1–In1–N1	144.08(5)

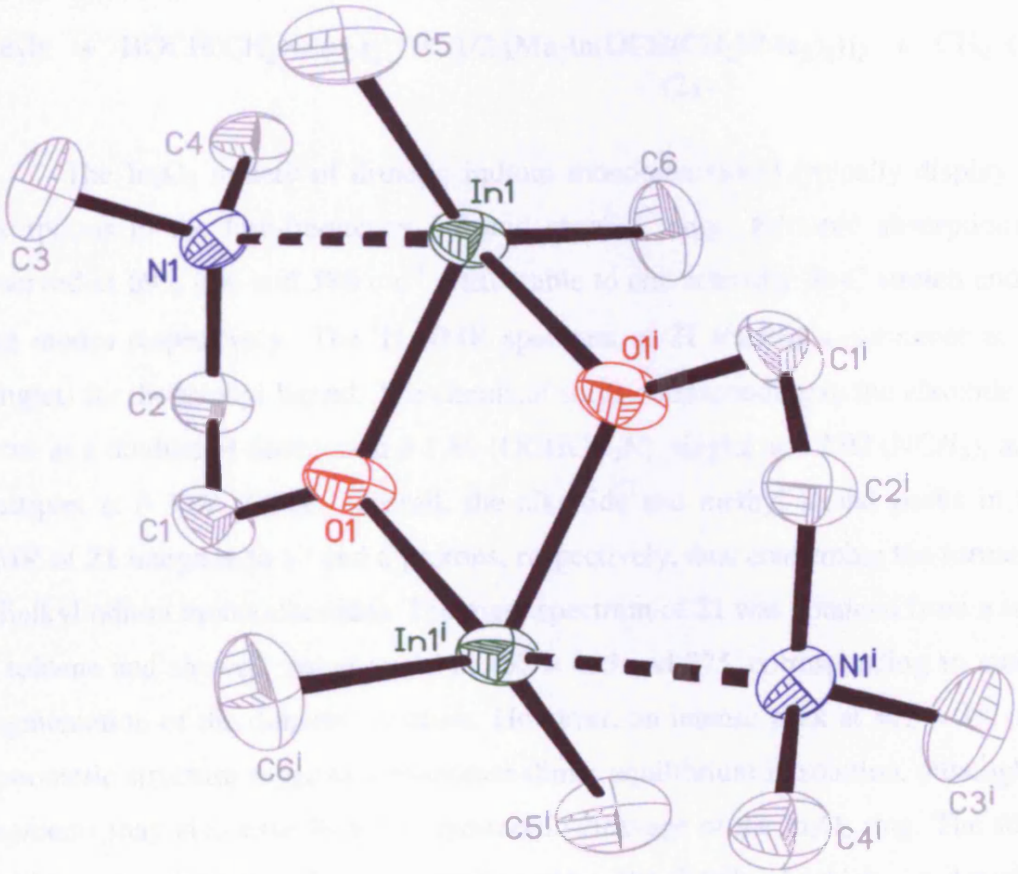

Figure 2.14: X-ray structure of $[Me_2In(OCH_2CH_2NMe_2)]_2$ **(20)**

2.2.33 Reaction of Me_3In and one equivalent of $HOCH(CH_2NMe_2)_2$

The reaction of Me_3In with one equivalent of $HOCH(CH_2NMe_2)_2$ in toluene at -78 °C resulted in a strongly exothermic reaction with evolution of methane. After work up, the resulting pale yellow oil was left to stand at room temperature for 24 h. Colourless crystals of compound **(21)** were isolated in a 69% yield. Analytical and spectroscopic data for **21** indicated that dimeric $[Me_2In(OCH(CH_2NMe_2)_2)]_2$ had formed, as shown in Equation 2.37.

$$Me_3In + HOCH(CH_2NMe_2)_2 \longrightarrow 1/2\,[Me_2In(OCH(CH_2NMe_2)_2)]_2 + CH_4 \quad \textbf{(2.37)}$$
$$\textbf{(21)}$$

The In_2O_2 moiety of dimeric indium mono(alkoxides) typically display strong absorptions in the low-frequency infrared spectral range. Infra-red absorptions were observed at 695, 666 and 588 cm^{-1} attributable to characteristic In–C stretch and In_2O_2 ring modes respectively. The ^1H NMR spectrum of **21** showed a resonance at δ 0.01 (singlet) for the methyl ligand. The chemical shifts corresponding to the alkoxide ligand occur as a doublet of doublets at δ 1.89 ($OCHCH_2N$), singlet at δ 2.02 (NCH_3), and as a multiplet at δ 3.80 (OCH). Overall, the alkoxide and methyl ligand peaks in the ^1H NMR of **21** integrate to 17 and 6 protons, respectively, thus confirming the formation of a dialkylindium mono(alkoxide). The mass spectrum of **21** was obtained from a solution of toluene and showed strong peaks at m/z = 435 and 275, corresponding to molecular fragmentation of the dimeric structure. However, an intense peak at m/z = 291 for the monomeric structure suggests a monomer-dimer equilibrium in solution, although these fragments may also arise from the symmetric cleavage of the In_2O_2 ring. The structure of **21** was confirmed by X-ray crystallography, the details of which are described in section 2.2.34.

2.2.34 X-ray structure of $[Me_2In(OCH(CH_2NMe_2)_2)]_2$ (21)

The X-ray structure of compound **21** was determined by X-ray crystallography, the results of which are shown in Figure 2.15; selected bond lengths and angles are given in Table 2.9. Compound **21** crystallised into the triclinic space group, $P\bar{1}$. As shown in Figure 2.15, compound **21** also exhibits a dimeric molecular arrangement similar to **18** and the gallium compounds, **3**, **6**, and **7**. The centrosymmetric, four-membered ring In_2O_3 ring is planar and each indium atom is six coordinate. The In–C

(*av.* 2.1475 Å) and In–O (*av.* 2.1927 Å) bond distances are elonagted with respect to the corresponding bonds in the gallium analogue **11**. In contrast to compound **11**, the alkoxide ligand coordinates to both indium centres simultaneously using the nitrogen atoms of the amino donor group. As expected, these dative In–N bond lengths are long (In1–N1 2.8329 Å and In1–N2 2.9302 Å) but shorter than the sum of the van der Waals radii of In and N.

The geometry of the indium coordination sphere in **21** can be considered as highly distorted octahedron. The distortions observed in **21** are the largest among the compounds described in this thesis. The most significant deviations from octahederal geometry are found in the N1–In–N2 angle (150.85°) and N1–In–O1, which is probably due to constraints imposed by the amino ligand. Significant deviations from octahedral geometry have been observed in other six-coordinate indium compounds.[56] Typically, distortions are observed due to constraints imposed by the ligands. In compound **21**, these would include a small O–In–O angle due to the In_2O_2 ring and the five-membered NInOCC rings.

Table 2.9: Selected bond lengths (Å) and angles (°) for $[Me_2In(OCH(CH_2NMe_2)_2)]_2$ **(21)**

In1–C8	2.141(3)	In1–C9	2.154(3)
In1–O1	2.1894(18)	In1–O1#1	2.1960(18)
In1–N1	2.8329(21)	In1–N2	2.9302(18)
C8–In1–C9	145.48(14)	C8–In1–O1	104.80(11)
C9–In1–O1	104.35(10)	C8–In1–O1#1	103.11(10)
C9–In1–O1#1	102.87(11)	O1–In1–O1#1	72.76(7)

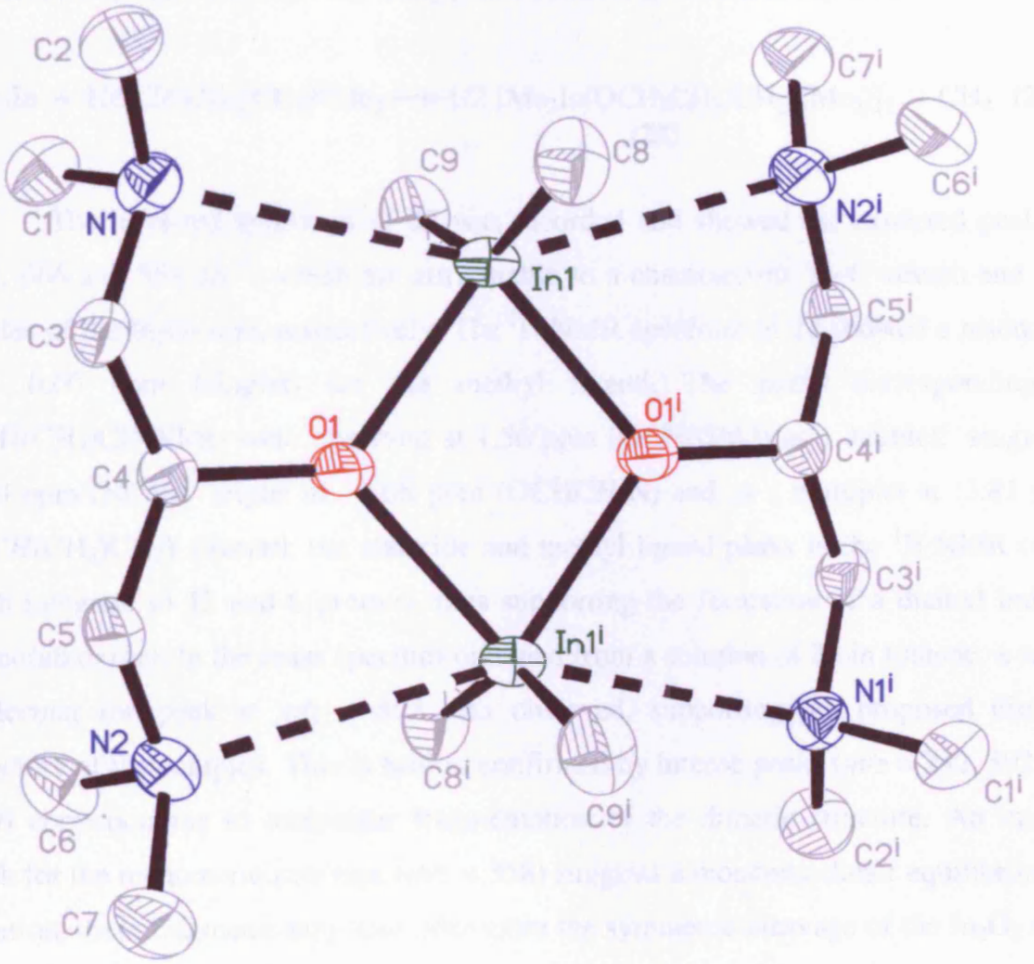

Figure 2.15: X-ray structure of $[Me_2In(OCH(CH_2NMe_2)_2)]_2$ **(21)**

2.2.35 Reaction of Me_3In with one equivalent of $HOCH(CH_3)CH_2NMe_2$

The analogous reaction of Me_3In with one equivalent of $HOCH(CH_3)CH_2NMe_2$ in toluene at -78 °C gave rise to a strongly exothermic reaction with violent evolution of methane gas. After work up, the resulting colourless oil was left to stand at room temperature for several days. X-ray quality colourless crystals of compound **(22)** in a 41% yield were obtained. Analytical and spectroscopic data for **22** indicated that dimeric $[Me_2In(OCH(CH_3)CH_2NMe_2)]_2$ had formed, as shown in Eq. 2.38.

$$Me_3In + HOCH(CH_3)CH_2NMe_2 \longrightarrow 1/2\,[Me_2In(OCH(CH_3)CH_2NMe_2)]_2 + CH_4 \quad \textbf{(2.38)}$$
$$\textbf{(22)}$$

The infra-red spectrum of **22** was recorded and showed the expected peaks at 695, 666 and 558 cm^{-1}, which are attributable to a characteristic In–C stretch and ring modes of the In_2O_2 unit, respectively. The ^1H NMR spectrum of **22** showed a resonance at 0.00 ppm (singlet) for the methyl ligand. The peaks corresponding to $OCH(CH_3)CH_2NMe_2$ were observed at 1.56 ppm ($OCH(CH_3)$) as a doublet, singlet at 1.90 ppm (NCH_3), triplet at 2.08 ppm ($OCHCH_2N$) and as a multiplet at 3.81 ppm ($OCH(CH_3)CH_2$). Overall, the alkoxide and methyl ligand peaks in the ^1H NMR of **22** each integrate to 12 and 6 protons, thus supporting the formation of a dialkyl indium mono(alkoxide). In the mass spectum obtained from a solution of **22** in toluene, a small molecular ion peak at m/z = 493 was observed, supporting the proposed dimeric structure of the complex. This is further confirmed by intense peaks (m/z = 232, 392 and 479) corresponding to molecular fragmentation of the dimeric structure. An intense peak for the monomeric structure (m/z = 358) suggests a monomer-dimer equilibrium in solution, these fragments may also arise from the symmetric cleavage of the In_2O_2 ring. Interestingly a large peak corresponding to the ligand fragment ($OCH(CH_3)CH_2NMe_2$) is observed and could provide some evidence of a potential decomposition pathway to indium oxide. The structure of **22** was confirmed by X-ray crystallography, the details of which are described in section 2.2.36.

2.2.36 X-ray structure of $[Me_2In(OCH(CH_3)CH_2NMe_2)]_2$ (22)

The X-ray structure of compound **22** was determined by X-ray crystallography, the results are shown in Figure 2.16: selected bond lengths and angles are given in Table 2.10. Compound **22** crystallised into the monoclinic space group $P2_1/n$. As shown

in Figure 2.16, compound **22** adopts a dimeric molecular arrangement. In the structure of **22** two independent molecules were present in the unit cell. The centrosymmetric, four-membered In_2O_2 ring that is common to this type of complex[32] is planar, and each indium atom adopts a distorted trigonal bipyramidal geometry with two methyl groups in equatorial positions. The bridging alkoxide groups are located in both axial and equatorial positions, while the nitrogen atom of the aminoalkoxide group is in the axial position with the average N–In–O bond angle to the opposite, axial alkoxide group being 146.50(5)°. This large deviation from 180° is due to the constraints of the internal In–O angle in the In_2O_2 ring and the geometry of the ligand. The sum of the bond angles in the equatorial plane of **22** is 359.96°, which is a measure of the planarity of the equatorial groups. The equatorial In–O bond lengths (*av.* 2.1342(12) Å) are significantly shorter than the axial In–O bond distance (*av.* 2.560(12) Å) indicative of two active bonding In–O bond types. The In–N distances (*av.* 2.5376(15) Å), can be attributed to N→In dative bonding and are slightly longer than the N→Ga in the related compound $[Me_2Ga(OCH_2CH_2NMe_2)]_2$. [12] This effect could be due to the larger Lewis acidity of indium in comparison to that of gallium.

Table 2.10: Selected bond lengths (Å) and angles (°) for $[Me_2In(OCH(CH_3)CH_2NMe_2)]_2$ **(22)**

In1–O1	2.1342(12)	In1–C7	2.150(2)
In1–C6	2.157(2)	In1–O1#1	2.2560(12)
In1–N1	2.5376(15)	In2–O11	2.1342(12)
In2–C17	2.1537(19)	In2–C16	2.1551(18)
In2–O11#2	2.2482(11)	In2–N11	2.5641(15)
O1–In1–C7	114.42(8)	O1–In1–C6	112.24(8)
C7–In1–C6	133.30(10)	O1–In1–O1#1	72.76(5)
C7–In1–O1#1	96.98(7)	C6–In1–O1#1	98.34(8)
O1–In1–N1	73.33(5)	C7–In1–N1	94.80(7)
C6–In1–N1	96.43(8)	O1#1–In1–N1	146.02(5)
O11–In2–C17	114.11(7)	O11–In2–C16	110.05(7)
C17–In2–C16	135.70(8)	O11–In2–O11#2	73.53(5)
C17–In2–O11#2	97.97(7)	C16–In2–O11#2	97.61(6)
O11–In2–N11	73.48(5)	C17–In2–N11	94.37(7)
C16–In2–N11	94.58(7)	O11#2–In2–N11	146.99(4)

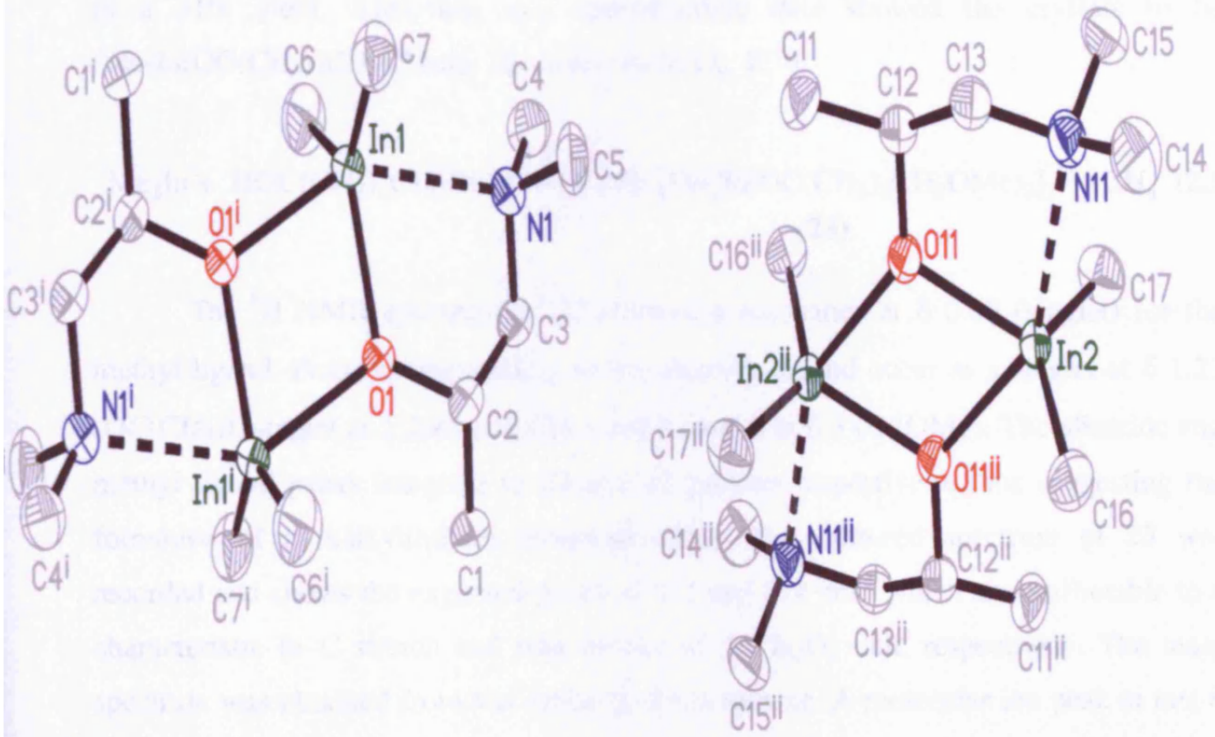

Figure 2.16: X-ray structure of $[Me_2In(OCH(CH_3)CH_2NMe_2)]_2$ **(22)**

2.2.37 Reaction of Me_3In and one equivalent of $HOC(CH_3)_2CH_2OMe$

The reaction of Me_3In with one equivalent $HOC(CH_3)_2CH_2OMe$ in toluene at -78 °C gave rise to a strongly exothermic reaction with violent evolution of methane gas. The resulting colourless solution was reduced in *vacuo* yielding a white solid. Recrystallisation from toluene at -20 °C afforded colourless crystals of compound **(23)** in a 51% yield. Analytical and spectroscopic data showed the crystals to be $[Me_2In(OC(CH_3)_2CH_2OMe)]_2$ **23**, as shown in Eq. 2.39.

$$Me_3In + HOC(CH_3)_2CH_2OMe \longrightarrow 1/2\ [Me_2In(OC(CH_3)_2CH_2OMe)_2]_2 + CH_4 \quad \textbf{(2.39)}$$
$$\textbf{(23)}$$

The ^1H NMR spectrum of **23** showed a resonance at δ 0.00 (singlet) for the methyl ligand. Peaks corresponding to the alkoxide ligand occur as a singlet at δ 1.23 ($OC(CH_3)$), singlet at δ 2.88 ($OCCH_2$) and a singlet at δ 3.03 (OMe). The alkoxide and methyl ligand peaks integrate to 22 and 12 protons respectively, thus suggesting the formation of a dialkylindium mono(alkoxide). The infra-red spectrum of **23** was recorded and shows the expected peaks at 612 and 514 cm^{-1} which are attributable to a characteristic In–C stretch and ring modes of the In_2O_2 unit, respectively. The mass spectrum was obtained from a solution of **23** in toluene. A molecular ion peak at *m/z* = 481 was observed for **23**. A further ion peak is observed at *m/z* = 393 arising from molecular fragmentation of the dimeric structure. The structure of **23** was confirmed by X-ray crystallography, the details which are described in section 2.2.38.

2.2.38 X-ray structure of $[Me_2In(OC(CH_3)_2CH_2OMe)]_2$ (23)

The X-ray structure of compound **23** was determined by X-ray crystallography, the results are shown in Figure 2.17; selected bond lengths and angles are given in Table 2.11. Compound **23** crystallised into the monoclinic space group, $P2_1/n$. As shown in Figure 2.17, compound **23** also exhibits a dimeric molecular arrangement as observed for **22**. The centrosymmetric, four-membered ring In_2O_2 is planar, and each indium atom adopts a distorted trigonal bipyramidal geometry with two methyl groups in equatorial positions. The bridging alkoxide groups are located in both axial and equatorial positions, while the oxygen atom of the methoxy group is in the axial position with the O–In–O bond angle to the opposite, axial alkoxide group being

143.37(4)°. The sum of the bond angles in the equatorial plane of **23** is 356.93°, which is a measure of the planarity of the equatorial groups. This is less than the expected 367° which is probably due to the O–In–O angles imposed by the In_2O_2 ring. The equatorial In(1)–O(1) bond length of 2.1433(13) Å is slightly shorter than that to the axial alkoxide oxygen atom with In(2)–O(2) distance of 2.2083(12) Å. The bond lengths observed in this compound are similar to those observed in the methyl derivative, $[Me_2Ga(O(CH_3)_2CH_2OMe)]_2$.[16] The equatorial Ga(1)–O(1) bond length in $[Me_2Ga(O(CH_3)_2CH_2OMe)]_2$ is 1.914(4) Å with the axial Ga(2)–O(2) distance being 1.999 (4) Å. As expected the Ga–O bond distances are shorter than the analogous In–O bond length in **23**. As expected the longest In-O bond distance is the O→In dative bond (2.5810(13) Å), resulting from interaction of the O atom of the methoxy group to the indium centre.

Table 2.11: Selected bond lengths (Å) and angles (°) for $[Me_2In(OC(CH_3)CH_2OMe)]_2$ **(23)**

In1–O1	2.1433(13)	In1–C7	2.146(2)
In1–C6	2.154(2)	In1–O1#1	2.2083(12)
In1–O2	2.5810(13)		
O1–In1–C7	113.75(8)	O1–In1–C6	111.04(7)
C7–In1–C6	132.14(9)	O1–In1–O1#1	74.17(5)
C7–In1–O1#1	103.54(7)	C6–In1–O1#1	103.99(7)
O1–In1–O2	69.27(4)	C7–In1–O2	89.25(7)
C6–In1–O2	91.31(7)	O1#1–In1–O2	143.37(4)

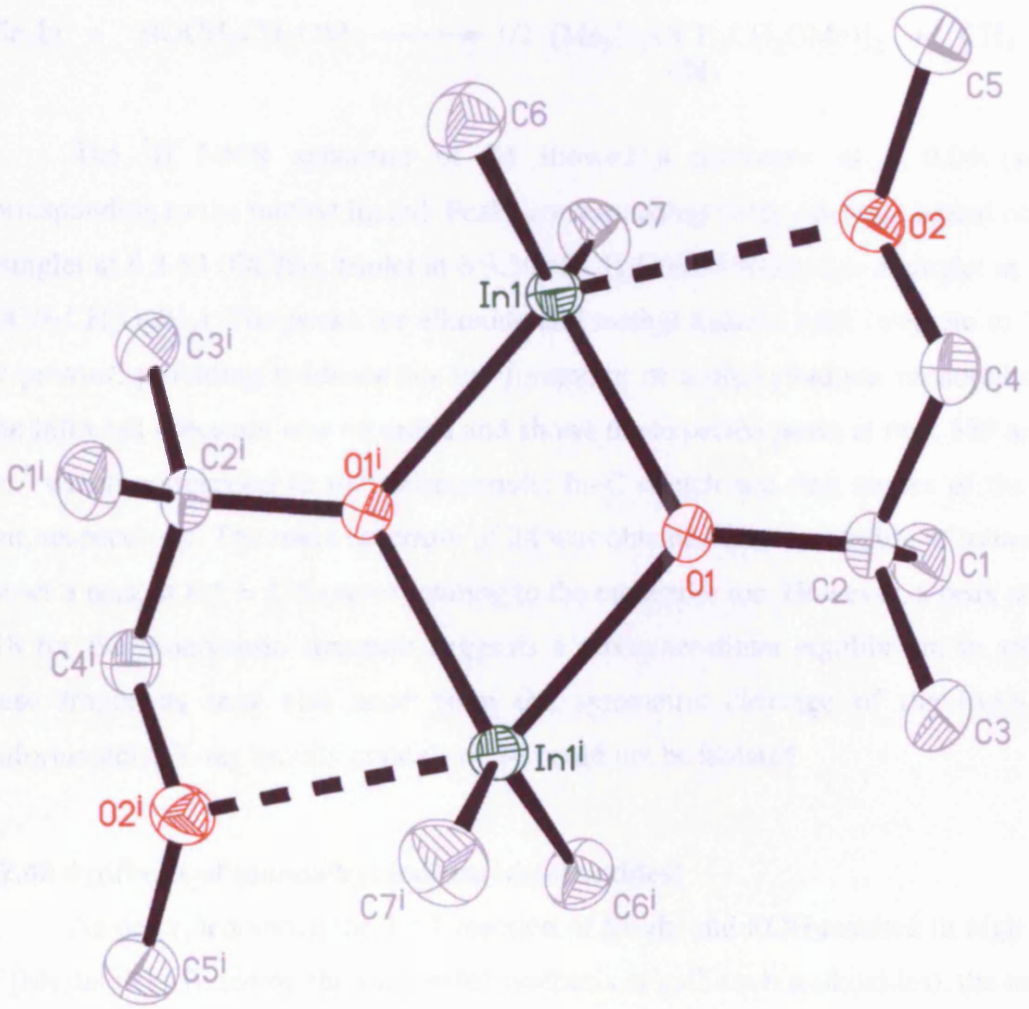

Figure 2.17: X-ray structure of $[Me_2In(OC(CH_3)_2CH_2OMe)]_2$ **(23)**

2.2.39 Reaction of Me_3In and one equivalent of $HOCH_2CH_2OMe$

Treatment of Me_3In with one equivalent of $HOCH_2CH_2OMe$ in toluene at -78 °C gave rise to a strongly exothermic reaction with violent evolution of methane gas. After work up, compound **(24)** was obtained as a white microcrystalline solid in a 91 % yield. Analytical and spectroscopic data for **24** indicated that dimeric $[Me_2In(OCH_2CH_2OMe)]_2$ had formed, as shown in Eq. 2.40.

$$Me_3In + HOCH_2CH_2OMe \longrightarrow \underset{\textbf{(24)}}{1/2\ [Me_2In(OCH_2CH_2OMe)]_2} + CH_4 \quad \textbf{(2.40)}$$

The ^1H NMR spectrum of **24** showed a resonance at δ 0.04 (singlet) corresponding to the methyl ligand. Peaks corresponding to the alkoxide ligand occur as a singlet at δ 3.33 (OCH_3), triplet at δ 3.39 ($OCH_2CH_2OCH_3$) and as a singlet at δ 3.73 ($OCH_2CH_2OCH_3$). The peaks for alkoxide and methyl ligands, each integrate to 14 and 12 protons, providing evidence for the formation of a dialkylindium mono(alkoxide). The infra-red spectrum was recorded and shows the expected peaks at 666, 589 and 518 cm^{-1} which correspond to the characteristic In–C stretch and ring modes of the In_2O_2 unit, respectively. The mass spectrum of **24** was obtained from a solution of toluene and shows a peak at *m/z* = 438 corresponding to the molecular ion. However, a peak at *m/z* = 218 for the monomeric structure suggests a monomer-dimer equilibrium in solution, these fragments may also arise from the symmetric cleavage of the In_2O_2 ring. Unfortunately, X-ray quality crystals of **24** could not be isolated.

2.2.40 Synthesis of monoalkyl indium bis(alkoxides)

As described above the 1 : 1 reaction of Me_3In and ROH resulted in high yields of $[Me_2InOR]_2$. Based on the successful synthesis of gallium bis(alkoxides), the reaction of Me_3In and excess alcohol at elevated temperatures was investigated in an attempt to isolate indium bis(alkoxides).

2.2.41 Reaction of Me_3In and 6 equivalents of $HOCH_2CH_2NMe_2$

Reaction of Me_3In with an excess of $HOCH_2CH_2NMe_2$ in toluene under reflux conditions for 24 h afforded a 1 : 7 mixture of the dimethylindium mono(alkoxide) $[Me_2In(OCH_2CH_2CH_2NMe_2)]_2$ **(20)** and the methylindium bis(alkoxide)

[MeIn(OCH$_2$CH$_2$NMe$_2$)$_2$] (**25**). Spectroscopic data confirmed the formation of a 1 : 7 mixture of compounds **20** and **25**.

$$Me_3In + 6\,HOCH_2CH_2NMe_2 \xrightarrow{\Delta} 1\,[Me_2In(OCH_2CH_2NMe)]_2\ (\mathbf{20}) + 7\,[MeIn(OCH_2CH_2NMe)_2]\ (\mathbf{25}) \qquad (2.41)$$

The ^{1}H NMR spectrum of the product identified a mixture of the dimeric dimethyl indium mono(alkoxide) complex **20** and methylindium bis(alkoxide) complex **25**. These two complexes can be distinguished by the difference in peak position of the Me-In resonances. In complex **20**, the Me–In peak is found at δ 0.09 (integrated to 12 protons) and in complex **25** at δ 0.12 (integrated to 21 protons). Although the proton resonances of the alkoxide ligand vary little within both complexes, the NC*H*$_3$ is observed in complex **20** at δ 3.06 (integrated to 12 protons) and at δ 3.09 in complex **25** (integrated to 18 protons). Analysis of the observed proton integrations correlate to the calculated values for a 1 : 7 product mixture of **25** and **20**. ^{13}C NMR shows two environments for each of the carbon atoms of the methyl and alkoxide groups further confirming the presence of the two species, **20** and **25**. Mass spectrum of the product also confirmed the presence of both complexes. A molecular ion peak at *m/z* = 466 was observed from the dimeric structure of **20**. A further strong ion peak was observed at 378 arising from the molecular fragmentation of the dimeric structure of the dimethyl indium alkoxide **20**. Additionally, a strong molecular ion peak at *m/z* = 218 was observed for the molecular fragmentation of **25**. Unfortunately, even after repeated crystallisations using a range of solvents, X-ray quality crystals of **25** could not be isolated. Furthermore, attempts to isolate crystals of **25** *via* sublimation also failed.

2.2.42 Reaction of Me$_3$In and 6 equivalents of HOCH(CH$_2$NMe$_2$)$_2$

Treatment of Me$_3$In with excess of HOCH(CH$_2$NMe$_2$)$_2$ in toluene under reflux conditions for 24 h afforded a 1 : 3 mixture of the dimethylindium mono(alkoxide) [Me$_2$In(OCH(CH$_2$NMe$_2$)$_2$)]$_2$ (**21**) and the methylindium bis(alkoxide) [MeIn(OCH(CH$_2$NMe$_2$)$_2$)$_2$] **26**. Analytical data confirmed the formation of a 1 : 3 mixture of compounds **21** and **26**.

$$Me_3In + 6\ HOCH(CH_2NMe_2)_2 \xrightarrow{\Delta} 1\ [Me_2In(OCH(CH_2NMe_2)_2)]_2\ (\mathbf{21}) + 3\ [MeIn(OCH(CH_2NMe_2)_2)_2]\ (\mathbf{26}) \quad (\mathbf{2.42})$$

The ^1H NMR spectrum of the product identified a mixture of the dimeric dimethylindium mono(alkoxide) complex **21** and monomethylindium bis(alkoxide) complex **26**. These two complexes can be distinguished by the difference in peak position of the methyl ligand resonances. In complex **26**, the Me–In peak is found at δ -0.03 (integrating to 9H) and in complex **21** at δ 0.01 (integrated to 12H). Peaks corresponding to the alkoxide ligand occur as a singlet at δ 2.09 (NCH_3), doublet of doublet at δ 2.19 and 2.30 ($OCHCH_2N$) and as a multiplet at δ 3.81 in complex **26**. In compound **21** these peaks are observed as a singlet at δ 2.02 (NCH_3), doublet of doublet at δ 1.84 and 2.10 ($OCHCH_2N$) and as a mulitpet at δ 3.89 (OCH). ^{13}C NMR shows two environments for each of the carbon atoms of the methyl and alkoxide groups further confirming the presence of the two species, complexes **26** and **21**. Mass spectrum of the product revealed strong ion peak at *m/z* = 435 arising from the molecular fragmentation of the dimeric structure **21** and one at *m/z* = 291 from the fragmentation of the monomeric structure if **26**. Additionally, a strong ion peaks at *m/z* = 275 was observed arising from the molecular fragmentation of the monomethylindium bis(alkoxide) **26**. Unfortunately, X-ray quality crystals of **26** could not be isolated.

2.2.43 Reaction of Me_3In and 6 equivalents of $HOCH(CH_3)CH_2NMe_2$

The analogous reaction of Me_3In with excess $HOCH(CH_3)CH_2NMe_2$ in toluene under reflux conditions for 24 h afforded a 1 : 3 mixture of the dimethylindium alkoxide $[Me_2In(OCH(CH_3)CH_2NMe_2)]_2$ **(22)** and the methylindium bis(alkoxide) $[MeIn(OCH(CH_3)CH_2NMe_2)_2]$ **(27)**. Spectroscopic data confirmed the formation of a 1 : 3 mixture of compounds **(22)** and **(27)**.

$$Me_3In + 6\ HOCH(CH_3)CH_2NMe_2 \xrightarrow{\Delta} 1\ [Me_2In(OCH(CH_3)CH_2NMe_2)]_2\ (\mathbf{22}) + 3\ [MeIn(OCH(CH_3)CH_2NMe_2)_2]\ (\mathbf{27}) \quad (\mathbf{2.43})$$

The ^{1}H NMR spectrum (Figure 2.20) of the product identified a mixture of the dimeric dimethylindium mono(alkoxide) complex **22** and monomethylindium bis(alkoxide) **27**. These two complexes can be distinguished by the difference in peak position of the Me–In resonances. In complex **27**, the Me–In peak is found at δ -0.03 (integrated to 9 protons) and in complex **22** at δ 0.01 (integrated to 12 protons). Although the proton resonances of the alkoxide ligand vary little within both complexes, the OCH(CH_3) is observed in complex **27** at δ 1.12 (integrated to 18 protons) and at δ 1.15 in complex **22** (integrated to 6 protons). Analysis of the observed proton integrations correlate to the calculated values for a 1 : 3 product mixture of **22** and **27**.

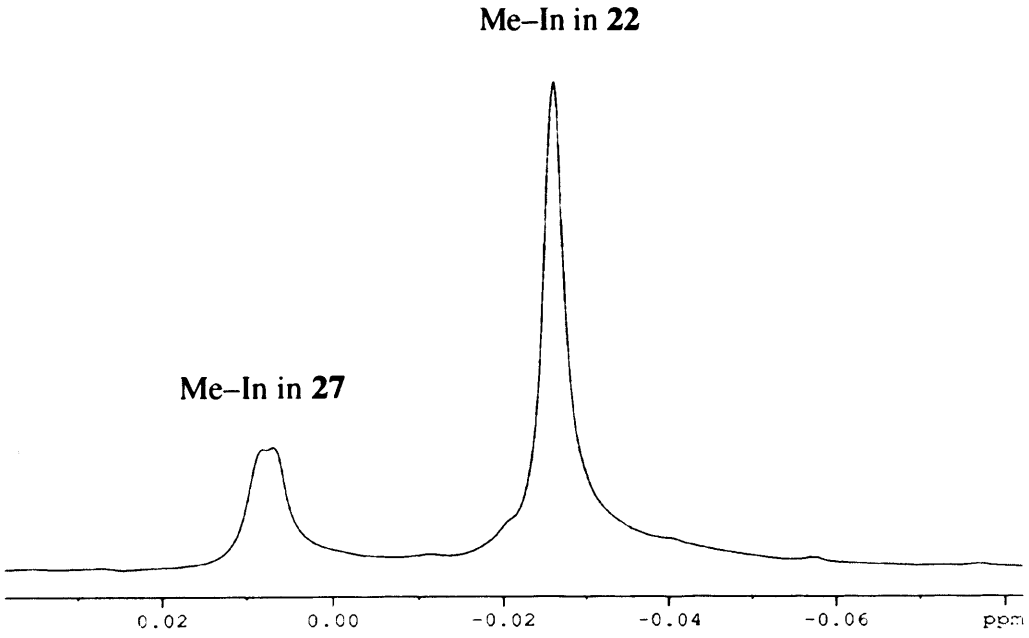

Figure 2.20: ^{1}H NMR spectrum showing two peaks arsisng from the Me–In in compounds **22** and **27**.

The ^{13}C NMR (Figure 2.21) shows two environments for each of the carbon atoms of the methyl and alkoxide groups further confirming the presence of two the species, **27** and **22**.

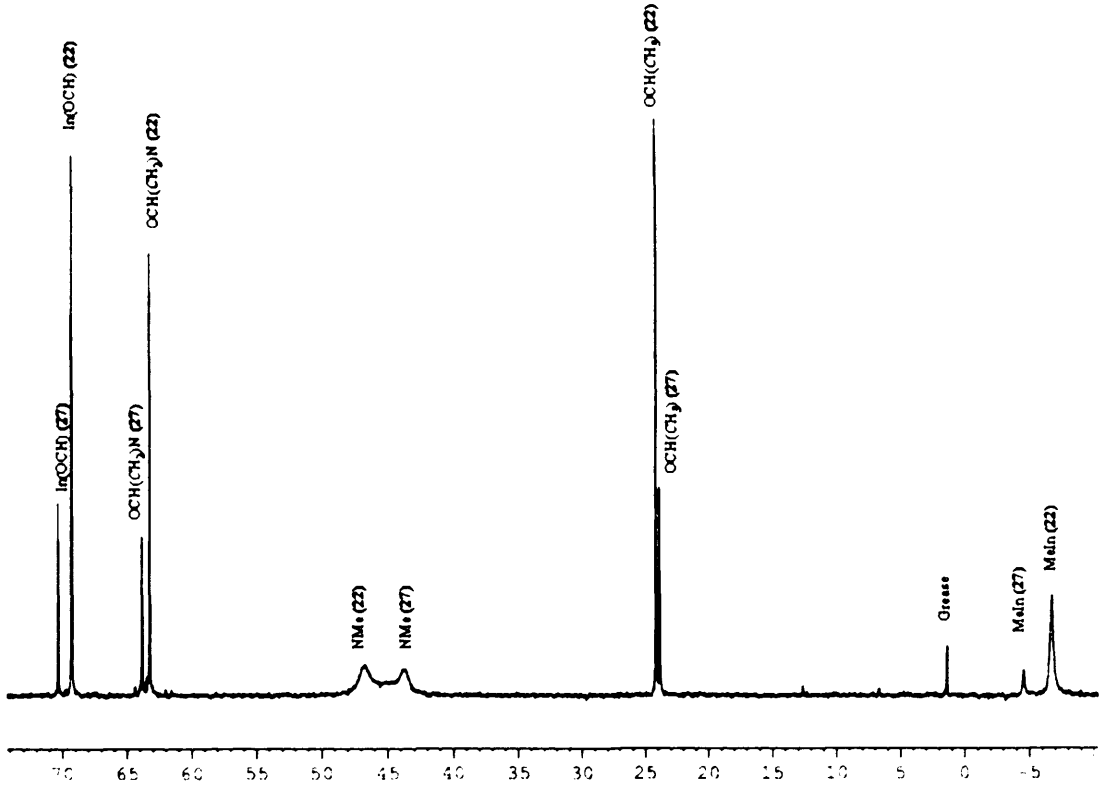

Figure 2.21: ^{13}C NMR spectrum for the reaction of Me_3In and six equivalents of $HOCH(CH_3)CH_2NMe_2$.

Mass spectrum of the product also confirmed the presence of both complexes (Figure 2.22). A molecular ion peak at *m/z* = 493 was observed from the dimeric structure of **22**. Strong ion peaks *m/z* = 479, 392 and 248 corresponding to molecular fragmentation of the dimeric structure of complex **22** are also observed. A strong ion peak at *m/z* = 232 corresponding to the molecular fragmentation of the monomeric structure of complex **22** was also present. Unfortunately, even after repeated crystallisations using a range of solvents, X-ray quality crystals of **27** could not be isolated. Furthermore, attempts to isolate crystals of **27** *via* sublimation also failed.

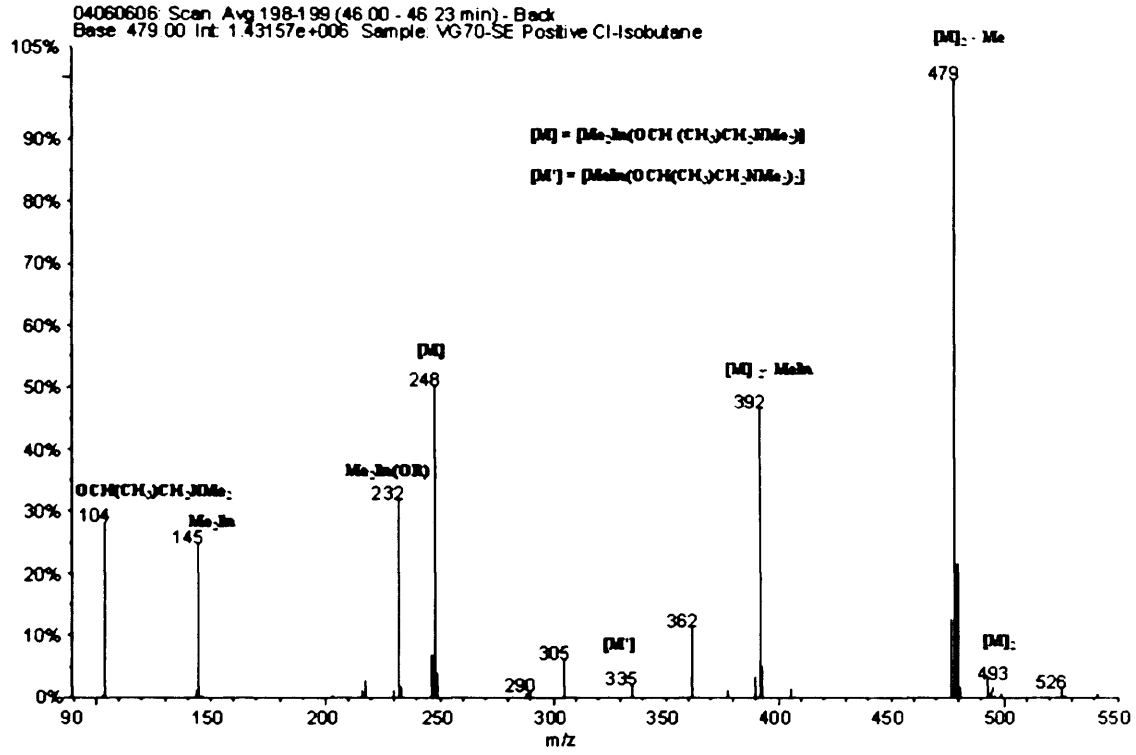

Figure 2.22: Mass spectrum of the reaction of Me_2In and six equivalents of $HOCH(CH_3)CH_2NMe_2$ showing the presence of the two complexes **22** and **27**.

2.2.43 Reaction of Me_3In and 6 equivalents $HOC(CH_3)_2CH_2OMe$

The reaction of Me_3In with excess of $HOC(CH_3)_2CH_2OMe$ in toluene under reflux conditions for 24 h afforded a 1 : 3 mixture of the dimethylindium alkoxide $[Me_2In(OC(CH_3)_2CH_2OMe)]_2$ **23** and the methylindium bis(alkoxide) $[MeIn(OC(CH_3)_2CH_2OMe)_2]$ **(28)**. Spectroscopic data confirmed the formation of a 1 : 3 mixture of compounds **23** and **28**.

$$Me_3In + 6\ HOC(CH_3)_2CH_2OMe \xrightarrow{\Delta} 1\ [Me_2In(OC(CH_3)_2CH_2OMe)]_2 + 3\ [MeIn(OC(CH_3)_2CH_2OMeMe)_2] \qquad (2.44)$$

(23) **(28)**

The ^{13}C NMR spectrum confirms that both the dimeric dimethylindium mono(alkoxide) complex **23** and monomethylindium bis(alkoxide) complex **28** were present, as two environments for methyl and alkoxide groups were observed. The ^{1}H NMR spectrum of the product identified a mixture of **23** and **28** due to the difference in

peak position of the Me–In resonances. In complex **28**, the Me–In peak is found at δ -0.018 (integrated to 9 protons) and in complex **23** at δ -0.016 (integrated to 6 protons). The proton resonances of the alkoxide ligand vary little within both complexes and so cannot be distinguished. The mass spectrum of the product also confirmed the presence of both complexes. A strong molecular ion peak was observed at *m/z* = 249 arising from the molecular fragmentation of the monomeric structure **28**. A strong molecular ion peak *m/z* = 481 was identified for the dimeric complex **23**. A further ion peaks at *m/z* = 393 arising from the molecular fragmentation of the dimeric structure is observed. Unfortunately, even after repeated crystallisations using a range of solvents, X-ray quality crystals of **28** could not be isolated.

2.2.45 Reaction of Me_3In and 6 equivalents of $HOCH_2CH_2OMe$

Treatment of Me_3In with excess of $HOCH_2CH_2OMe$ in toluene under reflux conditions for 24 h afforded a 1 : 2 mixture of the dimethylindium alkoxide $[Me_2In(OCH_2CH_2OMe)]_2$ **24** and the indium bis(alkoxide) $[MeIn(OCH_2CH_2OMe)_2]$ **(29)**. Spectroscopic data confirmed the formation of a 1 : 2 mixture of compounds **24** and **29**.

$$Me_3In + 6\ HOCH_2CH_2OMe \xrightarrow{\Delta} 1\ [Me_2In(OCH_2CH_2OMe)]_2\ (\mathbf{24}) + 2\ [MeIn(OCH_2CH_2OMe)_2]\ (\mathbf{29}) \quad \mathbf{(2.45)}$$

The ^1H NMR spectrum of the product identified a mixture of the dimeric dimethylindium mono(alkoxide) complex **24** and monomethylindium bis(alkoxide) complex **29**. These two complexes can be distinguished by the difference in peak position of the Me_2In resonances. In complex **24**, the Me–In peak is found at δ 0.02 (integrated to 12 protons) and in complex **29** at δ 0.00 (integrated to 6 protons). The OCH_3 peak is observed in complex **24** at δ 2.09 (6H) and at δ 2.34 in complex **29** (12H). Analysis of the observed proton integrations correlate to the calculated values for a 1 : 2 product mixture of **24** and **29**. The ^{13}C NMR shows two environments for each of the carbon atoms of the methyl and alkoxide groups further confirming the presence of the two species, **29** and **24**. The mass spectrum was obtained from a solution of in

toluene. An ion peak at *m/z* = 204 was observed for **29** arising from molecular fragmentation of the indium bis(alkoxide). Unfortunately, X-ray quality crystals of **29** could not be isolated.

2.2.46 Summary

A number of methods were attempted to separate the dimethylindium mono(alkoxide) from the methylindium bis(alkoxide). Sublimation was attempted, where the oils were warmed gently under vacuum. This was the method which was successful in yielding X-ray quality crystals of $[EtGa(OCH_2CH_2NMe_2)_2]$.[36] However, all attempts with these mixtures were unsuccessful. Fractional crystallisation methods also failed to separate the compounds and isolate the methylindium bis(alkoxide). The selected bond lengths and angles for the gallium and indium alkoxides are given in Table 2.12.

Table 2.12: Selected bond lengths and angles for gallium and indium alkoxides.

Compound	M–C (Å)*	M–O (Å)*	M–O' (Å)*	M–NMe_2 (Å)*	M–OMe (Å)*	O–M–O (°)	M–O–M (°)
3	-	1.841	1.842	2.1395	-	135.08	-
6	-	1.8381	1.8386	2.1606	-	118.80	-
8	-	1.886	1.9753	-	2.1613	76.30	103.7
10	1.9766	1.9229	2.0669	2.4398	-	74.48	105.50
11	1.9751	1.9152	2.0965	2.4398	-	74.83	105.17
12	1.979	1.919	2.088	2.5765	-	75.07	104.37
13	1.9742	1.9299	2.0141	-	2.626	77.27	102.73
20	2.1547	2.1432	2.2358	2.5765	-	71.75	108.25
21	2.1475	2.1894	2.1960	2.8816	-	72.76	107.24
22	2.1535	2.1342	2.2560	2.5509	-	72.76	107.24
23	2.150	2.1433	2.2083	-	2.5810	74.17	105.83

* Average bond lengths given

2.3 Experimental

2.3.1 General Procedures

All manipulations were performed under a dry, oxygen-free dinitrogen atmosphere using standard Schlenk techniques or in a Mbraun Unilab glovebox. All solvents used were stored in alumina columns and dried with anhydrous engineering equipment, such that the water concentration was 5–10 ppm. Epichem Ltd supplied triethylgallium and trimethylindium. All other reagents were procured commercially from Aldrich and used without further purification. Microanalytical data were obtained at University College London.

2.3.2 Physical Measurements

All ^{1}H and ^{13}C NMR spectra were obtained on a Bruker AMX300 and AMX400 spectrometer, operating at 299.87 MHz and 400.12 MHz respectively. All spectra were recorded using C_6D_6 and CD_2Cl_2 which were dried and degassed over molecular sieves prior to use; ^{1}H and ^{13}C chemical shifts are reported relative to $SiMe_4$ (δ 0.00). All IR spectra were recorded using a Shimadzu FTIR-8200 spectrometer, operating in the region of 4000-400 cm^{-1}. The IR samples were prepared using nujol. The mass spectra were obtained using a Micromass 70-SE spectrometer using Chemical Ionoisation (CI) with methne reagent gas. The Elemental Analysis (elemental analysis) was carried using Elemental Analyser (CE-440) (Exeter Analytical Inc). The instrument used for thermal analysis was the Netzsch Jupiter.

2.3.3 Synthesis of $[Ga(NMe_2)_3]_2$ (1)

A solution of $LiNMe_2$ (2.61 g, 51.1 mmol) in hexane (40 cm^3) was added dropwise to a stirred solution of $GaCl_3$ (3.00 g, 17.04 mmol) also in hexane (30 cm^3), at -78 °C with stirring over a 2 h period. The reaction mixture was allowed to warm slowly to room temperature and stirred for a further 24 h. The resulting white slurry was filtered using a filter stick and the solvent removed *in vacuo* to yield a clear solution. Cooling of this solution to -20 °C resulted in colourless crystals being formed after 24 h at this temperature. The crystals were dried under vacuum yielding $[Ga(NMe_2)_3]_2$ as a free-flowing white powder (4.29 g, 62%). Anal.Calc. (%) for $C_6H_{18}N_3Ga$: C, 35.68; H,

8.97, 20.81. Found (%): C, 35.17; H, 8.97; N, 20.14. ^{1}H NMR (CD_2Cl_2): δ/ppm 2.69 (s, μ-NCH_3, 12H), 2.68 (s, NCH_3, 24H). ^{13}C{^{1}H} NMR (CD_2Cl_2): δ/ppm 42.9 (NCH_3), 43.2 (μ-NCH_3). IR (cm^{-1}): 2814 s, 2767 s, 1463 s, 1259 s, 1128 m, 1040 w, 899 vs, 502 vs.

2.3.4 Synthesis of [Ga(OCH$_2$CH$_2$NMe$_2$)$_3$] (2)

HOCH$_2$CH$_2$NMe$_2$ (0.8 cm^3, 7.96 mmol) was added dropwise to a solution of [Ga(NMe$_2$)$_3$]$_2$ (0.5 g, 2.48 mmol) in hexane (20 cm^3) at -78 °C with stirring over a 0.5 h period. The reaction mixture was allowed to warm slowly to room temperature and stirred for 24 h. Removal of the solvent *in vacuo* afforded a clear oil (0.17g, yield 49%). ^{1}H NMR δ/ppm (C_6D_6): 2.00 (OCH$_2$CH_2N, 6H), 2.27 (NCH_3, 18H), 3.93 (OCH_2CH$_2$N, 6H). ^{13}C{^{1}H} NMR δ/ppm (C_6D_6): 43.9 (NCH_3), 58.7 (OCH$_2$$CH_2$N), 60.4 (O$CH_2CH_2$N). IR (cm^{-1}): 3256 vs, 2913 vs, 2191 s, 1974 vs, 1812 s, 1678 s, 1605 m, 1454 vs, 1405 s, 1368 s, 1350 s, 1327 m, 1272 s, 1185 m, 1156 m, 1084 s, 949 s, 887 s, 787 s, 731 s, 696 m, 623 vs, 561 s. Mass spec. (CI): (*m/z*) 474 ([Ga(OCH$_2$CH$_2$NMe$_2$)$_2$Cl–OCH$_2$CH$_2$NMe$_2$), 405 [Ga(OCH$_2$CH$_2$NMe$_2$)$_3$] OCH$_2$CH$_2$NMe$_2$Cl, 334 (Ga(OCH$_2$CH$_2$NMe$_2$)$_3$), 281 [Ga(OCH$_2$CH$_2$NMe$_2$)$_2$Cl], 245 (Ga(OCH$_2$CH$_2$NMe$_2$)$_2$), 194 Ga(OCH$_2$CH$_2$NMe$_2$)Cl, 158 (Ga(OCH$_2$CH$_2$NMe$_2$)), 88 (OCH$_2$CH$_2$NMe$_2$). The reaction flask was left at room temperature and X-ray quality crystals of compound **(3)** were obtained after several days.

2.3.5 Synthesis of [Ga(OCH(CH$_2$NMe$_2$)$_2$)$_3$] (4)

Compound **4** was prepared in the same manner as **2** using HOCH(CH$_2$NMe$_2$)$_2$ (1.18 cm^3, 6.37 mmol), [Ga(NMe$_2$)$_3$]$_2$ (0.5 g, 2.48 mmol) in hexane (20 cm^3). Removal of the solvent *in vacuo* afforded a yellow non-viscous oil. The reaction flask was left at room temperature and colourless crystals were obtained after several days (0.3 g, yield 48%). ^{1}H NMR δ/ppm (C_6D_6): 2.09 (s, NCH_3, 36H), 3.77 (m, OCHCH_2N, 12H), 4.12 (s, OCH, 3H). ^{13}C{^{1}H} NMR δ/ppm (C_6D_6): 46.1 (NCH_3), 64.6 (OCHCH$_2$N), 66.9 (OCH). IR (cm^{-1}): 3422 s, 2942 s, 2769 s, 1677 s, 1459 vs, 1326 s, 1263 s, 1198 s, 1172 vs, 1099 s, 12 s, 929 s, 877 s, 856 s, 832 s, 820 s, 654 s. Mass spec. (CI): (*m/z*) 433 Ga(OCH(CH$_2$NMe$_2$)$_2$Cl$_2$, 359 Ga(OCH(CH$_2$NMe$_2$)$_2$, 251 Ga(OCH(CH$_2$NMe$_2$)$_2$Cl, 147 (OCH(CH$_2$NMe$_2$)$_2$.

2.3.6 Synthesis of $[Ga(OCH(CH_3)CH_2NMe_2)_3]$ (5)

Compound **5** was prepared in the same manner as to **2** using $HOCH(CH_3)CH_2NMe_2$ (0.8 cm^3, 6.49 mmol), $[Ga(NMe_2)_3]_2$ (0.5 g, 2.48 mmol) and hexane (20 cm^3). Removal of the solvent *in vacuo* afforded a yellow non-viscous oil (0.22 g, yield 58%). ^1H NMR δ/ppm (C_6D_6): 1.09 (d, $OCH(CH_3)$, 6H, J = 5.8 Hz), 2.21–2.11 (broad, $OCHCH_2N$, 4H), 2.31 (broad, NCH_3, 12H), 3.86 (m, $OCH(CH_3)CH_2$, 2H). $^{13}C\{^1H\}$NMR δ/ppm (C_6D_6): 24.1 ($GaOCH(CH_3)$), 46.4 (NCH_3), 63.4 ($OCHCH_2N$), 69.4 ($GaOCH$). IR (cm^{-1}): 2924 s, 2361 m, 2342 m, 1457 vs, 1377 m, 1347 v, 1322 m, 1260 s, 1188 m, 1137 s, 1092 s, 1030 m, 1012 s, 955 s, 858 m, 836 m, 802 w, 722 s, 668 m, 637 s, 539 w, 496 m, 479 s. Mass spec. (CI): (*m/z*) 309 $[Ga(OCH(CH_3)CH_2NMe_2)_2Cl]$, 273 $(Ga(OCH(CH_3)CH_2NMe_2)_2)$, 102 $(OCH(CH_3)CH_2NMe_2)$. The reaction flask was left at room temperature and X-ray quality crystals of compound **(6)** were obtained after several. Anal. Calc. for $C_{10}H_{24}ClGaN_2O_2$: C, 39.06; H, 7.21; N, 9.11. Found: C, 38.88; H, 7.08; N, 7.97.

2.3.7 Synthesis of $[Ga(OC(CH_3)_2CH_2OMe)_3]$ (7)

Compound **7** was prepared in the same manner as **2** but using $HOC(CH_3)_2CH_2OMe$ (1.00 cm^3, 8.56 mmol), $[Ga(NMe_2)_3]_2$ (0.5 g, 2.48 mmol) in hexane (20 cm^3). Removal of the solvent *in vacuo* afforded a brown non-viscous oil (0.18 g, yield 60%). ^1H NMR δ/ppm (C_6D_6): 1.11 (s, $OC(CH_3)$, 6H), 2.89 (s, $GaOCCH_2$, 2H), 2.96 (s, OCH_3, 3H).). $^{13}C\{^1H\}$ NMR δ/ppm (C_6D_6): 26.3 ($OC(CH_3)$), 58.8 (OCH_3), 69.7 ($OCCH_2$), 81.4 ($OCCH_2$). IR (cm^{-1}): 2962 m, 2360 m, 1614 w, 1455 m, 1384 m, 1261 m, 1092 s, 1020 s, 799 s, 666 m. Mass spec. (CI): (*m/z*) 451 $Ga(OC(CH_3)_2CH_2OMe)_3Cl_2$, 379 $Ga(OC(CH_3)_2CH_2OMe)_3$-$OC(CH_3)CH_2OMe$, 290 $Ga(OC(CH_3)_2CH_2OMe)_2Cl_2$ - $OC(CH_3)_2CH_2OMe$, 245 $Ga(OC(CH_3)CH_2OMe)_2Cl_2$, 87 $(C(CH_3)_2CH_2OMe)$. The reaction flask was left at room temperature and X-ray quality crystals of compound **(8)** were obtained after several days Anal. Calc. for $C_5H_{11}Cl_2GaO_2$: C, 24.61; H, 4.55. Found: C, 25.02; H, 4.26.

2.3.8 Synthesis of $[Ga(OCH_2CH_2OMe)_3]$ (9)

Compound **9** was prepare in the same manner as **2** using $HOCH_2CH_2OMe$ (0.57cm^3, 6.37 mmol) and $[Ga(NMe_2)_3]_2$ (0.5 g, 2.48 mmol) in hexane (20 cm^3). Removal of the solvent *in vacuo* afforded a yellow non-viscous oil (0.19 g, yield 52%).

^{1}H NMR δ/ppm (C_6D_6): 3.23 (s, OCH_3, 9H), 3.43 (b, $OCH_2CH_2OCH_3$, 6H), 4.19 (t, $OCH_2CH_2OCH_3$, 6H). $^{13}C\{^1H\}$NMR δ/ppm (C_6D_6): 58.6 (OCH_3), 63.1 ($OCH_2CH_2OCH_3$), 72.6 ($OCH_2CH_2OCH_3$). IR (cm^{-1}): 2880 s, 2714 s, 2396 s, 2153 s, 1971 vs, 1606 s, 1455 vs, 1396 s, 1365 s, 1331 s, 1241 s, 1199 s, 1092 s, 964 s, 904 s, 842 s, 700 s, 733 s, 697 s. Mass spec. (CI): (*m/z*) 589 $[M]_2$, 515 $[M]_2$ - OCH_2CH_2OMe, 255 $Ga(OCH_2CH_2OMe)_2Cl$, 19 $Ga(OCH_2CH_2OMe)_2$.

2.3.9 Synthesis of $[Et_2Ga(OCH_2CH_2NMe_2)]_2$ (10)

$HOCH_2CH_2NMe_2$ (0.68 cm^3, 6.73 mmol) was added dropwise to a solution of Et_3Ga (1.00 cm^3, 6.37 mmol) in toluene (20 cm^3) at -78 °C with stirring over a 0.5 h period. The reaction mixture was allowed to warm slowly to room temperature and stirred for a further 24 h. Removal of the solvent *in vacuo* afforded a colourless oil. The reaction flask was left at room temperature and X-ray quality crystals were obtained after several days (2.65 g, yield 91%). Anal. Calc. for $C_8H_{20}NOGa$: C, 44.49; H, 9.33; N, 6.49. Found: C, 43.38; H, 9.32; N, 5.91. ^{1}H NMR δ/ppm (C_6D_6): 0.44 (quartet, $GaCH_2CH_3$, 4H, J = 8.1Hz), 1.29 (t, $GaCH_2CH_3$, 6H, J = 8.1 Hz), 1.98 (s, NCH_3, 6H), 2.01 (t, OCH_2CH_2N, 2H, J = 8.0 Hz), 3.49 (t, OCH_2CH_2N, 2H, J = 8.1 Hz). $^{13}C\{^1H\}$NMR δ/ppm (C_6D_6): 4.14 ($GaCH_2CH_3$), 11.0 ($GaCH_2CH_3$), 45.2 (NCH_3), 59.1 (OCH_2CH_2N), 61.7 (OCH_2). IR (cm^{-1}): 2924 vs, 2789 w, 2719 w, 2700 w, 1666 s, 1420 m, 1356 m, 1273 s, 1233 w, 1187 m, 1165 w, 1036 m, 1000 m, 954 m, 932 m, 894 m, 786 m, 629 m, 552 m, 504 m, 430 m. Mass spec. (CI): (*m/z*) 433 ([M]), 403 ([M]–Et), 344 ([M]–($OCH_2CH_2NMe_2$)), 216 ($Et_2Ga(OCH_2CH_2NMe_2)$), 186 ($EtGa(OCH_2CH_2NMe_2)$), 127 (Et_2Ga).

2.3.10 Synthesis of $[Et_2Ga(OCH(CH_2NMe_2)_2)]_2$ (11)

Compound **11** was prepared in the same manner as **10** using $HOCH(CH_2NMe_2)_2$ (2.35 cm^3, 6.37 mmol) and Et_3Ga (1.00 cm^3, 6.37 mmol) in toluene (20 cm^3). Removal of the solvent *in vacuo* afforded a yellow non-viscous oil. The reaction flask was left at room temperature and X-ray quality crystals were obtained after several days (1.64 g, yield 89%). Anal. Calc. for $C_{11}H_{27}ON_2Ga$: C, 48.38; H, 9.97; N, 10.26 Found: C, 48.37; H, 9.97; N, 10.63. ^{1}H NMR δ/ppm (C_6D_6): 0.58 (quartet, $GaCH_2CH_3$, 4H, J = 8.1 Hz), 1.41 (t, $GaCH_2CH_3$, 6H, J = 8.1 Hz), 2.04 (s, NCH_3, 12 H), 2.08 (d, $OCHCH_2N$, 2H), 3.81 (m, OCH, 1H). $^{13}C\{^1H\}$ NMR δ/ppm (C_6CD_6): 5.0 ($GaCH_2CH_3$), 10.8

($GaCH_2CH_3$), 46.2 (NCH_3), 66.7 ($OCHCH_2N$), 67.9 (OCH). IR (cm^{-1}): 3126 vs, 2927 vs, 2859 m, 2818 s, 2768 w, 2194 vs, 1323 s, 1262 vs, 1206 m, 1169 m, 1099 vs, 1033 vs, 959 w, 931 m, 901 m, 875 m, 855 w, 833 w, 820 w, 611 m, 615 m. Mass spec. (CI): (*m/z*) 401 ([M]–($OCH(CH_2NMe_2)_2$)), 243 ($Et_2Ga(OCH(CH_2NMe_2)_2)$),127 (Et_2Ga).

2.3.11 Synthesis of $[Et_2Ga(OCH(CH_3)CH_2NMe_2)]_2$ (12)

Compound **12** was prepared in the same manner as **10** using $HOCH(CH_3)CH_2NMe_2$ (0.83 cm^3, 6.37 mmol) and Et_3Ga (1.00 cm^3, 6.37 mmol) in toluene (20 cm^3). Removal of the solvent *in vacuo* afforded a yellow non-viscous oil. The reaction flask was left at room temperature and X-ray quality crystals were obtained after several days (1.42 g, yield 92%). Anal. Calc. for $C_9H_{22}NOGa$: C, 46.10; H, 9.64; N, 6.09. Found: C, 44.77; H, 9.28; N, 5.09. ^1H NMR δ/ppm (C_6D_6): 0.56 (quartet, $GaCH_2CH_3$, 4H, J = 8.0 Hz), 1.39 (t, $GaCH_2CH_3$, 6H, J = 8.0 Hz), 1.56 (d, $OCHCH_2N$, 2H, J = 6.10 Hz), 1.90 (s, NCH_3, 6H), 2.08 (t, $OCH(CH_3)CH_2$, 3H, 11.1 Hz)), 3.81 (m, $OCH(CH_3)CH_2$, 1H).$^{13}C\{^1H\}$ NMR δ/ppm (C_6D_6): 6.36 ($GaCH_2CH_3$), 11.6 ($GaCH_2CH_3$), 23.0 ($GaOCH(CH_3)$), 46.4 (NCH_3), 65.4 ($OCHCH_2N$), 69.5 (GaOCH). IR (cm^{-1}): 2926 vs, 2723 m, 1687 w, 1421 m, 1342 m, 1316 m, 1260 m, 1279 m, 1198 m, 1140 m, 1032 s, 947 s, 865 m, 837 m, 662 m, 619 m, 553 m, 519 m, 422 m. Mass spec. (CI): (*m/z*) 461 ([M]), 431 ([M]–Et), 358 ([M]–$OCH(CH_3)CH_2NMe_2$), 230 ($Et_2GaOCH(CH_3)CH_2NMe_2$), 200 ($EtGa(OCH(CH_3)CH_2$-$NMe_2)$), 127 (Et_2Ga).

2.3.12 Synthesis of $[Et_2Ga(OC(CH_3)_2CH_2OMe)]_2$ (13)

Compound **13** was prepared in the same way as **10** using $HOC(CH_3)_2CH_2OMe$ (0.79 cm^3, 6.37 mmol) and Et_3Ga (1.00 cm^3, 6.37 mmol) in toluene (20 cm^3). Removal of the solvent *in vacuo* afforded a caked white solid. The solid was redissolved in toluene (2 cm^3) and cooled to -20 °C. Compound **13** was obtained as a white microcrystalline solid after several days (1.50 g, yield 97%). Anal. Calc. for $C_9H_{21}O_2Ga$: C, 46.80; H, 9.16. Found: C, 46.26; H, 9.29. ^1H NMR δ/ppm (C_6D_6): 0.64 (quartet, $GaCH_2CH_3$, 4H, J = 16.1 Hz), 1.23 (s, $GaOC(CH_3)$, 6H), 1.40 (t, $GaCH_2CH_3$, 6H, J = 16.1 Hz), 2.88 (s, $GaOCCH_2$, 2H), 3.03 (s, OMe, 3H).$^{13}C\{^1H\}$ NMR δ/ppm (C_6D_6): 8.1 ($GaCH_2CH_3$), 10.5 ($GaCH_2CH_3$), 27.4 ($OC(CH_3)$), 58.4 (OCH_3), 72.6 ($OCCH_2$), 81.9 ($OCCH_2$). IR (cm^{-1}): 2923 vs, 2726 w, 1565 w, 1463 s, 1364 m, 1238

m, 1178 m, 1152 m, 1112 m, 1002 m, 961 m, 936 m, 918 m, 796 m, 658 m, 633 m, 556 m. Mass spec. (CI): (*m/z*) 433 ([M] – Et), 358/9 ([M] – ($OC(CH_3)_2CH_2OCH_3$), 231 ($Et_2Ga\ OC(CH_3)_2CH_2OCH_3$), 201 ($EtGaOC(CH_3)_2CH_2OCH_3$), 127 ($Et_2Ga$).

2.3.13 Synthesis of [$Et_2Ga(OCH_2CH_2OMe)$] (14)

Compound **14** was prepared in the same manner as **10** using $HOCH_2CH_2OMe$ (0.51 cm^3, 6.37 mmol), Et_3Ga (1.00 cm^3, 6.37 mmol) in toluene (20 cm^3). Removal of the solvent *in vacuo* afforded a caked white solid. The solid was redissolved in toluene (2 cm^3) and cooled to -20 °C. Compound **14** was obtained as a white microcrystalline solid after several days (1.50 g, yield 97%). ^1H NMR δ/ppm (C_6D_6): 0.75 (quartet, $GaCH_2CH_3$, 4H, J = 8.0 Hz), 1.58 (t, $GaCH_2CH_3$, 6H, J = 5.0 Hz), 2.99 (s, OCH_3, 3H), 3.45 (t, $OCH_2CH_2OCH_3$, 2H, J = 5.4 Hz), 3.83 (t, $OCH_2CH_2OCH_3$, 2H, J = 4.5 Hz). $^{13}C\{^1H\}$NMR δ/ppm (C_6D_6): 5.5 ($GaCH_2CH_3$), 10.1 ($GaCH_2CH_3$), 58.1 (OCH_3), 63.81 ($OCH_2CH_2OCH_3$), 73.9 ($OCH_2CH_2OCH_3$). IR (cm^{-1}): 2935 s, 2865 m, 2726 m, 2373 m, 2152 m, 2046 m, 1975 m, 1568 s, 1456 s, 1418 m, 1394 m, 1362 m, 1261 s, 1237 s, 1198 s, 1127 s, 1081 s, 1025 s, 960 s, 908 s, 849 s, 801 vs, 654 vs. Mass spec. (CI): (*m/z*) 438 $[M]_2$, 218 [M], 127 (Et_2Ga).

2.3.14 Synthesis of [$Et_2Ga(OCH(CH_3)_2)]_2$ (15)

Compound **15** was prepared in the same manner as **10** using $HOCH(CH_3)_2$ (1.78 cm^3, 6.37 mmol) and Et_3Ga (1.00 cm^3, 6.37 mmol) in toluene (20 cm^3). Removal of the solvent *in vacuo* afforded a caked white solid. The solid was redissolved in toluene (2 cm^3) and cooled to -20 °C. Compound **15** was obtained as a white microcrystalline solid after several days (1.13g, yield 90 %). Anal. Calc. for $C_7H_{17}OGa$: C, 46.80; H, 9.16. Found: C, 46.26; H, 9.29. ^1H NMR δ/ppm (C_6D_6): 0.62 (quartet, $GaCH_2CH_3$, 4H, J = 3.2, Hz), 1.32 (t, $GaCH_2CH_3$, 6H, J = 3.0 Hz), 0.99 (d, $OCH(CH_3)_2$, 6H, J = 1.95 Hz), 3.91 (septet, OCH, 1H, J = 3.0 Hz).$^{13}C\{^1H\}$ NMR δ/ppm (C_6D_6): 5.7 ($GaCH_2CH_3$), 10.0 ($GaCH_2CH_3$), 26.2 ($OCH(CH_3)_2$), 66.5 (OCH). IR(cm^{-1}): 2926 s, 2877 m, 2729 m, 2638 m, 1941 s, 1461 s, 1417 m, 1380 m, 1339 s, 1260 s, 1234 s, 1163 m, 1121 m, 1001 s, 962 m, 826 s, 653 s, 603 s. Mass spec. (CI): (*m/z*) 374 [M], 317 [M]-OR, 186 $Et_2Ga(OR)$, 127 (Et_2Ga).

2.3.15 Attempted synthesis of [EtGa(OCH$_2$CH$_2$NMe$_2$)$_2$]

$HOCH_2CH_2NMe_2$ (4.06 cm^3, 40.4 mmol) was added dropwise to a solution of Et_3Ga (1.00 cm^3, 6.37 mmol) in toluene (20 cm^3) at -78 °C with stirring over a 0.5 h period. The reaction mixture was allowed to warm slowly to room temperature and stirred for a further 24 h. Removal of the solvent *in vacuo* afforded a colourless oil of compound **10**. Anal. Calc. for $C_8H_{20}NOGa$: C, 44.49; H, 9.33; N, 6.49. Found: C, 44.18; H, 9.16; N, 6.41. ^{1}H NMR δ/ppm (C_6D_6): 0.57 (quartet, $GaCH_2CH_3$, 4H, J = 8.1Hz), 1.35 (t, $GaCH_2CH_3$, 6H, J = 8.1 Hz), 1.93 (s, NCH_3, 6H), 2.06 (t, OCH_2CH_2N, 2H, J = 8.0 Hz), 3.56 (t, OCH_2CH_2N, 2H, J = 8.1 Hz). ^{13}C {^{1}H} NMR δ/ppm (C_6D_6): 4.25 ($GaCH_2CH_3$), 11.1 ($GaCH_2CH_3$), 44.8 (NCH_3), 58.8 (OCH_2CH_2N), 61.3 (OCH_2). IR (cm^{-1}): 2926 s, 2860 w, 1461 s, 1420 m, 1379 w, 1356 s, 1262 s, 1187 s, 1096 s, 1036 s, 1000 m, 954 s, 932 s, 894 s, 786 m, 729 m, 629 s, 522 s, 504 vs, 429 vs. Mass spec. (CI): *(m/z)* 433 ([M]), 403 ([M]–Et), 344 ([M]–($OCH_2CH_2NMe_2$)), 216 ($Et_2Ga(OCH_2CH_2NMe_2)$), 186 ($EtGa(OCH_2CH_2NMe_2)$), 127 (Et_2Ga), 88 ($OCH_2CH_2NMe_2$).

2.3.16 Synthesis of [EtGa(OCH(CH$_2$NMe$_2$)$_2$)$_2$] (16) and (11)

Compound **16** was prepared in the same manner as **10** using $HOCH(CH_2NMe_2)_2$ (6.58 cm^3, 40.4 mmol), Et_3Ga (1.00 cm^3, 6.37 mmol) in toluene (20 cm^3). Removal of the solvent *in vacuo* afforded a yellow non-viscous oil. The reaction mixture was allowed to warm slowly to room temperature then heated under reflux for 24 h yielding a colourless solution. Removal of the solvent *in vacuo* afforded a pale yellow non-viscous oil composed of a 1 : 8 mixture of compound **11** and compound **16**. ^{1}H NMR δ/ppm (C_6D_6): Compound **11**: 0.57 (quartet, $GaCH_2CH_3$, 8H, J = 3.3 Hz), 1.41 (t, $GaCH_2CH_3$, 12H, J = 3.6Hz), 2.04 (s, NCH_3, 12H), 2.60 (broad, $OCHCH_2N$, 8H), 4.13 (m, OCH, 2H). Compound **16**: 0.55 (quartet, $GaCH_2CH_3$, 16H, J = 3.4 Hz), 1.44 (t, $GaCH_2CH_3$, 24H, J = 3.3 Hz), 2.16 (s, NCH_3, 192 H). ^{13}C {^{1}H} NMR δ/ppm (C_6D_6): Compound **11**: 4.8 ($GaCH_2CH_3$), 10.7 ($GaCH_2CH_3$), 45.7 (NCH_3), 64.3 (broad, $OCHCH_2N$), 67.9 (OCH). Compound **16**: 4.8 (broad, $GaCH_2CH_3$), 11.2 ($GaCH_2CH_3$), 46.6 (NCH_3), 64.3 (broad, $OCHCH_2N$), 66.8 (OCH). Mass spec. (CI): *(m/z)* Compound **16**: 273 $Et_2(Ga(OR))$. Compound **16**: 243 ([M]). Associated peaks: 186 ($[Et_2Ga(OCH(CH_2NMe_2))$, 128 (Et_2Ga).

2.3.17 Synthesis of [EtGa(OCH(CH$_3$)CH$_2$NMe$_2$)$_2$] (17) and (12)

Compound **17** was prepared in the same manner as **10** using HOCH(CH$_3$)CH$_2$NMe$_2$ (4.99 cm^3, 40.4 mmol), Et$_3$Ga (1.00 cm^3, 6.37 mmol) in toluene (20 cm^3). The reaction mixture was allowed to warm slowly to room temperature then heated under reflux for 24 h yielding a colourless solution. Removal of the solvent *in vacuo* afforded a pale yellow non-viscous oil composed of a 1 : 8 mixture of compound **12** and compound **17**. ^{1}H NMR δ/ppm (C_6D_6): Compound **12**: 0.50 (quartet, GaC*H*$_2$CH$_3$, 8H, J = 8.1 Hz), 1.24 (d, OCH(C*H*$_3$), 6H, J = 6.2 Hz), 1.38 (t, GaCH$_2$C*H*$_3$, 12H, J = 4.8 Hz), 1.75 (d, OCHC*H*$_2$N, 4H, J = 6.9 Hz), 2.16 (s, NC*H*$_3$, 12H), 3.98 (m, OC*H*(CH$_3$)CH$_2$, 2H). Compound **17**: 0.65 (quartet, GaC*H*$_2$CH$_3$, 16H, J = 7.6 Hz), 1.10 (d, OCH(C*H*$_3$), 48H, J = 6.1 Hz), 1.40 (t, GaCH$_2$C*H*$_3$, 24H, J = 4.9 Hz), 1.99 (t, OCHC*H*$_2$N, 32H, J = 10.8 Hz), 3.66 (m, OC*H*(CH$_3$)CH$_2$, 16H). ^{13}C{^{1}H} NMR δ/ppm (C_6D_6): Compound **12**: 11.2 (GaCH$_2$*C*H$_3$), 24.4 (OCH(*C*H$_3$)), 45.3 (N*C*H$_3$), 64.7 (OCH*C*H$_2$N), 68.4 (O*C*H). Compound **17**: 11.1 (GaCH$_2$*C*H$_3$), 24.1 (OCH(*C*H$_3$)), 45.7 (N*C*H$_3$), 64.4 (OCH*C*H$_2$N), 68.1 (O*C*H). Mass spec. (CI): *(m/z)* Compound **12**: (*m/z*) 431 ([M]$_2$ – Et), 373 ([M]$_2$–(CH$_3$-C(H)C(H)NMe$_2$)), 230 ([M]); Compound **17**: (*m/z*) 303 ([M]$^+$), 273 [M]–Et, 200 (EtGa(OCH(CH$_3$)CH$_2$NMe$_2$)). Associated peaks (*m/z*): 86 (CH$_3$C(H)C(H)NMe$_2$)

2.3.18 Synthesis of [EtGa(OC(CH$_3$)$_2$CH$_2$OMe)$_2$] (18) and (13)

Compound **18** was prepared in the same manner as **10** using HOC(CH$_3$)$_2$CH$_2$OMe (4.73 cm^3, 40.4 mmol) and Et$_3$Ga (1.00 cm^3, 6.37 mmol) in toluene (20 cm^3). The reaction mixture was allowed to warm slowly to room temperature then heated under reflux for 24 h yielding a colourless solution Removal of the solvent *in vacuo* afforded a white crystalline compound composed of a 1 : 3 mixture of compound **18** and compound **13**. ^{1}H NMR δ/ppm (C_6D_6): Compound **13**: 0.64 (quartet, GaC*H*$_2$CH$_3$, 8H, J = 8.00 Hz), 1.38 (t, GaCH$_2$C*H*$_3$, 12H, J = 8.01 Hz), 1.20 (s, GaOC(C*H*$_3$), 12H), 2.87 (t, GaOCC*H*$_2$, 4H, J = 8.2 Hz), 3.04 (OMe, 6H). Compound **18**: 0.60 (quartet, GaC*H*$_2$CH$_3$, 6H, J = 8.01 Hz), 1.27 (t, GaCH$_2$C*H*$_3$, 9H, J = 8.10 Hz). ^{13}C{^{1}H} NMR δ/ppm (C_6D_6): Compound **13**: 8.1 (GaCH$_2$CH$_3$), 10.4 (GaCH$_2$*C*H$_3$), 27.4 (OC(*C*H$_3$)), 58.4 (O*C*H$_3$), 72.6 (O*C*CH$_2$), 81.9 (OC*C*H$_2$). Compound **18**: 6.2 (GaCH$_2$CH$_3$), 10.2 (GaCH$_2$*C*H$_3$), 27.2 (OC(*C*H$_3$)), 58.1 (O*C*H$_3$), 72.2 (O*C*CH$_2$), 81.1 (OC*C*H$_2$). Mass spec. (CI): *(m/z)* Compound **18**: 433 ([M]–Et), 359 ([M]–(OC(CH$_3$)$_2$

CH_2OCH_3), 230 ($Et_2GaOC(CH_3)_2CH_2OCH_3$). Compound **18**: 301 [M^+], 201 ($EtGaOC(CH_3)_2CH_2OCH_3$). Associated peaks *(m/z)* 127 (Et_2Ga), 87 ($C(CH_3)_2CH_2OCH_3$).

2.3.19 Synthesis of [EtGa(OCH$_2$CH$_2$OMe)$_2$] (19) and (14)

Compound **19** was prepared in the same manner as **10** using $HOCH_2CH_2OMe$ (0.51 cm^3, 40.4 mmol) and Et_3Ga (1.00 cm^3, 6.37 mmol) in toluene (20 cm^3). The reaction mixture was allowed to warm slowly to room temperature then heated under reflux for 24 h yielding a colourless solution. Removal of the solvent *in vacuo* afforded a white crystalline compound composed of a 1 : 1 mixture of compound **19** and compound **14**. ^1H NMR δ/ppm (C_6D_6): Compound **14**: 0.68 (quartet, $GaCH_2CH_3$, 8H, J = 8.1 Hz), 1.29 (t, $GaCH_2CH_3$, 12H, J = 4.4 Hz), 3.04 (s, OCH_3, 6H), 3.51 (t, $OCH_2CH_2OCH_3$, 4H, J = 4.4 Hz), 3.73 (t, $OCH_2CH_2OCH_3$, 4H, J = 4.4 Hz). Compound **19**: 0.71 (quartet, $GaCH_2CH_3$, 2H, J = 8.2 Hz), 1.32 (t, $GaCH_2CH_3$, 3H, J = 4.7 Hz. $^{13}C\{^1H\}$ NMR δ/ppm (C_6D_6): Compound **14**: 4.3 ($GaCH_2CH_3$), 10.1 ($GaCH_2CH_3$), 58.3 (OCH_3), 62.7 ($OCH_2CH_2OCH_3$), 73.9 ($OCH_2CH_2OCH_3$). Compound **19**: 4.0 ($GaCH_2CH_3$), 9.9 ($GaCH_2CH_3$), 58.1 (OCH_3), 63.4 ($OCH_2CH_2OCH_3$), 74.5 ($OCH_2CH_2OCH_3$). Mass spec. (CI): *(m/z)* Compound **14**: 173 ($EtGa(OCH_2CH_2OCH_3)$). Compound **19**: 404 ($[M^+]_2$), 377 ($[M]_2$–Et), 331($[M]_2$–($OCH_2CH_2OCH_3$)), 202 ($Et_2Ga(OCH_2CH_2OCH_3)$), 173 (($Et_2GaOCH_2CH_2OCH_3$)–Et). Associated peaks: 127 (Et_2Ga).

2.3.20 Synthesis of [Me$_2$In(OCH$_2$CH$_2$NMe$_2$)]$_2$ (20)

$HOCH_2CH_2NMe_2$ (0.31 cm^3, 9.80 mmol) was added dropwise to a solution of Me_3In (1.00 cm^3, 9.80 mmol) in toluene (20 cm^3) at -78 °C with stirring over a 0.5 h period. The reaction mixture was allowed to warm slowly to room temperature and stirred for a further 24 h. Removal of the solvent *in vacuo* afforded a caked white solid. The solid was redissolved in toluene (2 cm^3) and cooled to -20 °C. Compound **20** was obtained as a white microcrystalline solid after several days (1.86 g, yield 58%). Anal. Calc. for $C_6H_{16}ONIn$: C, 30.93; H, 6.92; N, 6.01. Found: C, 30.45; H, 6.17; N, 5.80. ^1H NMR δ/ppm (C_6D_6): 0.04 (s, Me_2In, 3H), 2.99 (s, NCH_3, 6H), 3.89 (s, OCH_2CH_2N, 2H), 4.13 (s, OCH_2CH_2N, 2H). $^{13}C\{^1H\}$ NMR δ/ppm (C_6D_6): -8.5 (Me_2In), 44.5 (NCH_3), 58.1 (OCH_2CH_2N), 62.9 (OCH_2). IR (cm^{-1}): 2921 vs, 2694 w, 2271 m, 2206

m, 1990 vs, 1730 vs, 1660 vs, 1624 vs, 1455 s, 1406 m, 1377 m, 1353 s, 1275 m, 1261 m, 1184 w, 1168 w, 1150 s, 1096 vs, 1028 m, 947 s, 888 s, 783 s, 695 vs, 603 vs. Mass spec. (CI): *(m/z)* 642 $[M]_2$, 556 $[M]_2$-OR, 320 [M], 234 [M]-OR, 145 Me_2In, 115 In, 90 ($OCH_2CH_2NMe_2$).

2.3.21 Synthesis of $[Me_2In(OCH(CH_2NMe_2)_2)]_2$ (21)

Compound **21** was prepared in the same manner as **10** using $HOCH(CH_2NMe_2)_2$ (0.51 cm^3, 9.80 mmol) and Me_3In (1.00 cm^3, 9.80 mmol) in toluene (20 cm^3). Removal of the solvent *in vacuo* afforded a pale yellow non-viscous oil. The reaction flask was left at room temperature and X-ray quality crystals were obtained after 24h (1.94 g, 69% yield). Anal. Calc. for $C_9H_{23}N_2OIn$: C, 37.39; H, 7.67; N, 9.69. Found: C, 37.29; H, 8.26; N, 8.90. ^1H NMR δ/ppm (C_6D_6): δ 0.01 (s, Me_2In, 6H), 1.89 (dd, $OCHCH_2N$, 4H, J = 3.1 and J = 2.99 Hz), 2.02 (s, NCH_3, 12H), 3.80 (multiplet, OCH, 1H). $^{13}C\{^1H\}$ NMR δ/ppm (C_6CD_6): δ -5.3 (Me_2In), 46.1 (NCH_3), 64.3 ($OCHCH_2N$), 67.3 (OCH). IR (cm^{-1}): 2993 vs, 2854 vs, 2728 s, 2599 s, 2275 s, 1624 vs, 1455 m, 1366 m, 1337 w, 1312 w, 1280 m, 1257 m, 1195 m, 1138 s, 1089 s, 1024 s, 945 s, 863 m, 835 m, 801 s, 695 vs, 666 s, 588 s. Mass spec. (CI): (*m/z*) 435 ([M]–Me_2In), 291 (Me_2In ($OCH(CH_3)CH_2NMe_2$), 275 ($MeIn(OCH(CH_3)CH_2NMe_2)$), 145 (Me_2In).

2.3.22 Synthesis of $[Me_2In(OCH(CH_3)CH_2NMe_2)]_2$ (22)

Compound **22** was prepared in the same manner as **10** using $HOCH(CH_3)CH_2NMe_2$ (0.31 cm^3, 9.80 mmol) and Me_3In (1.00 cm^3, 9.80 mmol) in toluene (20 cm^3). Removal of the solvent *in vacuo* afforded a yellow non-viscous oil. The reaction flask was left at room temperature and X-ray quality crystals were obtained after 24h (1.97 g, yield 41%). Anal. Calc. for $C_7H_{18}NOIn$: C, 34.17; H, 6.96; N, 5.69. Found: C, 34.07; H, 6.66; N, 5.03. ^1H NMR δ/ppm (C_6D_6): δ 0.00 (s, Me_2In, 6H), 1.56 (d, $OCH(CH_3)$, 3H, J = 6.10 Hz), 1.90 (s, NCH_3, 6H), 2.08 (t, $OCHCH_2N$, 2H, J = 11.1 Hz)), 3.81 (m, $OCH(CH_3)CH_2$, 1H). $^{13}C\{^1H\}$ NMR δ/ppm (C_6D_6): δ -4.6 (Me_2In), 24.1 ($GaOCH(CH_3)$), 46.6 (NCH_3), 65.2 ($OCHCH_2N$), 69.2 (GaOCH). IR (cm^{-1}): 2923 s, 2728 m, 2599 m, 2276 m, 1624 s, 1456 m, 1366 w, 1337 w, 1313 w, 1280 m, 1195 w, 1138 m, 1089 m, 1024 s, 946 s, 863 w, 835 w, 801 vs, 695 vs, 666m, 588 vs. Mass spec. (CI): (*m/z*) 493 ($[M]_2$), 479 [M]-Me, 392 ([M]–MeIn), 248

(Me_2In–$OCH(CH_3)CH_2NMe_2$), 232 ($MeIn(OCH(CH_3)CH_2NMe_2)$), 145 (Me_2In), 104 ($OCH(CH_3)CH_2NMe_2$).

2.3.23 Synthesis of $[Me_2In(OC(CH_3)_2CH_2OMe)]_2$ (23)

Compound **23** was prepared in the same manner as **10** using $HOC(CH_3)_2CH_2OMe$ (0.36 cm^3, 9.80 mmol) and Me_3In (1.00 cm^3, 9.80 mmol) in toluene (20 cm^3). Removal of the solvent *in vacuo* afforded a caked white solid. The solid was redissolved in toluene (2 cm^3) and cooled to -20 °C. Compound **23** was obtained as a white microcrystalline solid after several days (1.25 g, yield 51%). Anal. Calc. for $C_5H_{13}O_2In$: C, 33.90; H, 6.91. Found: C, 33.19; H, 6.84. ^1H NMR δ/ppm (C_6D_6): 0.00 (s, Me_2In, 6H), 1.22 (s, $OC(CH_3)$, 6H), 2.74 (s, $OCCH_2$, 2H), 2.90 (s, (OCH_3, 3H). $^{13}C\{^1H\}$ NMR δ/ppm (C_6D_6): -3.94 (Me_2In), 28.6 ($OC(CH_3)$), 57.6 (OCH_3), 70.6 ($OCCH_2$), 82.7 ($OCCH_2$). IR (cm^{-1}): 2917 vs, 2279 m, 2185 m, 2032 s, 1924 s, 1732 vs, 1665 vs, 1631 vs, 1454 vs, 1377 vs, 1262 s, 1231 s, 1176 s, 1155 vs, 1103 vs, 1022 s, 996 s, 961 s. 912 s, 793 s, 704 s, 612 s, 514 s. Mass spec. (CI): (*m/z*) 481 ([M]), 393 ([M]-$OC(CH_3)_2CH_2OMe$), 145 (Me_2In).

2.3.24 Synthesis of $[Me_2In(OCH_2CH_2OMe)]_2$ (24)

Compound **24** was prepared in the same manner as **10** using $HOC(CH_3)_2CH_2OMe$ (0.25 cm^3, 9.80 mmol) and Me_3In (1.00 cm^3, 9.80 mmol) in toluene (20 cm^3). Removal of the solvent *in vacuo* afforded a caked white solid. The solid was redissolved in toluene (2 cm^3) and cooled to -20 °C. Compound **25** was obtained as a white microcrystalline solid after several days (1.96 g, yield 91%). Anal. Calc. for $C_5H_{13}O_2In$: C, 27.30; H, 5.96 Found: C, 27.06; H, 5.39. ^1H NMR δ/ppm (C_6D_6): 0.04 (s, Me_2In, 6H), 3.33 (s, OCH_3, 3H), 3.39 (t, $OCH_2CH_2OCH_3$, 2H, J = 4.6 Hz), 3.73 (t, $OCH_2CH_2OCH_3$, 2H, J = 4.6 Hz). $^{13}C\{^1H\}$NMR δ/ppm (C_6D_6): -6.6 (Me_2In), 57.8 (OCH_3), 63.1($OCH_2CH_2OCH_3$), 75. ($OCH_2CH_2OCH_3$). IR (cm^{-1}): 2923 s, 2722 w, 2705 w, 2272 m, 2036 m, 1632 m, 1271 s, 1237 s, 1197 m, 1149 m, 1122 w, 1079 vs, 1022 m, 903 m, 843 m, 720 s, 666 m, 589 s, 518 w. Mass spec. (CI): (*m/z*) 438 $[M]_2$, 218 [M], 145 (Me_2In), 115 (In).

2.3.25 Synthesis of [MeIn(OCH$_2$CH$_2$NMe$_2$)$_2$] (25) and (20)

$HOCH_2CH_2NMe_2$ (1.89 cm^3, 58.8 mmol) was added dropwise to a solution of Me_3In (1.00 cm^3, 9.80 mmol) in toluene (20 cm^3) at -78 °C with stirring over a 0.5 h period. The reaction mixture was allowed to warm slowly to room temperature then heated under reflux for 24 h yielding a colourless solution. Removal of the solvent *in vacuo* afforded a colourless oil composed of a 1 : 7 mixture of compound **20** and compound **25**. ^{1}H NMR δ/ppm (C_6D_6): Compound **20**: 0.09 (s, Me_2In, 12H), 3.06 (s, NCH_3, 12H), 4.02 (m, OCH_2CH_2N, 4H), 4.22 (m, OCH_2CH_2N, 4H, J = 2.6 Hz). Compound **25**: 0.12 (s, Me_2In, 21H), 3.09 (s, NCH_3, 84H). ^{13}C{^{1}H} NMR d/ppm (C_6D_6): Compound **20**: -2.91 (MeIn), 57.8 (NCH_3), 63.1 (OCH_2CH_2N), 75.7 (OCH2). Compound **25**: 58.6 (NCH_3), 62.1 (OCH_2CH_2N), 74.1 (OCH_2). Mass spec. (CI): (m/z) Compound **20**: 466 $[M]_2$, 378 $[M]_2$-$OCH_2CH_2NMe_2$. Compound **25**: 218 MeIn(OR). Associated peaks: 145 (Me_2In), 115 (In), 90 ($OCH_2CH_2NMe_2$).

2.3.26 Synthesis of [MeIn(OCH(CH$_2$NMe$_2$)$_2$)$_2$] (26) and (21)

Compound **26** was prepared in the same manner as **10** using $HOCH(CH_2NMe_2)_2$ (2.19 cm^3, 58.8 mmol) and Me_3In (1.00 cm^3, 9.80 mmol) in toluene (20 cm^3). The reaction mixture was allowed to warm slowly to room temperature then heated under reflux for 24 h yielding a pale yellow solution. Removal of the solvent *in vacuo* afforded a pale yellow non-viscous oil composed of a 1 : 3 mixture of compound **21** and compound **26**. ^{1}H NMR δ/ppm (C_6D_6): Compound **21**: -0.01 (s, Me_2In, 12H), 2.09 (s, NCH_3, 24H), 2.19 (dd, $OCHCH_2N$, 8H, 4.3, J = 12.3 Hz), 2.30 (dd, $OCHCH_2N$, 8H, 7.8, J = 12.3 Hz), 3.81 (m, OCH, 2H). Compound **26**: -0.013 (s, Me2In), 2.02 (s, NCH_3, 96H), 1.84 (dd, $OCHCH_2N$, 32H 2.9, J = 11.6Hz), 2.10 (dd, $OCHCH_2N$, 32H, J = 11.6 Hz), 3.89 (m, OCH, 16H). ^{13}C{^{1}H} NMR δ/ppm (C_6D_6): Compound **21**: -6.76 (Me_2In), 45.1 (NCH_3), 64.4 ($OCHCH_2N$), 66.2 (OCH). Compound **26**: -4.57 (Me_2In), 46.1 (NCH_3), 65.2 ($OCHCH_2N$), 67.3 (OCH). Mass spec. (CI): (m/z) Compound **21**: 435 ($[M]_2$-MeIn), 291 $Me_2In(OR)$, 405 ([M]-Me_2In). Compound **26**: 275 $MeIn(OCH(CH_2NMe_2)_2)$. Associated peaks: 145 (Me_2In), 86 ($OCH(CH_2NMe_2)$).

2.3.27 Synthesis of [MeIn(OCH(CH$_3$)CH$_2$NMe$_2$)$_2$] (27) and (22)

Compound **27** was prepared in the same manner as **10** using $HOCH(CH_3)CH_2NMe_2$ (2.31 cm^3, 58.8 mmol) and Me_3In (1.00 cm^3, 9.80 mmol) in

toluene (20 cm^3). The reaction mixture was allowed to warm slowly to room temperature then heated under reflux for 24 h yielding a colourless solution. Removal of the solvent *in vacuo* afforded a yellow non-viscous oil composed of a 1 : 3 mixture of compound **22** and compound **27**. ^1H NMR δ/ppm (C_6D_6): Compound **22**: -0.03 (s, Me_2In, 12H), 1.12 (d, $OCH(CH_3)$, 6H, J = 6.00 Hz), 1.98 (t, $OCHCH_2N$, 4H, J = 11.1 Hz), 1.82 (s, NCH_3, 12H), 3.83 (m, $OCH(CH_3)CH_2$, 2H). Compound **27**: 0.01 (s, MeIn, 9H), 1.15 (d, $OCH(CH_3)$, 18H, J = 6.00 Hz), 1.81 (s, NCH_3, 24H). $^{13}C\{^1H\}$ NMR δ/ppm (C_6D_6): Compound **22**: -6.76 (Me_2In), 24.15 ($OCH(CH_3)$), 46.8 (NCH_3), 63.8 ($OCHCH_2N$), 69.3 (OCH). Compound **27**: -4.8 (Me_2In), 23.8 ($OCH(CH_3)$), 43.7 (NCH_3), 64.4 ($OCHCH_2N$), 70.3 (OCH). Mass spec. (CI): (*m/z*) Compound **22**: 493 ($[M^+]$), 479 ([M]-Me), 392 ([M]-MeIn), 248 ($Me_2In(OCH(CH_3)CH_2NMe_2)$). Compound **27**: 232 ($MeIn(OCH(CH_3)CH_2NMe_2)$). Associated peaks: 145 (Me_2In), 104 ($OCH(CH_3)CH_2NMe_2$).

2.3.28 Synthesis of $[MeIn(O(CH_3)_2CH_2OMe)_2]$ (28) and (23)

Compound **28** was prepared in the same manner as **10** using $HOC(CH_3)_2CH_2OMe$ (3.06 cm^3, 58.8 mmol) and Me_3In (1.00 cm^3, 9.80 mmol) in toluene (20 cm^3). The reaction mixture was allowed to warm slowly to room temperature then heated under reflux for 24 h yielding a colourless solution. Removal of the solvent *in vacuo* afforded a caked white solid composed of a 1 : 3 mixture of compound **28** and compound **23**. ^1H NMR δ/ppm (C_6D_6): Compound **23**: -0.02 (s, Me_2In, 6H), 1.40 (s, $OC(CH_3)_2$, 6H), 2.88 (s, $OCCH_2$, 2H), 3.03 (s, OMe, 3H). Compound **28**: -0.016 (s, MeIn, 9H). $^{13}C\{^1H\}$ NMR δ/ppm (C_6CD_6): Compound **23**: -4.47 (Me_2In), 26.3 ($OC(CH_3)$), 57.6 (OCH_3), 71.3 ($OCCH_2$), 80.3 ($OCCH_2$). Compound **28**: -6.81 (Me_2In), 28.6 ($OC(CH_3)$), 58.4 (OCH_3), 72.6 ($OCCH_2$), 81.9 ($OCCH_2$). Mass spec. (CI): *(m/z)* Compound **23**: 249 ($Me_2In(OC(CH_3)_2CH_2OMe$), 481 ([M]), 451 ([M]-Me), 393 ([M]-$OC(CH_3)_2CH_2OMe$). Compound **28**: 233 ($MeIn(OC(CH_3)_2CH_2OMe$). Associated peaks: 233 ($MeIn(OC(CH_3)_2CH_2OMe$), 145 (Me_2In), 115 (In).

2.3.29 Synthesis of $[MeIn(OCH_2CH_2OMe)_2]$ (29) and (24)

Compound **29** was prepared in the same manner as **10** using $HOC(CH_3)_2CH_2OMe$ (0.68 cm^3, 58.8 mmol) and Me_3In (1.00 cm^3, 9.80 mmol) in toluene (20 cm^3). The reaction mixture was allowed to warm slowly to room

temperature then heated under reflux for 24 h yielding a colourless solution. Removal of the solvent *in vacuo* afforded a caked white solid composed of a 1 : 2 mixture of compound **24** and compound **29**. ^{1}H NMR δ/ppm (C_6D_6): Compound **24**: 0.02 (s, Me_2In, 12H), 2.34 (s, OCH_3, 6H), 2.89 (t, $OCH_2CH_2OCH_3$, 4H, J = 6.7 Hz), 3.62 (t, $OCH_2CH_2OCH_3$, 4H, J = 6.7 Hz). Compound **29**: 0.00 (s, MeIn, 6H), 2.09 (s, OCH_3, 12H). ^{13}C{^{1}H} NMR δ/ppm (C_6D_6): Compound **24**: -2.9 (Me_2In), 45.4 (OCH_3), 59.0 ($OCH_2CH_2OCH_3$), 63.6 ($OCH_2CH_2OCH_3$).Compound **29**: 46.1 (OCH_3), 60.7 ($OCH_2CH_2OCH_3$). Mass spec. (CI): (*m/z*) Compound **24**: 818 [MeIn(OCH_2CH_2OMe)]$_4$, 611 [MeIn(OCH_2CH_2OMe)]$_3$. Compound **29**: 204 [MeIn(OCH_2CH_2OMe)]. Associated peaks: 90 [Me(OCH_2CH_2OMe)], 145 (Me_2In).

2.4 References

1. C. J. Carmalt, S. J. King, *Coordination Chemistry Reviews*, 2006, 250, 682.
2. (a) P. P. Power, *Chem. Rev*, 1999, 99, 3463, (b) P. J. Brothers, P. P. Power, *Adv. Organomet. Chem*, 1996, 39, 1.
3. G. E. Coates, R. G. Hayter, *J. Chem. Soc*, 1953, 2519.
4. G. Mann, H. Olapinski, R. Ott, J. Weidlein, Z. *Anorg. Allg. Chem*, 1974, 410, 195.
5. H. -U. Schwering, E. Jungk, J. Weidlein, *J. Organomet. Chem*, 1975, 91, C4.
6. M. B. Power, W. M. Cleaver, A. W. Apblett, A. R. Barron, J. W. Ziller, *Polyhedron*, 1992, 11, 477.
7. M. D. Healey, J. T. Leman, A. R. Barron, *J. Am. Chem. Soc*, 1991, 113, 2776.
8. Y. Aleksandrov, N. Chikinova, G. I. Makin, V. I. Bregadze, L. M. Golubinskaya, *Metallorgan. Khim*, 1989, 2, 524.
9. Y. Aleksandrov, N. Chikinova, G. I. Makin, V. Alferov, I. Stepanova, *Zh. Obsh. Khim*, 1984, 54, 963.
10. S. Chitsaz, E. Iravani, B. Neumuller, *Z. Anorg. Allg. Chem*, 2002, 628, 2279.
11. G. E. Coates, R. G. Hayter, *J. Chem. Soc*, 1953, 2519.
12. S. J. Rettig, A. Storr, J. Trotter, Can. *J. Chem*, 1975, 53, 58.
13. J. Lewinski, J. Zachara, P. Horeglad, D. Glinka, J. Lipkowski, I. Justyniak, *Inorg. Chem*, 2001, 40, 6086.

14. K. -H. Thiele, E. Hecht, T. Gelbrich, U. Dumichen, *J. Organomet. Chem*, 1997, 540, 89.
15. H. Sun, Q. Zhao, Y. Liu, H. Hu, X. You, Z. Zhou, *J. Coord. Chem*, 1999, 47, 459.
16. H. Schumann, M. Frick, B. Heymer, F. Girgsdies, *J. Organomet. Chem*, 1996, 512, 117.
17. E. Hecht, Z. *Anorg. Allg. Chem*, 2000, 626, 1642.
18. M. Shenglof, D. Gelman, B. Heymer, H. Schumann, G.A. Molander, J. Blum, *Synthesis,* 2003, 302.
19. Y. Chi, T. -S. Chou, Y. -J. Wang, S. -F. Huang, A. J. Carty, L. Scoles, K.A. Udachin, S. -M. Peng, G. -H. Lee, *Organometallics,* 2004, 23, 95.
20. C. Zhu, F. Yuan, W. Gu, Y. Pan, *Chem. Commun*, 2003, 692.
21. G. E. Coates, R. A. Whitcombe, *J. Chem. Soc,* 1956, 3351.
22. H. Schmidbaur, *Angew. Chem. Int. Ed. Engl,* 1965, 4, 152.
23. B. M. Louie, S. J. Rettig, A. Storr, J. Trotter, *J. Chem*, 1985, 63, 3019.
24. D. A. Cooper, S. J. Rettig, A. Storr, *Can. J. Chem*, 1986, 64, 566.
25. E. C. Onyiriuka, A. Storr, *Can. J. Chem,* 1987, 65, 1367.
26. A. Mar, S. J. Rettig, A. Storr, J. Trotter, *Can. J. Chem*, 1988, 66, 101.
27. B. Armer, H. Schmidbaur, *Chem. Ber*, 1967, 100, 1521.
28. D. C. Bradley, D. M. Frigo, M. B. Hursthouse, B. Hussain, *Organometallics*, 1988, 7, 1112.
29. T. J. Trentler, S. C. Goel, K. M. Hickman, A. M. Viano, M. Y. Chiang, A. M. Beatty, P. C. Gibbons, W. E. Buhro, *J. Am. Chem. Soc*, 1997, 119, 2171.
30. T. Maeda, R. Okawara, *J. Organomet. Chem*, 1972, 39, 87.
31. T. -Y. Chou, Y. Chi, S. -F. Huang, C. -S. Liu, A. J. Carty, L. Scoles, K. A. Udachin, *Inorg. Chem*, 2003, 42, 6041.
32. M. Veith, S. Hill, V. Huch, *Eur. J. Inorg. Chem*, 1999, 1343.
33. B. Neumuller, *Chem. Soc. Rev*, 2003, 32, 50.
34. M. Veith, S. Faber, H. Wolfanger, V. Huch, *Chem. Ber*, 1996, 129, 381.
35. S. Chitsaz, B. Neumuller, *Organometallics,* 2001, 20, 2338.
36. S. Basharat, C. J. Carmalt, S. J. King, E. S. Peters, D. A. Tocher, *Dalton Trans*, 2004, 3475.

37. H. Schumann, R. Mohtachemi, M. Schwichtenberg, *Z. Naturforsch*, 1988, 43b, 1510.
38. R. C. Mehrotra, R. K. Mehrotra, *Curr. Sci*,1964, 33, 241.
39. H. Funk, A. Paul, *Z. Anorg. Allg. Chem*, 1964, 330, 70.
40. A. Tanner, R. Reinmann, *Z. Naturforsch*, 1965, 20b, 524.
41. H. Booch, A. Paul, H. Funk, Z. *Anorg. Allg. Chem*, 1965, 337, 145.
42. S. R. Bindal, V. K. Mathur, R. C. Mehrotra, *J. Chem. Soc*, 1969, 863.
43. J. G. Oliver, I. J. Worrall, *J. Chem. Soc*, A, 1970, 845.
44. J. G. Oliver, I. J. Worrall, *Inorg. Nucl. Chem. Lett*, 1969, 5, 455.
45. J. G. Oliver, I. J. Worrall, *J. Chem. Soc*, A 1970, 2347.
46. J. G. Oliver, I. J. Worrall, *Inorg. Nucl. Chem. Lett*, 1971, 33, 1281.
47. M. Valet, D. M. Hoffman, *Chem. Mater*, 2001, 13, 2135.
48. K. Folting, W. E. Streib, K. G. Caulton, O. Poncelet, L. Hubert- Pfalzgraf, *Polyhedron,* 1991, 14, 1639.
49. S. Suh, D. M. Hoffman, *J. Am. Chem. Soc*, 2000, 122, 9396.
50. L. Mîinea, S. Suh, S. G. Bott, J. -R. Liu, W. -K. Chu, D. M. Hoffman, *J. Mater. Chem*, 1999, 9, 929.
51. S. J. Rettig, A. Storr, J. Trotter, Can. *J. Chem*, 1975, 53, 58.
52. K. - H. Thiele, E. Hecht, T. Gelbrich, U. Dumichen, *J. Organomet. Chem*, 1997, 540, 89.
53. H. Schumann, M. Frick, B. Heymer, F. Girgsdies, *J. Organomet. Che*m, 1996, 512, 117.
54. C. J. Carmalt, S. Basharat, *Organometallic Derived I: Semiconductors (MS 166)*, Precursors to Semiconducting Materials, 2005.
55. T. – Y. Chou, S. –F. Huang, C. – S. Liu, *Inorg. Chem*, 2003, 42, 6041.
56. S. Abram, C. M.Mössmer, U. Abram, *Polyhedron*, 1997, 16, 2183.

Chapter 3

Chemical Vapour Deposition of Group 13 Oxides

Chapter 3 Chemical Vapour Deposition of Group 13 Oxides

3.1 Introduction

This chapter describes investigations into the suitability of a selection of the gallium and indium alkoxides, synthesised as described in Chapter 2, for chemical vapour deposition (CVD). The decomposition of the group 13 metal alkoxides was studied by thermogravimetric analysis and differential scanning calorimetry. The deposition of thin films from the metal alkoxides was achieved by aerosol assisted CVD and low pressure CVD.

3.2 Thermogravimteric analysis

3.2.1 Background

Thermogravimteric analysis (TGA) has been used to study the decomposition pathway of the precursors synthesised in Chapter 2. TGA continuously records changes in the mass of a material as it is heated in an inert controlled atmosphere. The total mass loss can predict whether the precursor will completely decompose to the required binary compound, e.g. whether a gallium alkoxide will decompose to give pure Ga_2O_3. TGA can also lead to the identification of decomposition products, and, where clean decomposition steps are identified, prediction of the decomposition pathway.

Differential scanning calorimetry (DSC) records the differences in heat flow into a sample and an inert reference, usually an empty pan, as the two are simultaneously heated. Hence, DSC gives information concerning chemical or physical changes that are accompanied by a gain or loss of heat. This is useful in determining whether a given complex will be a suitable CVD precursor, as compounds must be capable of vaporization and carry over to the substrate without decomposing. Therefore, a good candidate for a CVD precursor will exhibit a melting point at a temperature much lower than the onset of decomposition, allowing it to be thermally vaporized at a stable temperature. In addition, a good precursor will decompose to the relevant binary compound at a temperature below 600 ^{o}C to allow deposition on glass, as the glass

substrate will melt above this temperature. The analysis techniques described in this chapter, however, are carried out on bulk samples of the precursors, and so do not replicate a CVD experiment and therefore compounds which do not appear to be suitable precursors from these analytical results could still successfully produce thin films.

3.2.2 Decomposition pathway

The mechanism for the decomposition of group 13 alkoxides to the relevant oxide could involve β-hydride elimination. The loss of the alkoxide group, OCH_2CH_2OMe, via β-hydride elimination from a ethylgallium alkoxide is depicted in Eq. 3.1. If the alkoxide ligand is lost via β-elimination the alkene $H_2C=CH(OMe)$ would be eliminated. The β-hydrogen could react with the Ga–Et group resulting in the elimination of ethane.

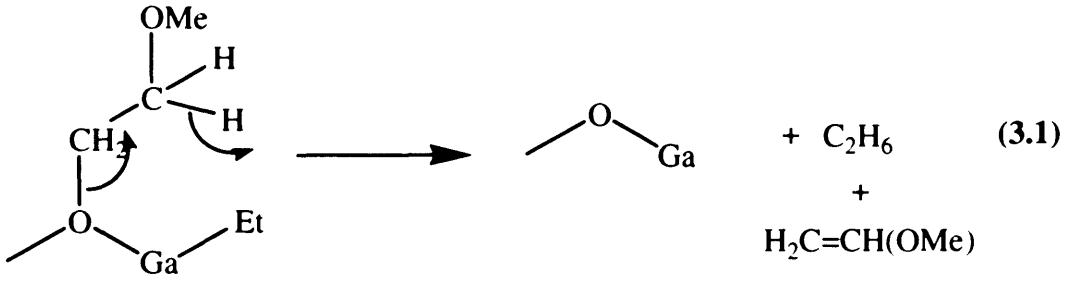

(3.1)

Alternatively, the ethyl group could be lost via β-elimination, as shown in Eq. 3.2. This mechanism would result in the loss of ethene and an alkane (e.g. CH_2CH_2OMe). TGA may provide information regarding the mechanism. Other methods to obtain mechanistic details about the decomposition process include pyrolysis studies and *in stiu* mass spectroscopy, which has not been investigated in this thesis.

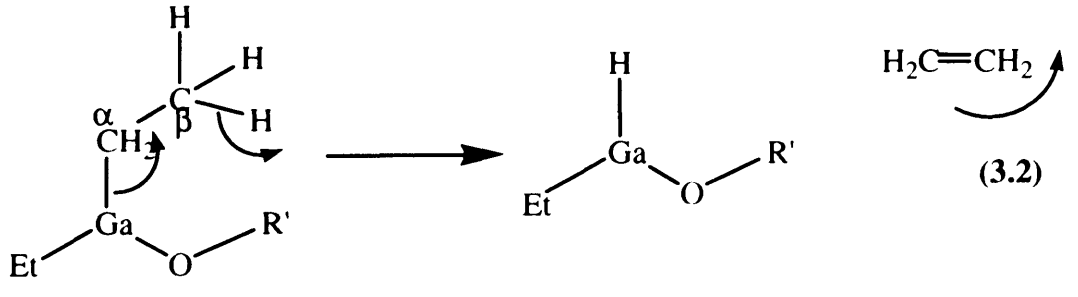

(3.2)

3.3 Chemical Vapour Deposition of Gallium and Indium Oxide Thin Films

3.3.1 Background - Deposition of Ga_2O_3 thin films

3.3.1.1 Single-source routes

Gallium oxide thin films have been grown by single-source chemical vapour deposition (CVD) routes using a range of techniques such as atmospheric pressure (AP)CVD and low pressure (LP)CVD. LPCVD has been found to be an effective method for growing Ga_2O_3 films using a range of precursors. These include homoleptic gallium alkoxides,[1] gallium tris(hexafloroacetylacetonate)[2,3] and gallium fluoroalkoxide.[4]

$[Ga(hfac)_3]$ (hfac = hexafluoroacetylacetonate)[2] and O_2 have been used to deposit amorphous Ga_2O_3 by low pressure CVD at substrate temperatures of 400-500 °C.[2,3] Similar results were obtained in a study by Mîinea *et al.* The gallium alkoxide complex $[Ga(OCH(CF_3)_2)_3(HNMe_2)]$,[1] has been reported to prepare Ga_2O_3 thin films by LPCVD in the presence of air, at substrate temperatures of 250 to 450 °C. Good quality films were obtained at 450 °C, which were shown to have the composition Ga_2O_3[1] with an optical band gap of 4.9 eV. Powder X-ray diffraction showed the film to be amorphous. The films were >90% transmittant in the mid-ultravoilet and visible regions. Attempted depositions using only the compound $[Ga(OCH(CF_3)_2)_3(HNMe_2)]$, or using if in combination with dry O_2 did not result in films in the same temperature range. This indicates that water vapour is the critical reactant in the $[Ga(OCH(CF_3)_2)_3(HNMe_2)]$ /air precursor system. However, the formation of GaF_3 was observed in the mass spectrum of $[Ga(hfac)_3]$ and the presence of fluorine in Ga_2O_3 films could cause problems for gas sensor applications, due to baseline resistance and sensor drift.[5]

LPCVD of $[Ga(\mu\text{-}O^tBu)(O^tBu)_2]_2$ and O_2 also resulted in the formation of Ga_2O_3.[6] Highly transparent films were grown at 300–700 °C. In comparison to $[Ga(OCH(CF_3)_2)_3(HNMe_2)]$, a good quality film was produced from compound $[Ga(O^tBu)(O^tBu)_2]_2$ at 400 °C without added air or O_2. The films were shown to be of composition Ga_2O_3 and amorphous with an optical band gap of 4.9 eV. Annealing the

film at 1000 °C produced an X-ray pattern consistent with polycrystalline Ga_2O_3. The films showed >80% transmittance in the 350-800 nm region.

The precursors $[ClGa(OC(CF_3)_2CH_2NMe_2)_2]$ and $[Me_2Ga(OC(CF_3)_2CH_2NMe_2)]$ have also been used to prepare Ga_2O_3 thin films with high-purity O_2 as the carrier gas at 500–600 °C via MOCVD.[4] The films showed 3–5 atom% carbon impurity but were fluorine-and chlorine-free. The reactions used to prepare these precursors employ $GaMe_3$ and $GaEt_3$, which are good CVD source reagents for depositing gallium oxide films, but their pyrophoric nature makes storage and handling difficult. A drawback of using these complexes as precursors is that the multi-step synthesis required for the ligands makes them less suitable for scale-up operations.[4]

Group 13 sesquialkoxides[7-10] are tetrameric compounds, which possess the desired ratio for M_2O_3. Hence, complexes of this type are ideal precursors to group 13 oxides. Recently, the LPCVD of the gallium sesquialkoxide, $[Ga(MeGa(OCH_2C_6H_4Me\text{-}4)_3)_3]$, has been used to deposit Ga_2O_3 thin films on glass substrates at 600 °C.[11] X-ray diffraction of the film obtained from $[Ga(MeGa(OCH_2C_6H_4Me\text{-}4)_3)_3]$, showed a diffraction pattern to be consistent with the monocline β-Ga_2O_3. UV-Vis data indicated that the film produced had an indirect band gap of 4.3 eV.

3.1.1.2 Dual- source routes

Gallium oxide thin films have been deposited by atmospheric pressure chemical vapour deposition from the reaction of gallium trichloride and methanol at temperatures above 400 °C.[12] The gallium oxide films were of a uniform phase Ga_2O_3 with a band gap of 4.3 eV. The films produced were amorphous, as shown by powder X-ray diffraction.

There have been no reports to date of gallium oxide films deposited by AACVD dual-source routes. This thesis reports the first range of examples of Ga_2O_3 thin films prepared by dual source routes using AACVD.

3.3.2 Background-Deposition of In_2O_3 thin films

3.3.2.1 Single-source routes

LPCVD of $[In(\mu\text{-}OCMe_2Et)(OCMe_2Et)_2]_2$ and O_2 produced highly conductive indium oxide films at 300–500 °C.[13] X-ray diffraction indicated (1 0 0)-orientated cubic

indium oxide had formed and EDXA analysis revealed that the film deposited at 500 °C was stoichiometric In_2O_3 with low levels of carbon contamination (less than 1%). A band gap value of 3.77 eV was obtained for the film deposited at 500 °C, this value is close to those reported previously for undoped In_2O_3 films prepared by MOCVD (3.5-3.8 eV).[14]

The LPCVD reaction of $[In(OCMe(CF_3)_2)_3(H_2N^tBu)]$ and oxygen resulted in the deposition of polycrystalline indium oxide at 400-500 °C.[15] X-ray diffraction studies on films grown at 400–550 °C indicated that they were polycrystalline cubic indium oxide with a (1 0 0) preferred orientation. Films deposited below 500 °C contained 2-3 atom% fluorine whilst films deposited at 550 °C had no detectable fluorine. X-ray photoelectron spectroscopy showed that the film contained virtually no carbon or nitrogen.

Similar results were obtained from the LPCVD of $[Me_2In(OC(CF_3)_2CH_2NHMe)]_2$ with O_2 at 400–500 °C. However, powder X-ray diffraction showed the formation of cubic In_2O_3 films with preferred (1 1 1)-orientation.[16]

3.3.2.2 Dual- source routes

There have been no reports to date of indium oxide films deposited by dual-source routes. This thesis describes the first example of indium oxide thin films prepared by dual source routes.

3.4 Results and Discussion-Deposition of Gallium Oxide Films by LPCVD

TGA was carried out on the compounds prepared as described in chapter 2, to get some information about the decomposition pathway and the temperature range. This section reports the deposition of Ga_2O_3 thin films by single-source routes using LPCVD. However, the *in situ* reaction between Et_3Ga and ROH, employed in the AACVD of Ga_2O_3 (section 3.5) presumably yields complexes analogous to the isolated compounds, therefore, the TGA or DSC results will also provide information for the necessary conditions for the AACVD reactions.

3.4.1 Thermal analysis of $[Et_2Ga(OCH_2CH_2NMe_2)]_2$ (10)

The decomposition properties of $[Et_2Ga(OCH_2CH_2NMe_2)]_2$ **(10)** were determined by TGA and the results are shown in Figure 3.1. The decomposition of **10** shows a total weight loss of 99.7% below 300 °C, which is much higher than the expected weight loss of 56.6% if Ga_2O_3 was formed from **10**. This difference could be due to sublimation of the precursor. The observation of a steep weight loss (0 - 300 °C) followed by a more gradual loss of weight (300-600 °C) suggest that most of the decomposition occurs below 300 °C. The DSC of **10** shows a sharp endotherm at 29.9 °C, which corresponds to the melting point. The three exotherms at 223.9, 259.2 and 289.2 °C could be an effect of the decomposition process. The decomposition of **10** begins at a higher temperature than the melting point suggesting that carry over of the intact molecule to the substrate could be successfully achieved. This would suggest that $[Et_2Ga(OCH_2CH_2NMe_2)]_2$ would make a good CVD precursor. The fact that **10** appears to sublime readily is an excellent characteristic for use as a CVD precursor.

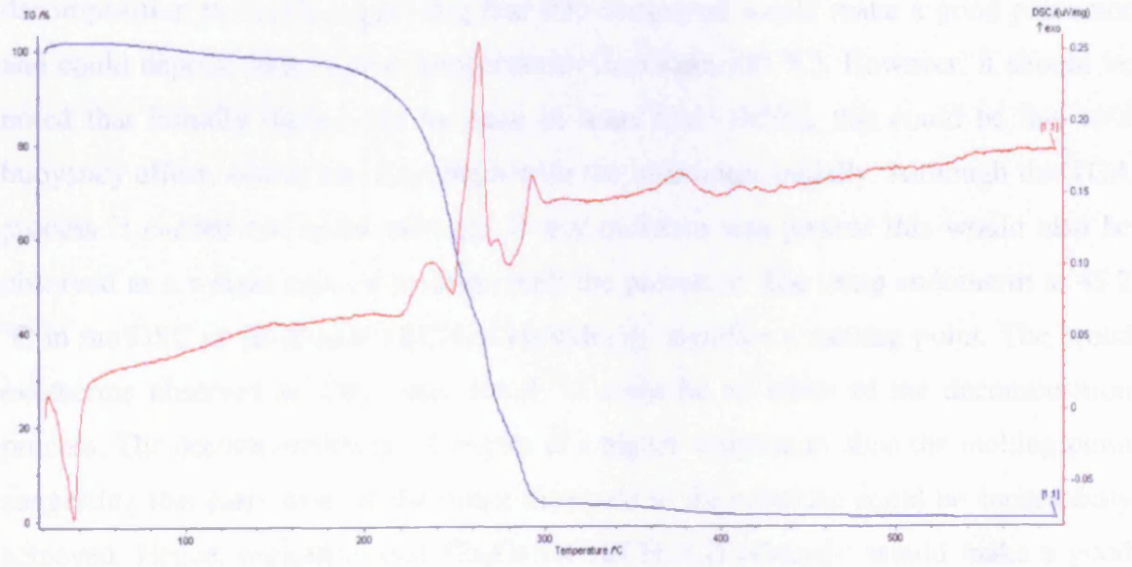

Figure 3.1: TGA/DSC for $[Et_2Ga(OCH_2CH_2NMe_2)]_2$ **(10)**

3.4.2 Thermal analysis of $[Et_2Ga(OCH(CH_2NMe_2)_2)]_2$ (11)

The TGA for $[Et_2Ga(OCH(CH_2NMe_2)_2)]_2$ **(11)** shows that decomposition occurs in one clean step. The overall mass loss measured is 68.9%, which is close to the 61.2% required for complete decomposition to Ga_2O_3 suggesting that this compound would make a good precursor and could deposit films at low temperatures (less than 400 °C). A broad endotherm at 40.5 °C signifies the melting point. The decomposition of this precursor also begins at a much higher temperature than the melting point suggesting that this complex would carry over to the substrate during the CVD process.

3.4.3 Thermal analysis of $[Et_2Ga(OCH(CH_3)CH_2NMe_2)]_2$ (12)

The thermogravimetric analysis of $[Et_2Ga(OCH(CH_3)CH_2NMe_2)]_2$ **(12)** shows an overall mass loss of 64.2% (Figure 3.2). The decomposition of **12** does not occur in clean, discrete stages but is continuous from the onset at *ca.* 150 °C throughout the temperature range studied and occurs in three stages. The first mass loss of 53.1% occurs at 200 °C, the second of 7.6% at 260 °C and finally the third mass loss of 3.5% at 380 °C. The overall mass loss of 64.2% is close to the 59.4% required for complete decomposition to Ga_2O_3 suggesting that this compound would make a good precursor and could deposit films at low temperatures (less than 400 °C). However, it should be noted that initially there is an increase in mass loss (105%), this could be due to a buoyancy effect, which was a problem with the instrument initially. Although the TGA process is carried out under nitrogen if any moisture was present this would also be observed as a weight gain on reaction with the precursor. The sharp endotherm at 45.2 °C in the DSC of $[Et_2Ga(OCH(CH_3)CH_2NMe_2)]_2$ signifies a melting point. The broad exotherms observed at 239.7 and 358.9 °C could be an effect of the decomposition process. The decomposition of **12** begins at a higher temperature than the melting point suggesting that carry over of the intact molecule to the substrate could be successfully achieved. Hence, indicating that $[Et_2Ga(OCH(CH_3)CH_2NMe_2)]_2$ would make a good CVD precursor. However, it should be noted that as the TGA does not occur in one clean stage, hence, some contamination could be observed in the film deposited.

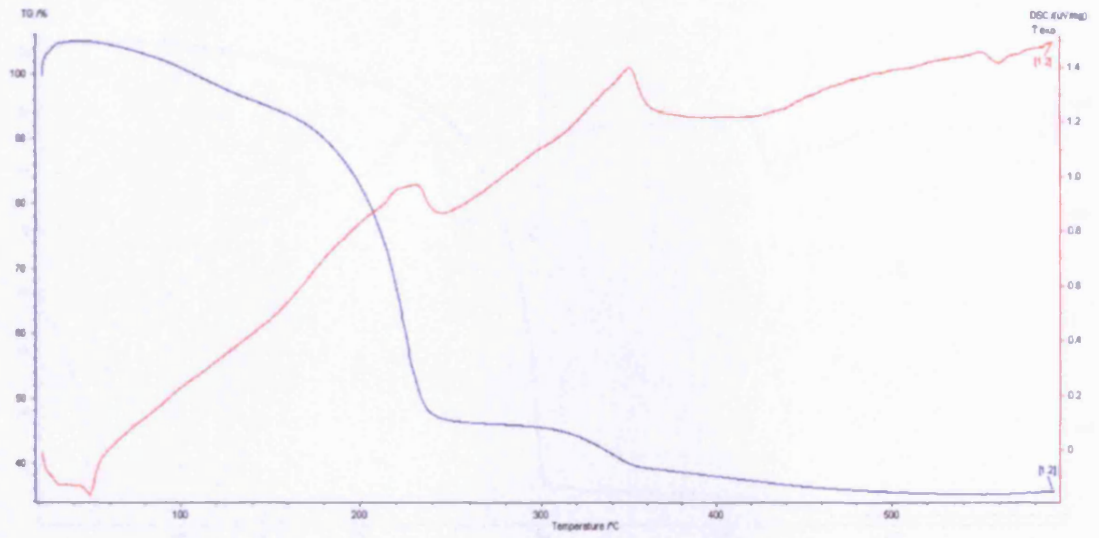

Figure 3.2: TGA/DSC for $[Et_2Ga(OCH(CH_3)CH_2NMe_2)]_2$ **(12)**

3.4.4 Thermal analysis of $[Et_2Ga(OC(CH_3)_2CH_2OMe)]_2$ (13)

The total mass loss of around 73.2% observed in the TGA of $[Et_2Ga(OC(CH_3)_2CH_2OMe)]_2$ **(13)** is significantly higher than the calculated mass loss of 59.4% for **13** to form Ga_2O_3. A higher measured mass loss than that expected often indicates that sublimation has occurred. As shown in Figure 3.3, the decomposition occurs in two stages. The mass change occurs in two steps, a steep weight loss of around 72.3% followed by a discrete mass loss of 4.7%. The second stage of mass loss corresponds well to a β-hydride elimination of an ethyl group (6.5% for the loss of ethene). The DSC of **13** shows a sharp endotherm at 45.3 °C, which corresponds to the melting point. The exotherms at 211.5, 271.4 and 297.9 °C could be as a result of the decomposition process. The decomposition of this precursor also begins at a higher temperature than the melting point suggesting that carry over of the intact molecule to the substrate could be successfully achieved. This would suggest that $[Et_2Ga(OC(CH_3)_2CH_2OMe)]_2$ would make a good CVD precursor with little contamination in the film formed as the decomposition pathway, as shown by TGA, is clean.

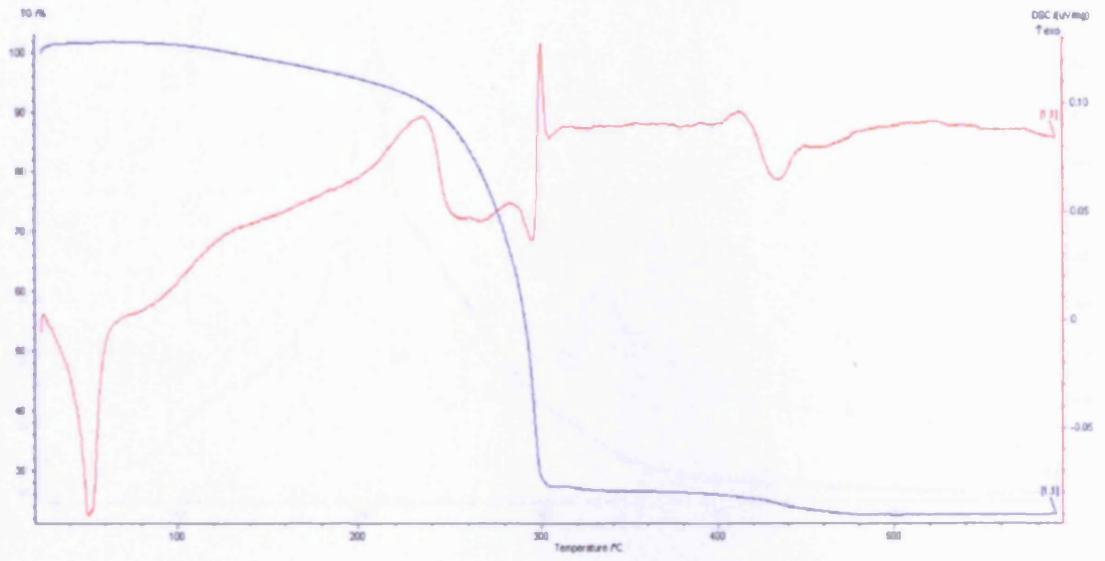

Figure 3.3: TGA/DSC for $[Et_2Ga(OC(CH_3)_2CH_2OMe)]_2$ **(13)**

3.4.5 Thermal analysis of $[Et_2Ga(OCH_2CH_2OMe)]_2$ (14)

The TGA for $[Et_2Ga(OCH_2CH_2OMe)]_2$ **(14)** shows that decomposition occurs, in two discrete steps (Figure 3.4). The overall mass loss measured (70.5%), although slightly higher is close to the 64% required for complete decomposition to Ga_2O_3 suggesting that this compound would make a good precursor and could deposit films at low temperatures (less than 400 °C). The broad endotherm at 45.3 °C signifies the melting point. The two exotherms at 194.3 and 322.5 °C could arise from the decomposition process. The decomposition of this precursor also begins at a much higher temperature than the melting point suggesting that this complex would deposit films easily.

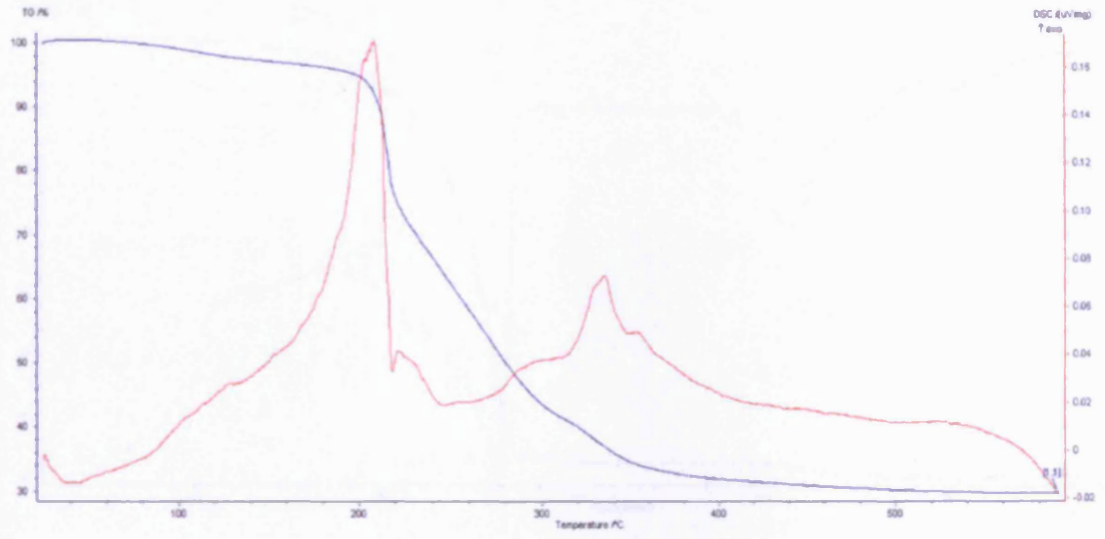

Figure 3.4: TGA/DSC for $[Et_2Ga(OCH_2CH_2OMe)]_2$ **(14)**

3.4.6 Thermal analysis of $[Et_2Ga(OCH(CH_3)_2)]_2$ (15)

The total mass loss of around 69.8% observed in the TGA of **(15)** $[Et_2Ga(OCH(CH_3)_2)]_2$ is higher than the calculated mass loss of 50.1% for **15** to form Ga_2O_3. A higher measured mass loss than that expected often indicates that sublimation has occurred. As shown in Figure 3.5, the decomposition occurs in two stages. The mass change occurs in two steps, a steep weight loss of around 66.8% followed by a discrete mass loss of 3.2%. The DSC of **15** shows a sharp endotherm at 97.6 °C, which corresponds to the melting point. Two endotherms at 260.9 and 415.4 °C could be as a result of the decomposition process. The decomposition of this precursor also begins at a higher temperature than the melting point suggesting that carry over of the intact molecule to the substrate could be successfully achieved. This would suggest that $[Et_2Ga(OCH(CH_3)_2)]_2$ would make a good CVD precursor.

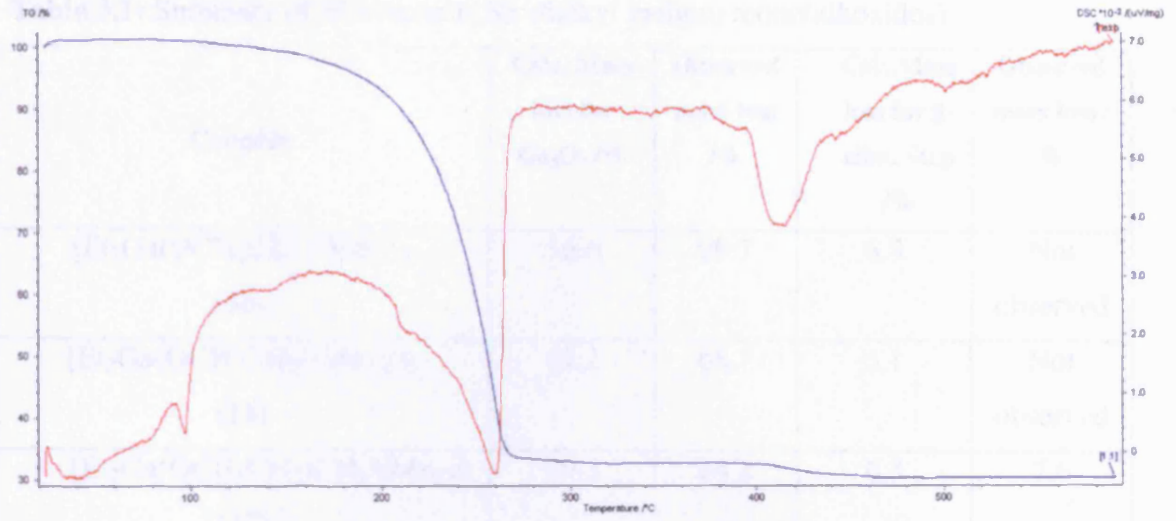

Figure 3.5: TGA/DSC for $[Et_2Ga(OCH(CH_3)_2)]_2$ **(15)**

3.4.7 Summary of TGA results

In general, the thermogravimetric analysis of the dialkyl gallium mono(alkoxides), gave total mass losses close to that required for the precursors to form Ga_2O_3. The results of are summarised in Table 3.1. The TGA results also suggest that all the precursors should decompose readily and carry over of the precursor in the CVD process could be achieved. The melting point of **15** is higher than the other compounds (**10**-**14**) with donor functionalised ligands. It is difficult to make a comparison due to sublimation of many of the compounds during TGA.

Table 3.1: Summary of TGA results for dialkyl gallium mono(alkoxides)

Complex	Calc. Mass loss for Ga_2O_3 /%	Observed mass loss /%	Calc.Mass loss for β-elim. Step /%	Observed mass loss / %
$[Et_2Ga(OCH_2CH_2NMe_2)]_2$ **(10)**	56.6	99.7	6.5	Not observed
$[Et_2Ga(OCH(CH_2NMe_2)_2)]_2$ **(11)**	61.2	68.7	5.1	Not observed
$[Et_2Ga(OCH(CH_3)CH_2NMe_2)]_2$ **(12)**	59.3	64.2	6.3	7.6
$[Et_2Ga(OC(CH_3)_2CH_2OMe)]_2$ **(13)**	59.4	73.2	6.5	4.7
$[Et_2Ga(OCH_2CH_2OMe)]_2$ **(14)**	64.0	70.5	5.0	11.8
$[Et_2Ga(OCH(CH_3)_2)]_2$ **(15)**	50.1	69.8	7.5	Not observed

3.4.8 LPCVD - Reaction conditions and appearance

Film deposition was carried out at 600 °C over 5 hours using 0.5 g of $[Et_2Ga(OCH_2CH_2NMe_2)]_2$ **(10)** $[Et_2Ga(OCH(CH_2NMe_2)_2)]_2$ **(11)**, $[Et_2Ga(OCH(CH_3)CH_2NMe_2))]_2$ **(12)**, and $[Et_2Ga(OC(CH_3)_2CH_2OMe)]_2$ **(13)**. All precursors deposited grey films, which were deposited over the middle two substrates (2 and 4 out of 6). The entire precursor was carried over during the deposition.

3.4.9 Film analysis

EDAX analysis and XPS on **11** and **12** revealed some carbon contamination (10%) was present in the resulting films, which have a Ga : O ratio of 1 : 1.3. However, XPS revealed binding energy shifts of 532.6 eV for O 1s and 1118.3 eV for Ga $2p_{3/2}$ and 1145.2 for Ga $2p_{1/2}$ These binding energy shifts are in agreement with previous literature values for Ga_2O_3.[17] Therefore, it is likely that Ga_2O_3 films have been formed but due to carbon contamination the ratio of Ga : O is not 1: 1.5. Scanning electron

microscopy analysis of the film deposited from $[Et_2Ga(OCH(CH_2NMe_2)_2)]_2$ **11** showed that deposition occurred *via* an island growth mechanism, with particle sizes of 1 μm in diameter, as shown in Figure 3.6.

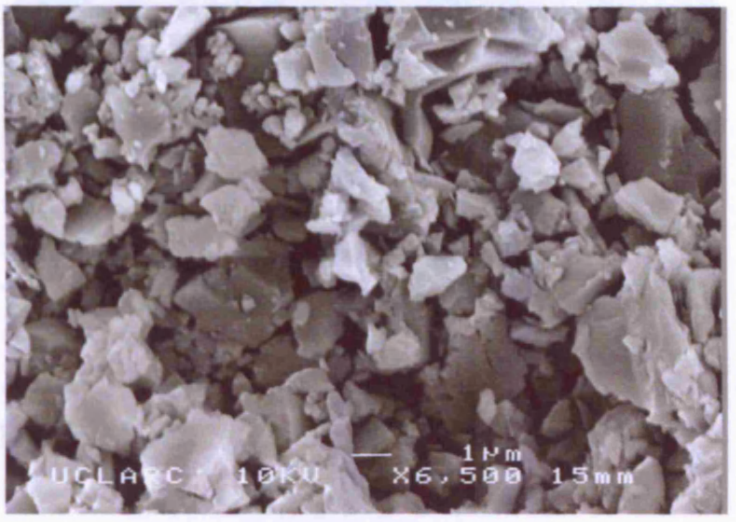

Figure 3.6: SEM image for a film deposited by LPCVD from $[Et_2Ga(OCH(CH_2NMe_2)_2)]_2$ **(11)** at 600 °C.

The film produced from $[Et_2Ga(OCH(CH_3)CH_2NMe_2)]_2$ **12** at 600 °C had slightly different morphology. Scanning electron microscopy analysis (Figure 3.7) of this film displays a Volmer-Weber type island growth mechanism. The size of the observed spherical particles is of the order 400 nm.

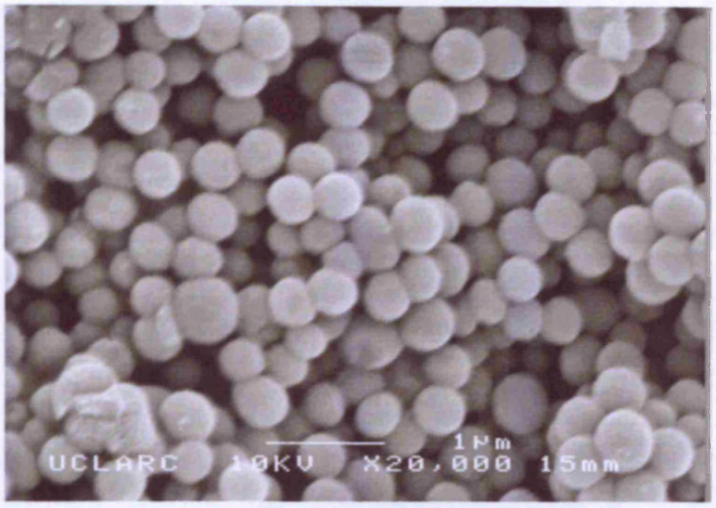

Figure 3.7: SEM image for a film deposited by LPCVD from $[Et_2Ga(OCH(CH_3)CH_2NMe_2))]_2$ **(12)** at 600 °C.

LPCVD of the related complexes $[Et_2Ga(OCH_2CH_2NMe_2)]_2$ **10** and $[Et_2Ga(OC(CH_3)_2CH_2OMe)]_2$ **13** also resulted in the deposition of thin films of Ga_2O_3 on glass and quartz substrates. EDXA and XPS analysis revealed some carbon contamination (10%) in the films which gave a Ga : O ratio of 1 : 1.2. These films were oxygen deficient due to the low oxygen content in the precursor. However, annealing the films in air at 900 °C produced highly crystalline β-Ga_2O_3 films. EDAX analysis and XPS of the annealed films revealed Ga : O ratios of 1 : 1.57 and 1 : 1.53 for films grown from **10** and **13**, respectively, in close agreement to the anticipated value for Ga_2O_3. XPS and EDXA indicate that there is little carbon contamination (<1 at.%). The binding energy shifts for O 1s and Ga $2p_{3/2}$ for the annealed films also agree with literature values for Ga_2O_3 (O 1s 531.2 eV and Ga $2p_{3/2}$ 1118.7 eV).[17] SEM of the annealed films showed (Figure 3.8) that they are crystalline with the formation of whiskers.

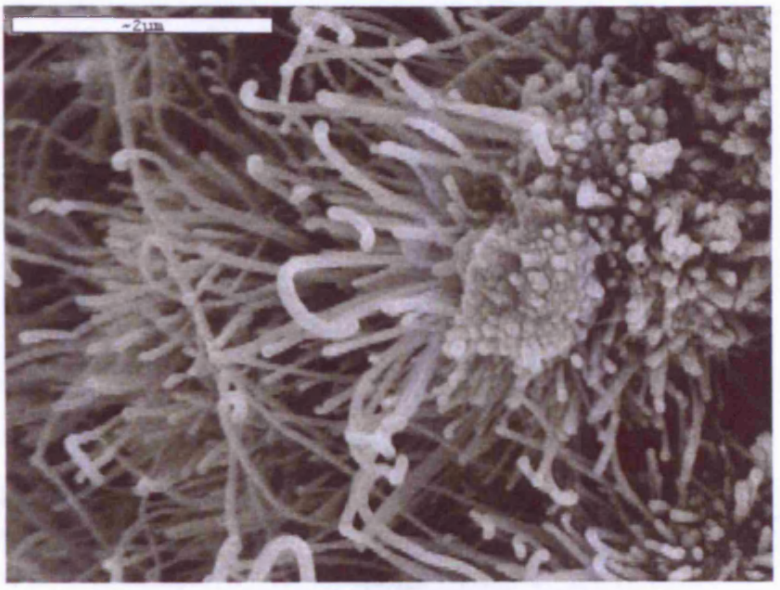

Figure 3.8: SEM image for a film deposited by LPCVD from $[Et_2Ga(OC(CH_3)_2CH_2OMe)]_2$ **(13)** at 600 °C.

The crystalline nature of the films was confirmed by glancing angle X-ray powder diffraction, Figure 3.9, shows the powder XRD of the annealed film grown from **13**, which is consistent with the reference standard for monoclinic β-Ga_2O_3. The film gave lattice constants a = 12.0(2), b = 2.99(1) and c = 5.7(1) Å and β = 103.5° in agreement with reported data for bulk Ga_2O_3.[5]

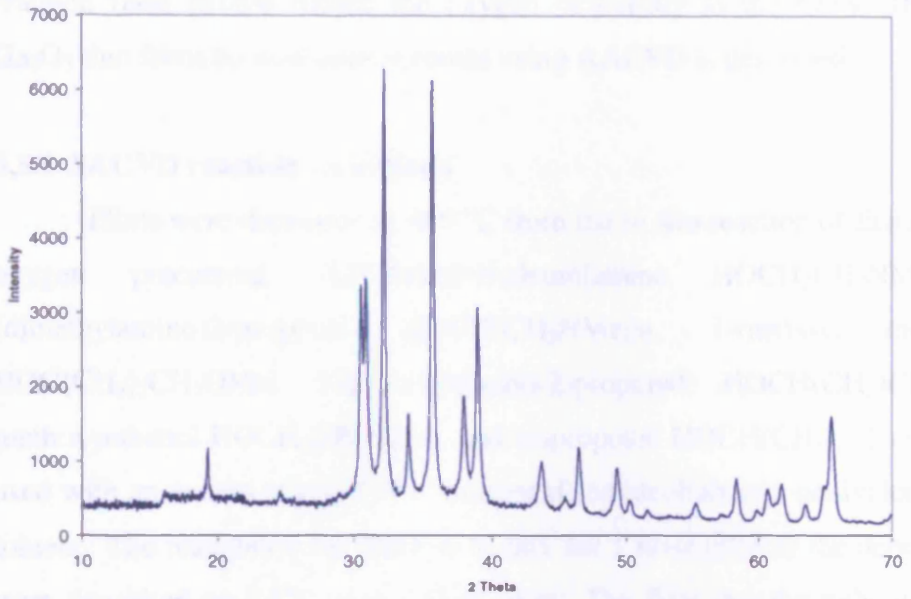

Figure 3.9: X-ray diffraction of Ga_2O_3 films deposited by LPCVD from $[Et_2Ga(OC(CH_3)_2CH_2OMe)]_2$ **(13)**.

All the films were investigated using Raman microscopy. In all cases no Raman scattering was observed and it is thought that gallium oxide is a poor Raman scatterer. However, Raman spectroscopy indicated the absence of graphitic carbon in the films. Conducting a Tauc plot[19] of the UV/visible data indicated that the films had a band gap of 4.5 eV, comparable to other values for Ga_2O_3 of 4.2–4.9 eV.[20] The films were shown to have contact angles for water droplets of 10°, suggesting that the films are hydrophilic. The annealed films had contact angles for water droplets of 1°, again suggesting that the films are hydrophilic. All films passed the scotch tape test and were resistant to marking by a wet towel or a brass stylus, but could be marked by a steel scalpel.

3.5 Deposition of Gallium Oxide Films from Et_3Ga and Donor Functionalised Alcohols by AACVD

Films grown from single-source precursors (section 3.4) were found to be deficient in oxygen. In an attempt to prepare stoichiometric Ga_2O_3 films the AACVD was investigated, involving the *in situ* reaction between Et_3Ga and excess ROH. This would presumably yielded complexes, of the type $[Et_2Ga(OR)]_2$, which were isolated and described in chapter 2. However, the presence of excess ROH in the AACVD

reaction flask should reduce the oxygen deficiency in the films. The deposition of Ga_2O_3 thin films by dual-source routes using AACVD is described.

3.5.1 AACVD reaction conditions

Films were deposited at 450 ^{0}C from the *in situ* reaction of Et_3Ga and a range of oxygen precursors, *N,N*-dimethylethanolamine $HOCH_2CH_2NMe_2$, 1,3 bis-(dimethylamino)2-proponal $HOCH(CH_2NMe_2)_2$, 1-methoxy-2-methyl-2-propanol $HOC(CH_3)_2CH_2OMe$, 1-dimethylamino-2-proponal $HOCH(CH_3)CH_2NMe_2$, 2-methoxyethanol $HOCH_2CH_2OMe_2$ and isoproponal $HOCH(CH_3)_2$. 1 cm^3 of Et_3Ga was used with an excess of the donor functionalised alcohols (six equivalents) in 30 cm^3 of toluene. The reagents were allowed to mix for 1 hour prior to the deposition. All films were deposited on SiCO coated float glass. The flow rate throughout the reactor was kept constant for all depositions at 1 L min^{-1}, after which the substrate was allowed to cool to room temperature under a nitrogen flow of 1 L min^{-1}. Deposition time was in excess of 3 hours due to the difficulty in forming a mist with toluene. Deposition was observed mainly on the substrate in the reactor, although there was some deposition on the top plate. The analysis from the substrate is reported.

3.5.2 Appearance and substrate coverage

In all cases films appeared transparent, unreflective, colourless and birefringence was observed indicating a variation of film thickness. The films deposited displayed deposition localised mainly towards the leading edge of the substrate. This is a feature of fast growth kinetics and suggests that the reaction at the surface is limited by mass transport.

3.5.3 Powder X-ray diffraction

All the films deposited from Et_3Ga and donor functionalised alcohols were amorphous to X-rays due to the low temperatures used. This is consistent with previous literature reports on Ga_2O_3 films.[12]

3.5.4 Wavelength Dispersive X-ray Analysis

WDX analysis revealed some carbon contamination (10%) in the films and gave a Ga : O ratio of 1 : 1.2. These films were oxygen deficient due to the low oxygen

content in the precursor, the results of which are summarised in Table 3.2. The films deposited were fairly thin, being approximately 300-400 nm thick. Breakthrough to the underlying glass can result in difficulties in obtaining accurate atomic ratios. However, annealing the films in air at 600 °C resulted in films with Ga : O ratios of 1 : 1.5, in agreement with the anticipated value for Ga_2O_3. Furthermore, EDAX indicated that there is little carbon contamination (< 0.1 at. %).

Table 3.2: Film stoichiometry obtained for the deposition of films by AACVD reaction of Et_3Ga and different oxygen precursors.

Oxygen precursor	WDX as deposited films Ga : O ratio	WDX after annealing Ga : O ratio
$HOCH_2CH_2NMe_2$	1:1.17	1:1.5
$HOCH(CH_3)CH_2NMe_2$	1:1.16	1:1.4
$HOCH(CH_3)CH_2NMe_2$	1:1.15	1:1.5
$HOC(CH_3)_2CH_2OMe$	1:1.17	1:1.5
$HOCH_2CH_2OMe_2$	1:1.16	1:1.5
$HOCH(CH_3)_2$	1: 1.16	1.1:5

3.5.5 Raman

All the films were investigated using Raman microscopy. In all cases no Raman scattering was observed and it is thought that gallium oxide is a poor Raman scatterer. However, Raman spectroscopy indicated the absence of graphitic carbon in the films.

3.5.6 X-ray Photoelectron Spectroscopy

X-ray photoelectron spectroscopy of a Ga_2O_3 sample deposited by the reaction of Et_3Ga and $HOCH(CH_2NMe_2)_2$ at 550 °C shows that there are two gallium environments present (Figure 3.10). The peaks at 105.1 and 108 eV correspond to Ga $3p_{3/2}$ and Ga $3p_{1/2}$ of Ga_2O_3. These values are in close agreement with literature values previously reported for Ga_2O_3.[17] XPS also revealed a shift at 529.8 eV for the O 1s peak (Figure 3.11), this shift is in agreement with previous literature values.[17]

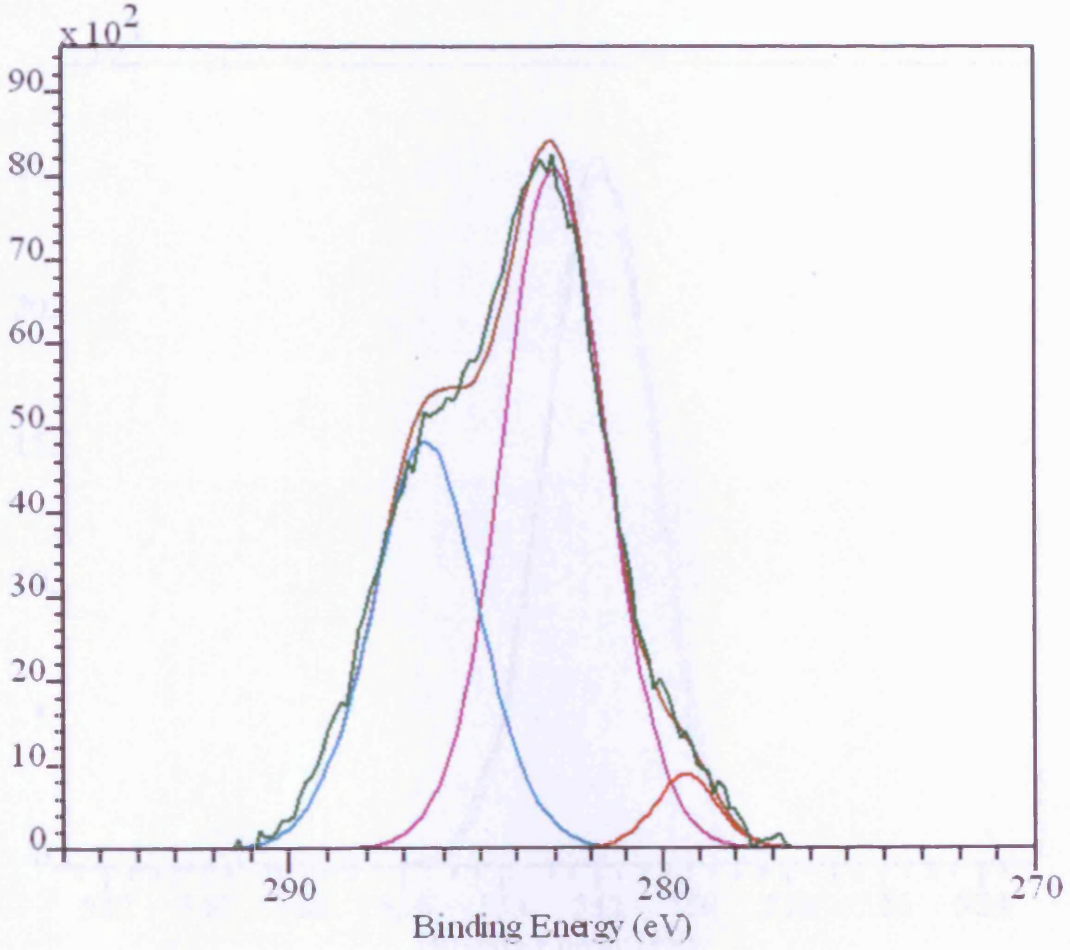

Figure 3.10: X-ray photoelectron spectrum for the Ga 3p peaks from a film deposited form the reaction of Et_3Ga and $HOCH(CH_2NMe_2)_2$ at 550 °C.

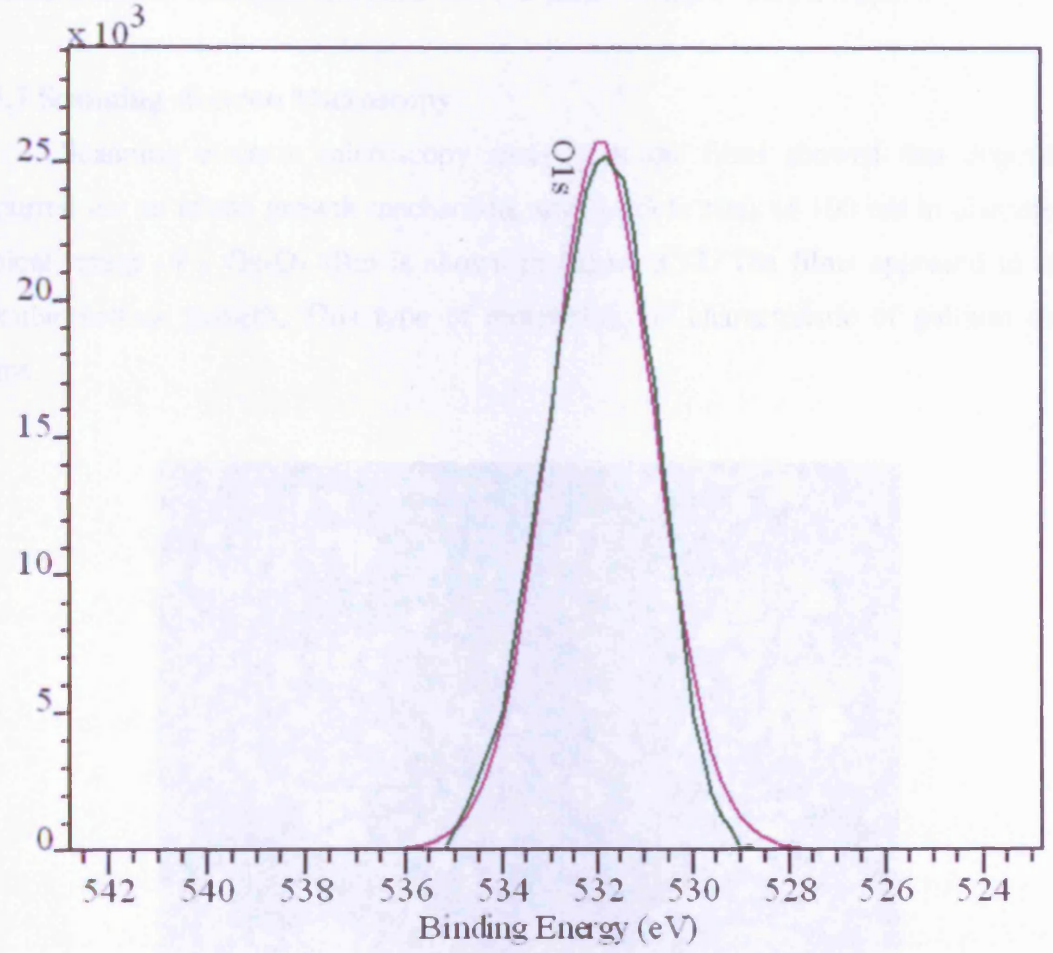

Figure 3.11: X-ray photoelectron spectrum for the O 1s peak from a film deposited form the reaction of Et_3Ga and $HOCH(CH_2NMe_2)_2$ at 550 °C.

X-ray photoelectron spectroscopy of a Ga_2O_3 sample deposited by the reaction of Et_3Ga and $HOCH_2CH_2NMe_2$ at 550 °C revealed binding energy shifts 106 and 109.3 eV corresponding to the Ga $3p_{3/2}$ and Ga $3p_{1/2}$ of Ga_2O_3. XPS revealed an additional peak at 531.6 eV for the O 1s peak. The binding shifts are in agreement with previous literature values of 105.1 and 108.7 eV for Ga $3p_{3/2}$ and Ga $3p_{1/2}$ and 530.5 eV for O 1s.[17]

XPS of a Ga_2O_3 film deposited by the reaction of Et_3Ga and $HOCH(CH_3)CH_2NMe_2$ at 550 °C revealed binding energy shifts 106.2 and 108.6 eV corresponding to the $3p_{3/2}$ and Ga $3p_{1/2}$ of Ga_2O_3. An additional peak corresponding to O

1s is observed at 529.7 eV. The binding energy shifts are in agreement with previous literature values. Nitrogen (1s) peak was not found in any of the XPS spectra.

3.5.7 Scanning electron Microscopy

Scanning electron microscopy analysis of the films showed that deposition occurred *via* an island growth mechanism, with particle sizes of 100 nm in diameter, a typical image of a Ga_2O_3 film is shown in Figure 3.12. The films appeared to have circular surface growth. This type of morphology is characteristic of gallium oxide films.

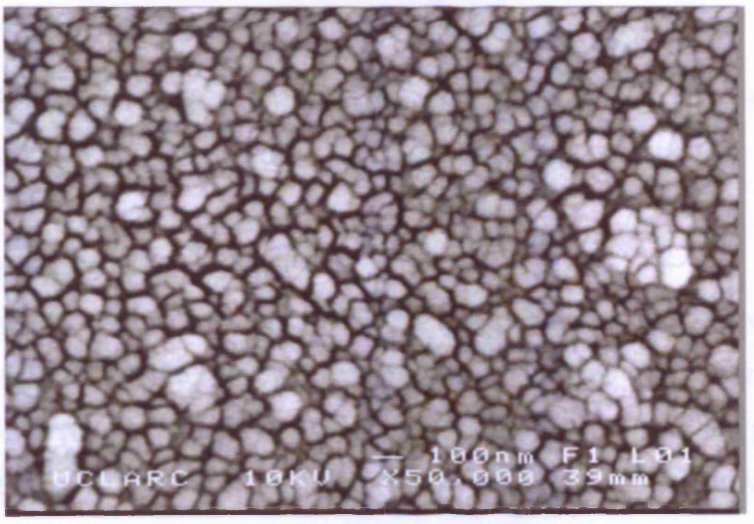

Figure 3.12: SEM image for Ga_2O_3 films deposited from the reaction of Et_3Ga and $HOCH_2CH_2NMe_2$ at 550 °C.

Annealing the films in air at 550 °C for 24 h gave slightly different morhpholgy, with a typical particle size of 1 μm and rods of about 10 μm. The SEM images, of films annealed and deposited from the reaction of Et_3Ga with $HOCH_2CH_2NMe_2$, or $HOCH(CH_2NMe_2)_2$ are shown in Figure 3.13.

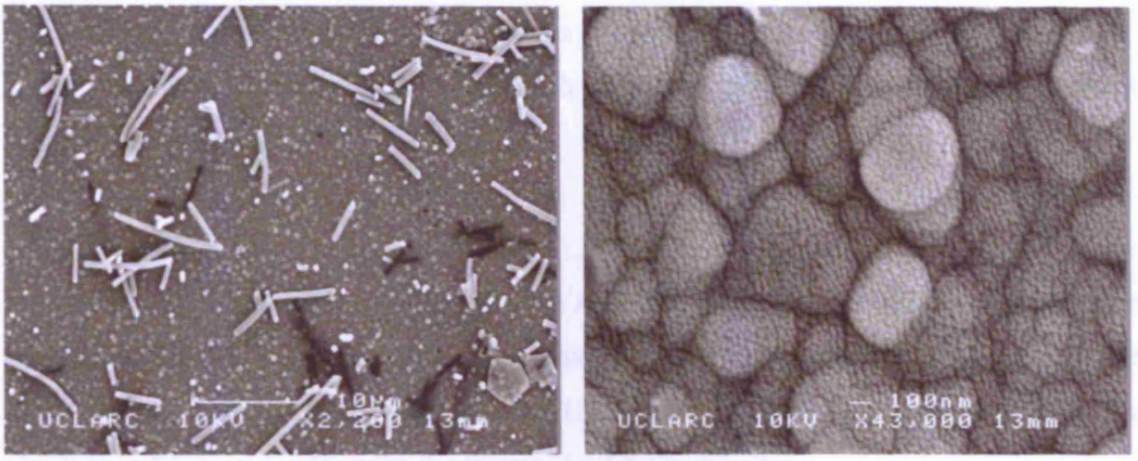

(a) (b)

Figure 3.13: SEM images if of annealed Ga_2O_3 films deposited from the reaction of Et_3Ga and a) $HOCH_2CH_2NMe_2$, and b) $HOCH(CH_2NMe_2)_2$ at 550 °C.

3.5.8 Optical properties

The optical properties of the films were investigated using reflectance transmission and UV/Visible measurements between 300-2500 nm. All samples showed a slight shift in the adsorption edge towards the visible relative to a plain glass substrate. The films displayed minimal reflectivity (5-10%) and very high transmission (80 – 90%).

3.5.9 Adherence

All films passed the scotch tape test. However, they were scratched by a brass or steel stylus.

3.5.10 Contact angle

The films were shown to have contact angles for water droplets of 24°, suggesting that the films are hydrophilic. This could be an effect of the large particle sizes allowing water to spread between the particles. The contact angles remain unchanged after photo-irradiation suggesting that the hydrophilicity is a permanent feature of the films rather than being photo-induced.

3.5.11 Band gap

Tauc plots[19], showed the films to have band gaps in the range of 4.5 and 4.7 eV as calculated from the UV-Vis data. These values are in agreement with values previously reported.[20]

3.5.12 Summary

The presence of excess ROH in the AACVD flask does not appear to reduce the oxygen deficiency. It is possible that stoichiometric films could be achieved if the carrier gas O_2 or wet ROH was employed. However, simple annealing of the films in air resulted in films of Ga_2O_3 with the correct 1 : 1.5 Ga : O ratio.

In general, dialkylgallium mono(alkoxides) thermally decompose initially to afford oxygen deficient Ga_2O_3 films *via* LPCVD on account of a low oxygen content in these precursors. However, the precursors prepared in this work do thermally decompose cleanly, as shown by the TGA data. Thin films of gallium oxide have been grown by the *in situ* reaction of Et_3Ga and excess alcohols via AACVD. These films were characterised by WDX, EDXA, XRD, XPS and UV-Vis and shown to be amorphous. The stiochiometric ratio of the Ga : O was low.

3.6 Deposition of Gallium Oxide Films from $[Ga(NMe_2)_3]_2$ and Donor Functionalised Alcohols by AACVD

In an effort to deposit stoichiometric Ga_2O_3 films using AACVD, the *in situ* reaction of $[Ga(NMe_2)_3]_2$ and excess ROH was investigated. This presumably yields complexes similar to the isolated compounds, as described in Chapter 2. Therefore, the gallium tris(alkoxides) are expected to form and such complexes possess a 1 : 3 ratio of Ga : O. These are expected to readily form stoichiometric Ga_2O_3 films with a 1 : 1.5 ratio of Ga : O. TGA was carried out on the isolated compounds to get some information about decomposition pathway and the temperature range. This section reports the deposition of Ga_2O_3 thin films by dual-source routes using AACVD.

3.6.1 Thermal analysis of $[Ga(OCH_2CH_2NMe_2)_3]_2$ (2)

The thermogravimetric analysis of $[Ga(OCH_2CH_2NMe_2)_3]_2$ **(2)** shows an overall mass loss of 79.8% (Figure 3.14). The decomposition of **2** does not occur in clean, discrete stages, but is continuous from the onset at *ca.* 100 °C throughout the temperature range studied, and occurs in four discrete stages. The first mass loss of 25.5% at 157 °C, the second of 30.0% at 180 °C, third mass loss of 21.2% at 265 °C and finally the fourth mass loss of 3.15% at 300 °C. The overall mass loss of 79.8% is close to the 72% required for complete decomposition to Ga_2O_3 suggesting that this compound would make a good precursor and could deposit films at low temperatures (less than 400 °C).

Two endotherms are observed, one small at 157.7 °C and a broad exotherm observed at 298.6 °C, which could be an effect of the decomposition process. Due to decomposition occurring in the experiment, it is difficult to distinguish the melting point for **2**.

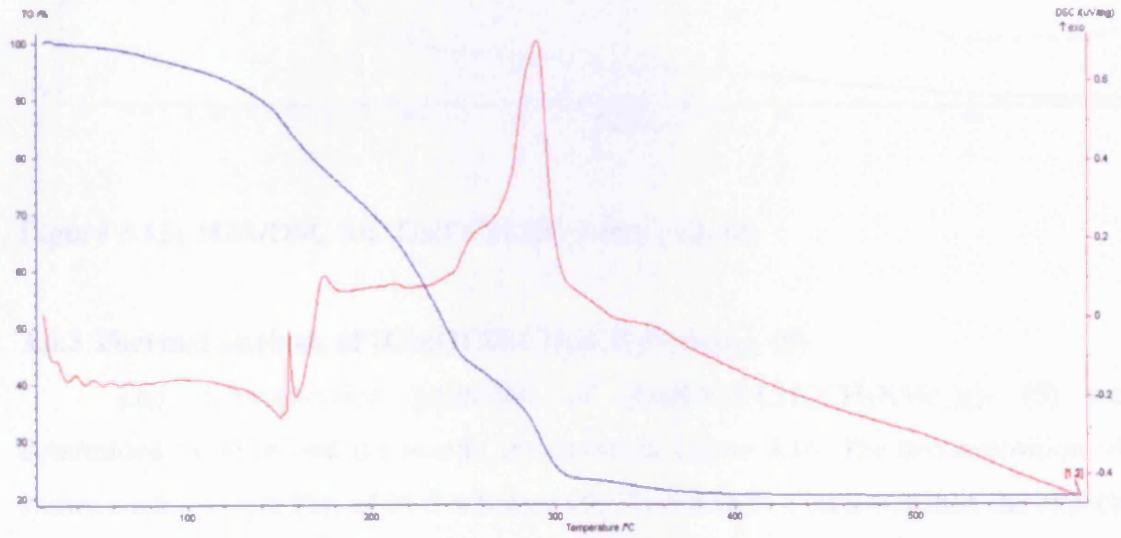

Figure 3.14: TGA/DSC of $[Ga(OCH_2CH_2NMe_2)_3]$ **(2)**

3.6.2 Thermal analysis of $[Ga(OCH(CH_2NMe_2)_2)_3]_2$ (4)

The TGA for $[Ga(OCH(CH_2NMe_2)_2)_3]_2$ **(4)** shows a total weight loss of 69.8% which is close to the 62.8% (below 200 °C) required for complete decomposition to Ga_2O_3 suggesting that this compound would make a good precursor and could deposit

films at low temperatures (less than 400 °C). Due to some decomposition occurring at the start of the experiment, it is difficult to distinguish the melting point, but appears to be below 100 °C. It is possible that decomposition of **4** has occurred before the melting point. The two exotherms at 133.2. and 198.2 °C could arise from the decomposition process. The decomposition of this precursor also begins at a much higher temperature than the melting point suggesting that this complex would deposit films easily.

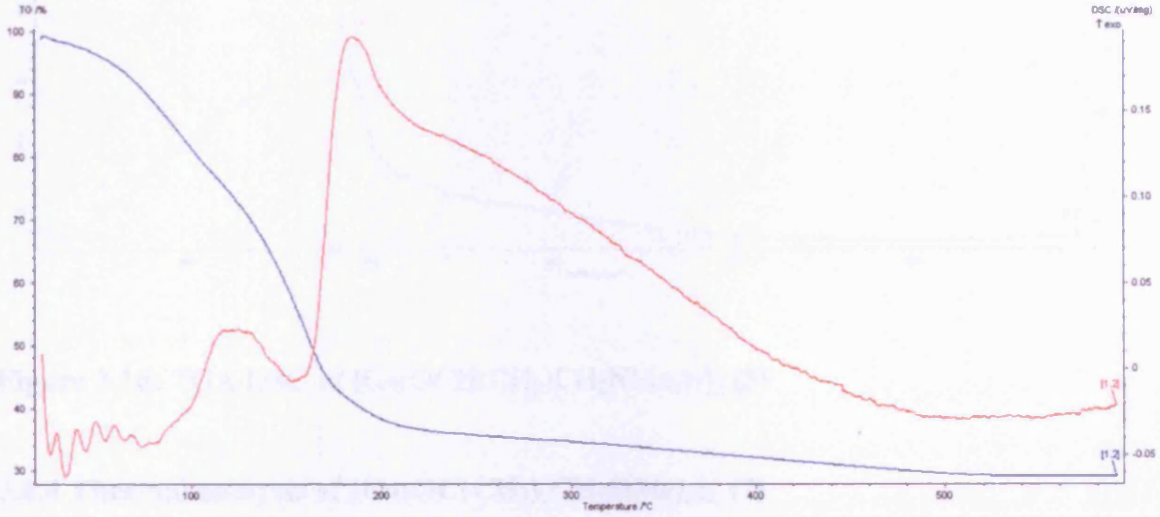

Figure 3.15: TGA/DSC for $[Ga(OCH(CH_2NMe_2)_2)_3]_2$ **(4)**

3.6.3 Thermal analysis of $[Ga(OCH(CH_3)CH_2NMe_2)_3]_2$ (5)

The decomposition properties of $[Ga(OCH(CH_3)CH_2NMe_2)_3]_2$ **(5)** were determined by TGA and the results are shown in Figure 3.16. The decomposition of **5** shows a total weight loss of 26.5% below 400 °C, which is a lot lower than the expected weight loss of 75.3% if Ga_2O_3 was formed. This behaviour indicates an incomplete decomposition to Ga_2O_3 up to 600 °C, although it is possible that the required weight loss could be attained at higer temperatures (the TGA set up allows analysis only to 600 °C). The observation of a steep weight loss followed by a more gradual loss of weight suggest that most of the decomposition occurs below 200 °C. However, it should be noted that initially there is an increase is mass (110%), this could be the result of buoyancy. The DSC of **5** shows a small endotherm at 63.9 °C, which corresponds to the melting point. The decomposition of **5** begins at a higher temperature than the melting

point suggesting that carry over of the intact molecule to the substrate could be successfully achieved. This would suggest that **5** would make a good CVD precursor.

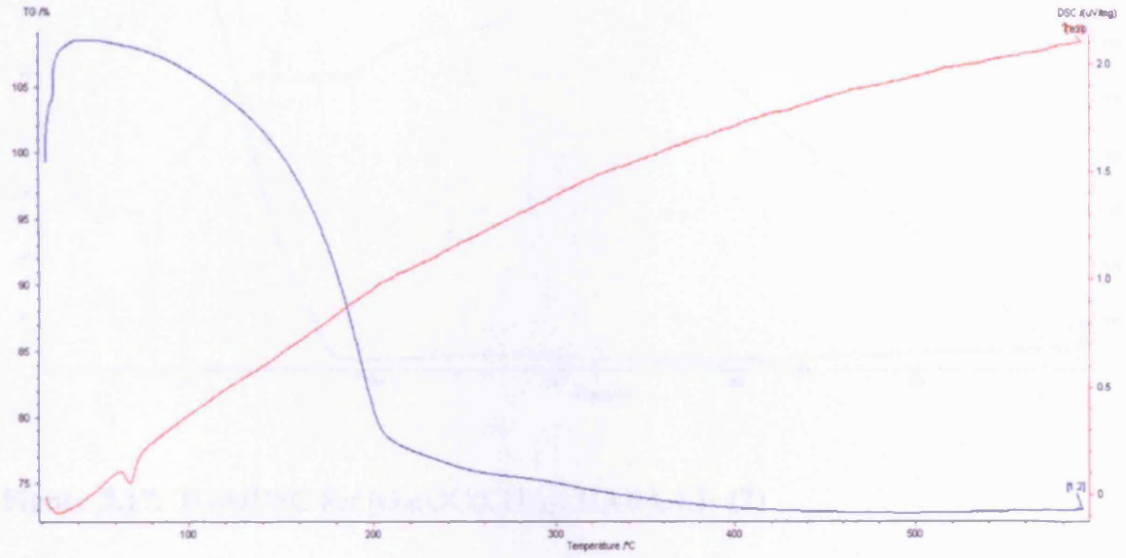

Figure 3.16: TGA/DSC of $[Ga(OCH(CH_3)CH_2NMe_2)_3]_2$ **(5)**

3.6.4 Thermal analysis of $[Ga(OC(CH_3)_2CH_2OMe)_3]_2$ (7)

The total mass loss of around 15.5% observed in the TGA of $[Ga(OC(CH_3)_2CH_2OMe)_3]_2$ **(7)** is lower than the calculated mass loss of 75.3% to form Ga_2O_3. A lower measured mass loss than that expected is an indication of incomplete decomposition. As shown in Figure 3.17, the decomposition occurs in a clean stage. The DSC of **7** shows a sharp endotherm at 83 °C, which corresponds to the melting point. A broad exotherm is observed at 328 °C, could be as a result of the decomposition process. It should be noted that the melting point of **7** is very close to the decomposition starting point suggesting that **7** may not be a good CVD precursor.

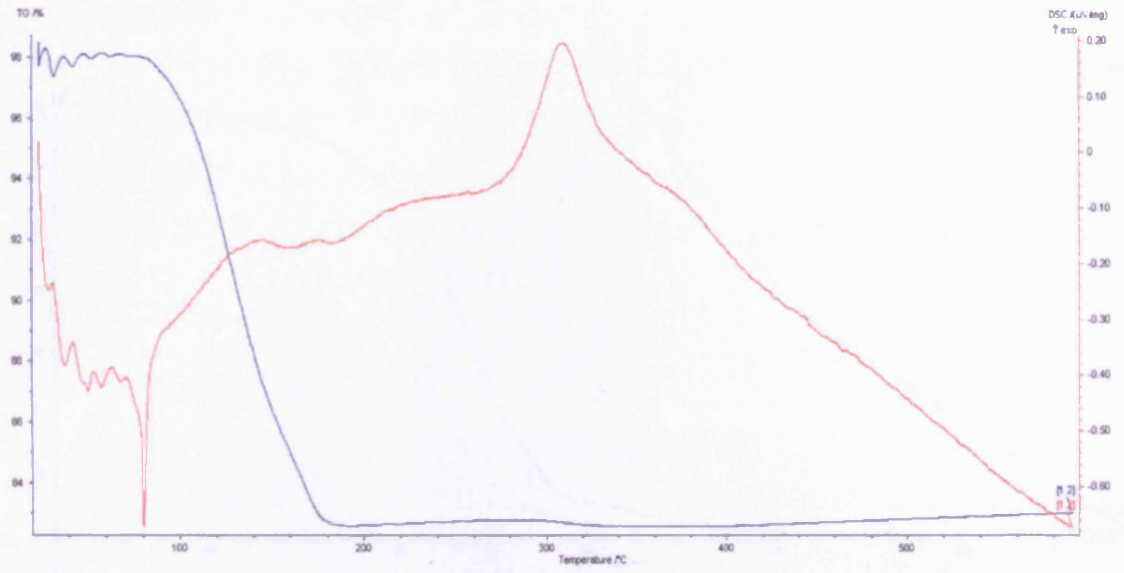

Figure 3.17: TGA/DSC for $[Ga(OC(CH_3)_2CH_2OMe)_3]_2$ **(7)**

3.6.6 Thermal analysis of $[Ga(OCH_2CH_2OMe)_3]_2$ (9)

The decomposition properties of $[Ga(OCH_2CH_2OMe)_3]_2$ **(9)** were determined by TGA and the results are shown in Figure 3.18. The decomposition of **9** shows a total weight loss of 34.5% below 400 °C, which is close to the expected weight loss of 43.8% if Ga_2O_3 was formed. As shown in Figure 3.18, the decomposition occurs in two stages. However, it should be noted that initially there is an increase is mass (110%), this is the result of the buoyancy. A broad exotherm is observed at 250.7 °C, which could be the result of a decomposition process. Due to some decomposition occurring at the start of the experiment, it is difficult to distinguish the melting point.

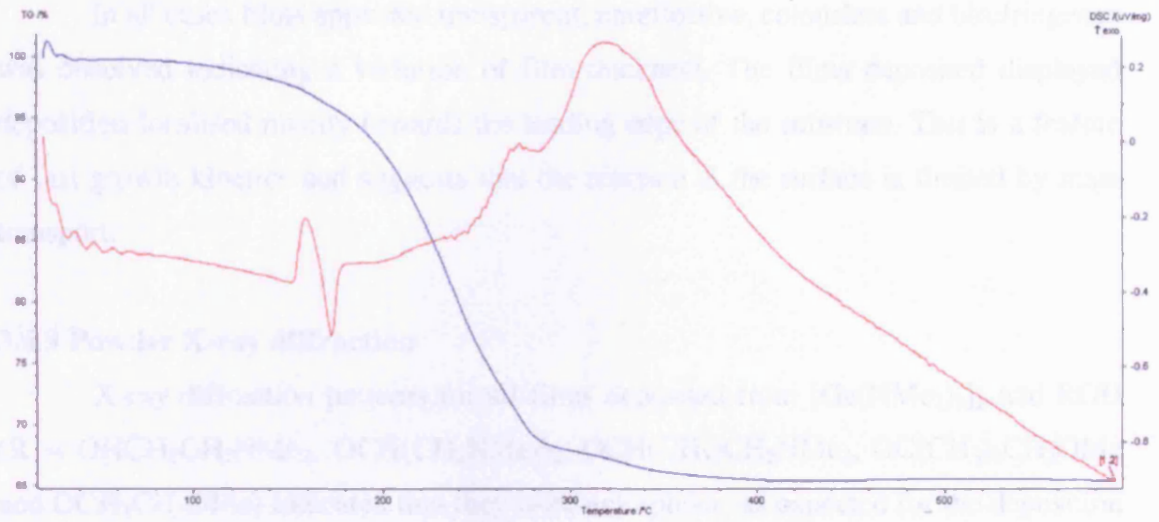

Figure 3.18: TGA/DSC for $[Ga(OCH_2CH_2OMe)_3]_2$ **(9)**

3.6.6 Summary of TGA results

In general, the TGA analysis of the homoleptic gallium alkoxides, gave total mass losses lower than that required for the precursors to form Ga_2O_3. The TGA was done on the mixtures formed from the reaction of $[Ga(NMe_2)_3]_2$ and alcohols, this could effect the total mass loss, due to the presence of impurities.

3.6.7 AACVD reaction conditions

Films were deposited at 450 °C from the *in situ* reaction of $[Ga(NMe_2)_3]_2$ and a range of oxygen precursors: *N,N*-dimethylethanolamine $HOCH_2CH_2NMe_2$, 1,3 bis-(dimethylamino)2-proponal $HOCH(CH_2NMe_2)_2$, 1-methoxy-2-methyl-2-propanol ($HOC(CH_3)_2CH_2OMe$), 1-dimethylamino-2-proponal $HOCH(CH_3)CH_2NMe_2$ and 2-methoxyethanol $HOCH_2CH_2OMe_2$. 0.5g of $[Ga(NMe_2)_3]_2$ was used with an excess of the donor functionalised alcohols (six equivalents) in 30 cm^3 of toluene. The reagents were allowed to mix for 1 hour prior to the deposition. All films were deposited on SiCO coated float glass. The flow rate throughout the reactor was kept constant for all depositions at 1 L min^{-1}, after which the substrate was allowed to cool to room temperature under a nitrogen flow of 1 L min^{-1}. Deposition time was in excess of 3 hours due to the difficulty in forming a mist with toluene. Deposition was observed mainly on the substrate in the reactor. The analysis from the substrate is reported.

3.6.8 Appearance and substrate coverage

In all cases films appeared transparent, unreflective, colourless and birefringence was observed indicating a variation of film thickness. The films deposited displayed deposition localised mainly towards the leading edge of the substrate. This is a feature of fast growth kinetics and suggests that the reaction at the surface is limited by mass transport.

3.6.9 Powder X-ray diffraction

X-ray diffraction patterns for all films deposited from $[Ga(NMe_2)_3]_2$ and ROH (R = $OHCH_2CH_2NMe_2$, $OCH(CH_2NMe_2)_2$, $OCH(CH_3)CH_2NMe_2$, $OC(CH_3)_2CH_2OMe$ and OCH_2CH_2OMe) indicated that they were amorphous, as expected for the deposition of gallium oxide at temperatures below 700 °C.[12]

3.6.10 Wavelength Dispersive X-ray Analysis

The films deposited from the AACVD reaction of $[Ga(NMe_2)_3]_2$ and ROH gave films that were oxygen deficient (Ga : O 1 : 2), despite the Ga : O ratio being correct in the precursor. This could be attributed to the presence of carbon in the film and the amorphous nature of the films. The films deposited were also very thin and breakthrough to the underlying glass made it difficult to analyse the oxygen content. Annealing the films in air at 600 °C gave films with stoichiometry close to Ga_2O_3 by WDX, the results of which are summarised in Table 3.3.

Table 3.3: Film stoichiometry obtained for the deposition of films by AACVD of $[Ga(NMe_2)_3]_2$ and different ROH

Oxygen precursor	WDX on deposited films	WDX after annealing
$HOCH_2CH_2NMe_2$	1.12	1.43
$HOCH(CH_2NMe_2)_2$	1.16	1.55
$HOCH(CH_3)CH_2NMe_2$	1.15	1.44
$HOC(CH_3)_2CH_2OMe$	1.12	1.39
$HOCH_2CH_2OMe_2$	1.11	1.37

3.6.11 Raman

Raman microscopy was used to investigate the films. Raman scattering was not observed in any instance. It is believed that gallium oxide is a poor Raman scatterer. However, no evidence of graphitic carbon was observed in any of the spectra.

3.6.12 X-ray Photoelectron Spectroscopy

The X-ray photoelectron spectrum for the Ga 2p peaks from a Ga_2O_3 film deposited from the reaction of $[Ga(NMe_2)_3]_2$ and $HOCH(CH_3)CH_2NMe_2$ at 550 °C shows that there are two gallium environments present (Figure 3.19). The peaks at 1119.4 and 1146.4 eV correspond to Ga $2p_{3/2}$ and Ga $2p_{1/2}$ of Ga_2O_3. However, it should be noted from the graph that there is some evidence of a small amount of impurity present in the film; the small peaks in the spectrum show this. This could be a gallium containg material, such as gallium carbide. These values for Ga_2O_3 are in close agreement with literature values previously reported for Ga_2O_3.[17] XPS also revealed a shift at 531.9 eV for the O 1s peak (Figure 3.20), this shift is in agreement with previous literature values of 530.5 eV for O 1s.[17]

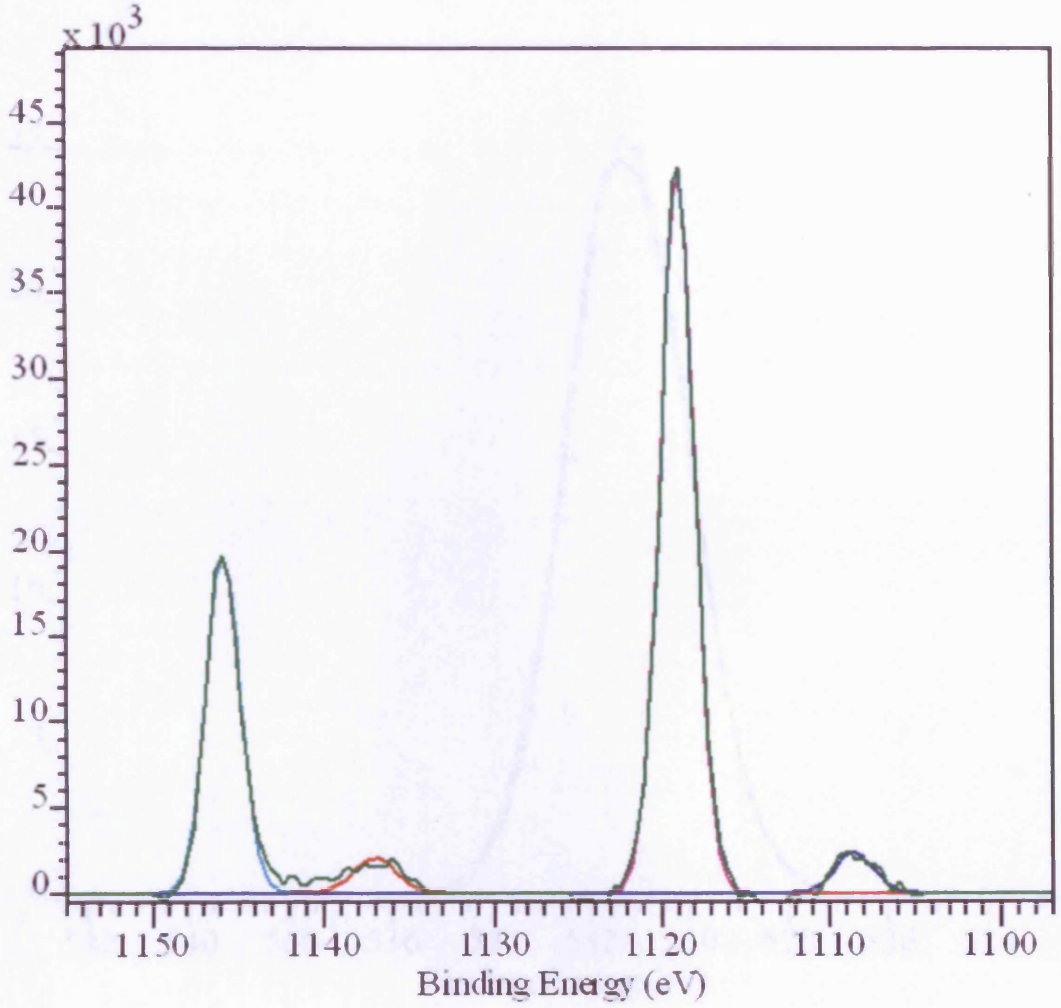

Figure 3.19: X-ray photoelectron spectrum for the Ga 2p peaks from a film deposited form the reaction of $[Ga(NMe_2)_3]_2$ and $HOCH(CH_3)CH_2NMe_2$ at 550 °C.

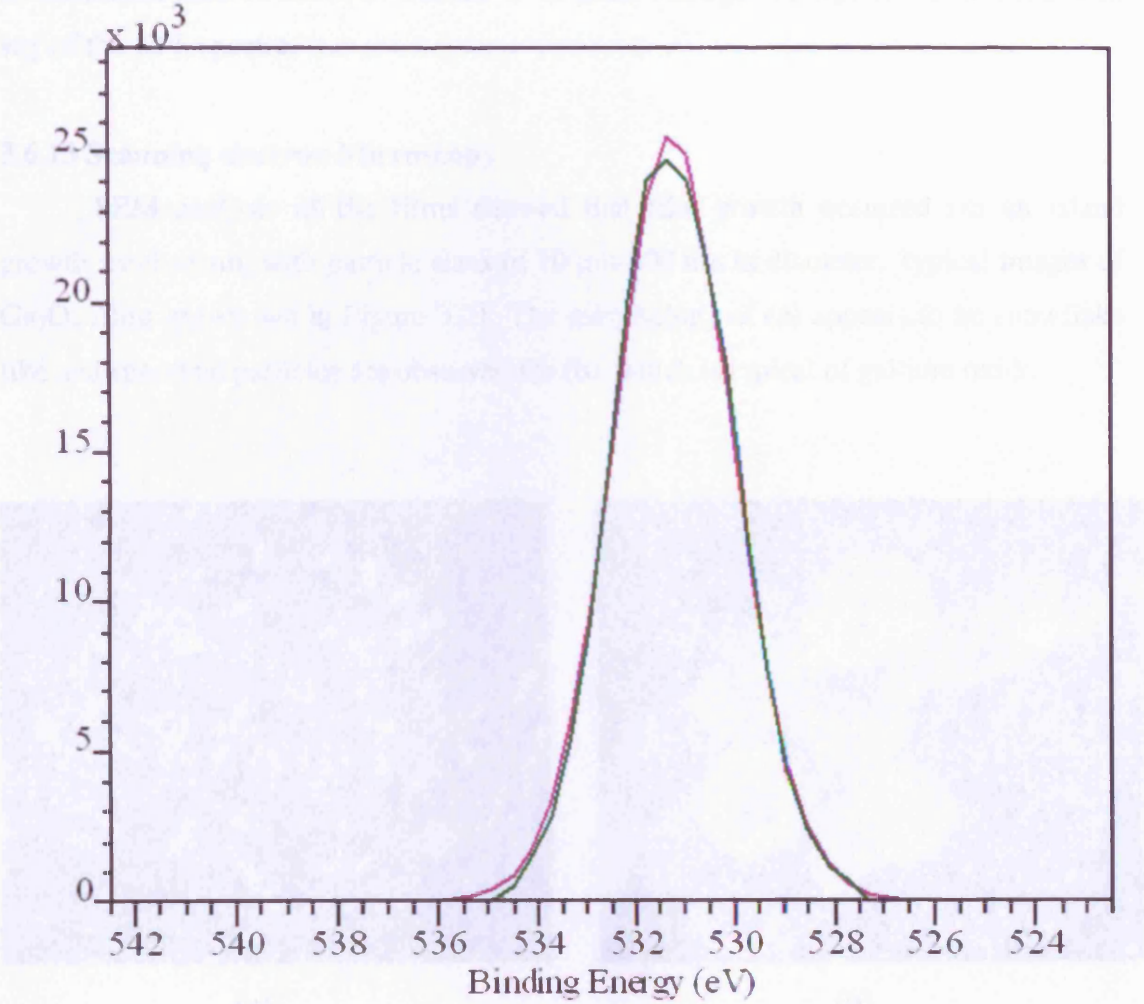

Figure 3.20: X-ray photoelectron spectrum for the O 1s peak from a film deposited form the reaction of $[Ga(NMe_2)_3]_2$ and $HOCH(CH_3)CH_2NMe_2$ at 550 °C.

The XPS of a Ga_2O_3 sample deposited by the reaction of $[Ga(NMe_2)_3]_2$ and $HOCH(CH_2NMe_2)_2$ at 550 °C revealed two different gallium environments, with binding energy shifts 1114.4 and 1141.2 eV corresponding to the $2p_{3/2}$ and Ga $2p_{1/2}$ of Ga_2O_3 and are within the range of values previously reported for this system. X-ray photoelectron spectroscopy also revealed a shift at 528.5 eV for the O 1s peak. This shift is in agreement with the previously reported literature value.[17]

X-ray photoelectron spectroscopy of a Ga_2O_3 sample deposited by the reaction of $[Ga(NMe_2)_3]_2$ and $HOCH_2CH_2NMe_2$ at 550 °C showed binding energy shifts at 1116.7 and 1143.7 eV corresponding to the $2p_{3/2}$ and Ga $2p_{1/2}$ of Ga_2O_3. XPS revealed

an additional peak at 531.0 eV for the O 1s peak. Nitrogen (1s) peak was not found in any of the XPS spectra.

3.6.13 Scanning electron Microscopy

SEM analysis of the films showed that film growth occurred *via* an island growth mechanism, with particle sizes of 10 μm-200 nm in diameter, typical images of Ga_2O_3 films are shown in Figure 3.21. The morphology of **(a)** appears to be snowflake like and spherical particles are observed for **(b)**, which is typical of gallium oxide.

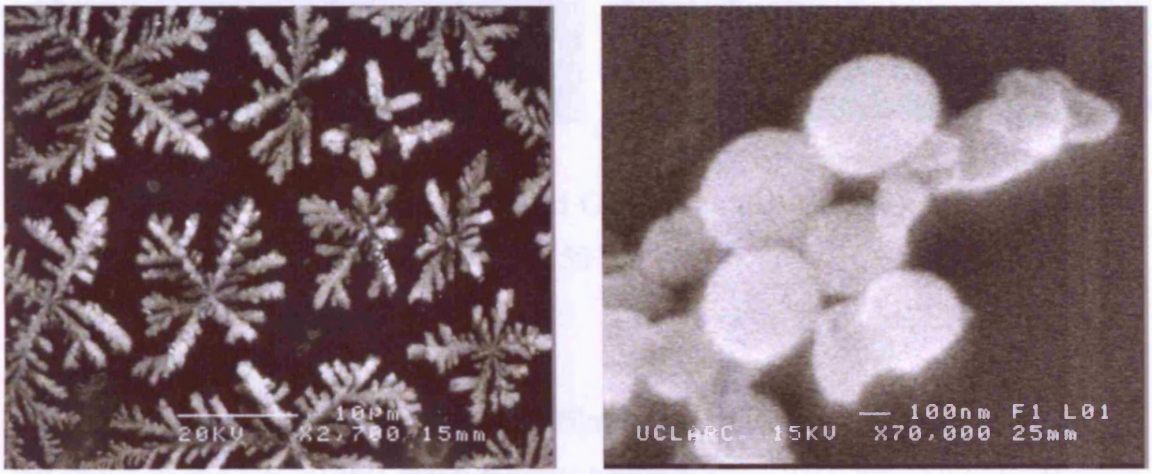

(a) **(b)**

Figure 3.21: SEM images for a Ga_2O_3 films deposited from the reaction of $[Ga(NMe_2)_3]_2$ and a) $HOCH(CH_3)CH_2NMe_2$, b) $HOCH(CH_2NMe_2)_2$ at 550 °C.

Annealing the films in air at 550 °C for 24 h gave films with similar morphology, with a typical particle of 1 μm, typical SEM images are shown in Figure 3.22.

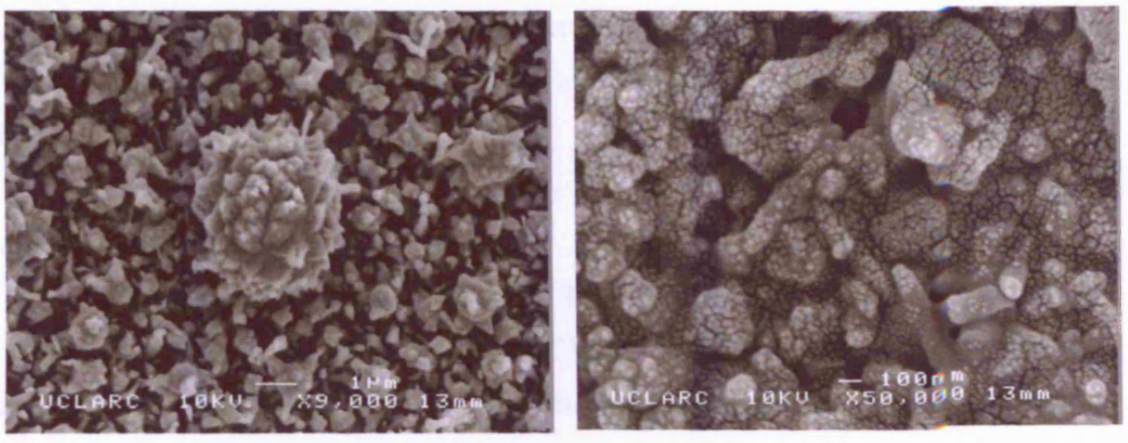

Figure 3.22: SEM images of an annealed Ga_2O_3 film deposited from the reaction of $[Ga(NMe_3)_2]_2$ and $HOCH(CH_2NMe_2)_2$ at 550 °C.

3.6.14 Optical properties

The optical properties of the films were investigated using reflectance transmission and UV-Visible measurements between 300 – 2500 nm. All films showed a slight shift in the adsorption edge towards the visible relative to a plain glass substrate. The films displayed minimal reflectivity (5-10%) and high transmission (80 – 90%).

3.6.15 Adherence

All films passed the scotch tape test. However, they were scratched by a brass or steel stylus.

3.6.16 Contact angle

The films were shown to have contact angles for water droplets of 20°, suggesting that the films are hydrophilic. Contact angle measurements are valuable in the glass industry in assessing whether films have self-cleaning properties.[4] Low contact angles arising from hydrophilic films give rise to the water spreading across the surface and hence washing away any loose dirt. However, the contact angles for these films did not change upon photo-irradiation suggesting that this low contact angle is not due to

some form of photo-induced hydrophilicity. Thus, the low contact angle is most likely due to a high-porosity within the films.

3.6.17 Band gap

Tauc plots[19] of the UV-Vis data were conducted and gave band gaps in the region of 4.2-4.5 in the range of 4.5-4.9 eV and are in agreement with literature values.[20]

3.6.18 Summary

Thin films of gallium oxide have been grown by the *in situ* reaction of $[Ga(NMe_2)_3]_2$ and excess alcohols via AACVD. These films were characterised by EDXA WDX, XRD, XPS and UV-Vis and shown to be amorphous. The stiochiometric ratio of the Ga : O was low for Ga_2O_3. However, annealing at 600 °C afforded films of the correct Ga : O

3.7 Deposition of Indium Oxide Films from Me_3In and Donor functionalised Alcohols by AACVD

The deposition of In_2O_3 thin films by dual-source routes using AACVD is discussed. The *in situ* reaction of Me_3In and ROH was used which presumably yielded complexes similar to the isolated compounds, $[Me_2InOR]_2$, as described in Chapter 2.

3.7.1 Thermal analysis of $[Me_2In(OCH_2CH_2NMe_2)]_2$ (20)

The TGA of $[Me_2In(OCHCH_2CH_2NMe_2)]_2$ **(20)** shows an overall mass loss of 52.3% (Figure 3.23). The decomposition of **20** does not occur in clean, discrete stages but is continuous from the onset at *ca.* 140 °C throughout the temperature range studied and occurs in four stages. The first mass loss of 13.2% at 180 °C, the second of 24.3% at 200 °C, the third mass loss of 13.8% at 238 °C, finally the fourth mass loss of 1.05% occurs at 300 °C. The overall mass loss of 52.3% is higher than the required total mass loss of 40.4% for complete decomposition to In_2O_3. This behaviour indicates sublimation of the precursor.

The sharp endotherm at 172.6 °C in the DSC of $[Me_2In(OCHCH_2CH_2NMe_2)]_2$ signifies a melting point. The sharp exotherm observed at 284.4 °C could be an effect of

the decomposition process. Due to some decomposition occurring at the start of the experiment, it is difficult to distinguish the melting point. It is possible that decomposition of **20** has occurred before the melting point.

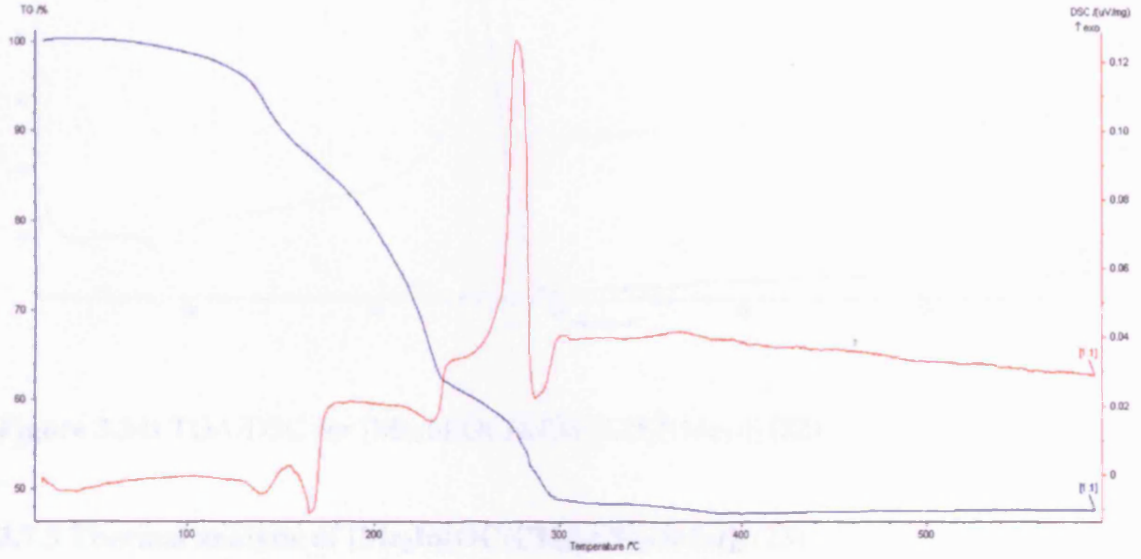

Figure 3.23: TGA/DSC for $[Me_2In(OCH_2CH_2NMe_2)]_2$ **(20)**

3.7.2 Thermal analysis of $[Me_2In(OCH(CH_3)CH_2NMe_2)]_2$ (22)

The decomposition properties of $[Me_2In(OCH(CH_3)CH_2NMe_2)]_2$ **(22)** were determined by TGA, the results of which are shown in Figure 3.24. The decomposition of **22** shows a total weight loss of 13.6% below 500 °C, which is a lot lower than the expected weight loss of 43.8% if In_2O_3 was formed. This could be due to incomplete decomposition to In_2O_3, the TGA equipment used only allows heating up to 600 °C. After 300 °C a slight weight gain is observed which could be due to hydrolysis. Further mass loss could be observed if the sample was heated to a higher temperature.

The DSC of **22** shows a small broad endotherm at 94.2 °C, which corresponds to the melting point. A further broad endotherm is observed at 285.8 °C. The sharp exotherm at 285.8 °C could be an effect of the decomposition process. Hence, suggesting that $[Me_2In(OCH(CH_3)CH_2NMe_2)]_2$ **22** would make a good CVD precursor, as the decomposition of **22** begins at a higher temperature than the melting point . However, the low weight loss indicated that decomposition of **22** may be incomplete.

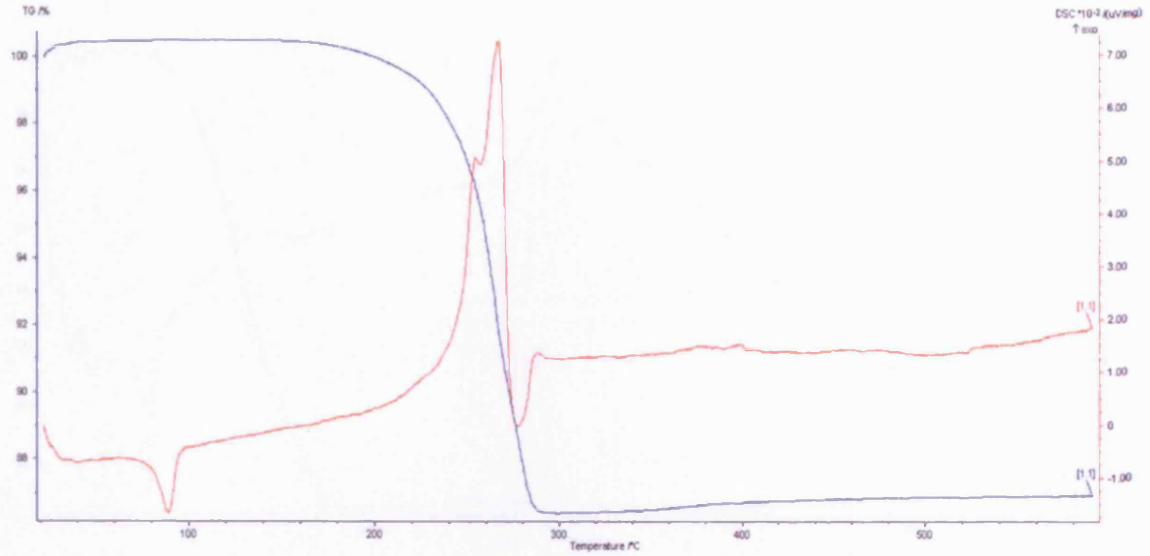

Figure 3.24: TGA/DSC for $[Me_2In(OCH(CH_3)CH_2NMe_2)]_2$ **(22)**

3.7.3 Thermal analysis of $[Me_2In(OC(CH_3)_2CH_2OMe)]_2$ (23)

The total mass loss of around 15.4% observed in the TGA (Figure 3.25) of $[Me_2In(OC(CH_3)_2CH_2OMe)]_2$ **(20)** is significantly lower than the calculated mass loss of 44.0% for **22** to form In_2O_3, which occurs around 100 °C. This lower measured mass loss than that expected could be due to incomplete decomposition. However, further mass loss could be observed if the sample was heated to a higher temperature.

The DSC of **22** shows a sharp endotherm at 180 °C, signifying the melting point. The exotherm at 320.6 °C could be as a result of the decomposition process. The poor weight loss can be due to the melting point and decomposition being very close.

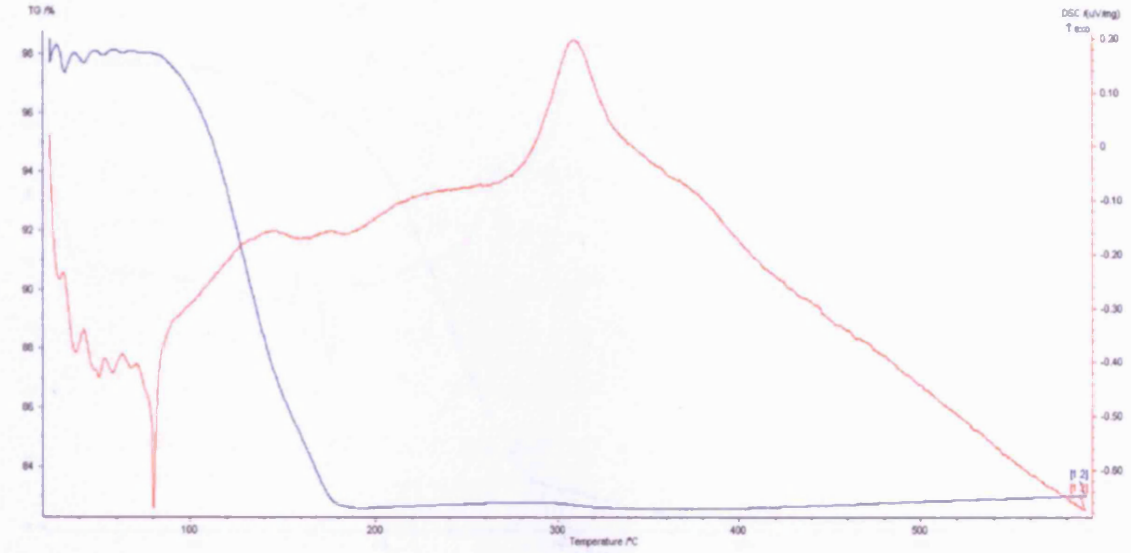

Figure 3.25: TGA/DSC for $[Me_2In(OC(CH_3)_2CH_2OMe)]_2$ **(23)**

3.7.4 Thermal analysis of $[Me_2In(OCH_2CH_2OMe)]_2$ (24)

The thermal analysis of $[Me_2In(OCH_2CH_2OMe)]_2$ **(24)** were determined by TGA and the results are shown in Figure 3.26. The initial increase in mass loss observed is due to the buoyancy. The overall mass loss of 34.5% is close to the 36.9% required for complete decomposition to In_2O_3 suggesting that this compound would make a good precursor and could deposit films at low temperatures (less than 400 °C). As the total mass loss as occurred below 300 °C.

Due to some decomposition occurring at the start of the experiment, it is difficult to distinguish the melting point. It is possible that decomposition of **4** has occurred before the melting point. The two exotherms at 172.0 and 349.7 °C could be an effect of the decomposition process.

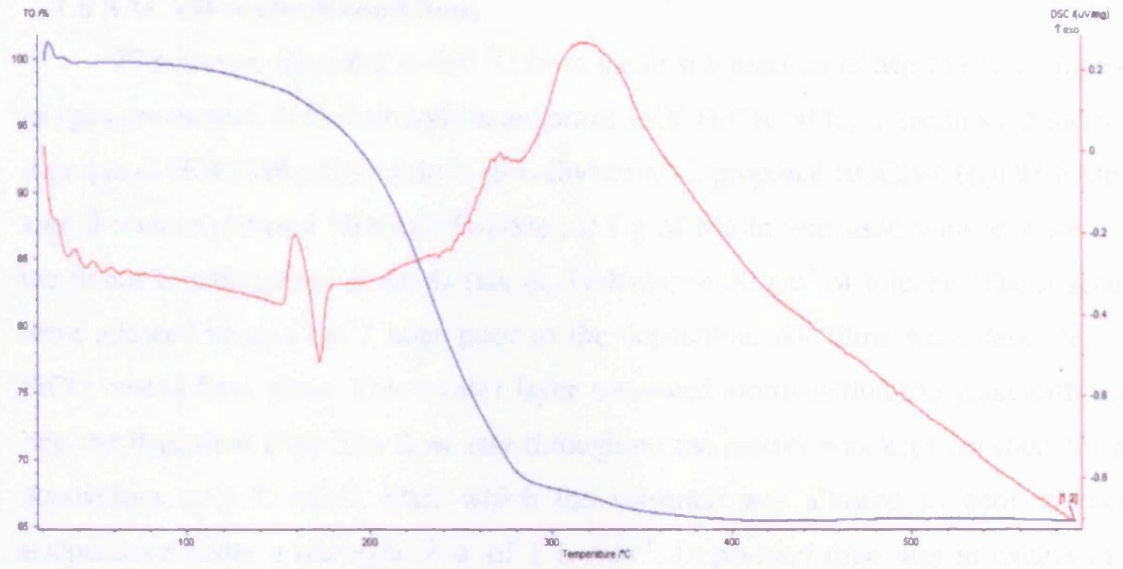

Figure 3.26: TGA/DSC for $[Me_2In(OCH_2CH_2OMe)]_2$ **(24)**

3.7.5 Summary of TGA/DSC results

The thermogravimetric analysis of two of the dialkyl indium mono(alkoxides) (**20** and **24**), gave total mass losses close to that required for the precursors to form In_2O_3. However, the observed mass loss for **22** and **23** were significantly lower than expected. These results could be due hydrolysis during the TGA process or incomplete decomposition. These results would need to be repeated to clarify this accuracy. The results of which are summarised in Table 3.4. The TGA results do suggest that all the precursors should decompose readily, as the total mass loss occurs below 300 °C, and carry over of the precursor in the CVD process could be achieved.

Table 3.4: Summary of TGA results of dialkyl indium mono(alkoxides)

Complex	Calc. Mass loss for In_2O_3 /%	Observed Mass loss for In_2O_3 /%
$[Me_2In(OCH_2CH_2NMe_2)]_2$ **(20)**	40.3	52.3
$[Me_2In(OCH(CH_3)CH_2NMe_2)]_2$ **(22)**	43.8	13.6
$[Me_2In(OC(CH_3)_2CH_2OMe)]_2$ **(23)**	40.0	15.4
$[Me_2In(OCH_2CH_2OMe)]_2$ **(24)**	34.5	36.9

3.7.6 AACVD reaction conditions

Films were deposited at 450 °C from the *in situ* reaction of Me_3In and a range of oxygen precursors, *N,N*-dimethylethanolamine $HOCH_2CH_2NMe_2$, 1-methoxy-2-methyl-2-propanol $HOC(CH_3)_2CH_2OMe$, 1-dimethylamino-2-proponal $HOCH(CH_3)CH_2NMe_2$ and 2-methoxyethanol $HOCH_2CH_2OMe_2$. 0.5 g of Me_3In was used with an excess of the donor functionalised alcohols (six equivalents) in 30 cm^3 of toluene. The reagents were allowed to mix for 1 hour prior to the deposition. All films were deposited on SiCO coated float glass. This barrier layer prevented atoms within the glass diffusing into the deposited film. The flow rate throughout the reactor was kept constant for all depositions at 1 L min^{-1}, after which the substrate was allowed to cool to room temperature under a nitrogen flow of 1 L min^{-1}. Deposition time was in excess of 2 hours due to the difficulty in forming a mist with toluene. Deposition was observed on the substrate in the reactor; analysis from the substrate is reported.

3.7.7 Appearance and substrate coverage

All the films were of brown/rainbow colour. The films deposited were uniform and covered the substrate completely. The films deposited displayed deposition localised equally over the whole substrate plate.

3.7.8 Powder X-ray diffraction

All the films obtained were composed of cubic crystalline In_2O_3 and the XRD patterns showed strong reflections for the (222) plane. A representative powder XRD of all In_2O_3 films is shown in Figure 3.27.

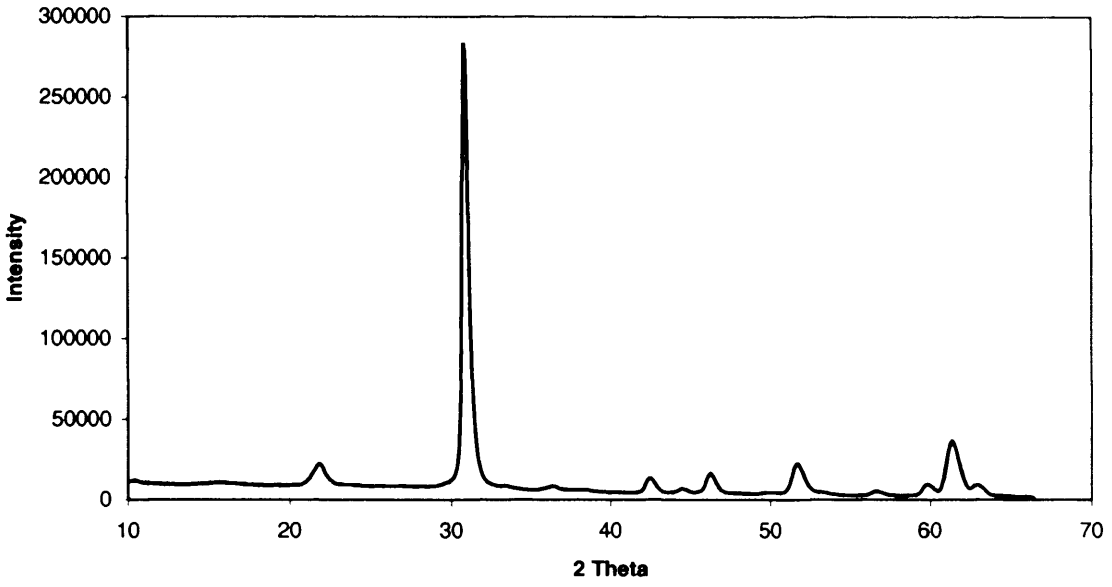

Figure 3.27: X-ray diffraction of In_2O_3 film deposited by AACVD from the *in situ* reaction of Me_3In and $HOCH_2CH_2OMe_2$ at 550 °C.

The In_2O_3 films were grown at 550 °C and showed only a single phase cubic In_2O_3. In general, indium oxide films are polycrystalline with a cubic structure in the bulk material, and a preferred orientation along the (222) plane is common.[20] The lattice constants obtained of cubic-In_2O_3 are summarised in Table 3.5. These values were found to be close to the anticipated value, 10.118 Å[21] for bulk In_2O_3.

Table 3.5: Lattice constants for the films deposited from the reaction of Me_3In and different oxygen precursors.

Oxygen precursor	Lattice constant, *a*
$HOCH_2CH_2NMe_2$	10.03
$HOCH(CH_3)CH_2NMe_2$	10.11
$HOC(CH_3)_2CH_2OMe$	10.03
$HOCH_2CH_2OMe_2$	10.03

3.7.9 Wavelength Dispersive X-ray Analysis

A summary of the WDX data for all the reactions is summarised in Table 3.6. The results show that films deposited from the *in situ* reaction of Me_3In and excess $HOCH_2CH_2NMe_2$ and $HOCH(CH_3)CH_2NMe_2$ produced films with the correct stiochiomtery. However, when using $HOC(CH_3)_2CH_2OMe$ and $HOCH_2CH_2OMe$ gave films which were slightly oxygen deficient, this could be due to the thickness of the films. However, within experimental error all films can be considered to be In_2O_3.

Table 3.6: Film stoichiometry obtained for the deposition of films by AACVD of Me_3In and different ROH

Oxygen precursor	WDX on deposited films
$HOCH_2CH_2NMe_2$	1:1.5
$HOCH(CH_3)CH_2NMe_2$	1:1.5
$HOC(CH_3)_2CH_2OMe$	1:1.4
$HOCH_2CH_2OMe_2$	1:1.3

3.7.10 X-ray Photoelectron Spectroscopy

The X-ray photoelectron spectrum for the In 2p peaks from a In_2O_3 film deposited from the reaction of Me_3In and $HOCH(CH_3)CH_2NMe_2$ at 550 °C shows that there are two indium environments present (Figure 3.28). The peaks at 444.5 and 452.1 eV correspond to In $2p_{3/2}$ and In $2p_{1/2}$ of In_2O_3. These values are in close agreement with literature values previously reported for In_2O_3.[17] XPS also revealed a shift at 530.1 eV for the O 1s peak (Figure 3.29), this shift is in agreement with previous literature value of 530.5 eV for O 1s.[17]

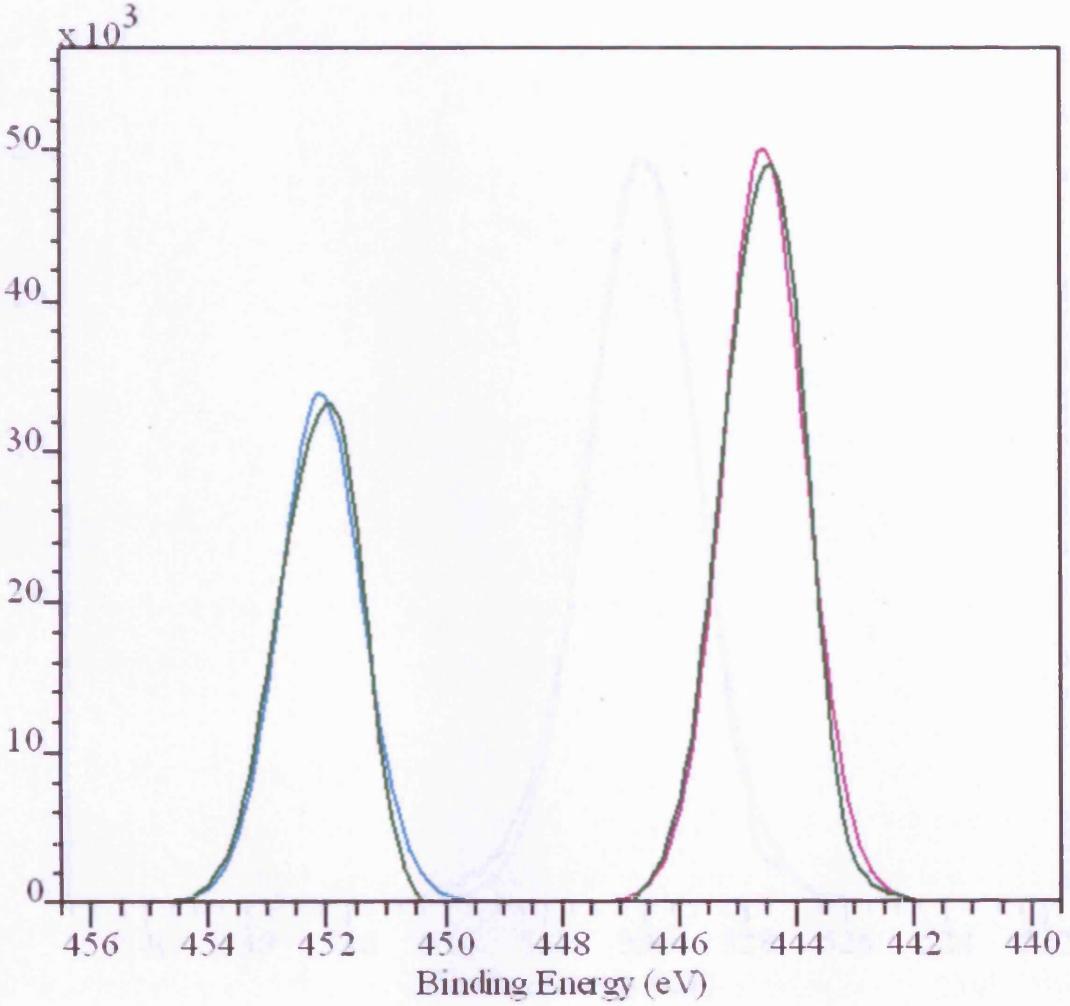

Figure 3.28: X-ray photoelectron spectrum for the In 2p peaks from a film deposited form the reaction of Me_3In and $HOCH_2CH_2NMe_2$ at 550 °C.

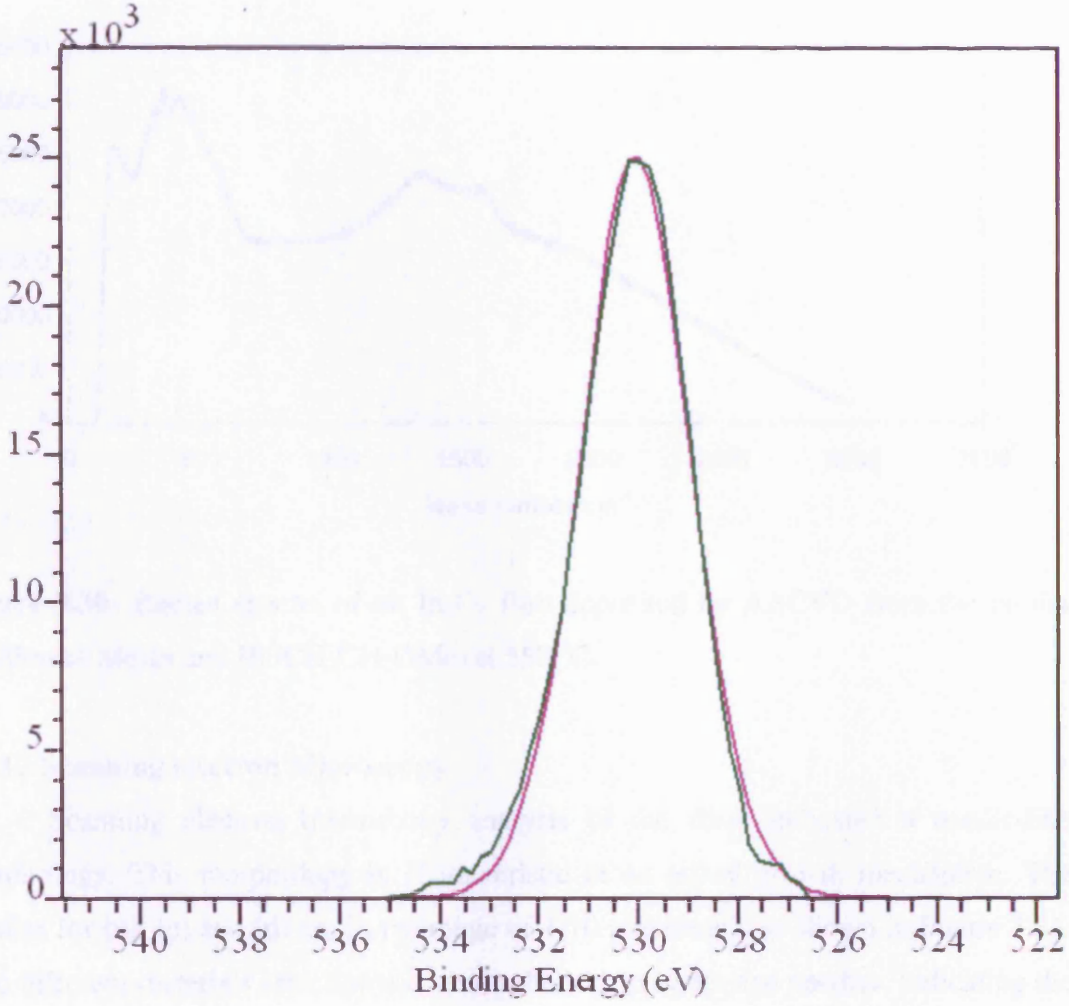

Figure 3.29: X-ray photoelectron spectrum for the O 1s peak from a film deposited form the reaction of Me_3In and $HOCH_2CH_2NMe_2$ at 550 °C.

3.7.11 Raman

The Raman pattern shown in Figure 3.30 is representative of all In_2O_3 films grown, absorption bands are observed, with a broad band at 363 cm^{-1}. The pattern is characteristic of In_2O_3 and matches well with those previously reported.[23] The strongest absorption bands for a standard commercial supply of In_2O_3 powders occurs near 308, 365, 504 and 637 cm^{-1}.[22]

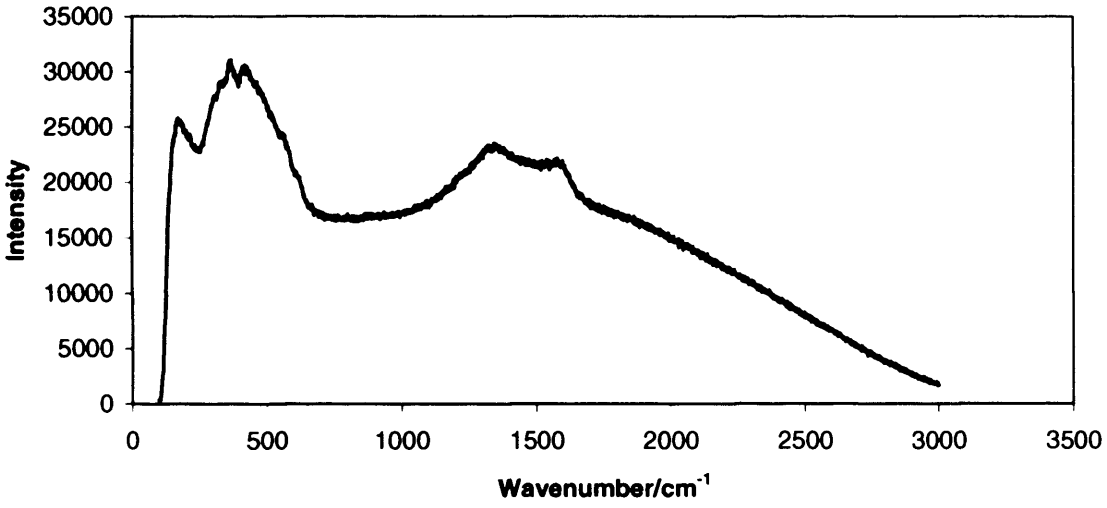

Figure 3.30: Raman spectra of an In_2O_3 film deposited by AACVD from the *in situ* reaction of Me_3In and $HOCH_2CH_2OMe_2$ at 550 °C.

3.7.12 Scanning electron Microscopy

Scanning electron microscopy analysis of the films indicated a needle-like morphology. This morphology is characteristic of an island growth mechanism. The needles for **(a)**, **(c)** and **(d)** are in the range of 4-10 μ in length, as shown in Figure 3.31. Two different materials are observed in **a**, spherical particles and needles, indicating the presence of two materials. This could be due to the thickness of the film or the presence of crystalline and amorphous material. However, the SEM image for the film deposited from the reaction of Me_3In and $HOCH_2CH_2NMe_2$, **(b)**, shows a slightly different morphology, that of spherical particles.

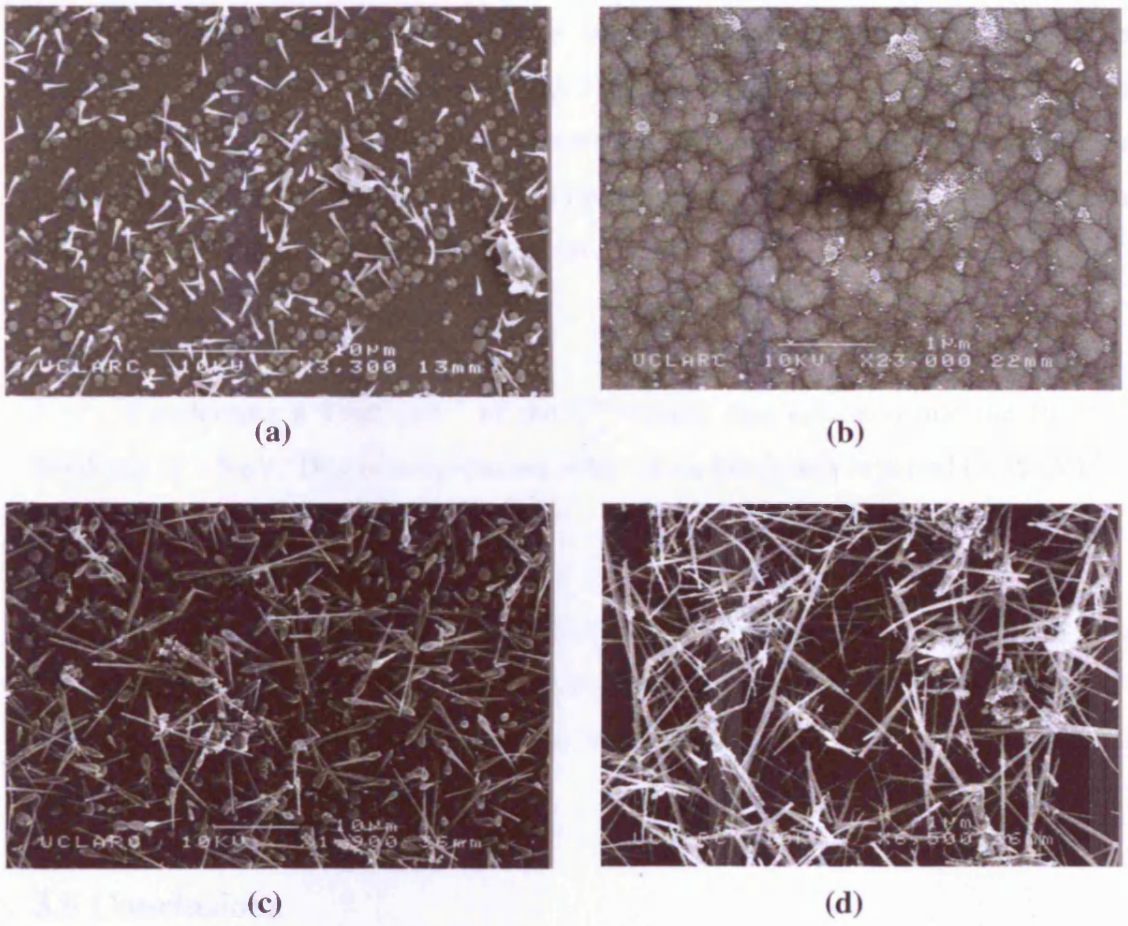

Figure 3.31: SEM images for In_2O_3 films deposited from the reaction of Me_3In and a) $HOCH(CH_3)CH_2NMe_2$, b) $HOCH_2CH_2NMe_2$, c) $HOC(CH_3)_2CH_2OMe$ and d) $HOCH_2CH_2OMe_2$ at 550 °C.

3.7.13 Optical properties

The optical properties of the films were investigated using reflectance transmission and UV-Visible measurements between 300 – 2500 nm. All films showed a slight shift in the adsorption edge towards the visible relative to a plain glass substrate. The films displayed minimal reflectivity (5-10%) and high transmission (70%).

3.6.14 Adherence

All films passed the scotch tape test and were resistant to marking by a wet towel or a brass stylus, but could be marked by a steel scalpel.

3.6.15 Contact angle

The films were shown to have contact angles for water droplets of 28°, suggesting that the films are hydrophilic. However, the contact angles for these films deposited did not change upon photo-irradiation suggesting that this low contact angle is not due to some form of photo-induced hydrophilicity. The porosity of the films could be responsible for this hydrophilic character.

3.6.16 Band gap

Conducting a Tauc plot[19] of the UV/visible data indicated that the films had band gap of 3.5 eV. This is in agreement with values previously reported (3.75 eV).[14]

3.7.17 Summary

Thin films of indium oxide have been grown by the *in situ* reaction of Me_3In and excess alcohols via AACVD. These films were characterised by WDX, XRD, XPS, Raman and UV-Vis and were shown to be crystalline. The films deposited had the correct ratio of In : O for In_2O_3.

3.8 Conclusions

In general, dialkylgallium mono(alkoxides) thermally decompose to afford oxygen deficient Ga_2O_3 on account of a deficiency of oxygen in these precursors. However, the precursors prepared in this work, do thermally decompose to form cleanly, as shown by the TGA data.

Thin films of gallium oxide have been grown successfully by the *in situ* reaction of $Et_3Ga/[Ga(NMe_2)_3]_2$ and excess alcohols *via* AACVD. These films were characterised by EDXA, WDX, XRD, XPS and UV-Vis and shown to be amorphous. Annealing the films at 600 °C afforded films of the correct Ga : O ratio. In comparison, Ga_2O_3 films were also prepared by single-source routes using LPCVD resulted in the deposition of a poorly adhesive grey film. The oxygen content was found to be low as revealed by EDXA.

Crystalline films of indium oxide have also been deposited by the *in situ* reaction Me_3In and excess alcohol in a similar manner to gallium. Surprisingly, the

In_2O_3 films were not oxygen deficient and little carbon contamination was observed. This could be due to the differences between Et–Ga and Me–In.

3.9 Experimental

3.9.1 AACVD Experimental

Nitrogen (99.99 %) was obtained from BOC and used as supplied. Depositions were obtained on SiCO coated float-glass. Prior to use the glass substrates were cleaned using petroleum ether (60-80 °C) and propan-2-ol and then dried in air. Glass substrates of *ca.* 90 mm x 45 mm x 4 mm were used. The precursor was dissolved in solvent and vaporized at room temperature by use of a PIFCO ultrasonic humidifier (Figure 3.32). This produced an aerosol of the precursor in the solvent used. Two-way taps were used to divert the nitrogen carrier gas through the bubbler. The aerosol was carried into the reactor in a stream of nitrogen gas through a brass baffle to obtain a laminar flow.

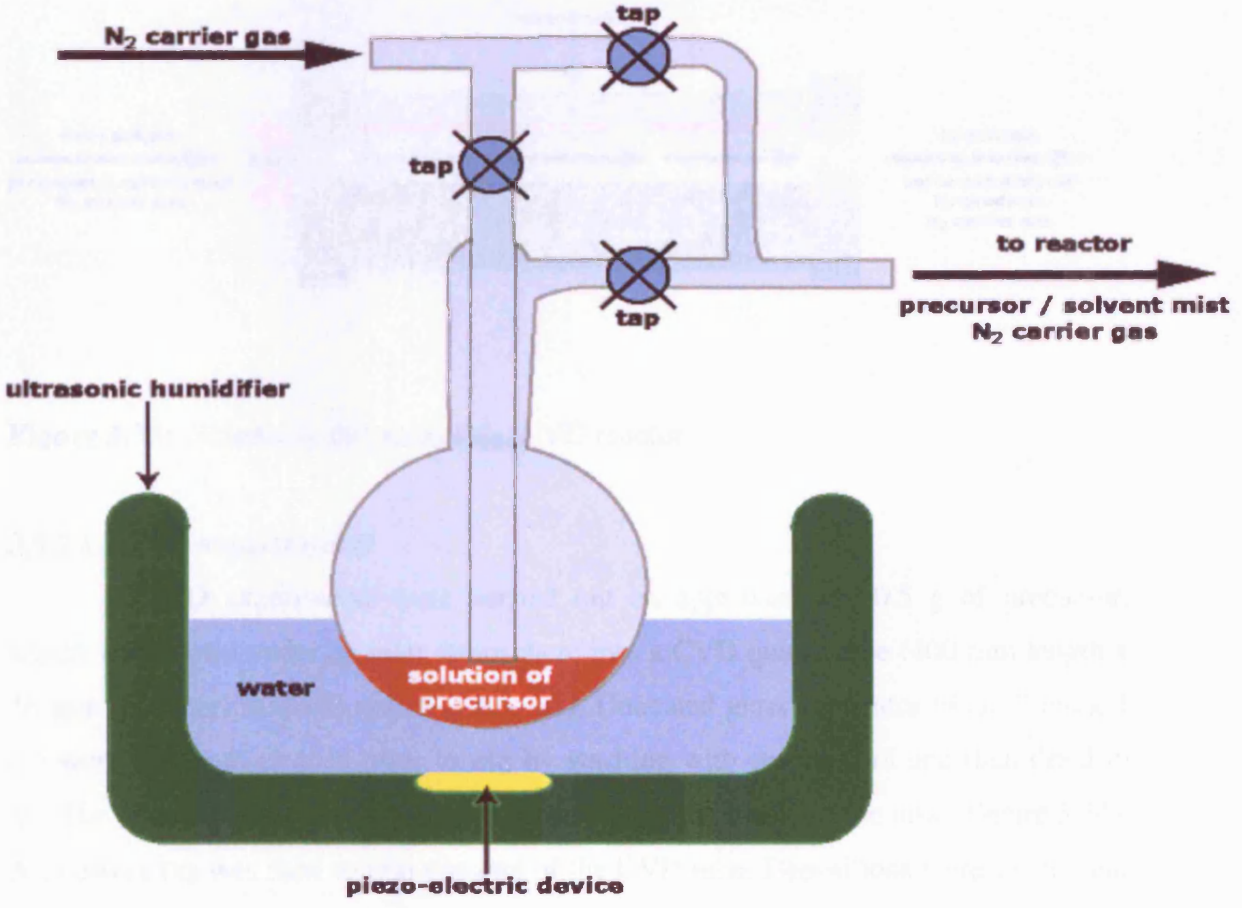

Figure 3.32: Schematic diagram of the aerosol delivery system

A graphite block containing a Whatman cartridge (Figure 3.33) heater was used to heat the glass substrate. The temperature of the substrate was monitored by a Pt-Rh thermocouple. Depositions were carried out by heating the horizontal bed reactor to the required temperature before diverting the nitrogen line through the aerosol and hence to the reactor. The total time for the deposition process was in the region of 2-3 hours. At the end of the deposition the nitrogen flow through the aerosol was diverted and only nitrogen passed over the substrate. The glass substrate was allowed to cool with the graphite block to less than 100 °C before it was removed. Coated substrates were handled and stored in air. Large pieces of glass (*ca* 4 cm x 2 cm) were used for X-ray powder diffraction. The coated glass substrate was broken into *ca.* 1 cm x 1 cm squares for subsequent analysis by SEM, XPS, transmission/reflectance and UV absorption studies. Annealing studies were performed by heating the coated substrates within a furnace at 550 °C for 24 h.

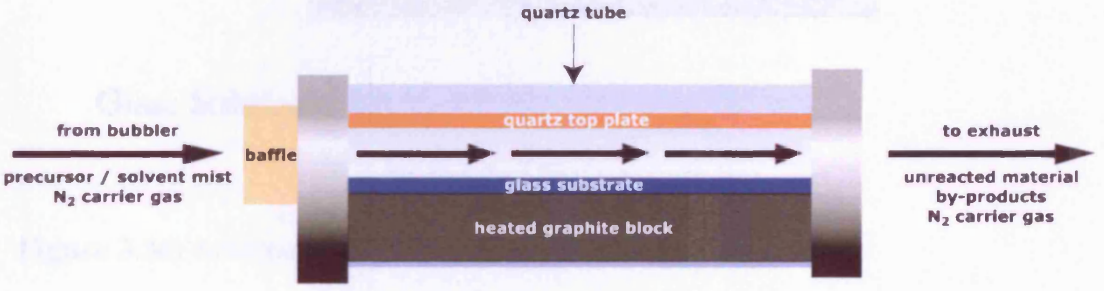

Figure 3.33: Schematic diagram of the CVD reactor

3.9.2 LPCVD experimental

LPCVD experiments were carried out on approximately 0.5 g of precursor, which was loaded under an inert atmosphere into a CVD quartz tube (400 mm length x 16 mm diameter) that was sealed at one end. Uncoated glass substrates of *ca.* 8 cm x 1 cm were used and cleaned prior to use by washing with propan-2-ol and then dried in air. The glass substrates were placed carefully along the inside of the tube (Figure 3.34). A two-way tap was used to seal one end of the CVD tube. Depositions were carried out by evacuating the CVD tube under a dynamic vacuum and placing it inside a cold

furnace such that 3.5 cm was inside the furnace and the end containing the sample protruded by 5 cm. The furnace was heated to 600 °C over a 1.5 h period under a dynamic vacuum (3.0 kPa) and was allowed to reach equilibrium. The CVD tube was slowly drawn into the furnace, *ca.* 5mm/10 min until the precursor started to melt. It was then held at that point until the precursor had decomposed. The total time for the deposition process was in the region of 60 minutes. The CVD tube remained under dynamic vacuum until it had cooled to room temperature. Coated glass substrates were handled in air but stored under an inert atmosphere in a Mbraun Unilab glove box.

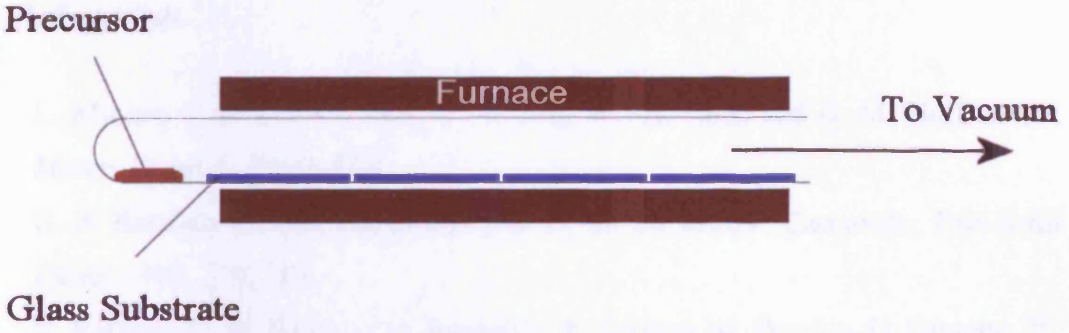

Figure 3.34: Schematic diagram for the LPCVD delivery system

3.9.3 Film Analysis Methods

X-ray powder diffraction patterns were measured on a Siemens D5000 diffractometer using monochromated $CuK_{\alpha 1}$ radiation (λ = 1.5400 A) radiation. The diffractometer used glancing incident radiation (1.5°). Glass substrates were indexed using Unit Cell and compared to database standards. Raman spectra were acquired using a Reinshaw Raman system 1000 using a helium-neon laser of wavelength 632.8 nm. The Raman system was calibrated against the emission lines of neon. SEM was carried out on a JEOL 6301 filament scanning electron microscope. Working distances between 0 and 15 mm were used. Accelerated voltages were between 5 and 10 eV depending on the sample. Magnification ranged from 10000 to 40,000. EDXA and WDX was obtained on a Philips XL30SEM instrument typically using an accelerating

voltage of 5 eV and a working distance of 10 mm. Al elements were standardised relative to cobalt. All the data were quantified using Oxford Link ISIS software. X-ray photoelectron spectra were recorded using a VG ESCALAB 220i XL instrument using focused (300 X spot) monochromatic Al Kα radiation at a pass energy of 20 eV. Scans were acquired with steps of 50 meV. A flood gun was used to control charging and binding energies were referred to an adventitious C 1s peak at 285.0 eV. Reflectance and transmission spectra were recorded between 300 and 1000 nm by a Zeiss miniature spectrometer. Reflectance measurements were standardised relative to a rhodium mirror and transmission relative to air. UV-Vis spectra were recorded using a Helios double beam instrument between 200 and 1000 nm.

3.10 References

1. L. Mîinea, S. Suh, S. G. Bott, J. –R. Liu, W. -K. Chuc and D. M. Hoffman, *J. Mater. Chem*, 9, 1999, 929.
2. G. A. Battison, R. Gerbasi, M. Porchia, R. Bertoncello, F. Caccavale, *Thin Solid Films*, 1996, 279, 115.
3. B. Ballarin, G. A. Battison, F. Benetollo, R. Gerbasi, M. Porchia, D. Favretto, P. Traldi, *Inorg. Chim. Acta*, 1994, 217, 71.
4. Y. Chi, T. –Y. Chou, Y. –J. Wang, and S. –F. Huang, A. J. Carty, L. Scoles, and K. A. Udachin, S. –M. Peng and G. –H. Lee, *Organometallics* 2004, 23, 95-103.
5. S. Basharat, C. J. Carmalt, S. J. King, E.S. Peters, D.A. Tocher, *Dalton Trans*, 2004, 3475.
6. M. Valet and D. M. Hoffman, *Chem. Mater,* 13, 2001, 2135-2143.
7. B. Neumüller, *Chem. Soc. Rev,* 2003, 32, 50.
8. S. Chitsaz, E. Iravani, B. Neumüller, *Z. Anorg. Allg. Chem,* 2002, 628, 2279.
9. D. A. Atwood, J. A. Jeiger, S. Liu, D. Rutherford, P. Wei, R. C. Tucker, *Organometallics,* 1999, 18, 976.
10. M. Munoz-Hernandez, P. Wei, S. Liu, D. A. Atwood, *Coord. Chem. Rev,* 2000, 210, 1.

11. S. Basharat, W. Betchley, C. J. Carmalt, S. Barnett, D. A. Tocher, and H. O. Davies, *Organometallics*, 2007, 26(2), 403.

12. R. Binions, C. J. Carmalt, I. P. Parkin, K. F. E. Pratt, G. A. Shaw, *Chem. Mater*, 2004, 16, 2489.

13. R. L. Weiher and R. P. Ley, *J. Appl. Phys*, 1966, 37, 299.

15. S. Suh, D. M. Hoffman, *J. Am. Chem. Soc*, 122, 2000, 9396.

16. L. Mîinea, S. Suh, D.M. Hoffman, *Inorg. Chem*, 38 , 1999, 4447.

17. Briggs, M. P. Seah Eds, *Practical Surface Analysis*, 2nd Edition, Volume 1- Auger and X-ray Photoelectron Spectroscopy, Wiley, 1990.

18. J. Tauc Ed, *Proceedings of the International School of Physics*, Enrico Fermi, Course XXXIV, The Optical Properties of Solids, 1966.

19. J. Passlack, *Appl. Phys*, 1995, 77, 686.

20. P. Lobinger, H. S. Park, H. Hohmeister and H. W. Roesky, *Chem. Vap. Deposition*, 2001, 3, 7.

21. JCPDS ®le 06-0416, International Centre for Diffraction Data, Swarthmore, PA.

22. G. Korotcenkova, V. Brinzaria, M. Ivanova, A. Cerneavschia, J. Rodriguezb, A. Cirerab, A. Cornetb, J. Morante, *Thin Solid Films*, 2005, 479, 38.

Chapter 4

Gas sensing Properties of Gallium Oxide

Chapter 4 Gas Sensing Properties of Gallium Oxide

This chapter describes the gas sensing properties of gallium oxide. The deposition of thin films was achieved by aerosol-assisted chemical vapour deposition. The production of thin films by CVD produces inexpensive, adhesive and reproducible films with low impurity levels,[1] and hence may be an advantageous method of producing gas sensors. CVD methods are directly compatible with Si-microfabrication technology. Typical solid state gas sensors are made by screen printing and tend to be very porous.

4.1 Introduction

A sensor is defined as "a device giving a signal for detection or measurement of a physical property to which it responds."[2] Gas sensing can be achieved in a variety of manners for example solid-state semiconducting metal oxide devices, electrochemical devices, metal phtalocyanine devices, infrared spectroscopy and electrolytic fuel cells.[3] Solid-state gas sensors are typically made up of semiconductor materials; the most widely used semiconductor in solid-state gas sensors is tin oxide. Currently there are three different types of metal oxide sensors in large-scale use. They are based on solid electrolytes, catalytic combustion and on resistance modulation of semiconducting oxides.

4.1.1 Semiconducting oxide gas sensors

A widely used type of sensor and one of the fastest growing of the three types is the semiconducting metal oxide gas sensor. A sensing element comprising of a semiconducting material presenting a high surface-to-bulk ratio is arranged on a heated insulating substrate between two interdigitated metallic electrodes. Reactions involving gas molecules can take place at the surface of the semiconductor leading to a change in the density of charge carriers available. Thus, the conductance of the device changes progressively with changing atmospheric compostion.[4]

The effectiveness of a sensor prepared from semiconducting metal oxides depends on the following factors:

- Operating temperature.
- Nature of the reaction taking place at the surface of the oxide.
- Catalytic properties of the surface.
- Electronic properties of the bulk oxide and the microstructure.

4.1.2 Categorising gas response type

The response of semiconducting metal oxide sensors is categorised depending on whether their conductivity displays a positive or a negative response on exposure to oxidising and reducing gases, as shown in Table 4.1.

Table 4.1: Resistance responses for reducing and oxidising gases on n- and p-type semiconducting oxides.[2]

Material type	Reducing gases	Oxidising gases
n-type	Resistance falls	Resistance rises
p-type	Resistance rises	Resistance falls

The two types of classifications arise from the changes, in the electronic charge carrier concentrations as a result of exposure of the metal oxide to gas. In the case of an n-type (negative) metal oxide, changes in the gas concentration effect the concentration of electrons in the conduction band. In the case of p-type (positive) metal oxide, changes in the gas concentration effect the concentration of holes in the valence band.

4.1.3 Sensor Response mechanism

The current widely held view of gas sensors[5] states that the conductivity of semiconducting metal oxides in air is determined by the trapping of electrons in surface states associated with surface absorbed oxygen.[6] The surface reaction controlling gas responses of semiconducting metal oxides involve changes in the concentration of surface oxygen species, such as O^{2-}. The formation of such ions by

oxygen adsorbed at the gas/solid interface abstracts electrons form the bulk of the solid; the oxygen can be regarded as a surface trap for electrons from the bulk.

Due to a micro-structural effect, part of the conductivity is gas sensitive due to modification in surface reactions, whilst the conductivity contributed by the bulk is not gas sensitive.[7] If the films are especially thin (100s of nm) then dense films such as those produced by CVD methodology may produce high quality gas sensors.[5]

Semiconductor gas sensors are either n-type or p-type; this affects the type of gas response they provide. In the case of an n-type semiconducting oxide, such as tin oxide, the electrons come from ionised donors *via* the conduction band, thus the charge density at the interface is reduced and a potential barrier to charge transport is developed. As the surface charge increases, the adsorption of any further oxygen is inhibited, thus the adsorption rate slows down because charge must be transferred to the adsorbate over the developing surface barrier, and the coverage saturates at a lower value.[3] In the case of a p-type semiconducting oxide in contrast, adsorbed oxygen acts as a surface acceptor state, abstracting electrons from the valence band and hence giving rise to an increase in the charge-carrier (hole) concentration at the interface.[8] Therefore, any decrease in the surface coverage of oxygen ions, results in a decrease in charge-carrier concentration and hence to an increase in the resistance of the material.

As stated in Chapter 1, below 900 °C, gallium oxide thin film operates as a surface-control-type sensor to reducing gases, *e.g.* EtOH.

4.2 Results and Discussion

4.2.1 Methods used

Gas sensor **(1)** was prepared by the reaction of $[Ga(NMe_2)_3]_2$ and $HOCH_2CH_2NMe_2$ under aerosol assisted chemical vapour deposition (AACVD) conditions. Sensors **(2)** and **(3)** were prepared by the reaction of Et_3Ga and donor functionalised alcohols, ROH (R = $OCH(CH_3)CH_2NMe_2$ and $OC(CH_3)_2CH_2OMe$) under AACVD conditions which produced Ga_2O_3 thin films on gas sensor substrates.

4.2.2 Gas Response

The Ga_2O_3 films showed an n-type response to ethanol at a variety of temperatures. Gas response was measured as the ratio between R (the resistance when exposed to ethanol) and R_0 (the resistance at the point immediately preceding the introduction of ethanol). The resistance was measured between the two electrodes of an interdigitized gold electrode structure on an alumina tile. All samples were tested across a range of operation temperatures; from 550 °C to 600 °C, for their response to ethanol gas at concentrations ranging from 8 ppm to 100 ppm.

4.2.2.1 Gas response from $[Ga(NMe_2)_3]_2$ and $HOCH_2CH_2NMe_2$

The Ga_2O_3 gas sensor prepared from the AACVD reaction of $[Ga(NMe_2)_3]_2$ and $HOCH_2CH_2NMe_2$ showed that at 600 °C **(a)** the gas response increased with ethanol concentration, as shown in Figure 4.1. The gas response was rapid and a near plateau was reached within minutes of exposure to ethanol. When the ethanol flow was stopped, the response drops slowly to near the baseline level and then tails off of at a similar rate to the baseline. The baseline remained fairly unstable throughout the experiment, showing slight downward drift. Signal noise is evident. The gas response level remained fairly constant and does not vary to a great extent throughout the experiment. Evaluation of response to a gas concentration of 100 ppm of ethanol indicates that the greatest response of R/R_0 at 1.128 occurred. Similar results were obtained from gas sensors at 550 °C **(b)**, evaluation of response to a gas concentration of 100 ppm of ethanol indicated that the greatest response of R/R_0 at 1.127 occurred.

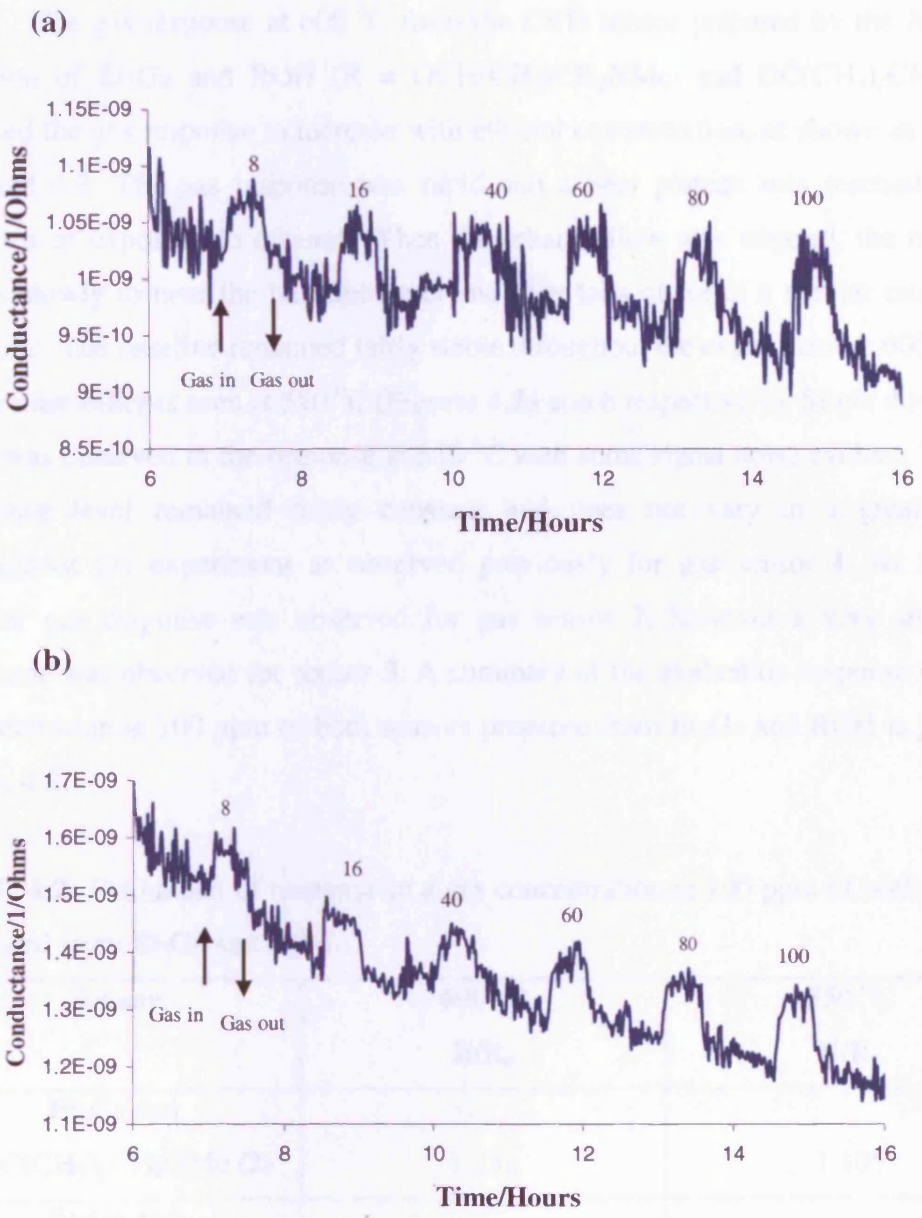

Figure 4.1: The gas response of a CVD prepared gallium oxide sensor **(1)** prepared from the *in situ* reaction of $[Ga(NMe_2)_3]_2$ and $HOCH_2CH_2NMe_2$ to varying concentrations of ethanol a) at 600 °C and b) at 550 °C.

4.2.2.2 Gas response from Et_3Ga and ROH

The gas response at 600 °C from the CVD sensor prepared by the AACVD reaction of Et_3Ga and ROH (R = $OCH(CH_3)CH_2NMe_2$ and $OC(CH_3)_2CH_2OMe$) showed the gas response to increase with ethanol concentration, as shown in Figures 4.2 and 4.3. The gas response was rapid and a near plateau was reached within minutes of exposure to ethanol. When the ethanol flow was stopped, the response drops slowly to near the baseline level and then tails off of at a similar rate to the baseline. The baseline remained fairly stable throughout the experiment at 600 °C but some unstability is seen at 550 °C (Figures 4.2a and b respectively). Slight downward drift was observed in the response at 550 °C with some signal noise evident. The gas response level remained fairly constant and does not vary to a great extent throughout the experiment as observed previously for gas sensor **1**. At 550 °C, similar gas response was observed for gas sensor **2**, however a very small gas response was observed for sensor **3**. A summary of the evaluation response to a gas concentration at 100 ppm of both sensors prepared from Et_3Ga and ROH is given in Table 4.2.

Table 4.2: Evaluation of response to a gas concentration at 100 ppm of both sensors prepared from Et_3Ga and ROH.

Sensor	**600 °C** $\mathbf{R/R_0}$	**550 °C** $\mathbf{R/R_0}$
Et_3Ga and $HOC(CH_3)_2CH_2OMe$ **(2)**	1.232	1.105
Et_3Ga and $HOCH(CH_3)CH_2NMe_2$ **(3)**	1.165	1.051

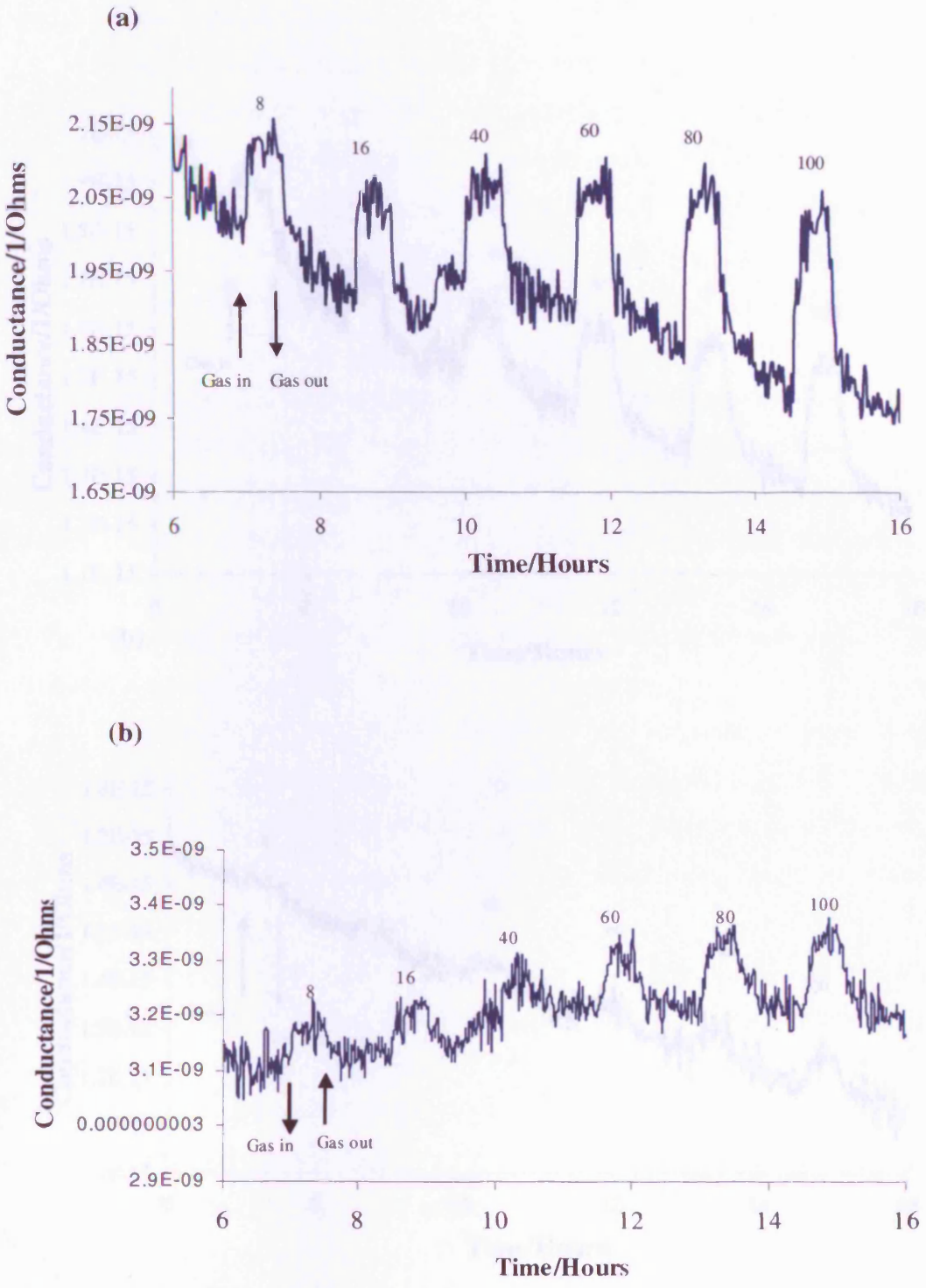

Figure 4.2: The gas response of a CVD prepared gallium oxide sensor prepared from the *in situ* reaction of Et_3Ga and $HOCH(CH_3)CH_2NMe_2$ to varying concentrations of ethanol a) sensor **(2)** at 600 °C and b) sensor **(2)** at 550 °C.

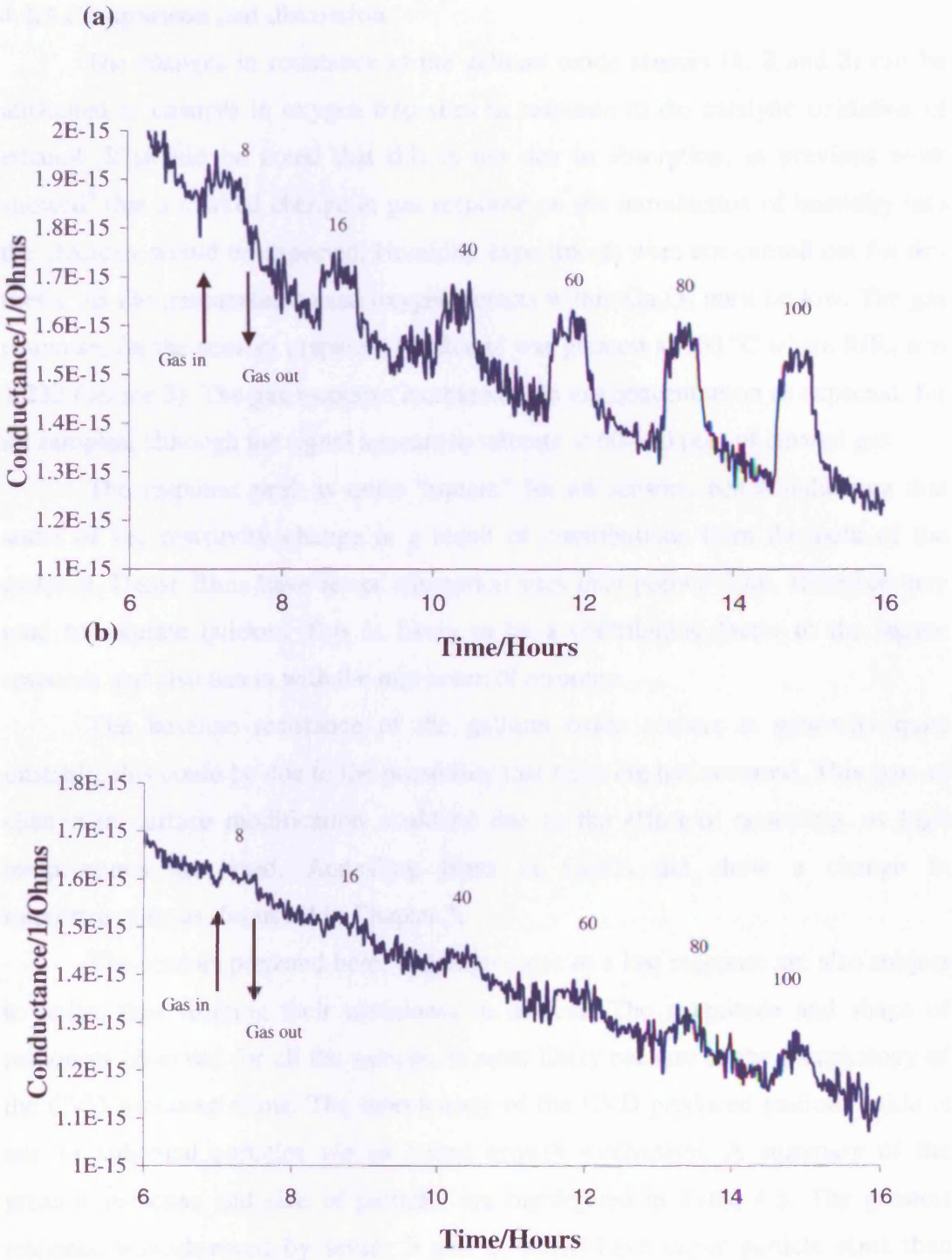

Figure 4.3: The gas response of a CVD prepared gallium oxide sensor prepared from the *in situ* reaction of Et_3Ga and ROH (R = $OC(CH_3)_2CH_2OMe$) to varying concentrations of ethanol a) **(3)** at 600 °C and b) sensor **(3)** at 550 °C

4.2.3 Comparison and discussion

The changes in resistance in the gallium oxide sensors (**1**, **2** and **3**) can be attributed to changes in oxygen trap sites in response to the catalytic oxidation of ethanol. It should be noted that this is not due to absorption, as previous work showed[5] that a marked change in gas response on the introduction of humidity into the chamber would be expected. Humidity experiments were not carried out for this thesis. At the temperatures used oxygen defects within Ga_2O_3 must be low. The gas response, for the sensors prepared, to ethanol was greatest at 600 °C where R/R_0 was 1.232 (sensor **3**). The gas response increased with gas concentration as expected, for all samples, although the signal appears to saturate at 60-100 ppm of ethanol gas.

The response peak is quite "square" for all sensors, hence indicating that some of the resistivity change is a result of contributions from the bulk of the material. Dense films have fewer adsorption sites than porous films, therefore they tend to saturate quicker. This is likely to be a contributing factor to the square response and also ties in with the maximum of response.

The baseline resistance of the gallium oxide sensors is generally quite unstable, this could be due to the possibility that sintering has occurred. This type of change in surface modification could be due to the effect of annealing, as high temperatures are used. Annealing films of Ga_2O_3 did show a change in microstructure, as discussed in Chapter 3.

The sensors prepared here, which give rise to a low response are also subject to noise, thus limiting their usefulness in devices. The magnitude and shape of responses observed for all the samples is most likely because of the morphology of the CVD produced films. The morphology of the CVD produced gallium oxide is one of spherical particles *via* an island growth mechanism. A summary of the greatest response and size of particles are highlighted in Table 4.3. The greatest response was observed by sensor **3** and **2**, which have larger particle sizes than sensor **1**. Hence, there are a greater number of available sites for adsorption and therefore giving a larger response.

Table 4.3: Summary of the particle size and response for all samples.

Sensor	Size	R/R_0 at 600 °C	R/R_0 at 550 °C
1	100 nm	1.128	1.127
2	1 μm	1.165	1.051
3	400 nm	1.232	1.105

Previous work has been carried out on gallium oxide sensors prepared by PVD. The gallium oxide films prepared by PVD showed a response to gases, such as methane and carbon monoxide.[9,10] The response was the greatest at higher temperatures. An example result indicates that the R/R_0 value for a sensor prepared by sputtering to 5000 ppm methane in dry air is 5 at 600 °C.

APCVD produced films had R/R_0 values between 1 and 2.84 for gas concentrations between 1 and 100 ppm. Similarly screen printed sensors had responses between 1 and 2.12 under the same conditions. The optimum response temperature was found to be 400 °C for CVD prepared sensors and 500 °C for screen-printed sensors.[6] The optimum working temperature for a sensor is dependent on the gas being detected and a similar decrease in response is observed away from the optimum temperature.[11] Lowering the optimum operational temperature in sensor devices is desirable as this results in the consumption of less energy.

Screen-printed tin oxide sensors give high responses to hydrocarbon gases at low temperature, typically 400 °C, the responses are in the order of 20 – 50.[12] Much work has been undertaken to improve the selectivity and stability of these sensors.[10] Metals such as antimony or platinum are routinely doped into the sensors to help achieve this.[13] PVD routes have been used to deposit SnO_2 films for gas sensor applications.[14] These sensors have optimum response while operating at 350 °C.[15] The sensors prepared by CVD give optimum responses at elevated temperature (600 °C), though this response is larger (1.86) compared to the optimum response given by the AACVD prepared sensors investigated here (1.2321 at 600 °C).

4.3 Conclusions

The response to reducing gas (ethanol) by AACVD prepared gallium oxide sensors was evaluated. It was found that out of the three sensors prepared by AACVD described here, the greatest response of 1.232 at 600 °C was observed for sensor **3**. It is likely that the morphology of this sensor is responsible for the increased sensitivity. Particle size of 400 nm is noted for the sensor; a large particle size would indicate the presence of a greater number of available sites for adsorption and therefore give a large response.

4.4 Experimental

For gas response, gallium oxide films were deposited by AACVD onto commercially produced sensor substrates. The sensor chips consist of a gold track printed on the top of an alumina tile and a platinum heater track printed on the reverse side of the tile. Gold electrodes were formed using laser trimming. This produced an interdigitized section with gap and finger widths of 50 μm.

Contacts to the devices were formed by spot welding 50 μm diameter platinum wire to pads of the track material in the corner of the sensor chip. The sensor heater was kept at constant resistance and hence constant temperature by incorporating it into a Wheatstone bridge. Electrical experiments were formed on a locally constructed test rig. Test gases were diluted from cylinders of synthetic air (79% nitrogen, 21% oxygen) containing ethanol (100 ppm). The devices were investigated over a variety of operating temperatures between 400 and 600 °C. Each device was duplicated and each experiment conducted twice.

4.5 References

1. F. Maury, CVD 2, 1996, 113.
2. The Concise Oxford Dictionary, Seventh Edition, Edited by J.B. Sykes, 1982, Oxford University Press, ISBN 0-19-861131-5

3. P. T. Moseley, J. O. W. Norris, D. E. Williams Eds. *Techniques and Mechanisms in Gas Sensing*, Adam Hilger, Bristol, 1991.
4. Basic Solid State Chemistry, Second Edition, A. R. West, 1999, John Wiley & Sons, ISBN 0-471-98756.
5. D. Niemeyer, D. E. Williams, P. Smith, K. F. E. Pratt, B. Slater, C.R.C.A. Catlow, A. M. Stoneham, *J. Mater. Chem.* 2002, 12, 667.
6. R. Binions, C. J. Carmalt, I. P. Parkin, K. F. E. Pratt, G. A. Shaw, *Chem Mater*, 2004, 16, 2489-2493.
7. D. E. Williams, K. F. E. Pratt, *Sens. Actuators B* 2000, 70, 214.
8. P. T. Moseley, *Meas. Sci. Technol.* 1997, 223-227.
9. T. Schwebel, M. Fleischer, H. Meixner, C.D. Kohl, *Sens. And Actuator , B* 49,1998, 46.
10. M. Fleischer, H. Meixner, *Sens. And Actuators B*, 26-27, 1995, 81.
11. R. Binions, C. J .Carmalt and I. P. Parkin, *Meas. Sci. Technol*, 2007, 18, 190.
12. K. Wada, M. Egashira, *Chem. Sens*, 15B, 1999, 109.
13. J. S. Bae, D. H. Yun, C. O. Park, J. S. Hwang, *Sens. And Actuators B* 75(3), 2001, 160.
14. C. A. Papadopoulos, J. N. Avaritsiotis, *Sens. And Actutors B*, 28, 1995, 201.
15. S. Gupta, R. K. Roy, M. P. Chowdhury, A. K. Pal, *Vacuum*, 75, 2004, 111.

Chapter 5

Conclusions

Chapter 5 Conclusions

The synthesis of a range of group 13 alkoxides has been achieved, as described in Chapter 2. The gallium tris(alkoxides), $[Ga(OCH_2CH_2NMe_2)_3]_2$, $[Ga(OCH(CH_2NMe_2)_2)_3)]_2$, $[Ga(OCH(CH_3)CH_2NMe_2)_3]_2$, $[Ga(OC(CH_3)_2CH_2OMe)_3]_2$ and $[Ga(OCH_2CH_2OMe)_3]_2$ were isolated from the reaction of $[Ga(NMe_2)_3]_2$ and excess alcohol. All the compounds have been characterised $^1H/^{13}C$ NMR, mass spectroscopy and FTIR. The synthesis of the gallium tris(alkoxides) also resulted in the isolation of the minor products, $[Ga(OCH_2CH_2NMe_2)_2Cl]$, $[Ga(OCH(CH_3)CH_2NMe_2)_2Cl]$ and $[Ga(OC(CH_3)_2CH_2OMe)Cl_2]$. These complexes have been characterised by X-ray crystallography, the results of which have been discussed. Although only minor products, $[Ga(OCH_2CH_2NMe_2)_2Cl]$ and $[Ga(OCH(CH_3)CH_2NMe_2)_2Cl]$ are of interest as gallium bis(alkoxides) are relatively rare.

Gallium mono(alkoxides) were made by the reaction of Et_3Ga and ROH (R = $OHCH_2CH_2NMe_2$, $OCH(CH_2NMe_2)_2$, $OCH(CH_3)CH_2NMe_2$, $OC(CH_3)_2CH_2OMe$ and OCH_2CH_2OMe) in a 1 : 1 reaction. The complexes $[Et_2Ga(OCH_2CH_2NMe_2)]_2$, $[Et_2Ga(OCH(CH_2NMe_2)_2)]_2$, $[Et_2Ga(OCH(CH_3)CH_2NMe_2)]_2$ and $[Et_2Ga(OC(CH_3)_2CH_2OMe)]_2$ have been structurally characterised and all compounds were characterised by analytical and spectroscopic methods. X ray crystallography showed that all the compounds adopt dimeric structures with four-membered Ga_2O_2 rings.

The synthesis of indium mono(alkoxides) were also investigated from the 1 : 1 reaction of Me_3In and ROH (R = $OHCH_2CH_2NMe_2$, $OCH(CH_2NMe_2)_2$, $OCH(CH_3)CH_2NMe_2$, $OC(CH_3)_2CH_2OMe$ and OCH_2CH_2OMe). The compounds $[Me_2In(OCH_2CH_2NMe_2)_2]_2$, $[Me_2In(OCH(CH_2NMe_2)_2)]_2$, $[Me_2In(OCH(CH_3)CH_2NMe_2)]_2$ and $[Me_2In(OC(CH_3)_2CH_2OMe)]_2$ were structurally characterised, and they also adopt dimeric structures.

A range of gallium bis(alkoxides) have been prepared by the reaction of Et_3Ga and excess alcohols (ROH = $HOCH(CH_2NMe_2)_2$, $HOCH(CH_3)CH_2NMe_2$, $HOC(CH_3)_2CH_2OMe$ and $HOCH_2CH_2OMe$) under reflux conditions. The complexes $[EtGa(OCH(CH_2NMe_2)_2)_2]$, $[EtGa(OCH(CH_3)CH_2NMe_2)_2]$ and $[EtGa(OC(CH_3)_2CH_2OMe)_2]$ and $[EtGa(OCH_2CH_2OMe)_2]$ were isolated as mixtures

with the corresponding gallium mono(alkoxides) $[Et_2Ga(OR)]_2$. The mixtures have been characterised by spectroscopic data but numerous attempts to separate them failed.

The reaction of Me_3In and ROH (R = $HOCH(CH_2NMe_2)_2$, $HOCH(CH_3)CH_2NMe_2$, $HOC(CH_3)_2CH_2OMe$ and $HOCH_2CH_2OMe$) at elevated temperatures in a 1 : 6 reaction yielded the compounds $[MeIn(OCH_2CH_2NMe_2)_2]$, $[MeIn(OCH(CH_2NMe_2)_2)_2]$, $[MeIn(OCH(CH_3)CH_2NMe_2)_2]$, $[MeIn(OC(CH_3)_2CH_2OMe)_2]$ and $[MeIn(OCH_2CH_2OMe)_2]$ were isolated as mixtures with the corresponding indium mono(alkoxides) $[Me_2In(OR)]_2$ and were characterised by spectroscopic data and have been discussed.

Chemical Vapour Deposition (CVD) using single-source precursors synthesised has been presented *via* low pressure CVD. Ga_2O_3 films have been deposited *via* LPCVD at 600 °C from $[Et_2Ga(OCH_2CH_2NMe_2)]_2$, $[Et_2Ga(OCH(CH_2NMe_2)_2)]_2$, $[Et_2Ga(OCH(CH_3)CH_2NMe_2))]_2$ and $[Et_2Ga(OC(CH_3)_2CH_2OMe)]_2$.

Dual-source routes towards the deposition of gallium and indium oxide thin films *via* aerosol assisted CVD were also investigated. Depositions were carried from the reaction of $[Ga(NMe_2)_3]_2$, Et_3Ga and Me_3In and excess alcohols.

The AACVD reaction of $[GaNMe_2)_3]_2$ and donor functionalised alcohols at 550 °C produced unreflective and birefringence films of Ga_2O_3. The films were amorphous and oxygen deficient. However, annealing the films in air at 600 °C gave gallium oxide thin films with the correct stiochiometry.

Gallium oxide thin films were deposited on glass from the AACVD reaction of Et_3Ga and excess alcohol at 550 °C. The films produced were unreflective and birefringence. The films produced were oxygen deficient and amorphous. Annealing the films in air at 600 °C produced films with the correct Ga : O ratio.

The AACVD of Me_3In and alcohols deposited crystalline films of In_2O_3 on glass substrates at 550 °C. SEM revealed the films to have needle like morphology WDX gave the correct ratio of In : O.

Gas sensing properties of gallium oxide were investigated. The response to reducing gas (ethanol) by AACVD prepared gallium oxide gas sensors has been evaluated. For the AACVD produced gas sensors it was found that the greatest gas response was at 600 °C.

List of Publications

1. S. Basharat, C. J. Carmalt, S. J. King, E. S. Peters, D. A. Tocher, *Dalton Trans*, 2004, 3475.
2. C. J. Carmalt, S. Basharat, *Organometallic Derived I: Semiconductors (MS 166)*, Precursors to Semiconducting Materials, 2005.
3. S. Basharat, W. Betchley, C. J. Carmalt, S. Barnett, D. A. Tocher, and H. O. Davies, *Organometallics*, 2007, 26(2), 403.

Appendix

Crystallographic data

Appendix – Crystallographic data

Crystal data and structure refinement for $[Ga(OCH_2CH_2NMe_2)_2Cl]$ (3)

Chemical formula	$C_8H_{20}ClGaN_2O_2$
Formula weight	281.43
Crystal colour	Colourless
Crystal size	$0.34 \times 0.29 \times 0.29$ mm^3
a (Å)	9.3818(8)
b (Å)	12.2919(10)
c (Å)	10.7257(9)
α (°)	90
β (°)	90
γ (°)	90
V (Å^3)	1236.89(18)
Z	4
Crystal system	Orthorhombic
Space group	*Pna*2$_1$
Radiation, wavelength	MoKα, 0.71073 Å
Calculated density	1.511 g/cm^3
Absorption coefficient μ	2.421 mm^{-1}
Reflections collected	10360
Independent reflections	2945 (R_{int} = 0.0220)
Reflections with $F^2>2\sigma$	2812
Final R indices ($F^2>2\sigma$)	R1 = 0.0273, wR2 = 0.0628
R indices (all data)	R1 = 0.0292, wR2 = 0.0637
Goodness-of-fit on F^2	1.115
Largest diff. peak and hole	0.718 and –0.296 e Å^{-3}

Bond lengths (Å) and angles (°) for $[Ga(OCH_2CH_2NMe_2)_2Cl]$ (3)

Ga1–O1	1.841(2)	Ga1–O2	1.842(3)
Ga1–N2	2.118(3)	Ga1–N1	2.161(3)
Ga1–Cl1	2.2433(8)	O1–C1	1.421(4)
C1–C2	1.521(5)	N1–C3	1.481(4)
N1–C4	1.453(5)	C11–C12	1.518(6)
O2–C11	1.407(4)	N2–C13	1.473(5)
C12–N2	1.466(5)	N2–C14	1.487(4)
O1–Ga1–O2	135.08(13)	O1–Ga1–N2	91.27(11)
O2–Ga1–N2	84.89(12)	O1–Ga1–N1	83.45(11)
N2–Ga1–N1	165.55(11)	O2–Ga1–N1	89.37(12)
O1–Ga1–Cl1	114.18(9)	N2–Ga1–Cl1	97.38(8)
O2–Ga1–Cl1	110.70(10)	N1–Ga1–Cl1	97.05(7)

Crystal data for $[Ga(OCH(CH_3)CH_2NMe_2)_2Cl]$ (6)

Chemical formula	$C_{10}H_{22}ClGaN_2O_2$
Formula weight	307.47
Crystal colour	Colourless
Crystal size	$1.22 \times 0.92 \times 0.23$ mm^3
a (Å)	7.7870(7)
b (Å)	7.9582(7)
c (Å)	12.0323(11)
α (°)	99.0680(10)
β (°)	93.109(2)
γ (°)	102.5140(10)
V (Å^3)	715.81(11)
Z	2
Crystal system	Triclinic
Space group	P $\bar{1}$
Radiation, wavelength	MoKα, 0.71073 Å
Calculated density	1.427 g/cm^3
Absorption coefficient μ	2.099 mm^{-1}
Independent reflections	3124 (R_{int} = 0.0230)
Reflections with $F^2>2\sigma$	3026
Final R indices ($F^2>2\sigma$)	R1 = 0.0359, wR2 = 0.0995
R indices (all data)	R1 = 0.0365, wR2 = 0.1000
Goodness-of-fit on F^2	1.071
Largest diff. peak and hole	1.010 and –0.934 e Å^{-3}

Bond lengths (Å) and angles (°) for [Ga(OCH(CH$_3$)CH$_2$NMe$_2$)$_2$Cl] (6)

Ga1–O1	1.8381(16)	Ga1–O2	1.8386(16)
Ga1–N1	2.1529(19)	Ga1–N2	2.1683(19)
Ga1–Cl1	2.2123(6)	N1–C2	1.473(3)
N1–C1	1.479(3)	N1–C3	1.486(3)
C3–C4	1.529(3)	C4–O1	1.414(3)
C4–C5	1.523(3)	N2–C12	1.477(3)
N2–C11	1.482(3)		
N2–C13	1.484(3)	C13–C14	1.529(3)
C14–O2	1.412(3)	C14–C15	1.524(3)
O1–Ga1–O2	118.80(8)	O1–Ga1–N1	84.31(7)
O2–Ga1–N1	90.32(7)	O1–Ga1–N2	89.78(7)
O2–Ga1–N2	84.25(7)	N1–Ga1–N2	168.86(8)
O1–Ga1–Cl1	121.63(6)	O2–Ga1–Cl1	119.57(6)
N1–Ga1–Cl1	95.41(5)	N2–Ga1–Cl1	95.73(5)
C2–N1–C1	109.14(19)	C2–N1–C3	110.92(19)
C1–N1–C3	110.37(19)	C2–N1–Ga1	114.19(15)
C1–N1–Ga1	114.08(14)	C3–N1–Ga1	97.68(13)
N1–C3–C4	108.91(18)	O1–C4–C5	109.54(19)
O1–C4–C3	110.14(18)	C12–N2–C13	111.01(18)
C5–C4–C3	110.1(2)	C11–N2–C13	110.06(19)
C4–O1–Ga1	116.26(13)		
C12–N2–C11	109.48(18)	C12–N2–Ga1	114.78(15)
C11–N2–Ga1	113.79(14)	C13–N2–Ga1	97.14(13)
O2–C14–C15	109.61(19)	O2–C14–C13	109.87(18)
C15–C14–C13	110.2(2)	C14–O2–Ga1	116.58(14)

Crystal data and structure refinement for $[Ga(OC(CH_3)_2CH_2OMe)Cl_2]$ (8)

Chemical formula	$C_5H_{11}Cl_2GaO_2$
Formula weight	243.76
Crystal colour	Colourless
Crystal size	$0.46 \times 0.37 \times 0.27$ mm^3
a (Å)	8.4505(10)
b (Å)	13.7024(17)
c (Å)	8.6396(11)
α (°)	90
β (°)	113.648(2)
δ (°)	90
V (Å^3)	916.4(2)
Z	4
Crystal system, space group	Monoclinic
Space group	$P2_1/n$
Radiation, wavelength	MoKα, 0.71073 Å
Calculated density	1.767 g/cm^3
Absorption coefficient μ	3.529 mm^{-1}
Reflections for cell refinement	5467 (θ range 2.899 to 28.146°)
Reflections collected	13241
Independent reflections	4429 (R_{int} = 0.0000)
Reflections with $F^2>2\sigma$	2353
Final R indices ($F^2>2\sigma$)	R1 = 0.0294, wR2 = 0.0818
R indices (all data)	R1 = 0.0325, wR2 = 0.0829
Goodness-of-fit on F^2	1.062
Largest diff. peak and hole	1.119 and –0.495 e Å^{-3}

Bond lengths (Å) and angles (°) for $[Ga(OC(CH_3)_2CH_2OMe)Cl_2]$ (8)

Ga1–O2	1.886(2)	Ga1–O2#1	1.9753(17)
Ga1–Cl2	2.1595(8)	Ga1–O1	2.1613(19)
Ga1–Cl1	2.1715(8)	O1–C1	1.442(3)
O1–C2	1.442(3)	O2–C3	1.454(3)
O2–Ga1#1	1.9753(17)	C2–C3	1.519(4)
C3–C5	1.517(4)	C3–C4	1.526(4)
O2–Ga1–O2#1	76.30(9)	O2–Ga1–Cl2	120.54(7)
O2#1–Ga1–Cl2	102.35(6)	O2–Ga1–O1	77.98(7)
O2#1–Ga1–O1	154.27(8)	Cl2–Ga1–O1	91.29(6)
O2–Ga1–Cl1	122.49(7)	O2#1–Ga1–Cl1	100.69(6)
Cl2–Ga1–Cl1	116.19(3)	O1–Ga1–Cl1	92.44(5)
C1–O1–C2	113.8(2)	C1–O1–Ga1	122.72(16)
C2–O1–Ga1	109.42(15)	C3–O2–Ga1	120.02(15)
C3–O2–Ga1#1	134.70(17)	Ga1–O2–Ga1#1	103.70(9)
O1–C2–C3	105.4(2)	O2–C3–C5	109.2(2)
O2–C3–C2	104.5(2)	O2–C3–C4	109.6(2)
C5–C3–C2	110.3(2)	C5–C3–C4	111.5(2)
C2–C3–C4	111.5(2)		

Crystal data and structure refinement for $[Et_2Ga(OCH_2CH_2NMe_2)]_2$ (10)

Chemical formula	$C_{16}H_{40}Ga_2N_2O_2$
Formula weight	431.94
Crystal colour	Colourless
Crystal size	$0.45 \times 0.36 \times 0.17$ mm^3
a (Å)	10.0583(7)
b (Å)	15.4421(11)
c (Å)	13.6263(10)
α (°)	90
β (°)	90.562(1)
δ (°)	90
V (Å^3)	2116.4(3)
Z	4
Crystal system, space group	monoclinic
Space group	$P2_1/n$
Radiation, wavelength	MoKα, 0.71073 Å
Calculated density	1.356 g/cm^3
Absorption coefficient μ	2.554 mm^{-1}
Reflections for cell refinement	9948 (θ range 2.417 to 28.235°)
Reflections collected	18939
Independent reflections	5273 (R_{int} = 0.0186)
Reflections with $F^2>2\sigma$	4665
Final R indices ($F^2>2\sigma$)	R1 = 0.0213, wR2 = 0.0522
R indices (all data)	R1 = 0.0240, wR2 = 0.0531
Goodness-of-fit on F^2	1.045
Largest diff. peak and hole	0.403 and –0.231 e Å^{-3}

Bond lengths (Å) and angles (°) for $[Et_2Ga(OCH_2CH_2NMe_2)]_2$ (10)

Ga1–O1	1.9229(10)	Ga1–C7	1.9786(14)
Ga1–C5	1.9843(14)	Ga1–O2	2.0669(9)
Ga1–N1	2.5068(12)	O1–C1	1.4041(16)
O1–Ga2	2.0910(9)	C1–C2	1.507(2)
C2–N1	1.4632(19)	N1–C4	1.4565(19)
N1–C3	1.467(2)	C5–C6	1.525(2)
C7–C8	1.527(2)	Ga2–O2	1.9337(9)
Ga2–C15	1.9848(14)	Ga2–C13	1.9856(14)
Ga2–N2	2.3727(11)	O2–C9	1.4110(16)
C9–C10	1.519(2)	C10–N2	1.4656(18)
N2–C11	1.4679(18)	N2–C12	1.4682(18)
C13–C14	1.529(2)	C15–C16	1.524(2)
O1–Ga1–C7	116.47(5)	O1–Ga1–C5	117.84(5)
C7–Ga1–C5	125.35(6)	O1–Ga1–O2	74.48(4)
C7–Ga1–O2	98.58(5)	C5–Ga1–O2	100.90(5)
O1–Ga1–N1	75.24(4)	C7–Ga1–N1	96.84(5)
C5–Ga1–N1	91.12(5)	O2–Ga1–N1	149.63(4)
C1–O1–Ga1	124.20(8)	C1–O1–Ga2	128.19(9)
Ga1–O1–Ga2	105.50(4)	O1–C1–C2	110.91(12)
C4–N1–C2	112.01(13)	N1–C2–C1	110.64(12)
C4–N1–C3	109.51(13)	C2–N1–C3	109.41(13)
C4–N1–Ga1	110.84(10)	C2–N1–Ga1	97.09(8)
C3–N1–Ga1	117.48(10)	C6–C5–Ga1	113.35(10)
C8–C7–Ga1	114.30(10)	O2–Ga2–C15	116.82(5)
O2–Ga2–C13	119.24(5)	C15–Ga2–C13	123.86(6)
O2–Ga2–O1	73.70(4)	C15–Ga2–O1	100.89(5)

Bond lengths (Å) and angles (°) for $[Et_2Ga(OCH_2CH_2NMe_2)]_2$ (10)

C13–Ga2–O1	97.00(5)	O2–Ga2–N2	75.45(4)
C15–Ga2–N2	94.42(5)	C13–Ga2–N2	96.43(5)
O1–Ga2–N2	149.11(4)	C9–O2–Ga2	122.44(8)
C9–O2–Ga1	129.72(8)	Ga2–O2–Ga1	106.04(4)
O2–C9–C10	109.93(11)	N2–C10–C9	109.34(11)
C10–N2–C11	111.16(11)	C10–N2–C12	111.35(12)
C11–N2–C12	109.03(12)	C10–N2–Ga2	98.84(8)
C11–N2–Ga2	111.51(9)	C12–N2–Ga2	114.67(9)
C14–C13–Ga2	115.94(10)	C16–C15–Ga2	115.03(10)

Crystal data for $[Et_2Ga(OCH(CH_2NMe_2)_2)]_2$ (11)

Chemical formula	$C_{11}H_{27}GaN_2O$
Formula weight	273.07
Crystal colour	Colourless
Crystal size	$0.65 \times 0.27 \times 0.17$ mm^3
a(Å)	8.5041(8)
b (Å)	8.9640(9)
c (Å)	9.9568(10)
α (°)	77.0570(10)
β (°)	83.2580(10)
γ (°)	82.2180(10)
V (Å^3)	729.93(12)
Z	2
Radiation, wavelength	MoKα, 0.71073 Å
Crystal system	Triclinic,
Space group	P $\bar{1}$
Calculated density	1.242 g/cm^3
Absorption coefficient μ	1.867 mm^{-1}
Reflections for cell refinement	4870 (θ range 2.346 to 28.202°)
Reflections collected	6413
Independent reflections	3344 (R_{int} = 0.0118)
Reflections with $F^2>2\sigma$	3199
Final R indices ($F^2>2\sigma$)	R1 = 0.0264, wR2 = 0.0702
R indices (all data)	R1 = 0.0277, wR2 = 0.0709
Goodness-of-fit on F^2	1.072
Largest diff. peak and hole	0.401 and –0.256 e Å^{-3}

Bond lengths (Å) and angles (°) for $[Et_2Ga(OCH(CH_2NMe_2)_2)]_2$ (11)

Ga1–O1	1.9152(11)	Ga1–C8	1.9738(19)
Ga1–C10	1.9764(19)	Ga1–O1#1	2.0965(11)
N1–C1	1.398(6)	N1–C2'	1.401(6)
N1–C3	1.437(3)	N1–C1'	1.461(7)
N1–C2	1.504(4)	N1–C3'	1.518(4)
C4–C3'	1.382(4)	C4–O1	1.386(2)
C4–C5	1.418(4)	C4–C5'	1.502(5)
C4–C3	1.516(3)	O1–Ga1#1	2.0965(11)
N2–C7	1.302(5)	N2–C5'	1.358(5)
N2–C6'	1.448(5)	N2–C5	1.485(4)
N2–C7'	1.633(5)	N2–C6	1.653(6)
C8–C9	1.520(3)		
O1–Ga1–C8	118.30(7)	O1–Ga1–C10	114.50(7)
C8–Ga1–C10	126.92(9)	O1–Ga1–O1#1	74.83(5)
C8–Ga1–O1#1	100.37(7)	C10–Ga1–O1#1	97.89(7)
C1–N1–C2'	134.0(4)	C1–N1–C3	115.5(3)
C2'–N1–C3	79.2(3)	C1–N1–C1'	27.1(3)
C2'–N1–C1'	111.4(5)	C3–N1–C1'	133.9(3)
C1–N1–C2	110.1(4)	C2'–N1–C2	31.3(3)
C3–N1–C2	109.1(2)	C1'–N1–C2	83.8(4)
C1–N1–C3'	82.9(3)	C2'–N1–C3'	109.9(4)
C3–N1–C3'	34.3(2)	C1'–N1–C3'	106.4(4)
C2–N1–C3'	134.7(3)	C3'–C4–O1	119.9(2)
C3'–C4–C5	124.9(3)	O1–C4–C5	115.2(2)
C3'–C4–C5'	120.0(3)	O1–C4–C5'	114.1(2)
C5–C4–C5'	27.8(2)	C3'–C4–C3	34.7(2)

Bond lengths (Å) and angles (°) for $[Et_2Ga(OCH(CH_2NMe_2)_2)]_2$ (11)

O1–C4–C3	114.96(17)	C5–C4–C3	115.5(2)
C5'–C4–C3	129.7(2)	C4–O1–Ga1	124.02(11)
C4–O1–Ga1#1	130.81(11)	Ga1–O1–Ga1#1	105.17(5)
C7–N2–C5'	133.1(3)	C7–N2–C6'	57.0(4)
C5'–N2–C6'	117.8(4)	C7–N2–C5	118.7(3)
C5'–N2–C5	28.3(2)	C6'–N2–C5	136.6(3)
C7–N2–C7'	44.8(4)	C5'–N2–C7'	106.1(3)
C6'–N2–C7'	100.7(4)	C5–N2–C7'	80.8(3)
C7–N2–C6	108.2(4)	C5'–N2–C6	74.9(3)
C6'–N2–C6	52.6(3)	C5–N2–C6	102.8(3)
C7'–N2–C6	144.6(3)	C9–C8–Ga1	114.60(16)
C4–C3'–N1	117.0(3)	N2–C5'–C4	119.3(3)

Crystal data for $[Et_2Ga(OCH(CH_3)CH_2NMe_2)]_2$ (12)

Chemical formula	$C_9H_{22}GaNO$
Formula weight	230.00
Crystal colour	Colourless
Crystal size	$0.82 \times 0.30 \times 0.20$ mm^3
a (Å)	8.4541(10)
b (Å)	8.7564(11)
c (Å)	16.944(2)
α (°)	77.893(2)
β (°)	80.226(2)
γ (°)	73.674(2)
Z	4
Crystal system	P $\bar{1}$
Space group	Triclinic
Radiation, wavelength	MoKα, 0.71073 Å
Calculated density	1.307 g/cm^3
Absorption coefficient μ	2.317 mm^{-1}
Reflections collected	9984
Independent reflections	5297 (R_{int} = 0.0282)
Reflections with $F^2>2\sigma$	4045
Final R indices ($F^2>2\sigma$)	R1 = 0.0417, wR2 = 0.1008
R indices (all data)	R1 = 0.0604, wR2 = 0.1097
Goodness-of-fit on F^2	1.033
Largest and mean shift/su	0.001 and 0.000
Largest diff. peak and hole	1.270 and –0.625 e Å^{-3}

Bond lengths (Å) and angles (°) for $[Et_2Ga(OCH(CH_3)CH_2NMe_2)]_2$ (12)

Ga1–O1	1.919(2)	Ga1–C8	1.978(3)
Ga1–C6	1.982(3)	Ga1–O1#1	2.088(2)
O1–C2	1.412(4)	O1–Ga1#1	2.088(2)
C1–C2	1.487(5)	C2–C3	1.518(5)
C3–N1	1.443(5)	N1–C4	1.466(5)
N1–C5	1.482(4)	C6–C7	1.531(5)
C8–C9	1.531(5)	Ga2–O2	1.920(2)
Ga2–C16	1.974(3)	Ga2–C18	1.982(3)
Ga2–O2#2	2.074(2)	O2–C12	1.399(5)
O2–Ga2#2	2.074(2)	C11–C12	1.470(5)
C12–C13	1.431(6)	N2–C14	1.473(6)
C13–N2	1.441(5)	N2–C15	1.431(6)
C16–C17	1.532(5)		
C8–Ga1–C6	127.04(14)	O1–Ga1–O1#1	75.07(10)
C8–Ga1–O1#1	98.38(12)	C6–Ga1–O1#1	100.72(12)
C2–O1–Ga1	122.8(2)	C2–O1–Ga1#1	130.4(2)
Ga1–O1–Ga1#1	104.93(10)	C1–C2–C3	113.1(3)
O1–C2–C1	112.7(3)	C4–N1–C5	107.0(3)
O1–C2–C3	108.3(3)	N1–C3–C2	112.5(3)
C3–N1–C4	111.3(3)	C3–N1–C5	109.7(3)
C7–C6–Ga1	114.6(3)	C9–C8–Ga1	114.4(2)
O2–Ga2–C16	114.93(13)	O2–Ga2–C18	115.46(12)
C16–Ga2–C18	128.90(15)	O2–Ga2–O2#2	75.63(10)
C16–Ga2–O2#2	99.51(13)	C18–Ga2–O2#2	100.39(12)
C12–O2–Ga2	123.6(2)	C12–O2–Ga2#2	130.9(2)
Ga2–O2–Ga2#2	104.37(10)	O2–C12–C13	113.5(4)

Bond lengths (Å) and angles (°) for $[Et_2Ga(OCH(CH_3)CH_2NMe_2)]_2$ (12)

O2–C12–C11	114.8(4)	C13–C12–C11	117.4(4)
C12–C13–N2	117.8(4)	C15–N2–C13	112.6(4)
C15–N2–C14	107.8(4)	C13–N2–C14	108.6(4)
C17–C16–Ga2	114.0(3)	C19–C18–Ga2	115.5(3)

Crystal data for $[Et_2Ga(OC(CH_3)_2CH_2OMe)]_2$ (13)

Chemical formula	$C_9H_{21}GaO_2$
Formula weight	230.98
Crystal colour	Colourless
Crystal size	$0.60 \times 0.48 \times 0.34$ mm^3
a (Å)	8.0695(8)
b (Å)	8.8229(9)
c (Å)	8.8587(9)
α (°)	108.355(2)
β (°)	105.923(2)
γ (°)	95.997(2)
V (Å^3)	562.92(10)
Z	2
Crystal system	Triclinic
Space group	P $\bar{1}$
Radiation, wavelength	MoKα, 0.71073 Å
Calculated density	1.363 g/cm^3
Absorption coefficient μ	2.409 mm^{-1}
Reflections for cell refinement	4160 (θ range 2.487 to 28.264°)
Reflections collected	4944
Independent reflections	2583 (R_{int} = 0.0116)
Reflections with $F^2>2\sigma$	2497
Final R indices ($F^2>2\sigma$)	R1 = 0.0184, wR2 = 0.0462
R indices (all data)	R1 = 0.0191, wR2 = 0.0465
Goodness-of-fit on F^2	1.058
Largest diff. peak and hole	0.426 and –0.270 e Å^{-3}

Bond lengths (Å) and angles (°) for $[Et_2Ga(OC(CH_3)_2CH_2OMe)]_2$ (13)

Ga1–O1#1	1.9299(9)	Ga1–C8	1.9737(13)
Ga1–C6	1.9748(13)	Ga1–O1	2.0141(9)
O1–C2	1.4337(15)	O1–Ga1#1	1.9299(9)
O2–C4	1.4195(17)	O2–C5	1.4202(17)
C6–C7	1.531(2)	C8–C9	1.5230(19)
C8–C9	1.5230(19)	C2–C3	1.5247(19)
C2–C4	1.5235(19)	C2–C1	1.5267(19)
O1#1–Ga1–C8	116.04(5)	O1#1–Ga1–O1	77.27(4)
O1#1–Ga1–C6	113.58(5)	C6–Ga1–O1	105.70(5)
C8–Ga1–C6	125.06(6)	C2–O1–Ga1	128.92(8)
C8–Ga1–O1	106.73(5)	C4–O2–C5	112.31(11)
C2–O1–Ga1#1	126.35(8)	C9–C8–Ga1	112.94(10)
Ga1#1–O1–Ga1	102.73(4)	C9–C8–Ga1	112.94(10)
C7–C6–Ga1	115.06(10)	O1–C2–C1	110.12(11)
O1–C2–C4	107.78(11)	C3–C2–C1	111.16(12)
C4–C2–C3	108.15(12)		
C4–C2–C1	110.44(12)		

Crystal data for $[Me_2In(OCH_2CH_2NMe_2)]_2$ (20)

Chemical formula	$C_6H_{16}InNO$
Formula weight	233.02
Crystal colour	Colourless
Crystal size	$0.46 \times 0.32 \times 0.15$ mm^3
a (Å)	11.6733(14)
b(Å)	15.6152(18)
c (Å)	10.3060(12)
α (°)	90
β (°)	90
γ (°)	90
V (Å^3)	1878.6(4)
Z	8
Crystal system	Orthorhombic
Space group	Pccn
Radiation, wavelength	MoKα, 0.71073 Å
Calculated density	1.648 g/cm^3
Absorption coefficient μ	2.453 mm^{-1}
Reflections for cell refinement	6075 (θ range 2.609 to 28.192°)
Reflections collected	10284
Independent reflections	2265 (R_{int} = 0.0188)
Reflections with $F^2>2\sigma$	2072
Final R indices ($F^2>2\sigma$)	R1 = 0.0201, wR2 = 0.0453
R indices (all data)	R1 = 0.0232, wR2 = 0.0466
Goodness-of-fit on F^2	1.112
Largest diff. peak and hole	404 and –0.384 e Å^{-3}

Bond lengths (Å) and angles (°) for $[Me_2In(OCH_2CH_2NMe_2)]_2$ (20)

In1–O1	2.1432(14)	In1–C5	2.1555(18)
In1–C6	2.1563(18)	In1–O1#1	2.2358(14)
In1–N1	2.5161(16)	O1–C1	1.387(2)
O1–In1#1	2.2358(14)	C1–C2	1.516(3)
C2–N1	1.471(2)	N1–C3	1.465(3)
N1–C4	1.471(3)		
O1–In1–C6	109.61(7)	O1–In1–C5	116.33(7)
C5–In1–C6	133.99(9)	O1–In1–O1#1	71.75(6)
C5–In1–O1#1	96.98(8)	C6–In1–O1#1	99.35(8)
O1–In1–N1	72.66(5)	C5–In1–N1	94.35(8)
C6–In1–N1	96.90(8)	O1#1–In1–N1	144.08(5)
C1–O1–In1	122.34(12)	C1–O1–In1#1	129.40(12)
In1–O1–In1#1	108.25(6)	O1–C1–C2	110.95(17)
N1–C2–C1	111.36(17)	C4–N1–C2	109.84(16)
C3–N1–C2	111.14(18)	C3–N1–In1	111.51(13)
C4–N1–In1	113.32(12)	C2–N1–In1	101.30(11)

Crystal data for $[Me_2In(OCH(CH_2NMe_2)_2)]_2$ (21)

Chemical formula	$C_9H_{22}InN_2O$
Formula weight	289.11
Crystal colour	Colourless
Crystal size	$0.40 \times 0.18 \times 0.05$ mm^3
a	8.3820(8)
b	8.4014(8)
c	10.1223(10)
α	66.1840(10)
β	85.316(2)
γ	82.575(2)
V (Å^3)	646.31(11)
Z	2
Crystal system	Triclinic
Space group	P $\bar{1}$
Radiation, wavelength	MoKα, 0.71073 Å
Calculated density	1.491 g/cm^3
Absorption coefficient μ	1.801 mm^{-1}
Reflections for cell refinement	4170 (θ range 2.201 to 28.280°)
Reflections collected	5495
Independent reflections	2915 (R_{int} = 0.0137)
Reflections with $F^2>2\sigma$	2763
Final R indices ($F^2>2\sigma$)	R1 = 0.0243, wR2 = 0.0601
R indices (all data)	R1 = 0.0261, wR2 = 0.0610
Goodness-of-fit on F^2	1.122
Largest diff. peak and hole	0.788 and –0.646 e Å^{-3}

Bond lengths (Å) and angles (°) for $[Me_2In(OCH(CH_2NMe_2)_2)]_2$ (21)

In1–C8	2.141(3)	In1–C9	2.154(3)
In1–O1	2.1894(18)	In1–O1#1	2.1960(18)
N1–C2'	1.418(7)	N1–C1	1.436(6)
N1–C3'	1.449(6)	N1–C2	1.470(6)
N1–C3	1.509(5)	N1–C1'	1.515(7)
N2–C6'	1.440(7)	N2–C5	1.443(6)
N2–C7'	1.475(7)	N2–C6	1.477(7)
N2–C7	1.479(6)	N2–C5'	1.485(6)
O1–C4	1.392(3)	O1–In1#1	2.1960(18)
C4–C5'	1.461(6)	C4–C3	1.469(5)
C4–C3'	1.496(6)	C4–C5	1.519(5)
C8–In1–C9	145.48(14)	C8–In1–O1	104.80(11)
C9–In1–O1	104.35(10)	C8–In1–O1#1	103.11(10)
C9–In1–O1#1	102.87(11)	O1–In1–O1#1	72.76(7)
C2'–N1–C1	129.2(4)	C2'–N1–C3'	114.1(4)
C1–N1–C3'	68.8(4)	C2'–N1–C2	35.1(4)
C1–N1–C2	110.3(4)	C3'–N1–C2	141.7(4)
C2'–N1–C3	71.8(4)	C1–N1–C3	109.9(4)
C3'–N1–C3	46.5(3)	C2–N1–C3	106.3(4)
C2'–N1–C1'	109.4(5)	C1–N1–C1'	40.4(4)
C3'–N1–C1'	109.1(4)	C2–N1–C1'	77.7(4)
C3–N1–C1'	144.3(4)	C6'–N2–C5	143.0(4)
C6'–N2–C7'	111.7(5)	C5–N2–C7'	66.1(4)
C6'–N2–C6	39.1(4)	C5–N2–C6	111.8(4)
C7'–N2–C6	130.2(4)	C6'–N2–C7	73.2(5)
C5–N2–C7	110.0(4)	C7'–N2–C7	44.4(4)
C6–N2–C7	107.5(4)	C6'–N2–C5'	109.4(4)

Bond lengths (Å) and angles (°) for $[Me_2In(OCH(CH_2NMe_2)_2)]_2$ (21)

C5–N2–C5'	46.7(3)	C7'–N2–C5'	109.0(4)
C6–N2–C5'	70.6(4)	C7–N2–C5'	145.3(4)
C4–O1–In1	125.61(16)	C4–O1–In1#1	127.15(16)
In1–O1–In1#1	107.24(7)	O1–C4–C5'	113.8(3)
O1–C4–C3	114.4(3)	C5'–C4–C3	131.8(3)
O1–C4–C3'	112.2(3)	C5'–C4–C3'	112.9(4)
C3–C4–C3'	46.4(3)	O1–C4–C5	113.3(3)
C5'–C4–C5	45.8(3)	C3–C4–C5	111.5(3)
C3'–C4–C5	134.5(3)	C4–C3–N1	112.9(3)
N2–C5–C4	114.7(4)	N1–C3'–C4	114.9(4)
C4–C5'–N2	115.7(4)		

Crystal data for $[Me_2In(OCH(CH_3)CH_2NMe_2)]_2$ (22)

Chemical formula	$C_{14}H_{36}In_2N_2O_2$
Formula weight	494.09
Crystal colour	Colourless
Crystal size	$0.58 \times 0.50 \times 0.33$ mm^3
a (Å)	15.5563(12)
b (Å)	8.1075(6)
c (Å)	16.7231(13)
α (°)	90
β (°)	96.9500(10)
γ (°)	90
V (Å^3)	2093.7(3)
Z	4
Crystal system	Monoclinic
Space group	$P2_1/n$
Radiation, wavelength	MoKα, 0.71073 Å
Calculated density	1.567 g/cm^3
Absorption coefficient μ	2.206 mm^{-1}
Reflections collected	17802
Independent reflections	4977 (R_{int} = 0.0149)
Reflections with $F^2>2\sigma$	4662
Final R indices ($F^2>2\sigma$)	R1 = 0.0183, wR2 = 0.0423
R indices (all data)	R1 = 0.0203, wR2 = 0.0431
Goodness-of-fit on F^2	1.078
Largest diff. peak and hole	0.357 and –0.414 e Å^{-3}

Bond lengths (Å) and angles (°) for $[Me_2In(OCH(CH_3)CH_2NMe_2)]_2$ (22)

In1–O1	2.1342(12)	In1–C7	2.150(2)
In1–C6	2.157(2)	In1–O1#1	2.2560(12)
In1–N1	2.5376(15)	N1–C4'	1.426(11)
N1–C3'	1.431(7)	N1–C5	1.457(4)
N1–C4	1.481(4)	N1–C3	1.501(3)
N1–C5'	1.514(9)	O1–C2'	1.368(8)
O1–C2	1.401(3)	O1–In1#1	2.2560(12)
C1–C2	1.534(5)	C2–C3	1.507(4)
In2–O11	2.1342(12)	In2–C17	2.1537(19)
In2–C16	2.1551(18)	In2–O11#2	2.2482(11)
In2–N11	2.5641(15)	O11–C12	1.413(3)
O11–C12'	1.427(5)	O11–In2#2	2.2482(11)
N11–C13	1.468(5)	N11–C15'	1.469(9)
N11–C13'	1.473(7)	N11–C14'	1.475(10)
N11–C14	1.476(6)	N11–C15	1.484(6)
C11–C12	1.518(10)	C12–C13	1.513(5)
C11'–C12'	1.516(13)	C12'–C13'	1.527(8)
O1–In1–C7	114.42(8)	O1–In1–C6	112.24(8)
C7–In1–C6	133.30(10)	O1–In1–O1#1	72.76(5)
C7–In1–O1#1	96.98(7)	C6–In1–O1#1	98.34(8)
O1–In1–N1	73.33(5)	C7–In1–N1	94.80(7)
C6–In1–N1	96.43(8)	O1#1–In1–N1	146.02(5)
C4'–N1–C3'	119.3(6)	C4'–N1–C5	128.3(5)
C3'–N1–C5	83.9(3)	C4'–N1–C4	20.5(4)
C3'–N1–C4	130.4(4)	C5–N1–C4	108.9(2)
C4'–N1–C3	91.9(5)	C3'–N1–C3	29.1(3)

Bond lengths (Å) and angles (°) for $[Me_2In(OCH(CH_3)CH_2NMe_2)]_2$ (22)

C4'–N1–C5'	107.6(6)	C3'–N1–C5'	111.6(5)
C5–N1–C5'	28.0(4)	C4–N1–C5'	87.0(4)
C3–N1–C5'	134.9(4)	C4'–N1–In1	106.4(6)
C3'–N1–In1	102.1(3)	C5–N1–In1	113.01(17)
C4–N1–In1	114.6(2)	C3–N1–In1	103.02(12)
C5'–N1–In1	109.3(4)	C2'–O1–C2	27.4(3)
C2'–O1–In1	115.5(3)	C2–O1–In1	121.60(14)
C2'–O1–In1#1	133.5(3)	C2–O1–In1#1	129.88(14)
In1–O1–In1#1	107.24(5)	O1–C2–C3	110.7(2)
O1–C2–C1	112.8(5)	C3–C2–C1	109.2(5)
N1–C3–C2	111.7(2)	C3'–C2'–C1'	105.1(11)
O1–C2'–C3'	108.6(6)	C17–In2–C16	135.70(8)
O1–C2'–C1'	106.1(12)	N1–C3'–C2'	109.5(6)
O11–In2–C17	114.11(7)	C17–In2–C16	135.70(8)
O11–In2–C16	110.05(7)	C17–In2–O11#2	97.97(7)
O11–In2–O11#2	73.53(5)		
C16–In2–O11#2	97.61(6)	O11–In2–N11	73.48(5)
C17–In2–N11	94.37(7)	C16–In2–N11	94.58(7)
O11#2–In2–N11	146.99(4)	C12–O11–C12'	33.4(2)
C12–O11–In2	119.85(14)	C12'–O11–In2	117.57(19)
C12–O11–In2#2	131.04(14)	C12'–O11–In2#2	131.18(19)
In2–O11–In2#2	106.47(5)	C13–N11–C15'	128.2(4)
C13–N11–C13'	22.4(2)	C15'–N11–C13'	110.1(4)
C13–N11–C14'	91.0(4)	C15'–N11–C14'	108.8(5)
C13'–N11–C14'	111.2(5)	C13–N11–C14	109.9(3)
C15'–N11–C14	88.3(5)	C13'–N11–C14	127.4(4)

Bond lengths (Å) and angles (°) for $[Me_2In(OCH(CH_3)CH_2NMe_2)]_2$ (22)

C14'–N11–C14	21.7(4)	C13–N11–C15	110.2(3)
C15'–N11–C15	22.6(4)	C13'–N11–C15	89.6(3)
C14'–N11–C15	127.4(5)	C14–N11–C15	108.9(4)
C13–N11–In2	102.1(2)	C15'–N11–In2	114.1(5)
C13'–N11–In2	102.7(3)	C14'–N11–In2	109.8(6)
C14–N11–In2	114.0(4)	C15–N11–In2	111.6(3)
O11–C12–C13	108.8(3)	O11–C12–C11	110.2(9)
C13–C12–C11	111.0(8)	N11–C13–C12	113.0(3)
O11–C12'–C11'	112.2(12)	O11–C12'–C13'	107.1(4)
C11'–C12'–C13'	107.2(13)	N11–C13'–C12'	111.9(5)

Crystal data for $[Me_2In(OC(CH_3)_2CH_2OMe)]_2$ (23)

Chemical formula	$C_7H_{17}InO_2$
Formula weight	248.03
Crystal colour	Colourless
Crystal size	$0.36 \times 0.22 \times 0.15$ mm^3
a (Å)	8.3096(9)
b (Å)	15.0739(16)
c (Å)	8.7685(9)
α (°)	90
β (°)	112.743(2)
γ (°)	90
V (Å^3)	1012.93(19)
Z	4
Crystal system	Monoclinic
Space group	$P2_1/n$
Radiation, wavelength	MoKα, 0.71073 Å
Calculated density	1.626 g/cm^3
Absorption coefficient μ	2.285 mm^{-1}
Reflections collected	5818
Independent reflections	2335 (R_{int} = 0.0155)
Reflections with $F^2>2\sigma$	2208
Final R indices ($F^2>2\sigma$)	R1 = 0.0180, wR2 = 0.0419
R indices (all data)	R1 = 0.0197, wR2 = 0.0427
Goodness-of-fit on F^2	1.078
Largest diff. peak and hole	0.364 and –0.265 e Å^{-3}

Bond lengths (Å) and angles (°) for $[Me_2In(OC(CH_3)_2CH_2OMe)]_2$ (23)

In1–O1	2.1433(13)	In1–C7	2.146(2)
In1–C6	2.154(2)	In1–O1#1	2.2083(12)
In1–O2	2.5810(13)	O1–C2	1.425(2)
O1–In1#1	2.2083(12)	C1–C2	1.524(3)
C2–C3	1.526(3)	C4–O2	1.430(2)
C2–C4	1.527(3)		
O1–In1–C7	113.75(8)	O1–In1–C6	111.04(7)
C7–In1–C6	132.14(9)	O1–In1–O1#1	74.17(5)
C7–In1–O1#1	103.54(7)	C6–In1–O1#1	103.99(7)
O1–In1–O2	69.27(4)	C7–In1–O2	89.25(7)
C6–In1–O2	91.31(7)	O1#1–In1–O2	143.37(4)
C2–O1–In1	122.71(11)	C2–O1–In1#1	128.48(11)
In1–O1–In1#1	105.83(5)	O1–C2–C1	110.71(16)
O1–C2–C3	109.39(15)	C1–C2–C3	110.80(16)
O1–C2–C4	107.50(14)	C1–C2–C4	110.40(16)
C3–C2–C4	107.95(16)	C4–O2–In1	107.04(10)
C5–O2–C4	112.91(15)	C5–O2–In1	121.27(12)